SOME STUDIES ON HIGH-T_C SUPERCONDUCTORS

by

V. P. N. PADMANABAN

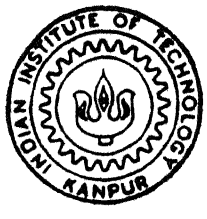

DEPARTMENT OF PHYSICS

INDIAN INSTITUTE OF TECHNOLOGY KANPUR

May, 1994

SOME STUDIES ON HIGH-T_C SUPERCONDUCTORS

A Thesis Submitted
in Partial Fulfilment of the Requirements
for the Degree of
DOCTOR OF PHILOSOPHY

by

V. P. N. PADMANABAN

to the

DEPARTMENT OF PHYSICS
INDIAN INSTITUTE OF TECHNOLOGY KANPUR
May, 1994

CERTIFICATE

It is certified that the work contained in the thesis entitled **"SOME STUDIES ON HIGH-T_C SUPERCONDUCTORS"**, by V.P.N. Padmanaban, has been carried out under my supervision and that this work has not been submitted elsewhere for a degree.

(K. Shahi)
Professor
Department of Physics
and Materials Science Program
I.I.T. Kanpur - 208 016

May, 1994

SYNOPSIS

An avalanche of research activities has resulted from the recent discoveries of superconductivity in such systems as La-Ba-Cu-O (T_c~30 K), $YBa_2Cu_3O_{7-\delta}$ (T_c~90 K), $Bi_2Sr_2Ca_2Cu_3O_{10}$ (T_c~110 K), $Tl_2Ba_2Ca_2Cu_3O_{10}$ (T_c~125 K), $HgBa_2Ca_2Cu_3O_{8+y}$ (T_c~133 K). Despite several years of sustained effort, the mechanism of superconductivity is far from understood and several problems remain to be sorted out before these high-T_c superconductors can be used in various technologies.

When this work was initiated in 1988, the primary aims were

(1) to develop new superconducting materials with possibly higher T_c and better superconducting properties and

(2) to contribute towards a better overall understanding of the mechanism of superconductivity in these new variety of ceramic superconductors.

Even during the initial stages of high-T_c superconductivity (HTSC) research, it was obvious that CuO plays the most crucial role in stabilizing the HTSCs, and this perception, of course, has been reinforced with every passing year. It was therefore imperative that any serious and systematic effort aimed at raising the T_c or developing altogether new materials of 123 type, potential substitutes or alternatives of copper oxides must be carefully identified. Since there were not many reports then, CuO itself was investigated by means of electric, thermoelectric, and dielectric measurements. Guided by these and other known properties of CuO such as

(A) the fluctuating valence state of its metallic (copper) ion,

(B) its anomalously high dielectric constant,

(C) that it is a p-type semiconductor with a band gap of ~1.4 eV,

(D) the anomaly in most physical properties at ~230 K, identified to be the paramagnetic to antiferromagnetic transition temperature, etc.,

oxides such as TiO_2, V_2O_3, and NiO were chosen as possible dopants for CuO in $YBa_2Cu_3O_{7-\delta}$. Besides, investigation on undoped and Pb- or Sb- doped (Bi, Pb, Sb)-Sr-Ca-Cu-O superconductors have been carried out in order to

(a) improve T_c and reduce ΔT_c,

(b) substantiate the paraconductivity analyses further,

(c) probe the normal-state behavior, etc.

Thus, in view of the above objectives, the following systems have been investigated and reported in that sequence:

(1) CuO, (2) $YBa_2Cu_3O_{7-\delta}$, (3) $YBa_2(Cu_{1-X}M_X)_3O_{7-\delta}$ (M=Ti, V, and Ni), and (4) (Bi, Pb, Sb)-Sr-Ca-Cu-O.

This thesis comprises seven Chapters. Chapter one gives a general introduction to superconductivity. A brief summary of various important experimental and theoretical developments concerning both low- and high-T_c superconductivity is given.

The details of various experimental set-ups and measurement techniques used in the present work are given in Chapter two. Design and fabricational details of (a) controlled atmosphere double stage (Pt-Rh and super-kanthal) furnace and other furnaces, (b) liquid nitrogen cryostat, and (c) various sample holders to perform measurements such as low-temperature (15-350 K) and high-temperature (300-1300 K) electrical resistivity (ρ), low-temperature (15-350 K) and high-temperature

(300-1300 K) thermoelectric power (S), and low-temperature (15-350 K) and high-temperature (300-1000 K) dielectric constant (ε') are also given.

Samples have been synthesized via ceramic, glass, and matrix routes. XRD, SEM, EDXA, DTA, TGA, and EPR techniques have been used for preliminary characterization of the samples. Details of density determination, and oxygen content measurement by iodometry are described. Besides, the measurements of ρ, S, and ε' involving LN_2 bath cryostat, closed cycle helium refrigerator, glove box, impedance analyzer, nanovoltmeter, DMMs, programmable temperature controllers, etc. are also discussed.

Chapter three reports $\rho(T)$, S(T), and $\varepsilon'(T)$ on CuO. All the three measurements, viz, $\rho(T)$, S(T), and $\varepsilon'(T)$ on CuO reveal an anomaly at ~230 K, the Neel transition temperature. CuO is a p-type, modest band gap (1.4 eV) semiconductor. Also, CuO has a large static dielectric constant. Besides, the anomaly at ~230 K, the large static dielectric constant, and the likely connection between antiferromagnetism and superconductivity have been analyzed.

Chapter four deals with the results and discussion on $YBa_2Cu_3O_{7-\delta}$ samples with different values of oxygen content. High-quality and high-density single-phase samples with T_c~93 K, $\Delta T_c < 0.5$ K, $\rho(300)$~600 $\mu\Omega$ cm, and $\rho(0)$~15 $\mu\Omega$ cm, have been used for paraconductivity analyses. Two different (normal-metal and Anderson-Zou) fitting procedures to the normal-state linear regions have been used to calculate the background resistivity. The Anderson-Zou fit to the data is found to work as well in polycrystals as in single crystals. The excess (or para-)

conductivity ($\Delta\sigma$) versus reduced temperature (ε) plots show the high-temperature, mean-field, crossover, and critical dynamics regions as the temperature approaches T_c.

The *in situ* high-temperature $\rho(T)$ measurements in controlled atmosphere up to 1200 K have furnished information regarding the linear $\rho(T)$ (absence of saturation, which implies weak electron-phonon coupling), the oxygen out-diffusion, and the high-temperature structural phase transition, etc. The low- and high-temperature S data are found to follow a relation of the type $S = (A/T) + BT$. The midband-filling and the phonon drag with the involvement of two carrier species (multiband conduction) seems to be operative in these systems.

Chapter five reports, besides $\rho(T)$, S(T), and $\Delta\sigma(\varepsilon)$, the structure, the solubility limit, the oxidation state, and the oxygen content in doped $YBa_2(Cu_{1-X}M_X)_3O_{7-\delta}$ (M=Ti, V, and Ni) systems. These results are compared with (1) each other, and (2) pure $YBa_2Cu_3O_{7-\delta}$ system, and (3) other doped $YBa_2Cu_3O_{7-\delta}$ systems, wherever possible to obtain a clearer picture of the properties of the materials studied.

Chapter six deals with the undoped and Pb- and/or Sb-doped Bi-Sr-Ca-Cu-O superconductors of various compositions with T_c varying from 40 to 110 K. The preparation process of 110 K phase has been optimized which requires a relatively short sintering time. The samples prepared via ceramic, glass, and matrix routes are characterized by XRD, EPR, $\rho(T)$, paraconductivity, S(T), and ε' measurements.

The last and the seventh Chapter summarizes the work and

TO MY PARENTS

ACKNOWLEDGEMENTS

I am grateful

to Profs. K. Shahi, A.K. Majumdar, D.C. Khan, D. Sahdev, O.P. Katyal, S.C. Sen, S.C. Agarwal, Y.R. Wagmare, H.D. Bist, R.C. Srivastava, R.C. Malhotra, K.K. Sharma, R.K. Theraja, R.M. Singru, K. Bannerji, G.S. Murthy, R. Ramachandran, N. Satyamoorthy, and others for their help and encouragement;

to Messrs B.Sharma, J.S. Sharma, J.N. Sharma, Sai Ram, V.P. Sharma, and B.K. Jain for their help in technical matters;

to Messrs T. Raj, Jawar Singh, Viswanath Singh, Lallu Singh, H.K. Panda, and A.K. Srivastava for their help in office matters;

to my friends Shiuli, Pandimani, Nagarajan, Sampathkumar, Srini, Whiteford, Jayaraj, Kumeresan, Srikanth, Ilango, Pandian, Manoravi, Venkat, Sivasubramaniam, Mungole, Bala, and others in various Halls of residence, GH, ISKCON, Vivekananda Samithi, Ramakrishna Mission, Tamil Mandram, Andra Association, etc.

to my adoptive father late T.P.R., adoptive mother, brothers, sisters, relatives, and friends for their support.

May, 1994, I.I.T. Kanpur V.P.N. Padmanaban

CONTENTS

LIST OF FIGURES XIII

LIST OF TABLES XXII

CHAPTER 1. INTRODUCTION 1

1.1 Historical Background 1

1.1.1 Discovery of Superconductivity 1

1.1.2 Critical Parameters 2

1.1.3 Magnetic Properties of a Perfect Conductor 3

1.1.4 Magnetic Properties of a Superconductor 3

1.1.5 Thermodynamics of the Transition 5

1.1.6 Isotope Effect 7

1.1.7 A.C. Resistivity, Tunneling, and Energy Gap 8

1.1.8 Phenomenological Theory 9

1.1.9 Microscopic Theory 11

1.2 Recent Developments 15

1.2.1 Discovery of High-T_c Superconductivity 15

1.2.2 The Structure 18

1.2.3 The Normal-State 31

1.2.4 The Superconducting-State 39

1.2.5 Different Classes of Superconductors 41

1.2.6 Towards a Theory 42

1.2.7 The RVB Theory and its Generalizations 44

1.2.8 The Spin Bags Theory 48

1.2.9 The Various Fermi-Liquid Theories 48

1.3 Superconductivity Applications 50

1.3.1 Physical Properties Important for Technology 50

1.3.2 Present Applications 51

1.3.3 Potential Applications 53

1.4 Statement of the Problem 53

CHAPTER 2. EXPERIMENTAL 55

2.1 Fabrication of Controlled Atmosphere Furnace 55

2.2 Materials Synthesis 55

2.3 General (Glovebox, Impedance analyzer, etc.) 63

2.4 Thermal Analysis (DTA, TGA) 64

2.5 X-ray Diffraction 65

2.6 Scanning Electron Microscopy 65

2.7 Electron Paramagnetic Resonance 65

2.8 Iodometry 65

2.9 Density Measurements 68

2.10 Cryostats and Sample Holders 68

2.11 Electrical Resistivity 74

2.12 Thermoelectric Power (TEP) 78

2.13 Dielectric Constant 83

CHAPTER 3. STUDIES ON CuO 87

3.1 Introduction 87

3.2 Properties of CuO and their Relevance to HTSC 89

3.3 Studies on CuO 93

3.4 Conclusions 105

CHAPTER 4. STUDIES ON $YBa_2Cu_3O_{7-\delta}$ 110

4.1 Introduction 110

4.2 Results and Discussion 111

4.2.1 XRD, SEM, EDXA, and DTA 111

4.2.2 EPR and Iodometry 112

4.2.3 Low-Temperature Resistivity 113

4.2.4 Paraconductivity 121

4.2.5 Low Temperature Thermoelectric Power 132

4.2.6 High Temperature Resistivity 138

4.2.7 High Temperature Thermoelectric Power 150

4.3 Conclusions 155

CHAPTER 5. STUDIES ON $YBa_2(Cu_{1-X}M_X)_3O_{7-\delta}$ (M = Ti, V, AND Ni) 156

5.1 Introduction 156

5.2 Results on $YBa_2(Cu_{1-X}M_X)_3O_{7-\delta}$ (M = Ti, V) 159

5.2.1 XRD, SEM, and EDXA 159

5.2.2 DTA, TGA, and Iodometry 159

5.2.3 EPR Studies 164

5.2.4 Electrical Resistivity 164

5.2.5 Thermoelectric Power (TEP) 167

5.3 Discussion ON $YBa_2(Cu_{1-X}M_X)_3O_{7-\delta}$ (M = Ti, V) 175

5.3.1 Solubility 175

5.3.2 Oxidation State 175

5.3.3 Electrical Resistivity 176

5.3.4 Paraconductivity 179

5.3.5 Thermoelectric power (S) 180

5.4 Results and Discussion on $YBa_2(Cu_{1-X}Ni_X)_3O_{7-\delta}$ 184

5.4.1 Solubility 184

5.4.2 Oxidation State 186

5.4.3 Electrical Resistivity 187

5.4.4 Paraconductivity 195

5.4.5 Thermoelectric Power 195

5.5 Conclusions 199

HAPTER 6. STUDIES ON (Bi,Pb,Sb)-Sr-Ca-Cu-O 201

6.1 Introduction 201

6.2 Results and Discussion 202

6.2.1 $Bi_2Sr_2CaCu_2O_Y$ 202

6.2.2 $Bi_{1.7}Pb_{0.3}Sr_{1.6}Ca_2Cu_{3.4}O_Y$ and $Bi_{1.9}Sb_{0.1}Sr_2Ca_2Cu_3O_Y$ 211

6.2.3 $Bi_{1.9}Pb_{0.3}Sr_2Ca_2Cu_3O_Y$ & $Bi_{1.6}Pb_{0.3}Sb_{0.1}Sr_2Ca_2Cu_3O_Y$ 222

6.3 Conclusions 234

HAPTER 7. SUMMARY AND CONCLUSIONS 235

EFERENCES 243

BLIOGRAPHY 275

PENDIX A LIST OF PUBLICATIONS 276

LIST OF FIGURES

Fig. 1.1. Increase in the T_c with time since the discovery of superconductivity. 19

Fig. 1.2. Structures for (a) tetragonal $YBa_2Cu_3O_6$ and (b) Ideal, orthorhombic $YBa_2Cu_3O_7$. (Adapted from ref. 96) 23

Fig. 1.3. Schematized structures of
(a) "1212" oxides, e.g., $TlBa_2CaCu_2O_7$ (m=2, n=2);
(b) "1223" oxides, e.g., $TlBa_2Ca_2Cu_3O_{10}$ (m=3, n=2);
(c) "2212" oxides, e.g., $Tl_2Ba_2CaCu_2O_8$ or $Bi_2Sr_2CaCu_2O_8$ (m = 2, n = 3); and
(d) "2223" oxides, e.g., $Tl_2Ba_2Ca_2Cu_3O_{10}$ or $Bi_2Sr_2Ca_2Cu_3O_{10}$ (m = 3, n = 3).
(Adapted from ref. 113) 27

Fig. 2.1. Controlled atmosphere double-statge (Pt-Rh and super Kanthal A) wire wound furnace (temperature range: 30-1600° C). 56

Fig. 2.2. Electrical resistivity, Thermopower, and Dielectric constant set up for the temperature range 77-400 K. 69

Fig. 2.3. Sample holder for TEP, two-probe electrical resistivity, and Dielectric constant measurements in the temperature range 77-500 K for DN 1710 Oxford Cryostat. 71

Fig. 2.4. Sample holder for thermopower measurement in the temperature range 15-300 K for closed cycle He cryostat. 73

Fig. 2.5. Sample holder for RT four-probe resistivity measurement. 76

Fig. 2.6. Experimental set up for HT four-probe resistivity measurement in the temperature range 300-1300 K. 77

Fig. 2.7. Controlled atmosphere set up for electrical resistivity and thermopower measurements in the temperature range 300-1300 K. 79

Fig. 2.8. Schematic diagram for TEP measurements. 82

Fig. 2.9. Micrometer cell for accurate RT capacitance measurement. 84

Fig. 2.10. Sample holder for two-probe resistivity and capacitance measurements in the temperature range 300-1000 K. 86

Fig. 3.1. Phase diagram for the system $YBa_2Cu_3O_{6+x}$. 91

Fig. 3.2. Ternary phase diagram for Y-Ba-Cu-O oxide. 91

Fig. 3.3. Log σ versus 1000/T plot of CuO at low-temperatures. 95

Fig. 3.4. Log σ versus 1000/T plot of CuO at high-temperatures. 96

Fig. 3.5. Plot of thermoelectric voltage (ΔV) versus the temperature difference (ΔT) across the sample. 98

Fig. 3.6. Plot of S versus 1000/T for CuO. 100

Fig. 3.7. Resistivity and thermopower versus 1000/T for CuO in the intrinsic region. 101

Fig. 3.8. Plot of the absorption spectrum of CuO. 102

Fig. 3.9. Plot of the real part of the dielectric constant (ε_r') versus temperature of CuO. 103

Fig. 3.10. Plot of the real part of the dielectric constant (ε_r') as a function of frequency. 104

Fig. 3.11. Plot of tan δ (loss) versus temperature for CuO. 106

Fig. 3.12. Relaxation time τ for dipole relaxation in CuO as a function of reciprocal temperature. 107

Fig. 4.1. Temperature dependence of the resistivity of three samples of $YBa_2Cu_3O_{7-\delta}$ with different room temperature resistivities. An anomaly is seen at around 220 K in sample 1. The dashed lines are the noncritical normal resistivity fitted to the form a+bT. 114

Fig. 4.2. Plot of ($d\rho/dT$) vs. T for samples 1, 2A and 2B. The transition widths (measured at half height) are $\leq$ 0.4 K. 118

Fig. 4.3. Anderson-Zou plot of the data in Fig.4.1. Fewer data points have been plotted for clarity. 120

Fig. 4.4. Log-log plot of the normalized excess conductivity ($\Delta\sigma/\sigma_{300}$) versus reduced temperature (ϵ) for sample 1 (2nd run); (N): $\Delta\sigma$ obtained by normal metal extrapolation ; (AZ): $\Delta\sigma$ obtained from the Anderson-Zou fit to the data. 127

Fig. 4.5. Log-log plot of the normalized excess conductivity ($\Delta\sigma/\sigma_{300}$) vs. reduced temperature (ϵ) for sample 2A ; (N): $\Delta\sigma$ obtained by normal metal extrapolation ; (AZ): $\Delta\sigma$ obtained from the Anderson-Zou fit to the data. 129

Fig. 4.6. Log-log plot of the normalized excess conductivity ($\Delta\sigma/\sigma_{300}$) vs. reduced temperature (ϵ) for sample 2B ; (N): $\Delta\sigma$ obtained by normal metal extrapolation ; (AZ): $\Delta\sigma$ obtained from the Anderson-Zou fit to the data. 130

Fig. 4.7. Thermopower as a function of temperature for $YBa_2Cu_3O_{7-\delta}$ compounds with different oxygen content (7-δ). 7-δ for curve 1 is 6.94 ± 0.02; for curve 2 is 6.85 ± 0.02. 134

Fig. 4.8. ST vs. T^2 plots for $YBa_2Cu_3O_{7-\delta}$ samples with different oxygen content (7-δ). 7-δ for curve 1 is 6.94 ± 0.02; for curve 2 is 6.85 ± 0.02. 136

Fig. 4.9. *In situ* resistivity vs. temperature curves for $YBa_2Cu_3O_{7-\delta}$ in oxygen ambient of sample 1 of Fig. 4.1. 142

Fig. 4.10. *In situ* resistivity vs. temperature curves for $YBa_2Cu_3O_{7-\delta}$ in oxygen ambient of sample 2 of Fig. 4.1. 143

Fig. 4.11. *In situ* resistivity vs. temperature curves for $YBa_2Cu_3O_{7-\delta}$ in Air (heating) and in helium (cooling) ambient. 149

Fig. 4.12. *In situ* thermopower vs. temperature curves for $YBa_2Cu_3O_{7-\delta}$ in oxygen ambient of sample 1 of Fig. 4.1. 151

Fig. 4.13. *In situ* thermopower vs. temperature curves for $YBa_2Cu_3O_{7-\delta}$ in oxygen ambient of sample 2 of Fig. 4.1. 152

Fig. 4.14. *In situ* thermopower vs. temperature curves for $YBa_2Cu_3O_{7-\delta}$ in air (heating) and in helium (cooling) ambient. 154

Fig. 5.1. Typical EDXA spectra (at 20 kV) of $YBa_2(Cu_{1-X}Ti_X)_3O_{7-\delta}$ (X = 0.025) sample. 160

Fig. 5.2. Typical EDXA spectra (at 20 kV) of $YBa_2(Cu_{1-X}V_X)_3O_{7-\delta}$ (X = 0.025) sample. 161

Fig. 5.3. Temperature dependence of the resistivity of $YBa_2(Cu_{1-X}Ti_X)_3O_{7-\delta}$ (X = 0 to 0.1) samples. 165

Fig. 5.4. Temperature dependence of the resistivity of $YBa_2(Cu_{1-X}V_X)_3O_{7-\delta}$ (X = 0 to 0.2) samples. 166

Fig. 5.5. The variation of $(d\rho/dt)$ versus T for $YBa_2(Cu_{1-X}V_X)_3O_{7-\delta}$ (X=0 to 0.025) samples. The temperature dependence of the resistivity in the transition region is also shown. 168

Fig. 5.6. Anderson-Zou plot of the data (with X=0.025) in Fig. 5.3. 169

Fig. 5.7. Anderson-Zou plot of the data (with X = 0.025, 0.05) in Fig. 5.4. 170

Fig. 5.8. Log-log plot of the normalized excess conductivity ($\Delta\sigma/\sigma_{300}$) vs. reduced temperature (ε) for the Ti-doped sample with X = 0.025; (N): $\Delta\sigma$ obtained by normal metal extrapolation; (AZ): $\Delta\sigma$ obtained from the Anderson-Zou fit to the data. 171

Fig. 5.9. Log-log plot of the normalized excess conductivity ($\Delta\sigma/\sigma_{300}$) vs. reduced temperature (ε) for the V-doped sample with X = 0.025; (N): $\Delta\sigma$ obtained by normal metal extrapolation; (AZ): $\Delta\sigma$ obtained from the Anderson-Zou fit to the data. 172

Fig. 5.10. Thermopower as a function of temperature for $YBa_2(Cu_{1-X}Ti_X)_3O_{7-\delta}$ (X = 0.025, 0.1) samples. 173

Fig. 5.11. Thermopower as a function of temperature for $YBa_2(Cu_{1-X}V_X)_3O_{7-\delta}$ (X = 0.025, 0.05, 0.1) samples. 174

Fig. 5.12. ST vs. T^2 plots for $YBa_2(Cu_{1-X}Ti_X)_3O_{7-\delta}$ (X = 0.025, 0.1) samples. 181

Fig. 5.13. ST vs. T^2 plots for $YBa_2(Cu_{1-X}V_X)_3O_{7-\delta}$ (X = 0.025, 0.05, 0.1) samples. 182

Fig. 5.14. Temperature dependence of the resistivity of $YBa_2(Cu_{1-X}Ni_X)_3O_{7-\delta}$ (X = 0.025 to 0.2) samples. 188

Fig. 5.15. The variation of ($d\rho/dt$) versus T for $YBa_2(Cu_{1-X}Ni_X)_3O_{7-\delta}$ (X=0.025) sample. 191

Fig. 5.16. The variation of transition temperature of $YBa_2(Cu_{1-X}Ni_X)_3O_{7-\delta}$ with concentration X. The dashed curve is a guide to the eyes. 192

Fig. 5.17. Anderson-Zou plot of the resistivity data reported in Fig. 5.14. for $YBa_2(Cu_{1-X}Ni_X)_3O_{7-\delta}$ samples (X = 0.025, 0.05, 0.075). 194

Fig. 5.18. Log-log plot of the normalized excess conductivity $(\Delta\sigma/\sigma_{300})$ versus reduced temperature (ε) for the Ni-doped sample with X = 0.025; (N): $\Delta\sigma$ obtained by normal metal extrapolation; (AZ): $\Delta\sigma$ obtained from the Anderson-Zou fit to the data. 196

Fig. 5.19. Thermopower as a function of temperature for $YBa_2(Cu_{1-X}Ni_X)_3O_{7-\delta}$ ($0.025 \leq X \leq 0.2$) samples. 197

Fig. 5.20. Variation of ST as a function of T^2 for $YBa_2(Cu_{1-X}Ni_X)_3O_{7-\delta}$ ($0.025 \leq X \leq 0.2$) samples. 198

Fig. 6.1. Ressistivity as a function of temperature for several samples of $Bi_2Sr_2CaCu_2O_y$ (2212) system. 203

Fig. 6.2. Resistivity as a function of temperature for several samples of $Bi_2Sr_2CaCu_2O_y$ (2212) system. 204

Fig. 6.3. ρT versus T^2 plots for $Bi_2Sr_2CaCu_2O_y$ (2212) system. 206

Fig. 6.4. Log-log plot of the normalized excess conductivity $(\Delta\sigma/\sigma_{300})$ versus reduced temperature (ε) for the Bi-2212 sample, with normal-metal background fitting. 208

Fig. 6.5. Log-log plot of the normalized excess conductivity ($\Delta\sigma/\sigma_{300}$) versus reduced temperature (ε) for the Bi-2212 sample, with Anderson-Zou background fitting. 209

Fig. 6.6. Thermopower (S) versus temperature behavior for the sample E of Fig. 6.2. 210

Fig. 6.7. XRD pattern for the sintered (840°C, 72h) $Bi_{1.7}Pb_{0.3}Sr_{1.6}Ca_2Cu_{3.4}O_X$ sample. 212

Fig. 6.8. Non-resonant microwave absorption signals of samples with the nominal compositions : ceramic $Bi_{1.7}Pb_{0.3}Sr_{1.6}Ca_2Cu_{3.4}O_X$ (1), crystallized glass $Bi_{1.7}Pb_{0.3}Sr_{1.6}Ca_2Cu_{3.4}O_X$ (2a) and ceramic $Bi_{1.9}Sb_{0.1}Sr_2Ca_2Cu_3O_Y$ (3) at 77K as a function of magnetic field H. 214

Fig. 6.9. Temperature dependence of the electrical resistance of sintered (840°C, 72h) $Bi_{1.7}Pb_{0.3}Sr_{1.6}Ca_2Cu_{3.4}O_X$ (1) and further annealed (400°C, 24h) and air quenched (1a) samples. 215

Fig. 6.10. DTA curve of melt-quenched sample of $Bi_{1.7}Pb_{0.3}Sr_{1.6}Ca_2Cu_{3.4}O_X$ (2). 216

Fig. 6.11. XRD patterns for the melt-quenched samples with the nominal compositions : $Bi_{1.7}Pb_{0.3}Sr_{1.6}Ca_2Cu_{3.4}O_X$ (2) $Bi_{1.9}Sb_{0.1}Sr_2Ca_2Cu_3O_Y$ (4). 217

6.12. Temperature dependence of the electrical resistance of crystallized $Bi_{1.7}Pb_{0.3}Sr_{1.6}Ca_2Cu_{3.4}O_X$ glass. 218

6.13. XRD patterns of samples with the nominal compositions : annealed (840°C, 15h) $Bi_{1.7}Pb_{0.3}Sr_{1.6}Ca_2Cu_{3.4}O_X$ [as grown few layers removed (2b)] and sintered (890°C, 15h) $Bi_{1.9}Sb_{0.1}Sr_2Ca_2Cu_3O_Y$ (3). 219

6.14. Temperature dependence of the electrical resistance of sintered $Bi_{1.9}Sb_{0.1}Sr_2Ca_2Cu_3O_Y$ sample (3). 221

6.15. Temperature dependence of the resistivity plots of $Bi_{1.9}Pb_{0.3}Sr_2Ca_2Cu_3O_y$ samples. 224

6.16. S versus T plot of Sample A of Fig. 6.15. 225

6.17. S versus T plot of sample B of Fig.6.15. 226

6.18. X-ray diffraction patterns for samples A and B of nominal composition $Bi_{1.9}Pb_{0.3}Sr_2Ca_2Cu_3O_y$. The Miller indices are noted above each peak. 228

6.19. Temperature dependence of the resistivity plots of $Bi_{1.6}Pb_{0.3}Sb_{o.1}Sr_2Ca_2Cu_3O_y$ samples. 229

6.20. X-ray diffraction patterns for samples C and D of nominal composition $Bi_{1.6}Pb_{0.3}Sb_{o.1}Sr_2Ca_2Cu_3O_y$. The Miller indices noted above each peak. 231

versus T plot of sample D of Fig. 6.19. 232

LIST OF TABLES

able 1.1. Basic composition of copper oxide superconductors and some of their variations. 20

able 4.1. Some resistivity parameters of $YBa_2Cu_3O_{7-\delta}$ samples. 117

able 4.2. The reduced-temperature range and exponent of AL equation, $\Delta\sigma = A\varepsilon^x$ for three differently processed Y-Ba-Cu-O polycrystalline samples. 128

able 5.1. Some resistivity parameters of $YBa_2(Cu_{1-x}Ti_x)_3O_{7-\delta}$ samples. 162

able 5.2. Some resistivity parameters of $YBa_2(Cu_{1-x}V_x)_3O_{7-\delta}$ samples. 163

able 5.3. Variation of cell parameters, thermal decomposition temperature, and oxygen content for $YBa_2(Cu_{1-x}Ni_x)_3O_{7-\delta}$ as a function of nominal Ni composition x. 185

able 5.4. Some resistivity parameters of $YBa_2(Cu_{1-x}Ni_x)_3O_{7-\delta}$. 189

able 6.1. Some parameters of (Bi,Pb,Sb)-Sr-Ca-Cu-O superconductors. 223

CHAPTER 1

INTRODUCTION

1.1 HISTORICAL BACKGROUND

1.1.1 Discovery of Superconductivity

In 1908, Kamerlingh Onnes, liquefied helium (He) and in 1911, he found no measurable resistance at 4.2 K [1] in a mercury (Hg) wire of high-purity. Soon he found that the addition of impurities to the Hg did not increase its resistance (R). Furthermore, R did not decrease smoothly but dropped almost discontinuously to zero within a temperature (T) range of 0.01 K. By 1913, he had concluded [2] that "*mercury has passed into a new state, which on account of its extraordinary electrical properties may be called the superconductive state.*" For this discovery, he was awarded the Nobel prize in 1913. Later, superconductivity has been found amongst metallic elements, intermetallic compounds, alloys, and semiconductors, although in many cases the measured T_c is well below 1 K. Nb is the *metallic element* with the highest T_c (9.3 K). Nb_3Ge is the *metallic compound* with the highest T_c (23.2 K). On cooling, the transition to the superconducting state may be extremely sharp if the specimen is pure and physically perfect. Quinn and Ittner [3] were able to deduce that the resistivity (ρ) of superconducting Pb (T_c=7.2 K) is less than 10^{-23} Ω cm whereas the ρ of a good normal metal at room temperature is about 10^{-6} Ω cm.

1.1.2 Critical Parameters

(1) CRITICAL (OR TRANSITION) TEMPERATURE

"*The temperature at which the transition, from a normal to a superconducting state, takes place is the critical (or transition) temperature* (T_c)." The temperature interval or the *transition width* (ΔT_c), over which the transition between the normal and superconductive states takes place, may be of the order of as little as 10^{-5} K or several K, depending on the material state. The narrow transition width was attained in 99.9999% pure Ga single crystals.

(2) CRITICAL MAGNETIC FIELD

In 1914, Onnes discovered another important property of superconductors, namely, that when the metal is placed in a sufficiently strong magnetic field, superconductivity gets destroyed [4]. However, it reappears when the field is removed. If the specimen is in the shape of a long cylinder and is placed parallel to the field, the transition is sharp and *the minimum field required to destroy the superconductivity is called the critical field* (H_c). Pure specimens of many materials which exhibit this behavior are called **type I superconductors** or *soft superconductors*. The value of H_c is independent of the volume (V) of the material but depends on T; it is zero at T_c and rises to a few hundred or a few thousand Gauss at the 0 K. Intermetallic compounds exhibit higher critical fields. In such cases the transition is not very sharp. They are known as **type II superconductors**.

(3) CRITICAL CURRENT

An interesting consequence of the existence of H_c is that there is also a critical strength (J_c) for the current flowing in a superconductor. The disturbance of superconductivity by a current was actually discovered [5] before that by a magnetic field. Silsbee [6] pointed out that the effect of a current in restoring the resistance might be merely due to the magnetic field which it produced. This has since been verified, and thus showing that the current effect is merely a secondary feature.

1.1.3 Magnetic Properties of a Perfect Conductor

If a superconductor can really be described by an infinite conductivity ($\rho=0$), then from Ohm's law, $\mathbf{E}=\rho\mathbf{j}$, and $\mathbf{E}=0$ inside, while $\mathbf{j}$ is held finite. From one of the Maxwell's equations $\partial\mathbf{B}/\partial t$ is proportional to curl $\mathbf{E}$, so that $\rho=0$ implies $\dot{\mathbf{B}}=0$; i.e., the magnetic induction ($\mathbf{B}$) is constant in time and the flux through the metal cannot change on cooling through the transition. That is, the state of magnetization of a perfect conductor is not uniquely determined by the external conditions but depends on the sequence by which these conditions were arrived at. This means that there is not a single superconductive state in a given external magnetic field but an infinite number which must be metastable.

1.1.4 Magnetic Properties of a Superconductor

(1) MEISSNER EFFECT (PERFECT DIAMAGNETISM)

Until 1933 it was assumed that the effect of a magnetic

field on a superconductor would be as described in section 1.1.3. However, in 1933, Meissner and Ochsenfeld [7] found that when a superconductor is cooled in a weak magnetic field, at the T_c persistent currents arise on the surface and circulate so as to cancel the flux density inside, in just the same way as when a magnetic field is applied after the metal has been cooled. "*This effect, whereby a superconductor never has a flux density inside* (B=0) *even when in an applied magnetic field is called the Meissner effect.*" Thus the superconductive state in a given external magnetic field is a single stable state to which the laws of thermodynamics apply. Thus, *perfect diamagnetism rather than infinite conductivity was taken to be the fundamental and most revealing property of superconductors.* Perfect diamagnetism and infinite conductivity are independent properties of superconductors, neither implying the other.

(2) PERMEABILITY AND SUSCEPTIBILITY OF A SUPERCONDUCTOR

Consider a long rod with the applied magnetic field, B_a, parallel to its length producing in the material a flux density equal to $\mu_r B_a$, where μ_r is the relative permeability of the material. For metals, $\mu_r \simeq 1$, so the flux density within is equal to B_a. But for a superconductor, $\mu_r=0$, so B=0 inside (the effect of screening currents is included in the statement $\mu_r=0$). The strength H_a of the applied magnetic field is given by $H_a=(B_a/\mu_o)$, and the flux density in a magnetic material is related to the strength of the applied field by $B=\mu_o(H_a+M)$, where M is the magnetization of the material. Thus, for a superconductor (B=0), $M=-H_a$ or $(M/B_a)=-(1/\mu_o)$, and the magnetic

susceptibility (χ), i.e., the ratio of the magnetization to the field strength, must be -1 (in CGS units, μ_o is replaced by 4π).

(3) PENETRATION DEPTH

If the metal is superconducting, B=0 inside, and so curl B=0 inside. Hence J=0 inside. So, if there is a current, it flows not through the metal but on the surface. But the current cannot be confined entirely to the surface because, if this were so, the current sheet would have no thickness and the current density would be infinite, which is a physical impossibility. In fact, the currents flow within a very thin surface layer whose thickness is of the order of 10^{-5} cm. The depth within which the currents flow is called the *penetration depth*, because it is the depth to which the flux of the applied magnetic field appears to penetrate. (This is somewhat like the *skin depth* to which high frequency alternating fields penetrate in a normal conductor.)

1.1.5 Thermodynamics of the Transition

(1) FREE ENERGY AND ENTROPY

The free energy of the superconducting state (F_S) is less than that of the normal state (F_N). At $T=T_c$, $F_S=F_N$ and there is no latent heat of transition at T_c. Thus the phase transition is *second-order.* The application of a magnetic field raises the free energy of the metal in the superconducting state by an amount $(1/2)\mu_o H_a^2$ due to the magnetization. The entropy of the superconducting state is less than that of the normal state. This means that the superconducting state is more ordered than the

normal state. Some or all of the electrons thermally excited in the normal state are ordered in the superconducting state.

(2) SPECIFIC HEAT AND LATENT HEAT

Since at T_c, $S_N=S_S$, and $(\partial F/\partial T)_N = (\partial F/\partial T)_S$. A phase transition which satisfies this condition (i.e. not only F is continuous but $\partial F/\partial T$ is also continuous) is known as a **second-order phase transition.** This has two important characteristics : at T_c there is no latent heat, and there is a jump in the specific heat. In the absence of any magnetic field the transition occurs at the T_c and $H_c=0$, but if there is a magnetic field the transition occurs at some lower temperature T where $H_c>0$. This latent heat arises because at temperatures between T_c and 0 K the entropy of the normal state is greater than that of the superconducting state, so heat must be supplied if the transition is to take place at constant temperature. In the presence of B_a magnetic field, therefore, the superconducting-normal transition is of the **first-order**, i.e., although F is continuous, dF/dT is not.

It is observed that at temperatures well below the T_c

$$(C_{el})_S = a \exp(-b/kT) \ , \qquad (1.1)$$

where a and b are constants. This suggests that as T is raised, electrons are excited across an energy gap above their ground state. The number of electrons excited across such a gap would vary exponentially with the temperature.

(3) THERMAL CONDUCTIVITY

In the superconducting state, the superelectrons no longer interact with the lattice in a way that they can exchange energy, and so they cannot pick up heat from one part of a specimen and deliver it to another. Consequently, if a metal goes into the superconducting state its thermal conductivity is reduced.

(4) THERMOELECTRIC EFFECTS

It is found both from theory and experiment, that the thermoelectric effects do not occur in a superconducting state. If a thermal emf were produced, there would be a strange situation in which the current would increase to the critical value, no matter how small is the temperature difference. It follows from the Thompson relations that, if there is no thermal emf in superconducting circuits, the Peltier and Thompson coefficients must be the same for all superconducting metals, and they are in fact zero. The absence of thermoelectric effects only applies to the type-I superconductors. Thermoelectric effects may appear in the type-II superconductors.

1.1.6 Isotope Effect

In 1950, Maxwell [8] and Reynolds et al. [9]. found in mercury that the T_c varies as the average atomic mass M varies. The results within each series of isotopes may be fitted by an equation of the form $M^{\alpha}T_c$= constant. This means that lattice vibrations and hence electron-lattice interactions are deeply involved in superconductivity.

1.1.7 A.C. Resistivity, Tunneling, and Energy Gap

That a superconductor has no resistance is strictly true only for a direct current of constant value. Up to 10^7 Hz the resistance is still zero, but for 10^9 Hz London [10] and Pippard [11] showed that there was a considerable resistance even below T_c. At infrared frequencies (~10^{13} Hz) the absorption of the metal (i.e., its resistivity) is the same and independent of temperature both in the normal and superconducting states. So somewhere in between infrared and microwave region an absorption mechanism at absolute zero must set in. The absorbed photons of sufficient energy excite the superelectrons into the higher state where they become as normal electrons, and thus responsible for the observed resistivity at finite temperatures. This suggests the existence of an energy gap in the electronic spectrum. As the temperature is increased not only does the gap decrease in energy, but the resistivity for photons below the gap energy no longer vanishes, except at zero frequency.

If the insulating barrier between two metals is sufficiently thin (<20 A°) there is a significant probability that an electron will pass from one metal to the other: this is called tunneling. Giaever [12] discovered that if one of the metals becomes superconducting, the I-V characteristic changes from the Ohmic or straight line behavior. When both metals are normal conductors, the current-voltage relation of the junction is Ohmic at low voltages [13,14]. In 1962, Josephson [15] predicted the tunneling of superconducting electron pairs from a superconductor through a layer of an insulator into another superconductor; such a junction is called a weak link. For this he was awarded Nobel

prize in 1973. The effects of pair tunneling include: (a) DC Josephson effect, (b) AC Josephson effect, and (c) Macroscopic long-range quantum interference. The tunneling technique also provides direct evidence on the density of states above the gap.

Apart from the above microwave, infrared, and tunneling of electron from one superconductor to another, the following are the further evidences for the existence of energy gap.

(1) Exponential decrease with decreasing temperature of thermal conductivity of a number of superconductors below $T_c/3$ [16].

(2) Exponential decrease of the electronic specific heat of a number of superconductors below $T_c/3$ [17].

(3) Decrease in the absorption of ultrasonic waves [18].

(4) Decrease in the spin-lattice relaxation time with decreasing temperature [19].

(5) Reflection from bulk material in the infrared [20].

These leave no doubt that in the soft superconductors, at least, there is an energy gap between the ground state and single-particle excited states, which is of the order of $3kT_c$. Typically $E_g \sim 10^{-4} \epsilon_F$. In a superconductor the gap is tied to the Fermi gas, Whereas in an insulator the gap is tied to the lattice. While in a *second-order* phase transition, the energy gap decreases continuously to zero as the temperature is increased to T_c, a *first-order* transition is characterized by a discontinuity in the energy gap.

1.1.8 Phenomenological Theory

In 1934, Gorter and Casimir [21] using the concept of two interpenetrating liquids (superconducting and normal ones),

described a *second-order* transition from a superconducting- to a normal-state when the magnetic field rises above the critical value H_c. In 1935, F. and H. London brothers [22] described the electrodynamics of superconductors based on the experimentally observed Meissner effect. After the discovery of superfluidity of He II which was presented in a finished form in 1938, it became more or less clear that superconductivity is the superfluidity of the electron liquid in a metal in the light of Landau's theory of superfluidity [23,24]. The connection between superfluidity and Bose-Einstein condensation of ^{4}He atoms was established in 1948 when ^{3}He was liquefied and its properties were found to differ sharply from those of liquid ^{4}He.

In 1950, Ginzburg and Landau (GL) [25] generalized the above phenomenological models assuming that some part of conduction electrons in a superconducting-state of metal forms a peculiar superfluid liquid (condensate), distributed with local density $N_s(r)$ over the whole volume of a crystal. The superfluid is capable of moving as a whole with local velocity $v_s(r)$. As the temperature rises, part of the electrons *evaporates* from the condensate and forms a *weakly excited gas* - a normal fluid which is also distributed over the whole volume of a crystal with local density $N_n(r)$ and capable of moving with local velocity $v_n(r)$. Remaining within the framework of London's local theory, Ginzburg and Landau made an important step towards constructing a quasi-microscopic (quantum) theory of superconductivity. They postulated that $N_s(r) \propto |\Psi_s(r)|^2$, where $\Psi_s(r)$ is some wave function of a superconducting-state, which is dependent only on one coordinate. So, a coherent state of all superconducting electrons

was postulated. In the state of dynamic equilibrium, when $T>T_c$, this function is equal to zero, and when $T<T_c$ it is different from zero. The GL theory is, strictly speaking, applicable to states near the T_c. However, it enables one to describe many qualitative features of the behavior of superconductors in a magnetic field. This theory introduced the important dimensionless parameter $c=\lambda/\xi_o$. For pure metals, the value of c is small. For example, c=0.16 for Hg (λ=500 A°, ξ_o=3000 A°). In 1957, Abrikosov showed [26] that the GL theory implied that two groups of superconductors are possible. Superconductors with $c(2)^{1/2}<1$ were referred to as superconductors of the first-kind. The conductors with $c(2)^{1/2}>1$ are called superconductors of the second-kind. They are characterized by two critical fields H_{c1} and H_{c2}. In this case, inside the specimen normal and superconducting phases coexist. This state called by Abrikosov a mixed state.

1.1.9 Microscopic Theory

The physical foundations of the quantum microscopic theory of superconductivity were formulated by F. London [27] in 1935. He introduced the concept of a very strong correlation between conduction electrons at low temperatures and assumed that the wave function describing the superfluid component applied to the whole crystal generally and was rigid. In 1950, employing the concept that the electron-phonon interaction plays a major role in superconductivity phenomenon, Fröhlich predicted [28] a very important feature of superconductors- the dependence of T_c on the isotopic composition (isotopic effect). The inapplicability of

perturbation theory to describe the properties of superconductors was first indicated by Schafroth [29]. He showed that the theory could not explain the Meissner effect to any finite order of perturbation theory, if the state involving no bound pairs was chosen as the initial state. In 1954, he [30] put forth the idea of pairing and suggested that the electron-phonon interaction could be responsible for it. Later, Schafroth et al. [31] developed their theory but left the question about the nature and mechanism of pairing unanswered. The pair size was assumed to be small (of atomic dimensions) and the T_c was determined to a first approximation by the formula for the temperature of Bose-Einstein condensation of an ideal gas.

The merit of the theory of superconductivity by Cooper [32] in 1956 and of the subsequent BCS theory [33], lies in the demonstration of pair formation (*large or Cooper pairs*) and of their collective *condensation* even under a weak attraction between electrons near the Fermi surface of the electron gas. An attractive interaction (indirect, i.e., via lattice) between electrons can lead to a ground state separated from excited states by an energy gap. The BCS theory, employed a model Hamiltonian based on the assumption that all electrons in a superconducting state near the Fermi surface are correlated in pairs with equal and oppositely directed momenta and spins. The basic equation in BCS theory is

$$T_c = 1.14\ \theta_D \exp(-1/\lambda)\ , \qquad N(E_F)\ U<1/2 \qquad (1.2)$$

where $\lambda=N(E_F)U$, $N(E_F)$ being the density of states at the Fermi energy and U the electron-phonon interaction, and $\theta_D=\hbar\omega_D/k_B$, $\hbar\omega_D$ being the average phonon energy. The value of the Debye temperature (θ_D) is determined from the heat capacity measurements. In metals, it is around 100-500 K. T_c is very sensitive to $N(E_F)U$, and less sensitive to θ_D; unfortunately only θ_D can be measured accurately in the normal-state. Increasing $N(E_F)U$ destabilizes the lattice and decreases ω_D.

The gap width becomes zero at $T=T_c$ with an infinite derivative, this corresponding to a *second-order* phase transition (from a superconducting into a normal state). At T=0, the ratio of the energy gap to k_BT_c for all the superconductors described by BCS theory is defined by the equality

$$2\Delta(0)/k_BT_c = 3.52 \ , \qquad (1.3)$$

which is well satisfied for many metals. At T below $0.6T_c$, the energy gap is slightly dependent on the temperature.

If one takes into account that only a small fraction $k_BT_c/E_F \sim 10^{-4}$ of electrons participates in pair formation near the Fermi surface, the distance between these pairs will be $\sim 10^6$ cm. With the density of electrons equal to 10^{22}, the volume occupied by a single pair $(10^{-4})^3$ will thus contain 10^6 other pairs. So, the wave function of a superconducting-state describes coherence of about a million quasiparticle pairs among which it is difficult to isolate any individual pair. Bardeen et al. [33] and Schrieffer [34] assert, *the picture of isolated pairs makes no sense,* and the superconducting transition is, strictly speaking,

not similar to Bose-Einstein condensation. Moreover, the pairs are not strictly Bose particles, because their creation operators do not satisfy the commutation relation for Bose-particles. Conceptually, a superconducting-state can be thought of as a kind of a *macromolecule* that consists of many millions of quasiparticles. Such a *molecule* occupies a large volume of a crystal and is capable of moving as a whole if there are rigid correlations between the particles constituting the molecule.

The BCS theory explains many experimental facts observed in superconductivity of simple metals and alloys. Yet, it incorporated some insufficiently substantiated assumptions and approximations. For a weak electron-phonon coupling, the theory was substantiated in a stricter way by Bogoliubov [35] and Valatin [36]. Taking into account the Coulomb interaction between the electrons, Bogoliubov, Tolmachev, and Shirokov derived

$$T_c = 1.44\ \theta_D \exp\{-1/(\lambda-\mu)\}, \qquad (1.4)$$

where μ is the Coulomb pseudopotential. The logarithmic weakening of the Coulomb repulsion results from the fact that the average distance of electrons in a Cooper pair, characterized by the correlation length $\xi_o \sim \hbar v_F/\Delta(0) \simeq 10^{-4}$ cm, (where v_F is the velocity on Fermi surface), is much greater than the lattice constant, a $\sim 10^{-8}$ cm. Therefore, the Coulomb repulsion is strongly screened.

The range of applicability of the BCS theory and of that developed by Bogoliubov was extended by Eliashberg [37] and Nambu [38]. Using the pseudopotential treatment of screened Coulomb interelectron repulsion proposed by Morel and Anderson [39],

McMillan [40] generalized the Eliashberg theory to include the coulomb interaction. The theories of BCS, Eliashberg, and McMillan are concerned with isotropic media. The T_c and the Δ in such superconductors are small (Δ=1.7 $k_B T_c$). However, the Fermi energy is large E_F ~10-14 eV due to the large density of charge carriers (~10^{22} cm^{-3}). Since the inequality $\Delta/E_F \ll 1$ is satisfied, only a very small part (~10^{-4}) of electrons with energies close to the Fermi energy participate in superconductivity in such metals. These superconductors are characterized by the large coherence length ξ_o=10^{-4} cm. If a is the lattice constant, then the coherence length can be evaluated by employing the uncertainty condition $\xi_o \approx a\ E_F/\Delta$.

1.2. RECENT DEVELOPMENTS

1.2.1 Discovery of High-T_c Superconductivity

Since superconductivity was discovered by Onnes [1,2], high-T_c superconductors (HTSCs) have been a goal and a dream of scientists in this field. This has stimulated the synthesis of a lot of novel materials like intermetallics, low-dimension structures, organic superconductors, excitonic superconductors, superconductivity under pressure, heavy fermion systems, and transition metal compounds. The discovery by Sleight et al. [41] of superconductivity in the pseudoternary alloy $BaPb_{1-X}Bi_XO_3$ (T_c~13 K, for X=0.25), which served as a prototype material for the ceramic superconductors that followed, was as surprising as that by Chevrel et al. [42] in the ternary sulfides which proved to contain HTSCs, represents a fundamental breakthrough in

crystal chemistry [43]. The T_c achieved in the material class of transition metal compounds, with A-15 structure for films of Nb_3Ge (T_c~23.2 K) in 1973 by Gavaler [44], has remained as the highest limit until 1986.

An avalanche of research activities has resulted from the recent discovery of possible high-T_c superconductivity (HTSC) in the multiphase mixtures with nominal composition $Ba_XLa_{5-X}Cu_5O_{5(3-Y)}$ at ~30 K by Bednorz and Müller [45] in 1986. Subsequent studies [46-49] confirmed that HTSC indeed exists in this system. Takagi et al. [50] further attributed the superconductivity in $La_{1.8}Ba_{0.2}CuO_4$ to the K_2NiF_4 phase. Substitution of Sr for Ba has produced ~40 K superconductivity [48,51,52]. Pressure was found to enhance the T_c of the La-Ba-Cu-O [48] at a rate greater than 10^{-3} K bar^{-1}. This unusually large pressure effect on T_c has led to suggestions that the HTSC in the La-(Ba,Sr)-Cu-O systems may be associated with interfacial effects arising from mixed phases; strong superconducting interactions due to the mixed valence states; or an yet unidentified phase.

In 1987, Wu et al. [53] found a new mixed phase Y-Ba-Cu-O compound at ambient pressure with the onset T_c (T_{co}) in the 90 K range which surpassed the so called technological and psychological temperature barrier of 77 K, the boiling point of liquid nitrogen, and made a new leap in this field. In strong contrast to what is observed in the La-(Ba,Sr)-Cu-O, pressure has only a slight effect on T_c [54]. Subsequently, the phase was identified [55-58] as an ordered, defect perovskite structure with composition $YBa_2Cu_3O_{7-\delta}$ (Y-Ba-Cu-O). Further,

crystal chemistry [43]. The T_c achieved in the material class of transition metal compounds, with A-15 structure for films of Nb_3Ge (T_c~23.2 K) in 1973 by Gavaler [44], has remained as the highest limit until 1986.

An avalanche of research activities has resulted from the recent discovery of possible high-T_c superconductivity (HTSC) in the multiphase mixtures with nominal composition $Ba_XLa_{5-X}Cu_5O_{5(3-Y)}$ at ~30 K by Bednorz and Müller [45] in 1986. Subsequent studies [46-49] confirmed that HTSC indeed exists in this system. Takagi et al. [50] further attributed the superconductivity in $La_{1.8}Ba_{0.2}CuO_4$ to the K_2NiF_4 phase. Substitution of Sr for Ba has produced ~40 K superconductivity [48,51,52]. Pressure was found to enhance the T_c of the La-Ba-Cu-O [48] at a rate greater than 10^{-3} K bar^{-1}. This unusually large pressure effect on T_c has led to suggestions that the HTSC in the La-(Ba,Sr)-Cu-O systems may be associated with interfacial effects arising from mixed phases; strong superconducting interactions due to the mixed valence states; or an yet unidentified phase.

In 1987, Wu et al. [53] found a new mixed phase Y-Ba-Cu-O compound at ambient pressure with the onset T_c (T_{co}) in the 90 K range which surpassed the so called technological and psychological temperature barrier of 77 K, the boiling point of liquid nitrogen, and made a new leap in this field. In strong contrast to what is observed in the La-(Ba,Sr)-Cu-O, pressure has only a slight effect on T_c [54]. Subsequently, the phase was identified [55-58] as an ordered, defect perovskite structure with composition $YBa_2Cu_3O_{7-\delta}$ (Y-Ba-Cu-O). Further,

superconductivity was achieved in $RA_2Cu_3O_{7-\delta}$ (R=rare earth elements except Ce,Pr, and Tb and A=Ba or Sr) [59-62] and in $YBa_2Cu_4O_8$ and $Y_2Ba_4Cu_7O_{15}$ systems [63,64].

In 1988, Maeda et al. [65] reported HTSC in the Bi-Sr-Ca-Cu-O system. Several attempts [66-72] have been made to obtain the pure 110 K- phase $Bi_2Sr_2Ca_2Cu_3O_{10}$(2223) without the presence of the 85 K- phase $Bi_2Sr_2CaCu_2O_8$ (2212) in this system. In the same year, Sheng and Hermann [73] reported superconductivity at 85-100 K in the Tl-Ba-Ca-Cu-O. Soon a much higher T_c (~125 K) has been reported [74-77] in the $Tl_2Ba_2Ca_2Cu_3O_{10}$ (2223 phase). Superconductivity has also been observed in other systems such as Nd-(Ce,Th)-Cu-O [78], $Ba_{1-X}K_XBiO_{3-Y}$ [79,80], A_3C_{60} (A=alkali metals) [81-85], $(Tl_{0.5}Hg_{0.5})Sr_2(Ca_{1-X}Y_X)Cu_2O_{7-\delta}$ (X=0.3) [86], $HgBa_2CuO_{4+\delta}$ [87], $HgBa_2Ca_2Cu_3O_{8+Y}$ [88], etc.

There have been many [89-94] reports of superconductivity at temperatures significantly higher than 125 K. A large number of these results are clearly due to experimental artifacts. Results which appear to be genuine, are difficult to verify, because the superconducting component is very small and unstable. If there is indeed a direct correlation between instability and the high-T_c, one might well expect that as one continues to raise the T_c the instabilities will become so pronounced that exceptional synthesis procedures will be required to produce reasonable superconducting fractions of these phases [95]. This is a considerable challenge for those attempting to raise the T_c. There are ~35 chemically or structurally unique copper oxide superconductors known to date. Although the theory of solid-sate

chemistry guides the choice of elements that might be combined to make new compounds, the materials are so complex that no theory can yet reliably predict the behavior of the new materials. The trick is to employ chemistry, intuition, and luck to find just the right combination of elements to drive the T_c even higher. Figure 1.1 shows the increase in the T_c with time since the discovery of superconductivity. Some of the basic composition of cuprate superconductors and their variants are presented in Table 1.1. Seven years of intensive research following the discovery of HTSC has produced over 20,000 publications. An overview of all physical properties is thus beyond the scope of this work, so focus on a few topics that are widely perceived to hold the key to understanding these fascinating compounds are discussed below.

1.2.2 The Structure

(1) $La_{2-x}A_xCuO_4$ (A = Ba, Ca, Sr) SYSTEM

The end member compound La_2CuO_4 exists in the tetragonal K_2NiF_4 structure [96]. The coordination polyhedra of La and Cu combine in a way that allows 3D space to be filled in a highly 2D manner. As a result, the planes of Cu and O interspace the inert double layer of La and O. La_2CuO_4 itself is not a superconductor but a semiconductor [97], because the remaining unpaired electrons on neighboring Cu atoms interact with one another and align antiferromagnetically. This pins the electrons to the crystal lattice, eliminating the possibility of superconductivity. The T_N (~ 240 K) which depends sensitively on the O content of La_2CuO_4, decreases with the introduction of

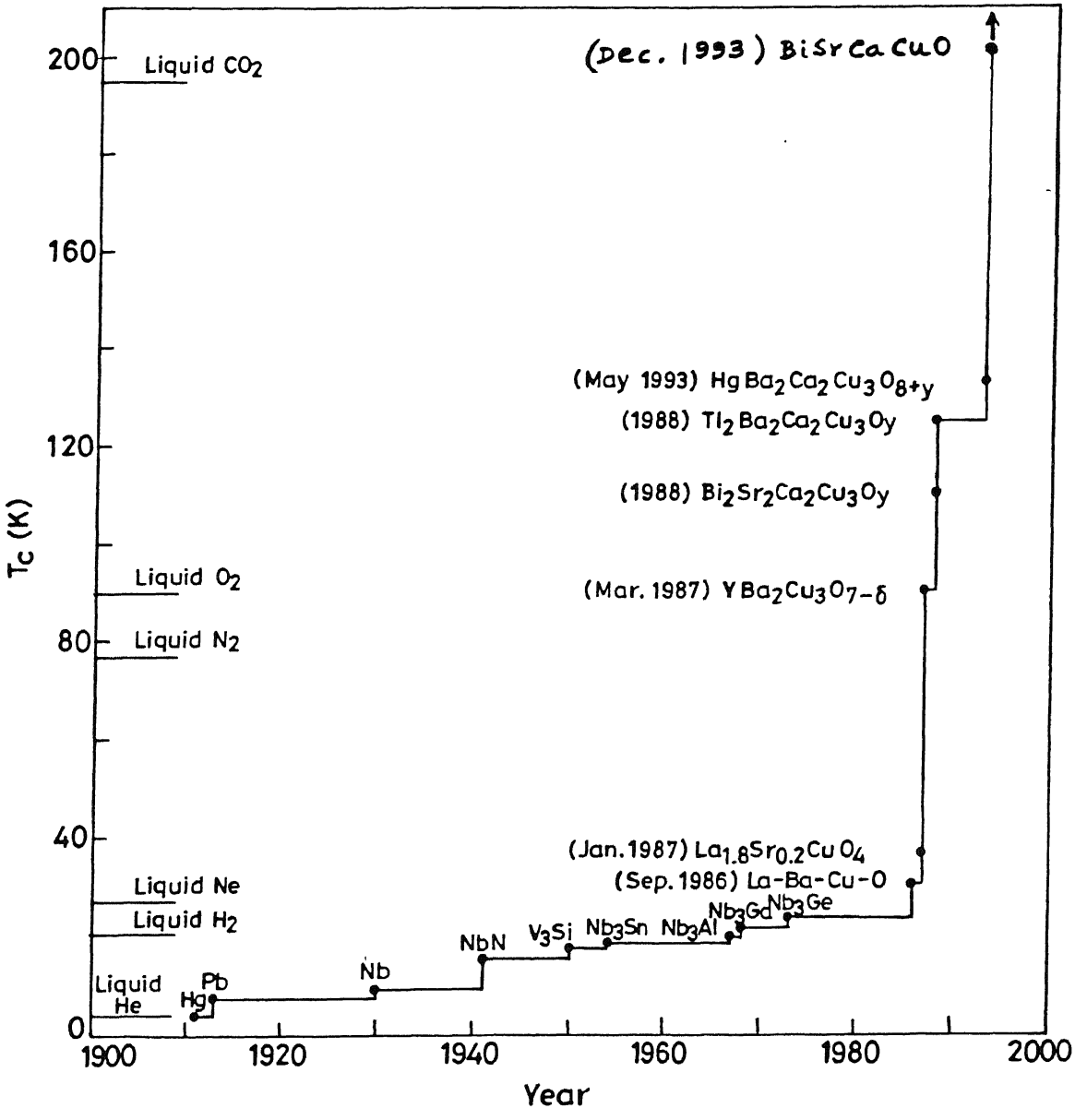

Fig. 1.1 Increase in the T_c with time since the discovery of superconductivity.

Table. 1.1. Basic composition of copper oxide superconductors and some of their variations.

parent structure	substitutions	T_c (K)	[Ref.]
$La_{2-X}Ba_XCuO_4$	Ca or Sr	20-40	[45,107-109]
$YBa_2Cu_3O_7$	La, Nd, Sm, Eu, Gd,Dy	85-95	[59-62]
	Ho, Er, Tm, Yb,or Lu;		
	Cu_4O_8 or Cu_7O_{15}	80-95	[63,64]
$(Bi,Pb)_2Sr_2CuO_6$	$CaCu_2O_8$ or $Ca_2Cu_3O_{10}$	10-110	[65-72, 120-123]
$Tl_2Ba_2CuO_6$	$CaCu_2O_8$ or $Ca_2Cu_3O_{10}$	80-125	[113-119]
$TlBa_2Cu_2O_5$	$CaCu_2O_7$, $Ca_2Cu_3O_9$	10-122	[113-119]
	$Ca_3Cu_4O_{11}$, or $Sr_2Cu_2O_7$		
$Tl_{0.5}Pb_{0.5}Sr_2CaCu_2O_7$	$Ca_2Cu_3O_9$	80-125	[118]
$(Tl,Bi)Sr_2Ca_{1-X}Y_XCu_2O_7$		80-100	[119]
$Pb_2Sr_2Ca_{1-X}Y_XCu_3O_8$		45-80	[125]
$Pb_{0.5}(Ca,Sr)_{2.5}Y_{1-X}Ca_XCu_2O_7$		50-80	[126]
$Nd_{2-X}Ce_XCuO_{4-Y}$	Pr, Sm, Th, or Eu	10-25	[78]
$Ba_{1-X}K_XBiO_Y$		25	[79,80]
A_3C_{60}	Na, K, Rb, or Cs	18-33	[81-85]
$YBa_2Cu_3O_XF_Y$		155-230 ?	[89-94]
$HgBa_2CuO_{4+\delta}$		~94	[87]
$HgBa_2Ca_2Cu_3O_{8+Y}$		~133	[88]
BiSrCaCuO		200	[89]

mobile holes into the CuO_2 sheets [98]. Thus, superconductivity has been evidenced in several $La_2CuO_{4+\delta}$ samples of a bulk nature or filamentary type [99-105]. Superconductivity is not La-defect-assisted as deduced from the off-stoichiometry effects on the Cu sites [99] as well as on the La sites [101]. Bulk superconductivity could appear when oxygenation suppresses the oxygen vacancies [99]. Bulk superconductors $La_2CuO_{4+\delta}$ have a stoichiometry of $\delta = 0.13$ and the excess charged O is introduced in the oxygenated samples as O_2^- [104]. Bulk superconductivity and antiferromagnetic (AFM) order have been found to coexist in several undoped $La_2CuO_{4+\delta}$ samples [106].

Charge neutrality is maintained in $La_{2-X}A_XCuO_4$ (A=Ba, Ca, or Sr) if one Cu atom is oxidized from 2+ to 3+ for every A atom substituted for a La atom. When the Cu atoms reach a critical valence (~2.2+), antiferromagnetism disappears and superconductivity appears [45, 107-109]. The $La_{2-X}Ba_XCuO_4$ (T_c~35 K for X=0.15) has a tetragonal structure in which Cu is coordinated to six O atoms that form the corners of an elongated octahedron. Because the coordination number increases roughly with the size of the atom, the La atoms, which are larger than Cu atoms, are coordinated to nine O atoms. The Ba atoms, which are similar in size to the La atoms, are also coordinated to nine O atoms. Within the crystal lattice, therefore, Ba atoms can occupy the same sites as the La atoms, and, in fact, they are distributed at random through the crystal lattice. Such a distribution of atoms in fixed crystallographic sites is known as a solid solution. Solid solution is generally formed if the sizes of the dopant and the host ions are relatively close and the

types of chemical bonds formed are similar. Thus, Ba, Ca, or Sr can form solid solutions in La_2CuO_4 by replacing some of the La leading to interesting results. For instance, when 10 at.% Sr is substituted, the result is $La_{1.8}Sr_{0.2}CuO_4$, where the Cu valence is 2.2+. The T_c of this compound is ~40 K, the highest among the solid solutions based on La_2CuO_4.

(2) $YBa_2Cu_3O_{7-\delta}$ SYSTEM

The structure [96] (Fig.1.2) of $YBa_2Cu_3O_{7-\delta}$ is similar to that of $(La, Sr)_2\ CuO_4$ in several respects: both are open, layered structures, with some similarity to perovskite in the sense that Cu could be octahedrally coordinated, i.e., in a formally filled structure $YBa_2Cu_3O_9$. The most obvious differences are the tripling of the unit cell of the latter along the c-axis, with two inequivalent Cu planes, labelled Cu(1) and Cu(2), sandwiched between Ba planes for Cu(1) and Ba and Y planes for Cu(2), and the removal of O from the Y plane and the Cu(1) plane. The small Y 3+ ions are always bonded to eight O ions; the large Ba 2+ ions to ten O ions. The chain copper site, Cu(1), primarily consists of a mixture of twofold {O(1)-Cu(1)-O(1)} dumbells and fourfold {Cu(1)-2 O(1)-2 O(4)} squares coordinations as a function of stoichiometry, with the sticks having shorter Cu(1)-O(1) bondlengths than the diamonds. The plane coppers, Cu(2) are coordinated to four Oxygen in the plane {two O(2)'s and two O(3)'s} and one Oxygen the apex of a pyramid, O(1), which it shares with Cu(1). Thus the 3D space is filled with a combination of 1D chains and 2D pyramidal planes.

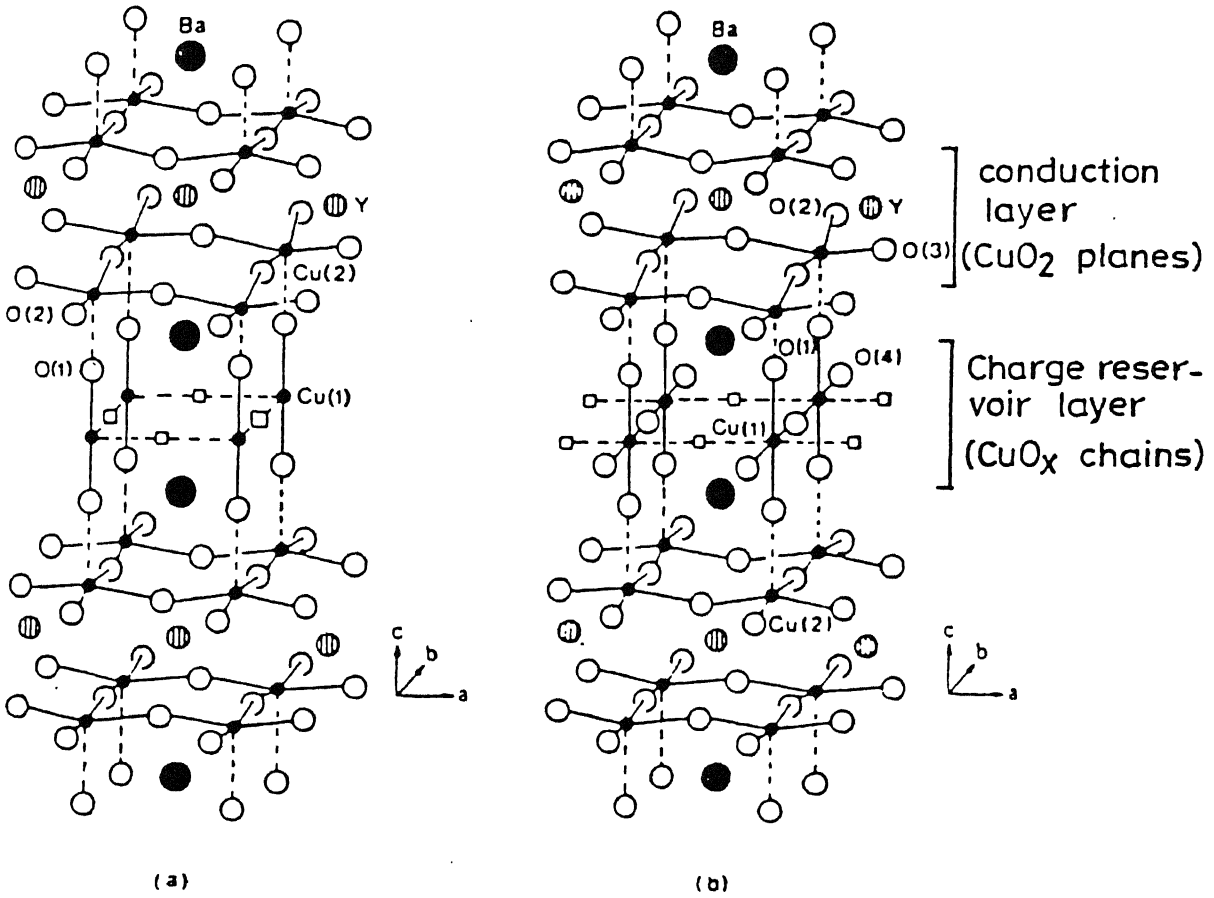

Fig. 1.2 Structures for (a) tetragonal $YBa_2Cu_3O_6$ and (b) ideal, orthorhombic $YBa_2Cu_3O_7$. (Adapted from ref. 96.)

When the O content is reduced from 7 to 6, the insulator $YBa_2Cu_3O_6$ with tetragonal structure is formed. $YBa_2Cu_3O_6$ being AFM with a well-defined T_N (~450 K) shows a clear anisotropic Cu^{2+} EPR signal. Oxygen is removed from one crystallographic site only, thereby transforming the Cu-O diamonds into sticks. The sticks are a stable coordination geometry for Cu in the 1+ state. The decrease in O content does not directly affect the Cu-O pyramids, but, as counting the charges reveals, the Cu atoms associated with the pyramids are now in the 2+ state. In this configuration the electrons are localized by the effect of antiferromagnetism. As the O content of $YBa_2Cu_3O_6$ is increased, O is added directly into the bonding environment of the sticks, and tries to form as many Cu-O diamonds as possible. At 6.5 O atoms, the resulting compound, $YBa_2Cu_3O_{6.5}$, pulls enough electrons away from the Cu atoms in the Cu-O pyramids to yield superconductivity (T_c ~60 K). This compound has a distinct crystal structure in which chains of diamonds and sticks form an ordered array. When the full chain structure is obtained, the T_c jumps to 90 K. It was shown [110] that there is a distinct step-like increase in the c-axis length and cell volume near a stoichiometry of 6.4 Oxygen per formula unit; it was also shown [111,112] that the c-axis step and the orthorhombic to tetragonal transition do not necessarily occur at the same composition.

A model that arises from the common structural features of the Cu-O superconductors is that the superconductivity occurs predominantly in the CuO_2 planes, while the other (intercalated) layers provide, in some fashion, carriers or the coupling mechanism necessary for superconductivity [110]. Thus holes are

created in the conduction layer when electrons are transformed to the charge reservoir layer. A precise measure of changes in the oxidation state of the plane Cu atom can be obtained from bond valence sum. For strongly hybridized systems such as superconducting copper oxides, the bond valence sums for the Cu atoms do not represent an ionic but rather covalent bond. The charge associated with chain Cu decreases in a linear manner with decreasing O content over the whole stoichiometry range. In contrast, the charge associated with the plane Cu displays a remarkable nonlinear variation with O stoichiometry. The total positive charge decreases by about 0.08 e per plane Cu as $(7-\delta)$ decreases from 7 to 6.

The bond valence sum shows [110] the same two plateau behavior as does T_c versus $(7-\delta)$. Thus the change from a 90 K to a 60 K superconductor is due to decrease in positive charge associated with the plane Cu(2) layer of approximately 0.03 e/Cu, near $(7-\delta)=6.6$ a reduction of the "hole" concentration. The transition from 60 K superconductor to semiconductor near $(7-\delta)=6.45$ involves an abrupt decrease in positive charge in the plane Cu(2) layer of approximately 0.05 e/Cu. It is also shown that the positive charge associated with the addition of O is accompanied entirely in the chain coppers. Apparently, no holes are doped into the CuO_2 layer until the superconducting-state appears at $(7-\delta)=6.45$. Therefore, any observed variation of T_N with composition in the tetragonal phase must be a secondary effect due for instance to increased electronic coupling between the plane coppers via the changing chain coppers.

(3) THALLIUM CUPRATES

The structures of the $TlBa_2Ca_{n-1}Cu_nO_{2n+3}$ and the $Tl_2Ba_2Ca_{n-1}Cu_nO_{2n+4}$ families are shown [113] in Fig. 1.3. Phases with n=1-5 have been identified [114-119]. These structures may be visualized as an intergrowth of superconductively active $Ca_{n-1}(CuO_2)_n$ layers and inactive BaO-TlO-BaO or BaO-TlO-TlO-BaO layers. Since only the outer CuO_2 sheets of the active layers have five-fold-coordinated Cu, one may anticipate that only these outer CuO_2 sheets of an active layer become oxidized and superconductive. This expectation finds support from the observed variation of the maximum T_c versus n, the number of CuO_2 sheets in an active layer. A maximum T_c=125 K is found for n=3; T_c decreases with increasing n>3. For n=2, a T_c=100 K is obtained. Communication across one Ca-CuO_2-Ca layer is probably maintained, but it apparently decreases with increasing separation of the outer CuO_2 sheets of the active layer [113]. Further superconductivity (T_c=80-125 K) has been observed in $Tl_{0.5}Pb_{0.5}Sr_2CaCu_2O_7$ [118] and $(Tl,Bi)Sr_2Ca_{1-X}Y_XCu_2O_7$ [119].

(4) BISMUTH CUPRATES

Although rather similar to the Tl-Cu the crystal chemistry of the Bi cuprates is less rich than that of Tl. Only two series of oxides have indeed been synthesized, both characterized by triple rock salt-type layers built up from Bi bilayers sandwiched by SrO layers. Thus, the existence of Bi bilayers seems absolutely necessary to stabilize such structure. The $Bi_2Sr_2Ca_{n-1}Cu_nO_{2n-4+X}$ family has an intergrowth structure. Similar to the Tl_2 family (Fig. 1.3), but with Bi substituted for

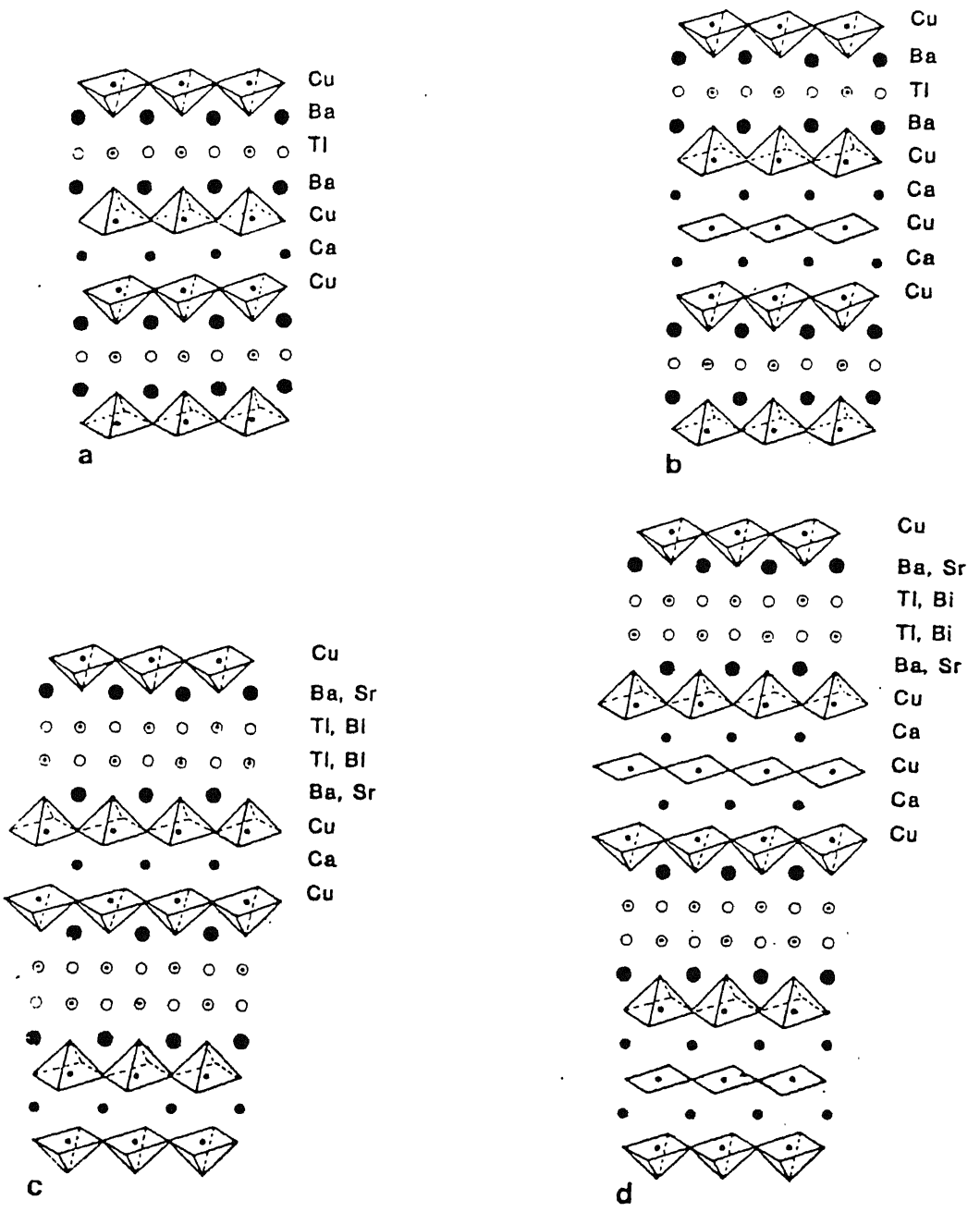

Fig. 1.3 Schematized structures of (a) "1212" oxides, e.g., $TlBa_2CaCu_2O_7$ ($m = 2, n = 2$); (b) "1223" oxides, e.g., $TlBa_2Ca_2Cu_3O_{10}$ ($m = 3, n = 2$); (c) "2212" oxides, e.g., $Tl_2Ba_2CaCu_2O_8$ or $Bi_2Sr_2CaCu_2O_8$ ($m = 2, n = 3$); and (d) "2223" oxides, e.g., $Tl_2Ba_2Ca_2Cu_3O_{10}$ or $Bi_2Sr_2Ca_2Cu_3O_{10}$ ($m = 3, n = 3$). (Adapted from ref. 113.)

Tl and, Sr for Ba. The 85 K superconductor $Bi_2Sr_2CaCu_2O_8$ [65,113,120,121] has its structure (Fig. 1.3) similar to that of the $Tl_2Ba_2CaCu_2O_8$, the Bi bilayers replacing the Tl bilayers. The 110 K superconductor $Bi_2Sr_2Ca_2Cu_3O_{10}$ detected for the first time by Tarascon et al. [122] is difficult to synthesize as a pure phase [66-72,122,123].

(5) Nd-(Ce,Th)-Cu-O SYSTEM

Tokura et al. [78] discovered the first n-type Nd-(Ce,Th)-Cu-O superconductors. The structure of the parent compound Nd_2CuO_4 [96] is similar to La_2CuO_4. But whereas La prefers nine O neighbors, the smaller Nd ion is usually coordinated to eight O atoms. In the compound Nd_2CuO_4 the O atoms form a square prism around the Nd atoms. As a result, the Cu atoms are coordinated to four O atoms in a square planar geometry. In the superconductor based on Nd_2CuO_4, some of the Nd atoms are replaced by Ce or Th, forming solid solutions $Nd_{2-X}Ce_XCuO_4$ and $Nd_{2-X}Th_XCuO_4$. When X equals 0.17, these materials reach their highest T_c = 25 K.

(6) LEAD AND MERCURY CUPRATES

$BaPbYSrCu_3O_8$ [124] is the only *pure lead* cuprate with triple Cu layers, but unfortunately it is not a superconductor. The superconductor $Pb_2Sr_2Ca_{1-X}Y_XCu_3O_8$ discovered by Cava et al. [125] is formed of Cu bilayers. Its structure consists of double pyramidal Cu layers alternatively with single Cu layers. The resistive transition is very broad with a T_{co}=80 K and T_{CRO}=46 K. The substitution of Bi for Pb allows the superconducting

properties of this phase to be considerably improved. The oxide $Pb_{0.5}Sr_{2.5}Y_{1-X}Ca_XCu_2O_{7-\delta}$ [126] is the only pure lead cuprate which exhibits double Cu layers. Its structure belongs indeed to the 1212 type already described for $TlA_2CaCu_2O_7$ (A=Ba, Sr) (Fig.1.3). Mixed Pb-Sr monolayers $[Pb_{0.5}Sr_{0.5}O]_\infty$ replace the $[TlO]_\infty$ monolayers in the double rock salt slabs. Again the resistive transition is very broad.

More recently, HTSC has been observed in Hg-based systems [86-88]. $T_c \simeq 90$-94 K has been reported in $(Tl_{0.5}Hg_{0.5})Sr_2(Ca_{1-X}Y_X)Cu_2O_{7-\delta}$ (X=0.3) [86] and in $HgBa_2CuO_{4+\delta}$ [87]. $HgBa_2CuO_{4+\delta}$ (Hg-1201) is the first member of $HgBa_2R_{n-1}Cu_nO_{2n+2+\delta}$ series with only one CuO_2 layer per unit cell. The availability of a material with high-T_c but only a single metal oxide (HgO) layer may be important for technological applications, as it seems that a smaller spacing between CuO_2 planes leads to better superconducting properties in a magnetic field. The structure consists of CuO_2-BaO-HgO_δ-BaO-CuO_2 layers. This is similar to that of Tl-1201 (T_c<10K). HTSC (T_c=133 K) has also been observed in $HgBa_2Ca_2Cu_3O_{8+Y}$ [88]. This consists of three CuO_2 layers per unit cell. More recently, an artificial cuprate compound belonging to the BiSrCaCuO family with eight adjacent CuO_2 layers in each building block was deposited on a single crystal of $SrTiO_3$ by sequentially imposed layer epitaxy. This compound undergoes a five order of magnitude resistivity drop with an onset near 280 K and an offset at 250 K. Electrical resistance dropped by a factor of 1,00,000 as it was cooled from 280 K to 250 K. It offered no resistance (within experimental error) to a small current at 235 K. It exhibit a diamagnetic

variation of susceptibility and magnetization below 290 K. Additional observed features, such as strongly nonlinear conductivity, suggest superconductivity as a plausible explanation of the properties of this compound. After several weeks of the preparation of the sample, it was structurally stable with a resistive transition over 200 K [89].

(7) COPPERLESS SYSTEMS

The discovery [79,80] of superconductivity in $Ba_{1-X}K_XBiO_{3-Y}$ (T_c~25 K) which does not have Cu has dramatically broadened and extended the scope. The superconducting phase ($0.37<X<0.5$) forms a cubic perovskite crystal structure [127] which shows none of the planar structures observed in the other HTSCs. $Ba_{1-X}K_XBiO_3$ is nonmagnetic [79] while the other related HTSCs, in their parent nonsuperconducting phases, display antiferromagnetism. Hall effect measurements [128] in $Ba_{1-X}K_XBiO_3$ indicate that the carriers are electrons, whereas in cuprates, with the exception of $R_{2-X}Ce_XCuO_4$ (R=Pr, Nd), the carriers are holes.

Another interesting discovery is, when intercalated with alkali metal atoms, to form the fullerides of the formula A_3C_{60} (A=alkali metals), the highly symmetric soccerball-shaped truncated icosahedral C_{60} (buckminsterfullerene) molecule becomes superconducting [81-85] at unprecedentedly high temperatures (T_c=18-33 K) for a molecular solid. For many purposes of solid-state chemistry and physics, the C_{60} molecule is a single atom-like entity. For example, its shape and size seem to be virtually identical [83] in the vapor phase, in solid C_{60} and in solid K_3C_{60}. Buckminsterfullerene cage may in fact behave much

like an atom with properties that are beyond the range of the usual atoms. The fullerides have been heralded as the first examples of three-dimensional organic superconductors, which would be important not only because of the relatively high value of T_c but also because three-dimensional materials are usually easier to understand and to exploit. The high-T_c copper oxides are highly anisotropic, quasi-two-dimensional materials, and the previously known organic superconductors are quasi- one-dimensional. Solid C_{60} forms a face-centered cubic (f.c.c.) lattice with 10 A° intercluster separation [84]. The calculated C_{60} diameter is 7.1 A°. K_3C_{60} has a f.c.c. structure [83] derived from that of C_{60} by incorporating potassium ions into all of the octahedral and tetrahedral interstices of the host lattice. The C_{60} solid is a weakly bonded material; but when it is intercalated with alkali atoms, electrons are transferred to the C_{60} cage, resulting in an ionically bonded solid. There have been indications that C_{60} has the ability to accept several electrons.

1.2.3 The Normal-State

(1) ELECTRICAL RESISTIVITY

The fundamental difficulty in understanding the HTSC arises from the fact that the exact nature of the metallic phase in the normal-state is not known. Currently much work is focused on whether the metallic cuprates are like ordinary metals such as Al or Pb, and on those unusual properties that are unique attributes of the metallic cuprates. More important is the fact that the understanding of these materials is closely tied to the *quality*

of experimental data, which in turn depends on sample quality [129]. As one might expect from the crystal structure, the electrical properties of the layered cuprates are highly anisotropic. The ρ of $Bi_2Sr_2CaCu_2O_8$, for example, can be up to 10^4 times larger in the c-direction than that in the a-b plane [130]. The degree of anisotropy is specific to a compound family and reflects how effectively the charge reservoir layers block the coherent motion of electrons between the CuO_2 planes. The in-plane ρ_{ab} behaves like that of a metal, while the perpendicular ρ_c is reminiscent of semiconductor behavior. A possible exception is found in $YBa_2Cu_3O_7$, which is the least anisotropic material. The semiconductor-like $\rho_c(T)$ can be several orders of magnitude greater than the maximum metallic value [131-133] ($\rho_c/\rho_{ab} \simeq 30\text{-}100$) at room-temperature; in some crystals of $YBa_2Cu_3O_7$, ρ_c has a metallic character [134-136], although it is still more than 10 times larger than ρ_{ab}. The value of ρ_{ab} varies from 120 to 170 $\mu\Omega$ cm at 295 K [132] and decreases to 50 $\mu\Omega$ cm at T_c. The resistivity in c-direction is ~10 mΩ cm and is weakly T dependent, displaying a shallow mimimum near 150 K.

The ρ_{ab} along the CuO_2 planes is almost similar for the various optimized compounds and depends nearly linearly on T over a wide temperature range [137-139]. The difference may be a combination of impurities (indicating oxygen vacancies) and degree of twinning in the a-b plane. This experiment is often taken to provide strong evidence against a Fermi-liquid picture. Phonons can give rise to this kind of T dependence provided $T_c > \omega_D/4$. For T_c above 50 K this inequality may be satisfied for a reasonable phonon spectrum. What is more persuasive is the

observation that in a particular cuprate [138], viz., $Bi_{2+X}Sr_{2-Y}Cu\ O_{6+Z}$ with T_c ~10 K, the ρ appears to be close to linear over the entire normal-state regime. This indicates that phonons are not the sole source of the linear T dependence. Even if electronic contribution to ρ is dominant, a crossover from T^5 to T behavior arising from a phonon *background* contribution should be evident somewhere below 50 K. That there is no deviation from linearity and thus no clear evidence for any additional (i.e., non-electronic) component of ρ is somewhat surprising and needs to be addressed further. It is difficult to believe that phonons play no role whatsoever in determining the T dependence of the ρ in the cuprates.

The qualitative difference in the ρ_{ab} and ρ_c suggests that two different conduction mechanisms may be operating in the two directions. While the a-b plane shows metallic resistivity, the origin of the c-axis resistivity is still controversial. The extrapolated residual resistivity to 0 K is quite small [140,141]. The high value of the slope $A=d\rho/dT$, and $B\simeq 0$ rules out the electron-phonon scattering mechanism as a dominant source of resistance. The striking similarity of the $\rho(T)$ curves for optimized compositions is evidence that the common CuO_2 planes are the electronically active building blocks in otherwise very different crystal structures. The mean-free path at 100 K is estimated to be 100-200 A° for Y-Ba-Cu-O [129], which is long compared to the lattice parameter of 3.8 A°. The electrons are thus only weakly scattered, and these metals are considered *clean*. Furthermore, the slopes $d\rho/dT$ fall in a narrow range near 0.5 $\mu\Omega$cm/K. The reported [142] dT_{co}/dp is small in

$YBa_2Cu_3O_{7-\delta}$, but is very large and positive in $La_{2-X}(Ba,Sr)_XCuO_4$. For X near 0.15, the observed values range between 0.1 and 0.3 K/kbar, whereas for A15 compounds typically $dT_{co}/dp \leq 10^{-2}$ K/kbar. The observed rounding off of the resistivity-temperature, $\rho(T)$, curve near and above the transition temperature (T_c) is that, the thermodynamic fluctuations can produce short-lived cooper-pairs, leading to an apparent increase in the conductivity called paraconductivity. This paraconductivity analysis give information about the dimentionality of the system.

(2) A.C. CONDUCTIVITY

One of the hallmarks of hopping conductivity in systems with localized electron states is a frequency (ω) dependent A.C. conductivity. The typical behavior seen in disordered semiconductors is $\sigma(\omega) \propto \omega^s (s \sim 0.8)$ where the ω dependence develops in the $\omega \sim 10^6$-10^7 Hz range at room-temperature and well below that at lower temperatures. Both metals and superconductors also show ω dependent A.C. conductivity [143] but at much higher ω . For metals the characteristic energy is $\omega\tau \sim 1$ (or $\omega \sim 10^{14}$ Hz) while for semiconductors it is $\hbar\omega \sim 2\varepsilon_g$. Measurements on single crystal Eu_2CuO_4 showed a ω dependent complex σ in the GHz frequency range [144]. Furthermore, it was found that an insulating, high-temperature quenched phase of polycrystalline Y-Ba-Cu-O exhibited a large dielectric constant [145-147]. The polarizability of the material could imply a ω dependent A.C. conductivity.

(3) OPTICAL CONDUCTIVITY

The unusual character of the charge dynamics of the cuprate is best seen by going beyond the T dependence of the D.C. conductivity $\sigma_o(T)=1/\rho_{ab}(T)$ to the optically measured frequency-dependent $\sigma(\omega,T)$ [143,148]. At first sight the low frequency parts of the rapidly decreasing $\sigma(\omega)$ curves are reminiscent of charge carriers being scattered at a ω independent rate of $1/\tau_o$, which increases with T as observed in simple metals. However, the simplest scattering form of this constant - τ_o model- a Lorentzian with a width $\hbar/\tau_o$ of approximately k_BT - deviates significantly from the measured $\sigma(\omega)$ curves. A consistent description of the observed $\sigma(\omega)$, within a model of carriers scattering from excitations (such as phonons), requires that the scattering rate depend on both T and ω.

(4) THERMOPOWER

In thermopower (S) measurements it seems that the phonon drag effects contribute through the normal-state because of the relatively high T_c's. These may partially obscure the characteristic features arising from the electronic contributions. S is positive and has a maximum at a characteristic temperature of 100-200 K. This is observed in ceramic samples of $La_{1.8}Ba_{0.2}CuO_4$ [149], $La_{1.85}Sr_{0.15}CuO_4$ [150], and Tl-Ca-Ba-Cu-O [151]. This behavior is in contrast to a linear T dependence which is expected for purely elastic scattering. While this is so, the situation in the Y-Ba-Cu-O family is less clear.

(5) HALL EFFECT

In a simple metal, the Hall effect is a measure of the carrier concentration and is only weakly T dependent. The observed strong T dependence of the inverse of the Hall coefficient of single crystals of Y-Ba-Cu-O [152] over a wide temperature range suggests that it is an intrinsic property of the cuprates. Strong T dependence of the Hall effect is observed in ordinary metals only at temperatures below a fraction (a fifth to a half) of the Debye temperature θ_D, which is the characteristic energy scale for phonons. In the so-called 123 compounds, θ_D is 400-450 K, which makes it unlikely that the observed strong T dependence is caused by electron-phonon scattering. Invoking more than one type of carriers (such as heavy and light electrons or holes and electrons described by different bands) to explain $\rho(T)$ and $R_H(T)$, would require a fortuitous and unlikely combination of temperature-dependent carrier concentrations and mobilities. Also the observed carrier concentration of the charge carriers is small ($\sim 10^{21}$ cm^{-3}). Recently Rao et al. [153] observed that the T_c becomes maximum when n_h is in the 0.12-0.15 range in cuprates containing a single Cu-O layer and around 0.2 in cuprates containing two Cu-O layers.

(6) MAGNETIC PROPERTIES

The magnetic moments of the nearly filled Cu^{2+} $3d^9$ shell form a spin 1/2 Heisenberg system on a 2D square lattice. Strong AFM superexchange J provides the dominant interactions between neighboring Cu atoms (J~10-130 meV). A weak interlayer coupling leads to long-range 3D AFM ordering [154] at a temperature much

lower than the in-plane exchange energy. A gradual change of the magnetic response is observed upon the introduction of carriers. The static susceptibility, χ, is only weakly T dependent between T_c and 400 K for optimized superconductors, and it increases systematically with the number of closely spaced CuO_2 layers, each layer contributing 1.2-1.5 X 10^{-3} emu/mole to the spin susceptibility [155]. The NMR Knight shift [156-158], which in essence is a local susceptibility probe, exhibits the same T dependence at the Cu and the O sites, and both closely follow the static, macroscopically measured χ. Thus a single-species spin-system description seems appropriate. The χ, NMR Knight shift and the nuclear relaxation rates , $T_1^{-1}(T)$ [159,160], decrease upon cooling below room-temperature. It has been suggested that these reductions indicate a suppression of low-frequency spin excitations due to the formation of a pseudogap in the excitation spectrum, reminiscent of the spin gaps in linear chains of s=1 antiferromagnets.

(7) THERMAL CONDUCTIVITY

Thermal conductivity, K(T), in the normal-state is observed to be nearly T independent. Since the conductivity, σ, is proportional to T^{-1}, the Wiedemann-Franz law is obeyed if one assume that the observed K(T)=constant is electronic. Wiedemann-Franz law holds if the scattering process for σ(T) and K(T) are the same and specific-heat varies linearly with temperature.

(8) RAMAN SCATTERING

Raman scattering experiments have revealed the existence of electronic excitations [161] that may be closely linked to the scattering that leads to $\sigma(\omega,T)$. Contrary to our experience with conventional metals, where light is scattered by particle-hole excitations up to frequencies of order 50 cm^{-1}, a broad continuum of electronic excitations is observed in the metallic cuprates [162]. It remains to be determined whether the broad Raman scattering, which is highly characteristic of the cuprates, is due to spin or charge excitations or both. The transport and light-scattering experiments suggest that there is no scale for low-energy excitations other than the temperature itself [163].

(9) ELECTRONIC STATES AND FERMI SURFACE

Bonding between nominal Cu^{2+} and O^{2-} has both ionic and covalent character and involves the Cu 3d and O 2p orbitals. The origin of the covalency is ultimately rooted in the proximity in energy of the 3d and 2p levels [164]. Thus, the highest occupied electronic states - the ones near E_F - have both 3d and 2p character, with a predominance of the latter. The measured energy bands confirm the presence of a Fermi surface [165,166]. The oscillatory component of the magnetic susceptibility de Hass-van Alphen (dHvA) effect [167] also confirm the presence of Fermi surface in its normal phase at low temperatures. According to Gor'kov and Kopnin's estimates [168], the Fermi energy E_F is ~0.37 eV in an yttrium crystal, and ~0.34 eV in La. The lifetime broadening of the electronic states at energy E grows like $|E-E_F|^n$, with the best value of n being approximately 1.

(10) ISOTOPE SHIFT

A small oxygen isotope shift had been found in Y-Ba-Cu-O [169]. The very small oxygen isotope shift observed in 123 was taken to indicate that pairing of the charge carriers in this system is not phonon mediated. However, the substantial oxygen isotope shift obtained in the partial replacement of Y by Pr and Ca doped samples [170] is consistent [171, 172] with pairing by high-frequency phonons, suggesting that modes involving oxygen motion are important in the mechanism responsible for high-T_c superconductivity.

It is widely accepted that the superconducting pairs are located in the conducting CuO_2 planes [173,174]. If the coupling which causes pairing is also located there, then one might expect the plane sites to give the oxygen isotope effect. A recent measurement [175] of T_c of the site-selectively (^{18}O in the CuO_2 plane sites, and primarily ^{16}O in the optical and chain sites) substituted samples is higher than that of the ^{16}O control samples by 0.10-0.14 K, in contrast to the decrease in T_c of 0.20-0.23 K for complete ^{18}O substitution at all sites. This result indicate that the phonon-mediated contribution to the pairing mechanism in $YBa_2Cu_3O_7$ involves the optical sites (O1) and not just the CuO_2 plane sites (O2, O3).

1.2.4 The Superconducting-State

Cuprate superconductivity involves the pairing of quasiparticles (electrons), as expressed in an effective charge of $e^*=2e$. For $YBa_2Cu_3O_7$, in the low-temperature limit, one finds $\xi_{ab}=14\pm2$ A°, $\xi_c=2\text{-}3$ A° , $\lambda_{ab}=1400$ A° , and $\lambda_c=7000$ A° [129]. A

quantitative surprise is the high ratio of the zero temperature gap to T_c, $2\Delta(0)/k_BT_c \simeq 8$, obtained through a remarkable series of photoemission experiments [176]. This value is consistent with tunneling measurements [177] when due account is taken of the anisotropy: $2\Delta(0)/k_BT_c \simeq 8$ for momentum in the plane and $2\Delta(0)/k_BT_c \simeq 3.5$ for momentum perpendicular to the plane. They are consistent with reflectivity measurements [178] or the Knight shift measurements [156-158]. For comparison, the values for Nb are λ=350 A° and $\xi \simeq$400 A°. The length scale in the cuprates are rather extreme, and they result from material specific properties. Cuprate superconductors are of extreme type II ($\lambda/\xi \gg 1$) and are in the *clean* limit- that is, ξ (T=0) is much shorter than the electron's mean-free path (100-200 A°) near T_c. Large anisotropy of coherence lengths and energy gaps indicates weak correlation between Cu-O planes in the unit cell. Since the energy gap width that is proportional to k_BT_c and the Fermi energy have comparable values, a substantial part of the charge carriers is involved in superconductivity.

An external magnetic field can penetrate the cuprates to a relatively large depth (λ) because the few carriers are not effective in shielding the field. Within the BCS pairing theory, $\xi_o = \hbar v_F/\pi\Delta(0)$, where v_F is the Fermi velocity and $\Delta(0)$ is the superconducting-gap parameter, which is proportional to T_c. A ξ_o of 15 A° is indeed consistent with V_F=1.1 X 10^7 cm/sec and $2\Delta(0)=6\ k_BT_c$, which are typical parameters for 123 compounds. Given the low electron concentration of less than 1 per CuO_2 and a coherence volume that includes only 5-10 CuO_2 units, one finds fewer than five pairs within one coherence volume. This is

several orders of magnitude smaller than that in a conventional superconductor such as Al, which has more than 10^4 pairs. This leads to pronounced fluctuation effects (perhaps observed in electrical resistivity, magnetic, thermopower measurements, etc.) at the transition to the superconducting-state.

1.2.5 Different Classes of Superconductors

So far, seven classes of electron superconductors, one hole superconductor, and two BCS fluids are identified. They are:

1. Free-electron-like (s-p and lower d-band) metals. These all fit the theory and can be predicted.
2. Strong-coupling, old-fashioned high-T_c materials such as Nb_3Sn and $Pb(Mo_6S_8)$. These seems to have phonons, but they have many unusual properties in both their normal- and superconducting-states.
3. Organic superconductors. Still almost a complete mystery.
4. Heavy-electron superconductors. These are now proven to be BCS-like but anisotropic ; so-called d-wave superconductors, perhaps. No phonon mechanism is proposed.
5. $BaBiO_3$-based superconductors. These have phonons but cannot fit the simple theory because their electron density is too low, Coulomb repulsion seems nearly absent and they have their highest T_c's at dopings where conventional superconductors become normal, that is, at the metal-insulator transition.
6. High-T_c cuprates. In addition to their abnormal T_c's, these materials have very abnormal normal-state properties.
7. A_3C_{60} crystals. Too early to comment.

8. Nd-(Ce,Th)-Cu-O. These are the first hole superconductors. This will put various theories to serious test.

9 & 10. Helium-3 and neutron-star matter. Both of which are paired BCS superfluids.

1.2.6 Towards a Theory

The discovery of HTSCs have raised few important issues.

(A) what is the nature of the normal-state?

(B) what is the nature of the superconducting-state?

(C) what is the mechanism of pairing in these compounds?

One question is whether or not the normal-state of the HTSCs can be described by Fermi-liquid theory. The observation of a Fermi edge [179], along with many band structure-like features in angular resolved photoemission experiments [176] have led to some support for a Fermi-liquid description. On the other hand, as discussed in section 1.2.4 that many of the normal-state properties such as the $\rho(T)$, the thermal conductivity K(T), the optical conductivity $\sigma(\omega)$, the Raman scattering intensity $s(\omega)$, tunneling conductance g(v), the nuclear relaxation rate T_1^{-1} (T), small isotope effect, and the Hall coefficient $R_H(T)$ are all anomalous and are unlike those observed in any other metal or expected for a Fermi-liquid. Also, the superconducting-state in the cuprates is rather un-remarkable: i.e., the major new features are the high-T_c, absence of the *coherence peak* in T_1^{-1} near T_c, and the high value of $2\Delta(0)/k_BT_c \simeq 8$. Thus, the mechanism for superconductivity should follow relatively easily once the much harder problem of the normal-state is worked out [180]. At present no theory can account for all the normal phase data. So

far, it is not possible to calculate with confidence the T_c of a particular model. One do not even know with certainty whether its ground state is that of normal-metal, antiferromagnetic insulator, charge-density- Peierls insulator, or a superconductor. The field of HTSC forces us to unify such concepts as superconductivity, antiferromagnetism, Hubbard subbands, and correlated electron states. One or possibly a small set of closely related approaches will fully explain high-T_c, as BCS did for low T_c.

The main issues cited as responsible for the failure of Fermi-liquid theory are:

(1) The dimensionality D = 2 is low.

(2) The superconducting phase is in close proximity with a long range magnetically ordered AFM phase. Thus, the exchange interactions J in the metal are too strong.

(3) The carrier concentration number is too small.

(4) The normal-state temperatures may be too high; in other words the T_c is simply too high.

(5) The dominant wave vectors **q** and frequencies ω may be high.

(6) The Coulomb interactions themselves may be too strong, so that the adiabatic assumptions implicit in Landau's theory may be incorrect.

(7) The small isotope effect, the frequency dependence of the relaxation rate (which implies a vanishing quasiparticle amplitude), the controversial existence of the energy gap, and the failure of the sum rules for the photoemission data.

Given the concentration of mobile holes in the CuO_2 planes that determines the magnitude of T_c [181,182] and the electronic

structure [164], T_c for these materials has been estimated [183] from the strong-coupling theory (Eliashberg) to be less than 30 K for the electron-phonon coupling constant $\lambda \to \infty$. Thus, having generally agreed upon the fact that the conventional mechanism of pairing via electron-phonon interaction won't do, two principal varieties of models have been developed. They are:

(a) based on magnetic origins (uses the apparent relationship between antiferromagnetism and superconductivity).

(b) based on electronic origins.

There is as yet no consensus on this issue. The following major theories are in the fray:

(1) the *Resonating valence bond* (RVB) theory [184,185] and its various generalizations: Luttinger liquid [186,187]; Gauge field theory [188,189]

(2) the *spin bags* [190,191]

(3) the *almost localized* Fermi-liquids [192-194]

(4) the *almost magnetic* Fermi-liquids [195,196]

(5) the *marginal* Fermi-liquids [197,198]

Also, there are many other theories such as exciton mechanism [199,200], nested Fermi-liquid scheme [201], magnon and plasmon pairing mechanisms [202,203], bipolaron, soliton, and bisoliton mechanisms [204], and generalized BCS pairing theory [205].

1.2.7 The RVB Theory and its Generalizations

Anderson claimed on the basis of the small spin values s=1/2 and the 2D nature of the system that quantum spin fluctuations may thus lead to a novel quantum spin liquid ground state. This RVB state is argued [185] to be more stable than the Néel state

for small hole concentrations. It is assumed, furthermore, that this state persists for the entire superconducting concentration regime. Normal-state with separate spin and charge excitations, and deconfinement by interlayer Josephson tunneling as the driving force for superconductivity. In this, the normal-state is both more conservative and more radical than spin bags and perhaps even *anyons*. It is more conservative in that there is still a Fermi surface satisfying Luttinger's theorem. The Fermi surface is, however, not the surface of a Fermi sea of quasielectrons; rather it is the surface of neutral, spin-carrying fermions that we call *spinons*. One of the main motivations for introducing these neutral, spin-1/2 excitations is that they exist in the one-dimensional Hubbard model, which can be solved exactly. Oddly enough, they have a longer mean free time than the transport time τ determined from $\sigma=ne^2\ \tau/m$, which is proportional to 1/T in good, pure cuprate single crystals. Thus they have a very sharp Fermi surface.

As the spinons do not carry charge, a second branch of the excitation spectrum, *holons*, which are charged, spinless objects has been introduced. Holons are a limit of collective excitations near the spanning vectors $2k_F$ of the Fermi surface and are clearly present in 1D. What has thus happened is what is called *separation of charge and spin*. There are two different Fermi velocities for charge and spin fluctuations. When one removes an electron from this metal, it leaves behind not a simple hole quasiparticle with a definite energy, as in normal Landau-liquid metals, but at least one spinon excitation and one holon excitation and also a small shower of soft collective

excitations. The breadth of this spectrum, into which the hole can be thought of as decaying, is equal to its original energy-hence the observed transport relaxation rate, which is just the decay rate. But the spectrum has a sharp feature, a cusp at the spinon energy.

This holon and spinon liquid has two very unusual properties. First, transport current is very weakly scattered by charge fluctuations such as phonons or impurities because it is carried by a collective displacement of the whole spinon Fermi surface. Spin impurities, on the other hand, cause residual resistivity -a crucial and quite striking experimental fact. In a sense this liquid is a *T_c=0 superconductor* in the absence of spin scattering. Second, the liquid is strictly *confined* to the two-dimensional CuO_2 planes, in almost the same sense that quarks are confined to nuclei. The only objects that can move coherently from one plane to another are real electrons, but these break up incoherently into holons and spinons when they arrive. Thus there is no coherent 3D motion in the third direction, along the c-axis. The absence of c-axis motion even between the very close planes in $YBa_2Cu_3O_{7-\delta}$ and $Bi_2Sr_2CaCu_2O_8$ is also attested by, for instance, the absence of strong infrared absorption of c-axis-polarized photons. This absence represents a rather large increase in kinetic energy caused by the confinement. This energy provides the motivation for T_c-namely, that pairs of electrons can tunnel coherently from plane to plane, even if single electrons cannot, and this begins to occur at a $T_c \propto t_1^2/J$, where t_1 is the interlayer matrix element and J the width of the spinon band. The superconductive T_c is thus a crossover from two-to

three-dimensional behavior. This is confirmed by various measurements, such as the remarkable observation of large splittings in the photoemission below T_c [206].

In this theory the normal-state resistivity for good metallic samples (whether solid or compacted) is almost invariably: $\rho \propto (A/T) + BT$ [207]. With the holon-spinon picture, the AT term is in-plane scattering of holons by spinons, which is linear in T because of the absence of final state exclusion principle. Thus, Anderson [180] claims that the number of crucial experiments testing his theory is sufficient to preclude the possibility of going back to conventional theories. He also claims that the anyon theory of these flux phases is not, so far, a theory of our HTSCs based on the strong experimental data that there is no spin gap and that there is a Fermi surface in the normal-state. He also suggested the model that must serve as a basis for any further progress on the theory of HTSC as: Simple one-band Hubbard model; focus on the 2D case; the relatively large self-exchange energy U.

Here it is interesting to note that the carriers in the normal state are hole-like in nature in the a-b plane [208] and these carriers move in an energy band which arises from a strong hybridization of the $2p_x$, $2p_y$ oxygen levels with the $3d_{X^2-Y^2}$ copper level. So essentially it is three band problem [209]. whereas, in developing his Luttinger liquid theory Anderson has considered only a one-band problem.

quasi-localized and thus have nearly integral magnetic moment and valence state. Thus only O electrons were itinerant (within the Fermi-liquid approaches, the conservation of carrier number, i.e., Luttinger's theorem, requires that the d-electrons are also itinerant). Levin et al. [211] have given a detail discussion on these Fermi-liquid based theories.

(2) THE "ALMOST MAGNETIC" FERMI-LIQUIDS

Two groups [195,196] have primarily studied these theories. The motivation derives from nuclear magnetic relaxation and Knight shift measurements on the Y-Ba-Cu-O family of cuprates. The following observations have led to the conclusion that AFM correlations are important:

(1) The Cu NMR deviates from Korringa behavior for T ~ 120 K.

(2) Also NMR relaxation on the O site (as well as Y) obeys the Korringa law.

(3) This behavior coexists with a relatively temperature independent Pauli susceptibility.

Points (1) and (3) imply a T dependence in the dynamical susceptibility away from $\mathbf{q}=0$. Within a one component picture, (1) and (2) suggest form factor cancellations at the O site.

(3) THE "MARGINAL" FERMI-LIQUIDS

According to Varma and his coworkers [197,198] the universal normal state anomalies follow from the hypothesis that, over a wide range of momentum $\mathbf{q}$, there exist both charge and spin density excitations with a polarizability which has a contribution of the forms

$$\mathrm{Im}P\ (q,\omega) \simeq -\ N(0)\ \omega/T \quad \text{for} \quad |\omega|<T \tag{1.5}$$

and

$$\mathrm{Im}P\ (q,\omega) \simeq -\ N(0)\ \mathrm{sgn}\ \omega, \quad \text{for} \quad |\omega|>T \tag{1.6}$$

where N(O) is the unrenormalized one-particle density of states. In addition to these anomalous terms it is assumed that there is also a usual Fermi-liquid contribution to ImP. This approach predicts a number of normal state properties [198,212,213]. The above hypothesis characterizes these materials in the normal state as marginal Fermi liquids, and leads, as well, to an attractive particle-particle interaction for superconductive pairing. Calculation of the superconducting state yield results quantitatively consistent with experiments.

1.3 SUPERCONDUCTIVITY APPLICATIONS

1.3.1 Physical Properties Important for Technology

Maintaining the superconducting state requires that both the magnetic field and the current density, as well as the temperature, remain below critical values that depend on the material. A rule of thumb for general applications is that materials must be operated at a temperature of (3/4) T_c or below. At about (3/4)T_c, critical fields have reached roughly half their low temperature limit, and critical current densities roughly a quarter of their limit. The upper critical fields in $YBa_2Cu_3O_7$ samples are ranging from 30 T (c-axis) to 150 T (a- or b- axes) at 4.2 K. In bulk ceramic conductors of $YBa_2Cu_3O_7$, a $J_c \sim 10^3$ A/cm^2 has been achieved at 77 K and 6 T. Measurements on

epitaxially grown thin films indicate J_c values in excess of 10^6 A/cm^2 at 77 K. Almost all of the applications currently envisaged for high-temperature superconductors are extrapolations of devices already operated at liquid helium temperatures. Much of the excitement has been stirred by the speculations concerning applications as low-loss electric power transmission or magnetically levitated trains.

1.3.2 Present Applications

* *SUPERCONDUCTING QUANTUM INTERFERENCE DEVICES (SQUIDS)*

  Simple circuits incorporating Josephson junctions, which can

  - detect the very faint signals produced by the human heart (10^{-6}G) and brain (10^{-9}G)
  - measure a wide variety of other electromagnetic signals (anything with an associated magnetic signature from DC up to microwave frequencies)
  - sense the disturbances in the earth's magnetic field caused by a submarine deep in the ocean and hence detect submarines
  - detect field distributions caused by geologic formations holding oil or mineral deposits
  - measure infinitesimally small voltages, currents and resistances
  - study seismic activity
  - study gravitational radiation

- be used to maintain a voltage standard in terms of the voltage generated across the junction irradiated by microwaves at a precise frequency
- be used in high-speed analog signal processors for such functions as filtering, convolution, correlation, Fourier transformation and analog-to-digital (A-to-D) conversion

* *SUPERCONDUCTING MICROWAVE AND FAR-INFRARED RADIATION DETECTORS*

Quasiparticle mixtures; superconducting bolometers

High-Q waveguides, phase shifters, and antenna arrays

* *ELECTRO-MAGNETIC SHIELDING*

* *DEFENSE SYSTEMS*

Shielding against nuclear blasts

High-speed computers

Motor-generators for ships; ship propulsion

Coil/ rail guns

Waveguides, sensors, magnetic shielding, magnetic energy storage for powering ground-based free-electron lasers, etc., for Strategic Defense Initiative (SDI) program

* *COMMERCIAL AND INDUSTRIAL USES*

Magnetic shielding

Ore-refining

Medical diagnostics and research (magnetic resonance imaging and spectroscopy)

R & D magnets (high magnetic fields (>15 T) with a possible stored energy of ~100 MJ over a working volume of a m^3 for a future possible J_c > 100,000 A/cm^2)

* *PHYSICS MACHINES*

Radio frequency devices

Superconducting super collider (SSC)

Magnetic fusion machines

1.3.3 Potential Applications

* *COMPUTERS*

Semiconducting superconducting hybrids

Active superconducting elements

* *POWER UTILITY APPLICATIONS*

Energy production (magneto hydrodynamics, magnetic fusion)

Energy storage

Electrical power transmission

Large turbogenerators

* *TRANSPORTATION*

High-speed trains (magnetic levitation)

Ship drive systems

1.4 STATEMENT OF THE PROBLEM

The critical point concerned with the high-T_c cuprates is that, for transition-metal compounds (mainly oxides), the parent compounds are AFM insulators (CuO, La_2CuO_4, Nd_2CuO_4, $YBa_2Cu_3O_6$, etc.). Also CuO is considered to be the likely key material of most of the CuO based HTSCs, because of its interesting physical and structural (Jahn-Teller effect) properties. So understanding cupric oxide (CuO) becomes important.

The Cu-O assembly is responsible for the superconductivity, and the main contribution to the density of states, $DOS(E_F)$, comes from the Cu 3d and the O 2p hybridization states. The role of Y and Ba is supportive, helping to stabilize the structure and to the charge transfer mechanism between copper sites. Thus, the substitution of Cu by particularly the 3d transition-metals, should produce substantial changes in the superconducting properties which will elucidate the electronic structure, the mechanism, and the possible technological applications. Also, understanding such defects can guide our search for new superconducting compounds. Thus, Synthesis of high-quality material of undoped and Ti, V, or Ni-doped Y-Ba-Cu-O superconductors and the study of the various physical properties such as resistivity, paraconductivity, and thermoelectric power have been carried out.

Besides, investigation on undoped and Pb and/or Sb-doped Bi-Sr-Ca-Cu-O superconductors have been carried out in order to (1) improve T_c and reduce ΔT_c , (2) substantiate the paraconductivity analyses further, and (3) probe the normal-state behavior.

Thus in view of the above objectives, the following systems have been investigated and reported in that sequence:

(1) CuO

(2) $YBa_2Cu_3O_{7-\delta}$

(3) $YBa_2(Cu_{1-X}M_X)_3O_{7-\delta}$ (M = Ti, V, and Ni) and

(4) (Bi, Pb, Sb)-Sr-Ca-Cu-O.

CHAPTER 2

EXPERIMENTAL

2.1 Fabrication of Controlled Atmosphere Furnace

Figure 2.1 shows the block diagram of the furnace with the required electronic feedback. It is a controlled atmosphere double-stage (Pt-Rh and super kanthal A) furnace, which can go up to 1600°C. The super kanthal A heating element arrangement is switched on first to preheat the furnace (and hence the Pt-Rh element) before the electronic feedback of the Pt-Rh heating element arrangement is switched on. A proper fuse has been used across the Pt-Rh heating element to protect the same in case of accidental excessive power supply. The Al_2O_3 powder used for insulation provides good thermal inertia. Pt versus Pt-13% Rh thermocouple (TC) is used with a programmable microprocessor temperature controller (Indotherm MPC 500) to control the temperature to within ±1°C. Samples placed in Pt/Al_2O_3 crucible/boat, can be heat-treated in partial vacuum, air, or in controlled atmosphere, such as O_2, He, Ar, N_2, etc.

2.2 Materials Synthesis

(1) CuO

The as-received high-purity (5N) CuO (tenorite) powder (Aldrich) was further ground in an agate mortar and pestle to obtain fine particles, and pelletized (8-10 ton/cm^2) using high-carbon high-chromium (HCHC) steel dies of different diameters. (These dies were fabricated locally, after machining the die, the piston, and the punch and were hardened by heat

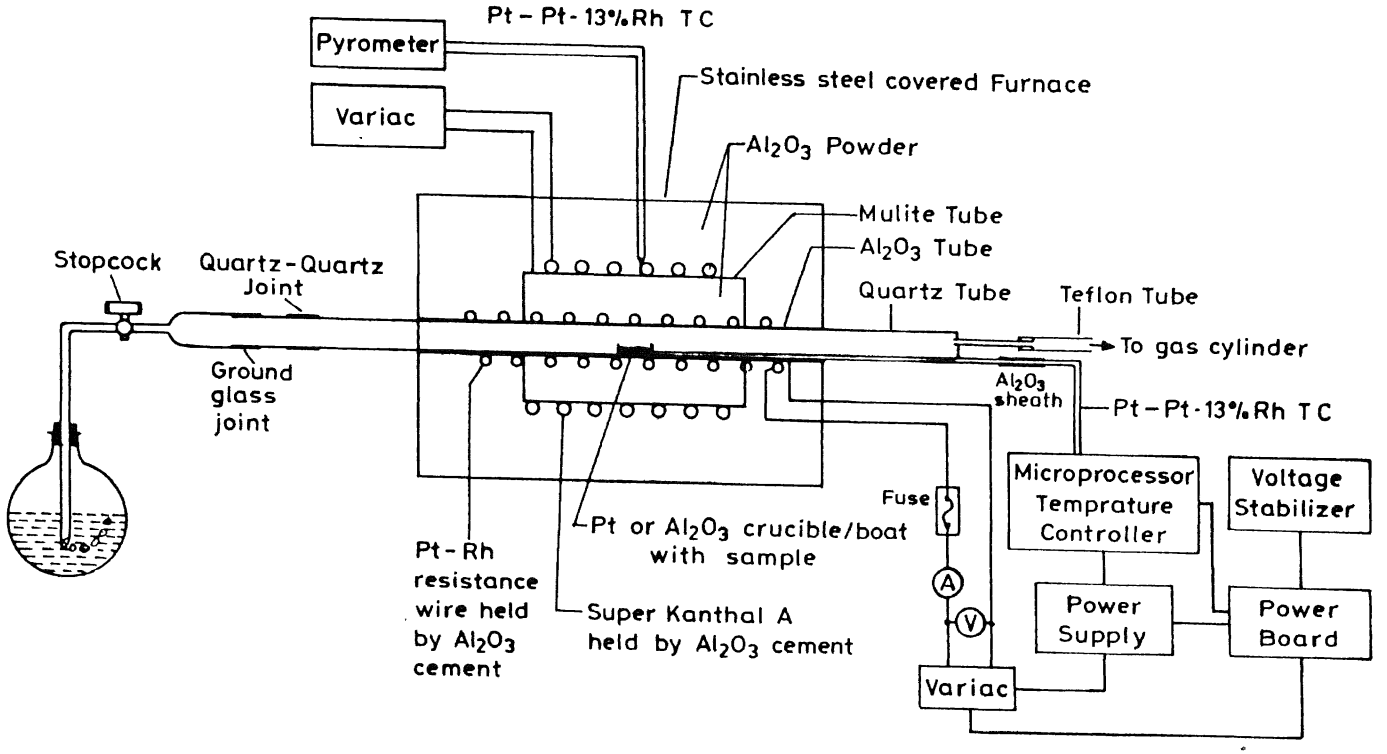

Fig. 2.1. Controlled atmosphere double-stage (Pt-Rh and super Kanthal A) wire wound furnace (temperature range: 30 - 1600°C).

treating at ~960°C for 15 min, followed by oil quenching; further, these pieces were polished by grinding and then were tempered by heat treating at ~350°C till a bluish color thin surface layer appears over it followed by oil quenching). The pellets were then sintered at 930-950°C for about 24 h in air and then furnace cooled. Different preparational conditions have also been tried. The density of the samples were ~90% of the single crystal value.

(2) $YBa_2Cu_3O_{7-\delta}$

The lack of thermodynamic stability is one of the predominant issues in the synthesis of HTSCs. Metastability may arise in different ways in various superconductors and thus it is desirable to synthesize these materials under conditions where they are thermodynamically stable. Then, if the compound possesses sufficient kinetic stability, it may be studied and used at conditions where it is metastable. Due to lack of thermodynamic stability at low temperatures, ordinary solution precursor methods which employ low-temperature synthesis have not been particularly useful. Thus most, but not all, solid solutions are prepared at temperatures high enough for entropy to stabilize the defects inherent in the solid solution [95]. In general, oxides containing several cations are generally prepared by heating intimate mixtures of solid reactants to temperatures where solid-state diffusion becomes sufficiently rapid and hence the reaction rates appreciable. The reactants may be either oxides or salts that decompose on heating to yield the corresponding oxides.

Ceramic $YBa_2Cu_3O_{7-\delta}$ samples with different room temperature resistivities were prepared by the solid-state reaction method. Appropriate amounts of high-purity (4-5N) Y_2O_3, $BaCO_3$, and CuO were mixed thoroughly in acetone medium carried in an agate mortar. For *calcination*, the mixtures were lightly pressed (1-2 ton/cm^2) into pellets, which were heated slowly up to 300°C (to remove solvent and water vapor) and then rapidly to 920°C in flowing O_2 gas (to facilitate better removal of carbon from $BaCO_3$) for 24 h followed by furnace cooling. The product was ground, pelletized (5 ton/cm^2), and heat treated at 960°C in O_2 for 16 h and then furnace cooled to 200°C in oxygen atmosphere before being removed from the furnace. The above pellets were further heat treated at 960°C in O_2 with intermittent grinding steps for *better homogeneity and phase purity*. The product was again reground and pressed (7 ton/cm^2) into disc-shaped pellets (~8 mm diameter and 2-3 mm thickness) and were finally *sintered* at ~980°C for 24 h in O_2 atmosphere and then slow cooled to 600°C, held there for about 24 h followed by furnace cooling to room temperature. Thus high density (~85%) black samples with a lot of microcrystallites were obtained this way (Sample 1).

In another batch of samples the above preparational steps were repeated except the final sintering. In this case, the product was pelletized (8-9 ton/cm^2) and sintered at ~990°C for 24 h in O_2 and then slow cooled to 700°C, and held there for 12 h, then cooled to 650°C, and held there for 6 h, and at 600°C for 6 h followed by slow cooling to room temperature. All these heat treatments were carried out in O_2 atmosphere. In the high density (90-95%) deep-black samples that resulted this way, it was

noticed that a few layers of highly blackish insulating phase had formed which were subsequently removed and the core superconducting phase containing a lot of microcrystallites was isolated (Sample 2A). Some of these pellets (sample 2A) were heated slowly (0.5°C/min) up to 900°C and then slow cooled (<0.5°C/min) to 650°C and held there for several hours followed by slow cooling (<0.5°C/min) to room temperature. All these steps were done in O_2. These are referred to as Sample 2B.

(3) $YBa_2(Cu_{1-X}M_X)_3O_{7-\delta}$ *(M=Ti, V)*

Ceramic $YBa_2(Cu_{1-X}M_X)_3O_{7-\delta}$ (M=Ti, V) samples are prepared by the solid-state reaction method. Appropriate amounts of high-purity (3 to 5N) Y_2O_3, $BaCO_3$, CuO, and TiO_2, or V_2O_3 were mixed well in acetone medium carried in an agate mortar. The mixture was calcined at ~940°C in air/O_2 for 24 h followed by furnace cooling. The product was ground, pelletized, and presintered at ~960°C for 24 h and furnace cooled. The above procedure was repeated with intermittent grinding steps to homogenize the samples. The products were reground, pelletized (8-9 ton/cm^2), and finally sintered in the temperature range 975-985°C (depending upon the composition) for 24 h in air/O_2. These samples were then slow cooled (1°C/min) to 700°C and held there for 12 h, followed by cooling in 100°C-steps to 400°C, holding for 12 h at each step. The samples were then furnace cooled to 200°C before their removal from the furnace. Thus high density (90-95%) black samples were obtained.

(4) $YBa_2(Cu_{1-X}Ni_X)_3O_{7-\delta}$

Samples of $YBa_2(Cu_{1-X}Ni_X)_3O_{7-\delta}$ ($0 \leq X \leq 0.2$) were also prepared by the solid-state reaction method, as described below. Appropriate amounts of high-purity (3 to 5N) Y_2O_3, $BaCO_3$, CuO, and NiO were mixed well in acetone medium carried in an agate mortar. The mixtures were calcined at ~940°C in O_2 for 24 h followed by furnace cooling. The resulting products were ground, pelletized, and presintered at ~950°C for 24 h in air and furnace cooled. The above procedure was repeated, as usual, with intermittent grinding steps to homogenize the samples. These products were reground, pelletized (8-9 ton/cm^2), and finally sintered at ~980°C for 24 h in flowing O_2. The samples were then slow cooled to 700°C and held there for 12 h, followed by cooling in 100°C-steps to 400°C, holding for 12 h at each step. Then the samples were furnace cooled to 200°C before they were removed from the furnace. High density (90-95%) black samples were thus obtained.

(5) (Bi,Pb,Sb)-Sr-Ca-Cu-O SYSTEMS

(A) $Bi_2Sr_2CaCu_2O_Y$

Ceramic $Bi_2Sr_2CaCu_2O_Y$ samples were prepared by matrix method. High-purity (3 to 4N) $SrCO_3$, $CaCO_3$, and CuO powders in appropriate ratios were thoroughly mixed and calcined at 950°C for 16 h followed by furnace cooling. The resultant matrices were reground and mixed thoroughly with Bi_2O_3 powder in proper ratio and calcined at 820-825°C for 24 h in air followed by furnace cooling. The black products thus obtained were pelletized (7

ton/cm^2) and heat treated at ~840°C for 24 h in air, followed by cooling (3°C/min) to room temperature. These pellets were further ground, pelletized (8 ton/cm^2), and sintered at ~850°C for 24 h in air, followed by fast furnace cooling. These are referred to as Sample 1. Some of the pellets of these Sample 1 were heat treated at ~850°C for 1 h, and then slow cooled (5°C/h) until 800°C and further cooled (10°C/h) to 400°C followed by furnace cooling to room temperature. These are referred to as Sample 2.

Some of the pellets of sample 2 were heated to 900°C then cooled (10°C/min) to 870°C, held there for 6 h, and then cooled (5°C/min) to 400°C followed by furnace cooling to room temperature (RT). These are referred to as Sample 3. Some of the Sample 3 specimen were heat treated at 900°C for 1 h, slow cooled (1°C/min) to 850°C and then furnace cooled to 400°C followed by quenching in air to RT. These have been labelled as Sample 4. Some of the Sample 4 specimen were heat treated at 930°C and then cooled (10°C/min) to 850°C followed by furnace cooling to 400°C and then quenching in air to RT. These are referred to as Sample 5. Some of the pellets of Sample 5 were heated to 860°C, held there for 6 h, and then slow cooled (1°C/min) to 800°C followed by furnace cooling to room temperature (Sample 6).

(B) $Bi_{1.7}Pb_{0.3}Sr_{1.6}Ca_2Cu_{3.4}O_Y$ *and* $Bi_{1.9}Sb_{0.1}Sr_2Ca_2Cu_3O_Y$

Ceramic Route

Appropriate amounts of high-purity (99.99%) powder reagents Bi_2O_3, PbO, Sb_2O_3, $SrCO_3$, $CaCO_3$, and CuO were well mixed and ground in acetone medium carried in an agate mortar. The mixtures

were calcined in air/O_2 at 810-840°C for 15-24 h. They were then reground, pelletized (6-8 ton/cm^2), and heat-treated in air at 840-860°C for 24 h with intermittent grinding. The products obtained in this manner were reground and pelletized, and the pellets were finally sintered in air at 870°C for 24 h, cooled to 840°C, and held there for 72 h, in the case of $Bi_{1.7}Pb_{0.3}Sr_{1.6}Ca_2Cu_{3.4}O_Y$ (Sample 1) and at 890°C for 15 h, in the case of $Bi_{1.9}Sb_{0.1}Sr_2Ca_2Cu_3O_Y$ (Sample 2), followed by furnace cooling.

Glass Route

The dense chunks of the prereacted materials of the above compositions were melted in an alumina crucible by keeping them at 1100-1150°C for about 15 min, and the melts were rapidly quenched (10^2-10^3°C/sec) by sandwiching them between two polished copper plates, resulting in opaque black sheets of about 0.5-1 mm thicknesses (referred to as Samples 3 and 4, respectively). For crystallization, the above dense glass plates were annealed in air at 840°C for 15 h, in the case of $Bi_{1.7}Pb_{0.3}Sr_{1.6}Ca_2Cu_{3.4}O_Y$ (Sample 5) and at 890°C for 15 h in the case of $Bi_{1.9}Sb_{0.1}Sr_2Ca_2Cu_3O_Y$ (Sample 6), followed by furnace cooling .

(C) $(Bi, Pb, Sb)_2Sr_2Ca_2Cu_3O_Y$

Samples of nominal compositions $Bi_{1.9}Pb_{0.3}Sr_2Ca_2Cu_3O_y$ and $Bi_{1.6}Pb_{0.3}Sb_{o.1}Sr_2Ca_2Cu_3O_y$ were prepared in air by a three-step reaction process involving matrix method. High-purity (3 to 4N) Bi_2O_3 , PbO, $CaCO_3$, and $SrCO_3$ powders in appropriate ratios were thoroughly mixed and calcined at 820°C for 12 h. The resultant

matrix was reground and mixed thoroughly with CuO powder in proper ratio and pressed (7 ton/cm^2) into disc-shaped pellets. These pellets were heat treated at 900°C for about 5-10 min and then quenched in air to room temperature. The black pellets so obtained were reground and repelletized (10 ton/cm^2).

Samples A and B with nominal composition $Bi_{1.9}Pb_{0.3}Sr_2Ca_2Cu_3O_y$ were prepared by finally sintering the above pellets at 852°C for 20 h and at 860°C for 16 h, respectively, followed by furnace cooling to 400°C and annealing at this temperature for ~12 h, and then air quenching to room temperature. Samples C and D with nominal composition $Bi_{1.6}Pb_{0.3}Sb_{o.1}Sr_2Ca_2Cu_3O_y$ were prepared by finally sintering the pellets at 860°C for 12 h and at 850°C for 12 h, respectively, followed by furnace cooling to 400°C and annealing at this temperature for 6 h, and then air quenching to room temperature.

2.3 General (Glovebox, Impedance analyzer, etc.)

All the surfaces of the samples were polished and where necessary the main surfaces were faced-off before taking any measurements. For resistivity, thermoelectric power (TEP), and dielectric constant measurements a number of electrodes such as Cu/Pt foils, silver paint, evaporated Cu, Ag, and Au were tried. During the evaporation of film electrodes, the sides of the samples were covered by teflon tapes to prevent them getting coated. These samples were usually heat treated at 300-400°C for few hours in inert atmosphere glove box (model GB-80, Mecaplex, Switzerland). AC resistivity and dielectric constant measurements were done using HP-4192A impedance analyzer. Optical absorption

measurement were performed using UV spectrophotometer (model 160 Shimadzu) by applying a thin layer of fine powder on a filter paper with reference to another empty filter paper.

2.4 Thermal Analysis (DTA, TGA)

Differential thermal analysis (DTA) was performed on a LINSEIS (Type L40/311) DTA equipment. Thermogravimetric analysis (TGA) was done using Ainsworth (USA) TG equipment. The measurements were carried out in air with a heating/cooling rate of 5°C/min. The weight of the sample taken was in the range of 50-100 mg. Pt versus pt-13% Rh thermocouple was used to monitor the temperature. In the case of DTA, Pt crucibles with α-Al_2O_3 as reference were used. The measurements were standardized by means of several high-purity materials of known melting points. The sensitivity range used in DTA was 0.1 mV. The DTA/TGA analyses were carried out in the range 25° to 1100°C.

2.5 X-Ray Diffraction

X-ray diffraction (XRD) patterns were recorded using a Iso-Debyeflex 2002 diffractometer with Ni filtered Cu Kα radiation. Samples in the form of fine powder packed in the sample holder were used for this purpose. The range of 2θ values analyzed was from 10° to 60° with a scanning speed of 0.3°/min, using a time constant of 1-10 sec. The lattice parameters were found by a standard computer program, including the intensity and the angle.

2.6 Scanning Electron Microscopy

Scanning electron microscopy (SEM) and energy dispersive X-ray analysis (EDXA) were carried out using a JEOL JSM-840A scanning microscope coupled with Kevex detector and software. Polished, fractured, or etched samples were used in this study.

2.7 Electron Paramagnetic Resonance

Microwave absorption by various samples was recorded using a Varian E-109 X-band EPR spectrometer operating at a frequency of ~9.4 GHz. Through-zero-field detection was achieved by using a pair of current-carrying Helmholtz coils producing an auxiliary field in a sense opposite to that of the electromagnet. The range of temperature covered was 77-450 K.

2.8 Iodometry

In certain samples, the oxygen content was determined by iodometric titration [214,215]. The indirect method (iodometry) deals with the titration of iodine liberated in chemical reactions. If a strong oxidizing agent is treated in neutral or more usually acid solution with a large excess of iodine ion, the later reacts as a reducing agent and the oxidant will be quantitatively reduced. In such cases, an equivalent amount of iodine is liberated, and is then titrated with a standardized solution of a reducing agent, which is usually sodium thiosulfate.

Method 1

Accurately weighed 40 to 50 mg of the sample (which roughly contain about 0.2 mmol of Cu in finely powdered form was dissolved in 2 ml of ice-cold ~4.4 M HBr (made by dissolving the commercial 48% HBr in 1:1 with triple distilled water) in a 4 ml vial provided with a small teflon coated magnet and stirred well for at least 10 min. This was transferred to a 50 ml conical flask (glass stoppered) containing 20 ml of ice-cold 0.2 M KI and enough NH_3 (to neutralize all but about 1 mmol of the added acid). The solution in the flask was stirred gently during addition. The 4 ml vial and the transfer pipet were washed twice with 2 ml portions of 2M KBr. 5 ml of 1M sodium citrate was then added to the flask, and the solution was brought to room temperature and stirred until dissolution of the Cu I precipitate was complete.

The iodine present was titrated with standardized 0.1 M sodium thiosulfate (3.567 g of pure dry KIO_3, dissolved in 1000 cm^3 of cold, boiled-out distilled water. 25 ml of this solution was treated with 1g of pure iodate-free KI, the absence of iodate was indicated by no immediate blue color formation when starch is added, followed by 3 ml of 1 M H_2SO_4, and the liberated iodine was titrated with the thiosulfate solution with constant shaking. When the color of the liquid has become pale yellow, it was diluted to about 200 cm^3 with distilled water, and 2 cm^3 of starch solution was added and the titration was continued until the color changes from blue to colorless), with the use of a microburet. When the solution begins to change color, two drops of freshly prepared starch solution (1 g of soluble starch into

100 cm^3 of boiling distilled water and 2-3 g of KI to the cooled solution) was added, and the titration was continued until the dark blue color changes to pale blue.

The oxygen coefficient y of an oxide $R_rA_aC_cO_y$, where R is a rare earth and A is an alkaline earth, may be calculated from the titration results using the following formula

$$y = (\alpha E + \beta)/(2-16E) \ , \qquad (2.1)$$

where E = mol of $S_2O_3^{2-}$ used/g of sample or

E = mol of Cu(III)/g of sample,

$$\alpha = rM_r + aM_a + 63.54\ c \qquad (2.2)$$

(M_r, M_a=molar masses of metals r and a, respectively), and

$$\beta = 3r+2a+2c \ . \qquad (2.3)$$

Method 2

45-50 mg of powdered sample was dissolved under He in 15 ml of 1 M KI and 15 ml of 0.7 M HCl solution. The solution was diluted by 20 ml of triple-distilled water and the liberated iodine was titrated with standardized sodium thiosulfate solution. This method is mainly used when the value of y in $R_rA_aCu_cO_y$ is less than 6.5 in which case the just described *method 1* is not applicable.

2.9 Density Measurements

Density measurements were carried out using a specific gravity bottle. A known weight, W_1, of the powdered sample was taken in the bottle which was then about half-filled with Xylene. This was put in a vacuum desiccator and the whole system was evacuated so as to expel all the air bubble trapped within the powder. Then the bottle was completely filled with Xylene and weighed (W_2). The bottle was then weighed after filling it with Xylene only (W_3). With known density, d, of Xylene, the density, D, of sample can readily be calculated from

$$D = W_1 \, d \, / \, (W_3+W_1-W_2) \, . \qquad (2.4)$$

2.10 Cryostats and Sample Holders

(1) FABRICATION OF LN_2 CRYOSTAT WITH SAMPLE HOLDER

Figure 2.2 shows the LN_2 bath cryostat with the sample holder suitable for electrical resistivity, thermoelectric power (TEP), and dielectric constant measurements. This set-up could cover a temperature range 77-400 K. The system is equipped with three copper versus constantan thermocouples, TC1, TC2, and TC3, to measure respectively (1) the cold end, (2) the hot end, and (3) the average temperature of the sample. For TEP measurements the sample is held between the two high-purity Cu blocks with the help of a spring. The manganin heating element wound non-inductively over the GE-varnished Cu/Al block serves as an auxiliary heater to maintain the temperature gradient across the sample. For electrical resistivity measurements four phosphor

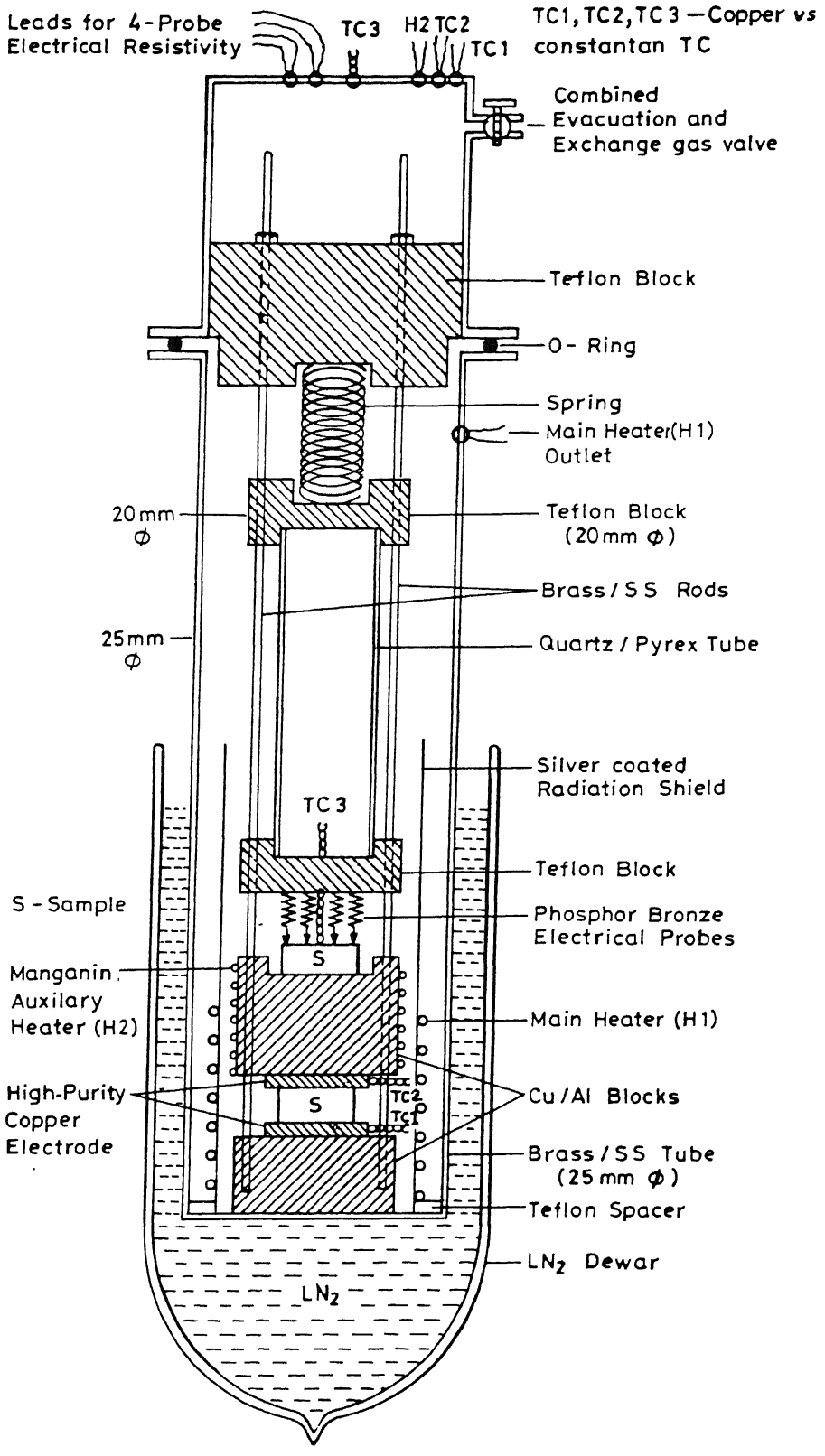

Fig. 2.2. Electrical resistivity, Thermopower, and Dielectric constant set up for the temp. range 77-400K.

bronze probes were mounted on a teflon block, which can be moved with the help of the spring load assembly. As the spring is located outside the dewar it maintains the spring constant. Loops in the nanovoltmeters' leads pick up small magnetic field changes and induce a current in the leads. This current shows up as a noise voltage in the meters' readings. This noise can be significantly reduced by twisting the leads together and by keeping them as short as possible.

(2) FABRICATION OF SAMPLE HOLDER FOR OXFORD LN_2 CRYOSTAT

The Oxford DN 1710 cryostat operates on the principle of the controlled continuous transfer of LN_2 from a reservoir to a heat exchanger which surrounds the sample space. It is designed mainly for variable temperature (77-500 K) magneto-measurements of either solid or liquid samples. The cold region extends ~ 50 mm above the bottom of the sample space and has a clear diameter of 20 mm. The sample is top loaded and is cooled by a static column of exchange gas which thermally links the sample to a heat exchanger. A Pt temperature sensor and a heater are fitted to the heat exchanger. A temperature controller (Oxford model ITC4) is used to control the temperature of the cryostat.

Figure 2.3 shows the sample holder fabricated for this cryostat. It can be used for TEP, two-probe resistivity, and dielectric constant measurements. The sample is held between the two high-purity Cu electrodes (which are in turn attached with Al blocks) with the help of a spring loaded assembly. The manganin heating element (H) wound non-inductively over the GE-varnished Cu/Al block serves as an auxiliary heater to maintain the

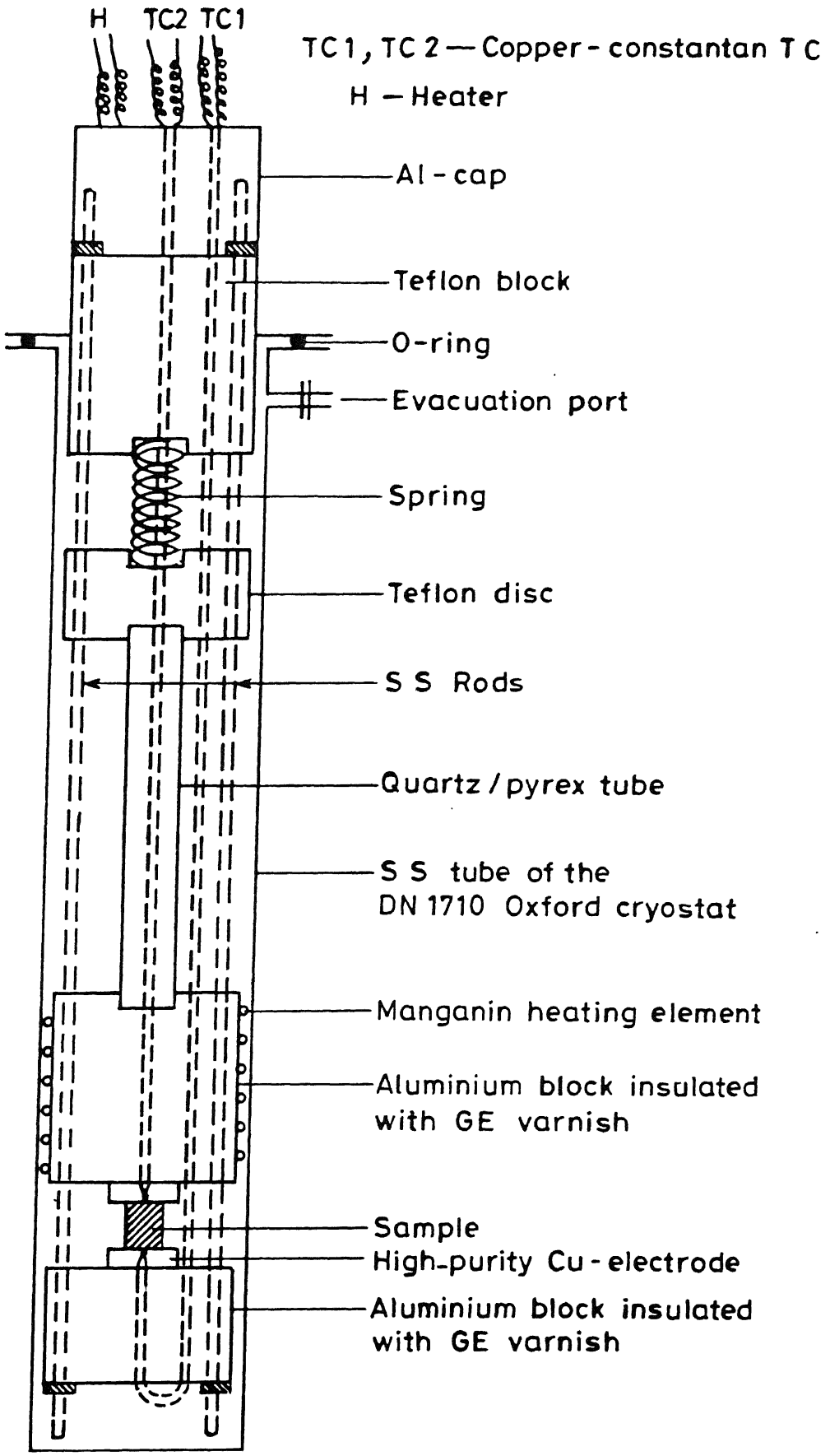

Fig. 2.3. Sample holder for TEP, two-probe electrical resistivity, and Dielectric constant measurements in the temperature range 77 - 500 K for DN 1710 Oxford Cryostat.

temperature gradient across the sample in the case of TEP measurements. The tip of the copper versus constantan thermocouples (TC1, TC2) are placed just above and at the center of the sample surface so that it can sense the exact temperature of the sample.

(3) FABRICATION OF SAMPLE HOLDER FOR CLOSED CYCLE HE CRYOSTAT

The APD superconductor characterization cryostat provides a 19 mm dia, 180 mm long isothermal refrigerated sample well for characterizing materials as a function of temperature from 12 to 350 K. The sample well is thermally attached to the expander of a closed cycle refrigerator (which comprises an expander, a compressor, and interconnecting flex hoses). He gas is filled in the sample space to facilitate good thermal equilibrium and to avoid moisture condensation while keeping the sample electrically isolated. The sample well and the cold section of the expander are enclosed in an insulating vacuum shroud. The standard sample holder is a 13 mm diameter tube which can hold up to 9.5 mm dia 150 mm long samples. The sample well temperature is controlled by a resistance heater on the expander cold tip and a temperature sensor (Si diode). A microprocessor-based temperature controller (Scientific Instruments, Inc. model 5500-1-25) is coupled with the cryostat to control the temperature. A calibrated Si diode with a 10 mK resolution is used to sense the temperature of the sample.

Figure 2.4 shows the sample holder designed for this cryostat to carry out the TEP measurements. Sample is held between two Al blocks with the help of minute amount of silver

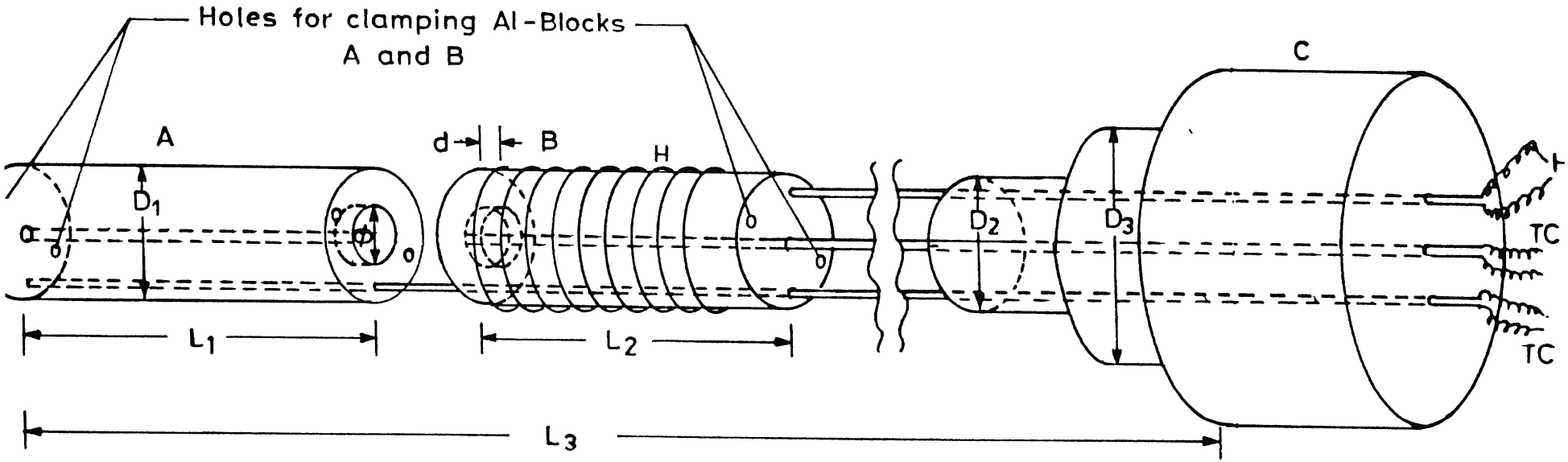

VARIOUS DIMENSIONS	
L_1 = 25 mm	D_1 = 10 mm
L_2 = 25 mm	D_2 = 12.7 mm
$L_3 \approx$ 55 cm	D_3 = 28.7 mm
ϕ = 6 mm	d = 1.0 mm

DESCRIPTION

A, B - Aluminium block
C - Brass cap for He-cryostat
H - Heater wire
TC1, TC2 - Thermocouple (Cu-Constantan)

Fig. 2.4. Sample holder for thermopower measurement in the temperature range 15-300 K for closed cycle He cryostat.

paint as well as by twisted Cu wires. Manganin heating element (H) serves as an auxiliary heater to provide the temperature gradient across the sample. Two copper-constantan (TC1, TC2) thermocouples are used to measure the temperature gradient across the sample.

2.11 Electrical Resistivity

Electrical resistivity (ρ) measurements were performed using standard dc/ac, two/four-probe methods depending upon the magnitude of the resistivity. The temperature range covered was from 15 to 1250 K. Different experimental arrangements have been used for these purposes. Precision constant current source (Knick model JS 300), DMMs (Keithley models 197 and 195 A), electrometer (Keithley model 619), nanovoltmeter (Keithley model 181), Lock-in amplifier (Stanford model SR 530), and HP-4192A low frequency impedance analyzer have been used for these measurements. Checks have been made for Ohmic contact. The samples in the form of circular disc (8mm in diameter and 1mm thick) were generally used for ρ measurement. For low resistivity measurements, four-probe technique [216] was generally preferred as it eliminates the lead resistance, cancels the thermo-emfs, and controls the electrical and magnetic noise. The temperatures in the transition region were measured within ±0.1 K. A calibrated Si diode with a 10 mK resolution was used for this purpose. Measurements were performed by using current values in the range of 5 to 50 mA. At each temperature the voltage readings were taken for both forward and reverse directions of the flow of current to correct for any thermo-emfs at the contacts. The experimental system was able to

detect changes of resistivity of the order of 1 $\mu\Omega$ cm. The resistivity can readily be calculated [216] from

$$\rho = R\ T\ G\ , \qquad (2.5)$$

where R is the ratio V/I, T is the effective thickness, and G is the geometrical factor. Figure 2.5 shows the square four-probe sample holder used to accurately calculate the room temperature (RT) resistivity of the sample for comparison and calibration purposes. The speciality of this sample holder is that the geometrical factor G in the above formula is known to a reasonable accuracy. AC four-probe measurements were also performed in the frequency range 1-100 KHz.

Figure 2.6 shows the experimental arrangement used for the four-probe resistivity measurements in controlled atmosphere above room temperature. It can be used in the temperature range from 300-1300 K. The thin rods used in this sample holder are made up of *inconel 600* superalloy material (high-temperature and corrosion resistance alloy), which can withstand temperatures up to ~1400°C. The nuts, screws, and the bushes (which carry the inconel screws through the lava stone) are all made out of the same material. The tips and the heads of the inconel screws have been welded with pt, so that the electrical connection will always be maintained through Pt tip-core material of the inconel screw-Pt wire, though the surfaces of the inconel screws get oxidized and hence become insulating. The lava discs are made up of pyrophyllite material which has been machined in proper dimension and hardened by heat treatment at ~ 1000°C for 24 h.

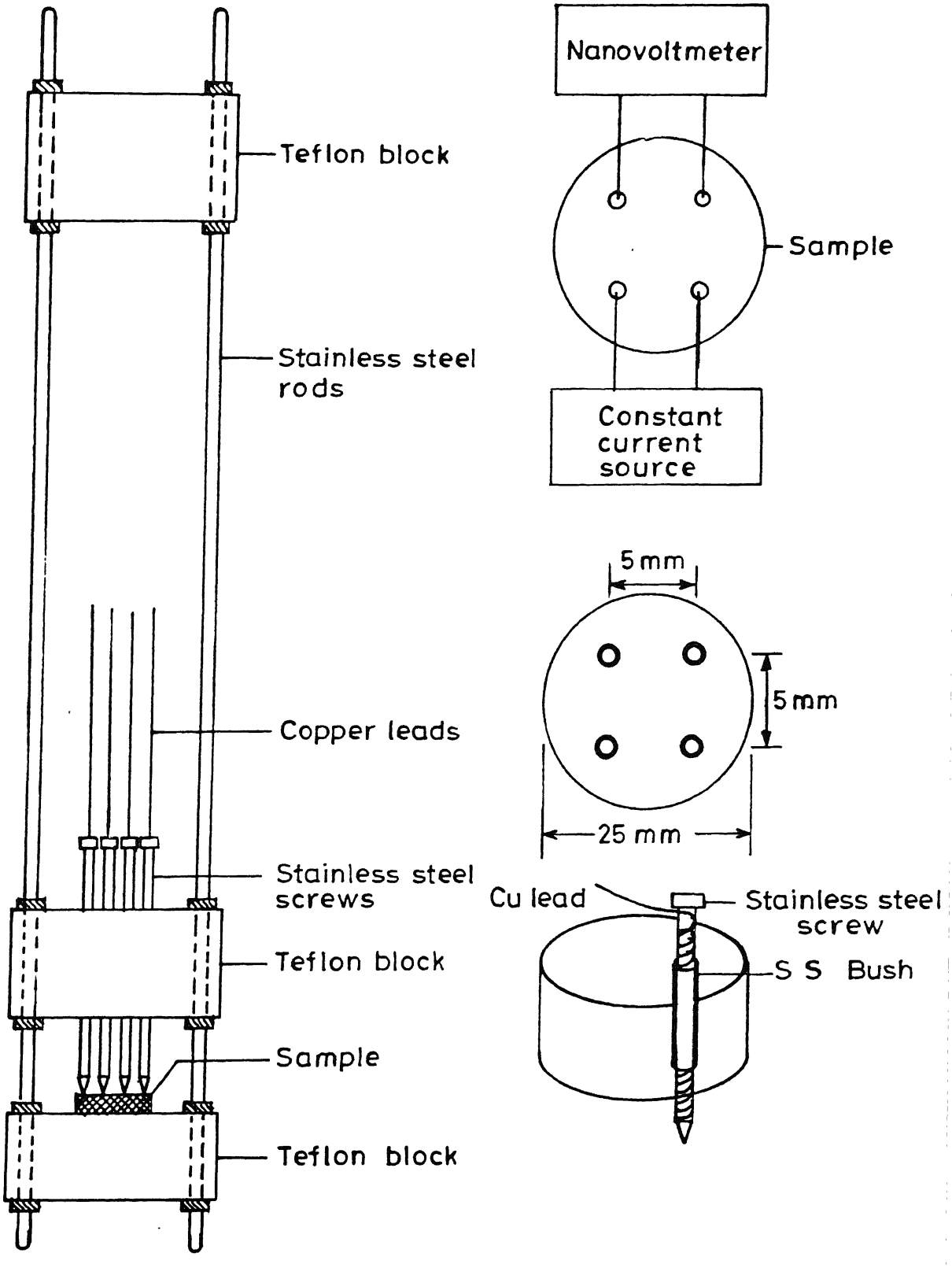

Fig. 2.5. Sample holder for R T four-probe resistivity measurement.

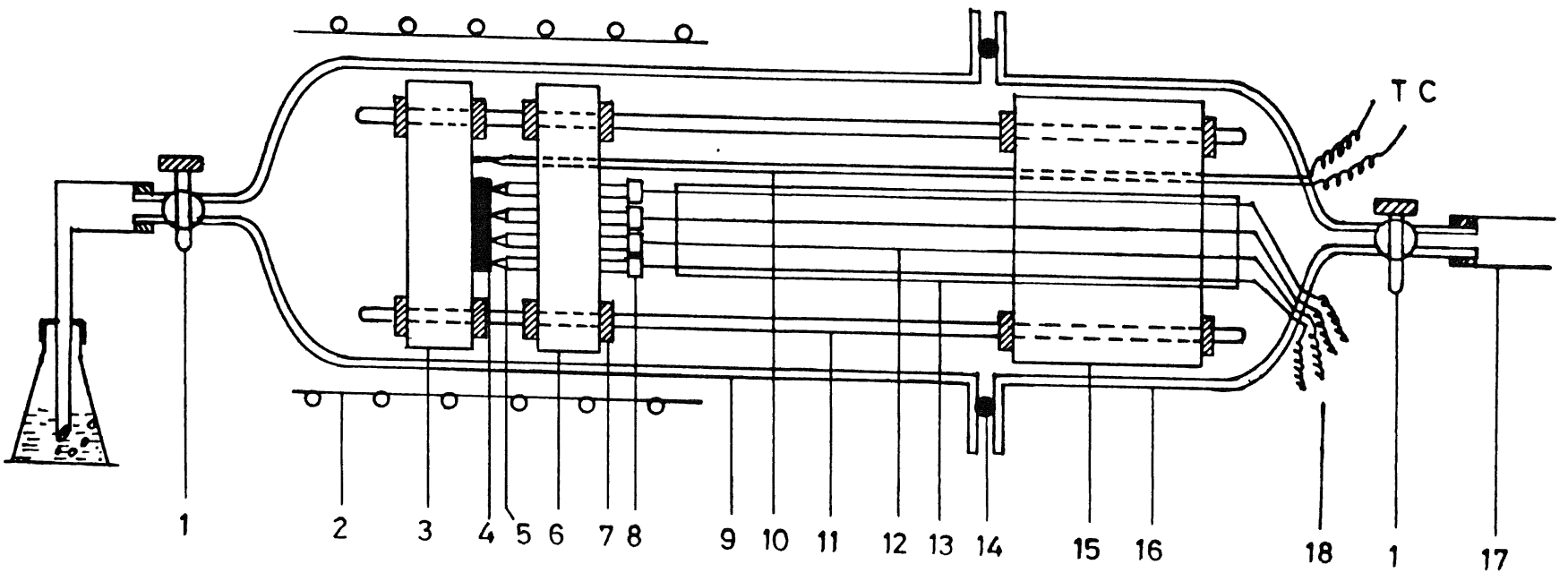

1 - Stopcock; 2 - Furnace; 3 - Pyrophyllite disc; 4 - Sample; 5 - Pt-tips; 6 - Pyrophyllite disc with inconel bushes; 7 - Inconel nuts; 8 - Inconel screws; 9 - Quartz tube; 10 - T C (type K or S in twin bore Al_2O_3 tube); 11 - Inconel rods; 12 - Pt lead wires; 13 - Four-bore Al_2O_3 tube; 14 - O-ring; 15 - Teflon block; 16 - Quartz tube; 17 - To gas cylinder with pressure regulator; 18 - Four-probe electrical lead wires.

Fig. 2.6. Experimental set up for H T four-probe resistivity measurement in the temperature range 300 - 1300 K.

For resistivity measurements the sample in the form of thin circular discs are placed under the four probes, which are arranged in square form. Ag, Au, or Pt paints were applied under the Pt tips in case there was surface poisoning between the sample and the Pt tips; for example, poisoning at the contact occurs in the form of formation of semiconducting alloy layer between the Pt tips and the $YBa_2Cu_3O_{7-\delta}$ sample and thereby preventing to make any meaningful measurements at higher temperatures. The whole assembly was fitted inside a quartz tube with necessary arrangements so as to enable measurements under controlled atmosphere.

2.12 Thermoelectric Power (TEP)

Measurement of TEP can provide evidence relating to (1) the type of majority carrier, (2) the details of the Fermi surface, and (3) the scattering processes. Separate experimental set ups have been used for low-temperature (15-300 K; Figs. 2.2-2.4) and high-temperature (300-1300 K; Fig. 2.7) TEP measurements. The high-temperature sample holder shown in Fig. 2.7 consists of lava/pyrophyllite blocks. These blocks, which can be moved smoothly along the two parallel inconel rods, applies uniform pressure and ensure a firm contact between the electrodes and the sample, by acting in combination with the spring and the quartz tube assembly. The length of the sample holder is such that the spring is located outside the furnace so that it can maintain its spring constant. Pt disc and foils have been used as electrodes. Two Pt versus Pt-13% Rh thermocouple pairs (marked TC1 and TC2) have been welded at the backside of the electrodes to serve as

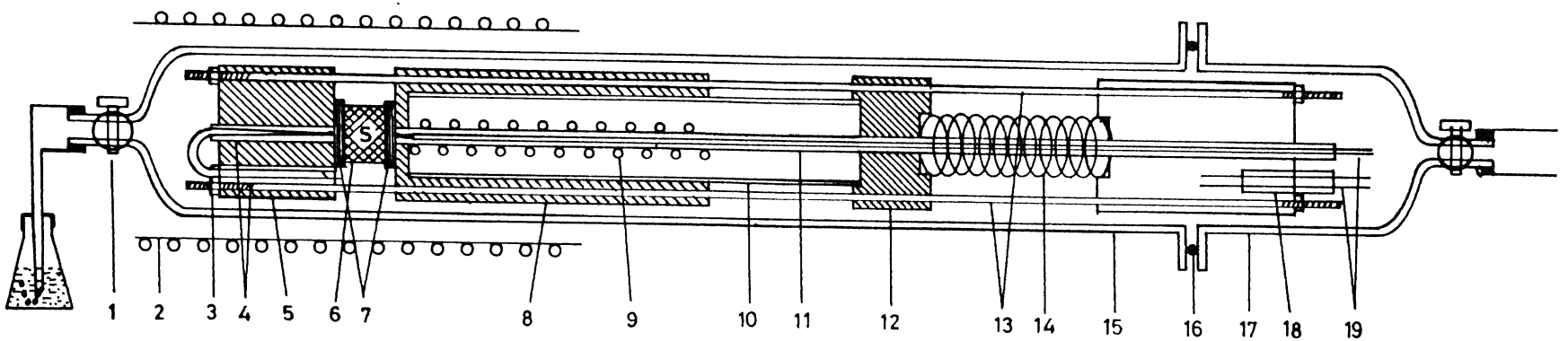

1- Stopcock ; 2 - Furnace ; 3 - Inconel nuts ; 4 - Twin-bore alumina tube ; 5 - Pyrophyllite block ; 6 - Sample ; 7 - Pt - electrodes ; 8- Pyrophyllite / Inconel block ; 9 - Super Kanthal A auxiliary heater ; 10 - Quartz tube ; 11 - Twin-bore alumina tube ; 12 - Pyrophyllite disc ; 13 - Inconel rods ; 14 - Spring ; 15 - Quartz tube ; 16 - O-ring ; 17 - Quartz tube ; 18 - Twin-bore alumina tube ; 19 - Pt - Pt-10% Rh.

Fig. 2.7. Controlled atmosphere set up for electrical resistivity and thermopower measurements in the temperature range 300 - 1300 K.

electrical lead wires as well as temperature probes. The reference junctions were kept in an oil bath whose temperature was constantly monitored to make accurate temperature measurements. A super kanthal A resistance-wire wound on the alumina thermocouple sheath, which is placed inside the long pyrophyllite/inconel-600 cylinder, served as an auxiliary heater to maintain the temperature gradient across the sample. The entire assembly was fitted inside a quartz tube with the necessary arrangements so as to enable the measurements under controlled atmosphere.

The main source of error in TEP measurements lies in the determination of the temperature difference ΔT between the two ends of the sample. Care was taken to minimize this error by securing good thermal (as well as electrical) contact between the heat source, the sample, and the sink, and between the thermocouple (TC) and the sample by placing the small thermocouple junction just above and at the center of the sample by suitable techniques appropriate for low-temperature (LT) and high-temperature (HT) set ups. In order to minimize the heat conduction between the thermocouple junction and the leads, very thin wires were used as leads. Further, the thermocouples used to measure the temperature difference across the sample were made from the same batch materials. To reduce thermal convection current, in the case of high-temperature measurements, the apparatus was mounted horizontally in the furnace. Supplementary heating was provided by means of an auxiliary heater. The sample and electrode assemblies were held in place by means of a spring arrangement. The temperature was measured using a chromel versus

alumel (Type K), a copper versus constantan (Type T), a Pt versus Pt-10% Rh (Type S), or a Pt versus Pt-13% Rh (Type R) thermocouple depending upon the temperature range. The other ends of the junctions was maintained at an appropriate reference temperatures (LN_2 or oil bath). Figure 2.8 shows the schematic diagram for TEP measurements. The difference in temperature between the hot junction (T_h) and the cold junction (T_c) gives the value of ΔT. The voltage (ΔV) developed across the sample due to this temperature difference (ΔT) was measured by the nanovoltmeter (Keithley model 181). Thus, the thermopower ($S=\Delta V/\Delta T$) at various average temperatures $\{T=(T_h+T_c)/2\}$ was measured. In the case of low-temperature, the sample S in the form of a circular cylinder (5 mm dia and 5 mm thick) were closely-fitted between two Cu/Al blocks with a minute amount of silver paint. A temperature difference of ~1 K was generally applied across the sample in the case of superconductors and 5-10 K in the case of semiconductors with the help of an auxiliary heater.

In the case of low-temperature TEP measurements, due to the poor thermal conductivity of Y-Ba-Cu-O, a direct use of Pb (a universally accepted TEP standard) is not the best choice, as it is difficult to draw Pb wires sufficiently thin to (1) prevent shunting of heat away from the sample which obviously will disturb its temperature profile and (2) avoid error due to cold working, impurity etc., and thereby causing problem in the reproducibility of the data. In this work, copper has been opted as thermopower reference leads, as it can be drawn into very thin wires, effectively eliminating the heat shunting, and has a small

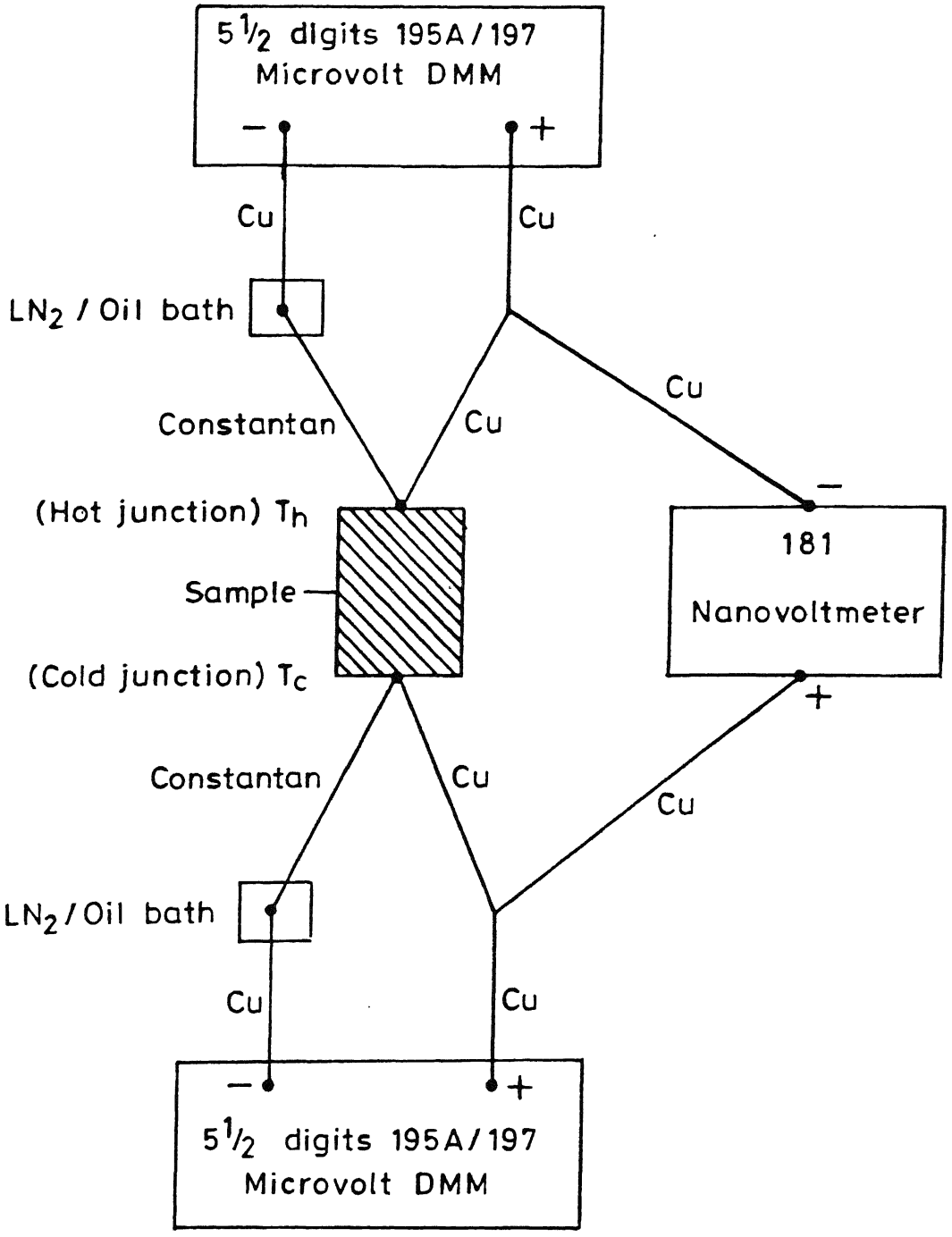

Fig. 2.8. Schematic diagram for TEP measurements.

(<2 μv/K even at 300 K) and reproducible thermopower in the temperature range of interest (77-300 K). The TEP data of the copper leads have been calibrated against high-purity (99.999 %) Pb, using the data reported recently by Roberts [217], and were found to agree well with the values of Crisp et al [218]. In addition to this the TEP of Cu above 90 K joins smoothly the data below 90 K where Y-Ba-Cu-O is superconducting and the measurements yields the absolute TEP of Cu directly. This absolute TEP of Cu was used to correct and calculate the absolute TEP of the samples under investigation. In the case of high-temperature studies, Pt has been opted as thermopower reference leads. The absolute TEP of Pt was used to correct and calculate the absolute TEP of the sample.

2.13 Dielectric Constant

Figures 2.2-2.4 shows the sample holders used for dielectric constant and loss measurements of the samples below room temperature. A teflon spacer, whose diameter is much less than, and the thickness about the same as that of the sample has been used to determine the effective capacitance of the sample. For further comparison, a micrometer cell (Fig. 2.9) was used to measure the capacitance of the sample accurately at room temperature (RT). The samples for dielectric constant measurements were flat discs having a diameter smaller than those of electrodes by at least twice there thicknesses, to avoid the need for edge corrections. This procedure of measuring dielectric constant is preferable as it eliminates the errors due to edge capacitance and stray capacitance due to leads etc. The

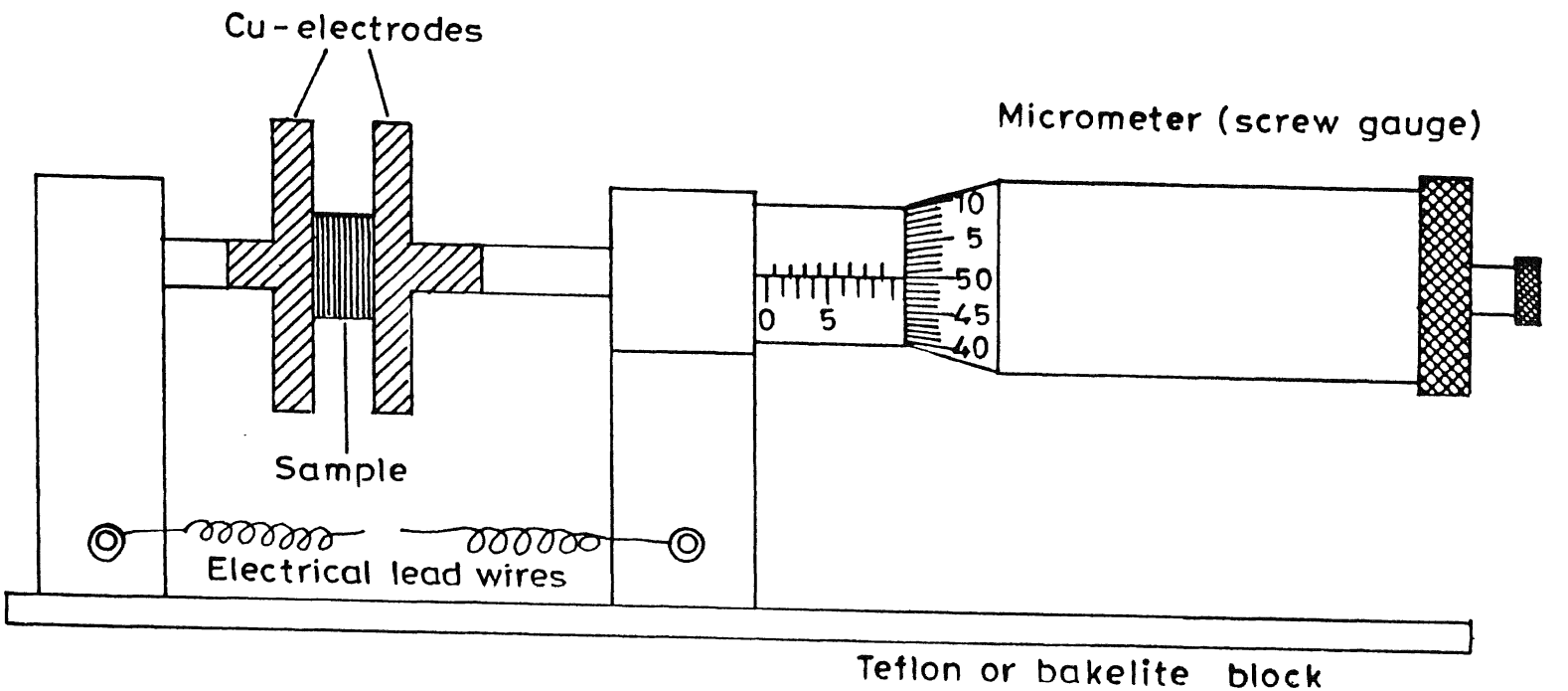

Fig. 2.9. Micrometer cell for accurate RT capacitance measurement.

capacitance measurements in general were more accurate in the frequency range 1 KHz-1 MHz. HP-4192A was used for this purpose. The real part (ϵ_r') of the complex dielectric constant $\epsilon_r^* = \epsilon_r' - j\,\epsilon_r''$ was calculated from

$$\epsilon_r' = (\Delta C_p\ t/A_s\ \epsilon_o) + 1\ , \qquad (2.6)$$

where ΔC_p is the difference between the capacitances (parallel mode) of the assembly with and without sample, t is the thickness of the sample, A_s is the area of the sample and ϵ_o the permittivity of free space.

Figure 2.10 shows the general sample holder used for two-probe resistivity and capacitance measurements above room temperatures. The lava/pyrophyllite discs, which can be moved smoothly along the two parallel stainless steel (ss) rods, in combination with the spring and the quartz tube applies uniform pressure to ensure a firm contact between the electrodes and the sample. The length of the sample holder is such that the spring is located outside the furnace so that it can maintain its spring constant. Pt discs/foils are used as electrodes. Silver or platinum wires welded at the back of the electrodes served as electrical lead wires. A chromel versus alumel (Type K) or Pt versus Pt-13% Rh (Type R) thermocouple is used to monitor the temperature. The reference junction is kept in an oil bath whose temperature is constantly monitored to make corrections for variation in the room temperature.

CHAPTER 3

STUDIES ON CuO

3.1. Introduction

In most of the HTSCs discovered so far, CuO is an essential ingredient. Its substitution by any other salt severely affects the T_c. Besides, the Cu-O assembly is believed to be responsible for the superconductivity, and the main contribution to the density of states, DOS (E_F), comes from the Cu 3d and the O 2p hybridization states. The role of Y and Ba is understood to be supportive; their presence helps stabilize the structure and the charge transfer mechanism between the Cu sites. Among the transition metal mono oxides (TMO) MnO, FeO, CoO, NiO, CuO, etc., CuO is a rather poorly studied compound. The band model of solids predicts that the materials with incompletely filled 3d shells should exhibit metallic-conductivity. However, the above oxide materials in their stoichiometric forms are as good insulators as Cu_2O which has a completely filled 3d shell. In general, the microscopic origin of their insulating nature and their inter-atomic magnetic coupling is not clear. When there are less than ten electrons, their distribution among the d orbitals is such that some electrons remain unpaired and a net spin moment results. This experimental fact, inferred from the optical absorption and magnetic moment measurements, supports the point of view that the unpaired electrons in the transition metal ions are essentially localized.

The variability in valence and hence in possible coordination polyhedra increases the variety of geometries that Cu-based compounds can have, but has also turned out to be critical in allowing the accommodation of nonideal oxygen stoichiometries. Because of the energetics of copper's outer shell in its 2+ state, oxygen atoms at two opposite corners of the octahedron will always be farther from the Cu than O atoms at the four other corners. This structural distortion, known as the *Jahn-Teller effect*, is what first led Bednorz and Müller to focus on Cu-O as possible superconductors. This effect suggests that the electrons interact strongly with the positions of Cu and O atoms in the crystal lattice, an interaction considered very important for the occurrence of superconductivity.

Obviously a thorough understanding of the basic properties of CuO is extremely important in order to (1) understand the HTSC better and (2) identify equivalent (oxide) materials to develop new possible HTSCs. When this work was initiated in 1988, the available studies on CuO were few and far between. These include resistivity [219], magnetic susceptibility [220,221], and optical studies [222]. However, soon after the discovery of HTSCs and while this work was in progress, several reports dealing with antiferromagnetic transition [223], presence of twin boundaries [224], optical [225], neutron scattering [226], magnetic susceptibility [227-229], microwave [230,231], and specific heat [232], etc., on CuO have appeared. In the next section, the properties of CuO are briefly reviewed, and in the following section the results of our own investigations on CuO are presented.

The next three chapters, viz, the 4th, 5th, and 6th deal with pure $YBa_2Cu_3O_{7-\delta}$ system and systems with defects involving chemical substitutions at the various sites in the structure of Y-Ba-Cu-O and (Bi, Pb, Sb)-Sr-Ca-Cu-O superconductors.

3.2. Properties of CuO and their Relevance to HTSC

Structurally CuO consists of CuO_4 clusters which are basic structural elements of a wide range of high-T_c cuprate superconductors. For this reason, CuO can be thought of as a sort of model system for studying the semiconducting phase of the corresponding superconductors. CuO has a monoclinic lattice with the cell parameters a=4.683 A° ; b=3.422 A° ; c=5.128 A° ; β=99.54 ; y=0.416. According to neutron diffraction, CuO is an antiferromagnet with an intermediate helicoidal structure at $T_{N2} \simeq 212\ K \leq T \leq T_{N1} \simeq 230\ K$ and a collinear structure at $T<T_{N2}$. At high temperatures, $T>T_{N1}$, CuO has reduced - dimensionality spin correlations.

In pure CuO, both Cu and O compete for the lone electron, but the oxygen "wins" mostly because a filled oxygen orbital is a slightly more stable configuration than a filled outer copper orbital. Thus, bonding between nominal Cu^{2+} and O^{2-} has both ionic and covalent character and involves the Cu 3d and O 2p orbitals. If copper oxide is doped with other elements, the delicate energy balance can be shifted, so that Cu and O can share electrons to complete their outer shells. This sharing of electrons forms a "covalent" bond between copper and oxygen. Because the electrons are now free to move between the Cu and O atoms, materials containing copper, oxygen, and other elements

can be good conductors. Hence, the properties of CuO may be varied from insulator to semiconductor to semimetal to metal and to superconductor. Copper can donate 1,2, or 3 electrons in a chemical bond with oxygen. The most stable of the three valence states is 2+. Hence, the 1+ state (found, for example, in Cu_2O) is called "reduced" Cu and the 3+ state (found, for instance, in $NaCuO_2$) is known as "oxidized" copper.

The Cu-O distance in copper oxide is 1.95 A° ; This cluster is also the basic structural unit of the CuO_2 planes of the high-T_c compounds, having comparable Cu-O distances: 1.89 Å in the La-Sr and 1.96 Å in the Y-Ba copper oxide compounds. This indicates also that the transfer integrals and hybridizations are comparable. The important difference is, in CuO, the clusters are connected via their sides to form a ribbon, whereas in the high-T_c compounds the clusters are connected via each of their corners to form a plane. This might cause some differences in polarization and screening effects in the lattice, etc.

Figures 3.1 and 3.2 show the phase diagrams for cuprates. Starting with an insulating, long-range ordered antiferromagnet, the ordering (Neel) temperature (T_N) drops rapidly when the carrier concentration per CuO_2 is changed. Transition occurs to an insulator with only short-range magnetic order (and a spin-glass ground state), to a metal with a superconducting ground state, and finally to a normal metal. The two classes of magnetic insulators are: Mott insulators and Heisenberg magnets. The Mott insulators order antiferromagnetically below the T_N and undergo a transition to the metallic phase at T_N. The Heisenberg magnets are insulating in both the antiferromagnetic (AFM) and

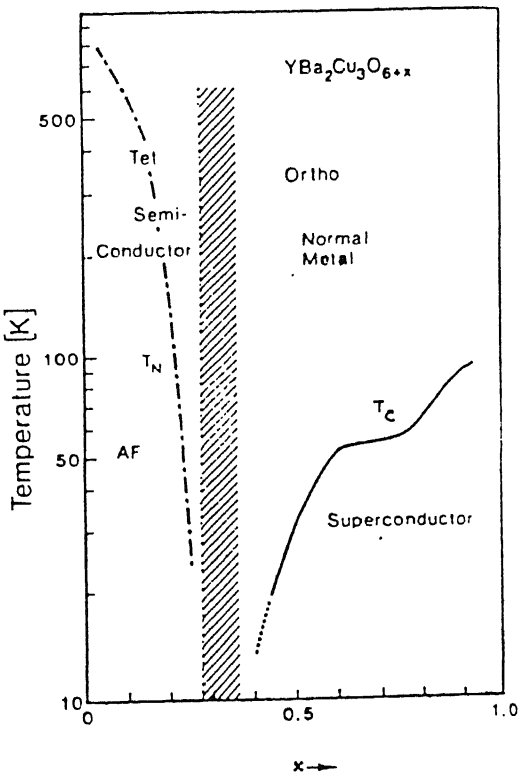

Fig. 3.1 Phase diagram for the system $YBa_2Cu_3O_{6+x}$.

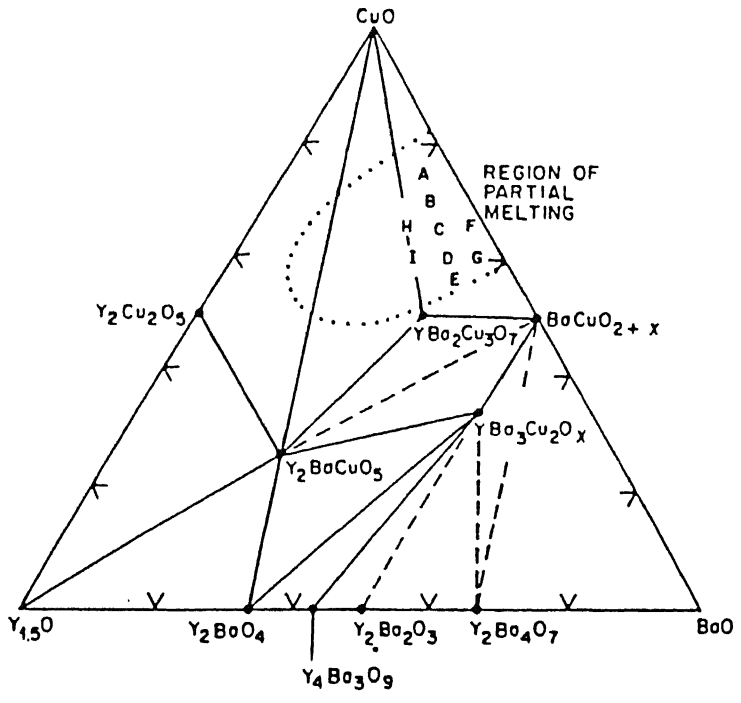

Fig. 3.2 Ternary phase diagram for Y-Ba-Cu oxide.

the paramagnetic temperature regimes. Between simple metals and magnetic insulators is a regime in which spectacular metal-insulator transition takes place (eg. V_2O_3). This metallic phase, which under relatively small changes in either temperature, alloy composition, or pressure transforms into a Mott insulator, is called an "almost localized" Fermi-liquid.

The study of the entire area of transition-metal compounds (mainly oxides) has gained enormous interest since the discovery of HTSCs. The critical point for these systems is that the parent compounds are AFM insulators (e.g. CuO, La_2CuO_4, Nd_2CuO_4, $YBa_2Cu_3O_6$, etc.). The presence of AFM ordering may prove to be as important as the isotope effect in classical superconductors.

Defects and thermodynamic instability play a major role in oxide superconductors. High defect concentrations are common in oxide superconductors, especially those with the highest T_c's. At high temperatures, defects may be thermodynamically stable due to their entropy contribution to the overall free energy of the phase. Thus, broad ranges of solid solutions may be thermodynamically stable at high-temperatures. At equilibrium, at low-temperatures, however, solid solubility is eliminated, and only the end-member compounds and possibly intermediate compounds of fixed composition remain. Defects can also destroy superconductivity in copper oxide compounds that would otherwise be superconducting. The defects are oxygen atoms that can occupy, in a random or ordered way, available lattice sites in the chain region of the structure, allowing the properties to be varied from insulating to superconducting.

Many metals M are known to alloy substitutionally with Cu over a wide solubility range and to add or subtract electrons from the Cu conduction band. Thus, it is of interest to study the effect of such alloying on $YBa_2Cu_{3-X}M_XO_{7-\delta}$. Perhaps the most widely studied are defects involving chemical substitution at the various sites in the structure, for example, Fe, Co, Ni, Zn etc., on the Cu sites in $YBa_2Cu_3O_{7-\delta}$, and Pr on the Y site. Such deliberately created defects have been useful as probes of the properties of the Cu-O superconductors. Also, understanding such defects can guide our search for new superconducting compounds.

In general, one still has to understand the synthesis of metastable and highly defective structures, the measurements on highly anisotropic crystals, the properties of grain boundaries, and so on. *Thus, there must be a systematic study of metallic oxides, non-superconducting oxides, and superconducting oxides.* Investigation of the metallic oxide systems, with structural arrangement similar to their superconducting counterparts, could lead to mechanistic and structural insight into the behavior of the superconducting materials.

The following section 3.3 reports our results on resistivity, TEP, dielectric constant, and EPR, and brings out the anomalous behavior of CuO.

3.3. Studies on CuO

The sample preparation and other experimental details have been given in Section 2.2. The four-probe electrical conductivity measurements on CuO were carried out using evaporated silver and gold (point) electrodes in the temperature range 140-1200 K.

Below 140 K the resistance becomes too high to be measured accurately. The log σ versus $10^3/T$ plots (Figs. 3.3 and 3.4) exhibit several distinct linear regions as indicated below:

$\sigma = A_1 \exp(-0.25\ eV/kT)$: 140 - 230 K

$\sigma = A_2 \exp(-0.14\ eV/kT)$: 230 - 400 K

$\sigma = A_3 \exp(-0.08\ eV/kT)$: 400 - 800 K

$\sigma = A_4 \exp(-0.71\ eV/kT)$: 800 - 1200 K

The conductivity of CuO is $\sim 5\times10^{-3}\ \Omega^{-1}cm^{-1}$ at room temperature. The four linear regions in Figures 3.3 and 3.4 are associated with activation energies of 0.25, 0.14, 0.08, and 0.71 eV, respectively, from low- to high-temperatures. The log σ versus 1000/T plot (Fig. 3.3) shows a change in slope at ~230 K. This indicates some sort of phase transition at ~230 K. It should be pointed out that the magnetic susceptibility studies have also revealed a transition at ~230 K which is attributable to antiferromagnetic (AFM) ordering in CuO. This anomaly at ~230 K is also observed in some of the non-superconducting and high-temperature superconducting cuprates. For such systems it is generally agreed upon that the one-electron band theory is inadequate to describe the ground-state electronic structure. This temperature T=230 K corresponds to the Neel transition temperature (T_N). Below this temperature ($T<T_N$) the material is antiferromagnetic, and above T_N ($T>T_N$) the material undergoes a

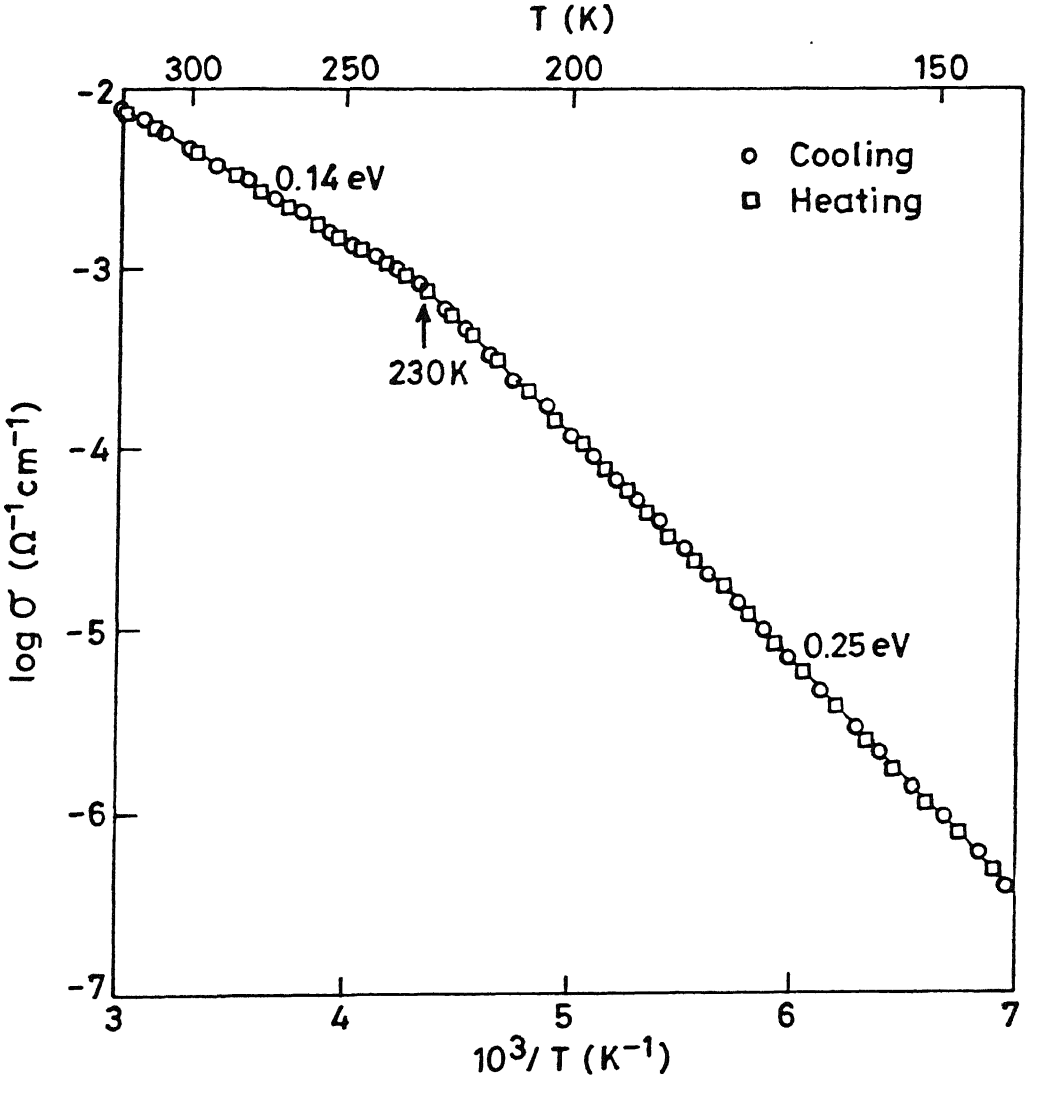

Fig. 3.3. Log σ versus 1000/T plot of CuO at low-temperatures.

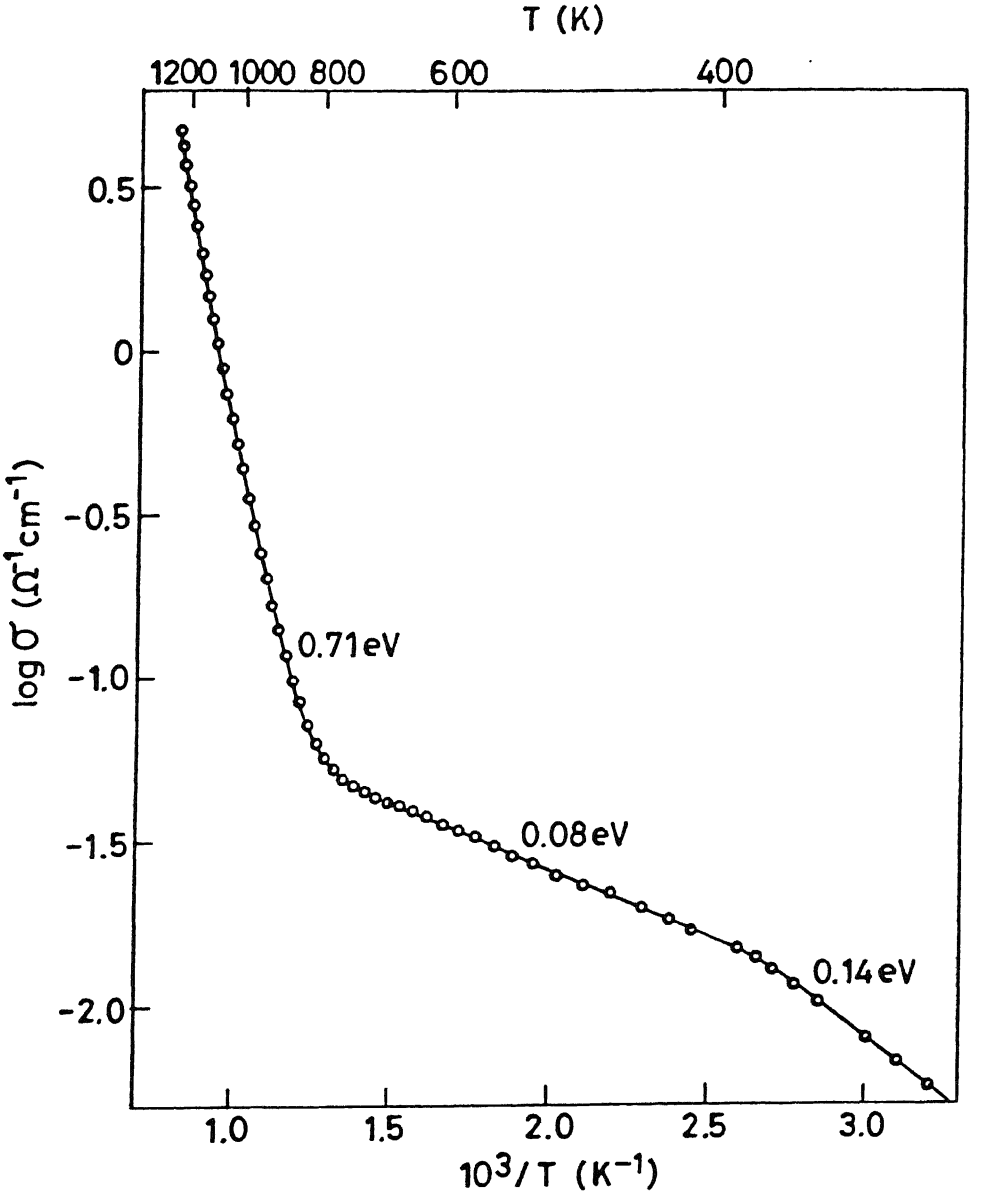

Fig. 3.4. Log σ versus 1000/T plot of CuO at high-temperatures.

different (paramagnetic) phase transition. This so called paramagnetic regime is complex in the sense that it does not display any EPR signal around g=2 (paramagnetic ion would generally give rise to Cu^{2+} EPR signal around g=2).

In fact, the as-received high-purity CuO has no Cu^{2+} EPR signal around g=2 from 77-400 K, although impure CuO displays Cu^{2+} signal at RT with varying intensity depending on the impurity concentration. Similarly, single-phase $YBa_2Cu_3O_{7-\delta}$ with optimal oxygen composition, has no Cu^{2+} EPR signal near g=2, because it has no curie moment, although multiphase Y-Ba-Cu-O gives Cu^{2+} EPR signal of varying intensity depending on the concentration of the impurity phase. It seems that the effective density of states of the VB is probably influenced by the magnetic transition at the Neel temperature (T_N).

The excellent agreement between the heating and cooling data (Fig. 3.3) and the complete lack of any hysteresis suggests that the stoichiometry (Cu/O ratio) remains undisturbed over the temperature range of investigation. The activation energy in the intrinsic region at high-temperatures, yields a band gap of 1.42 eV for CuO which is in very good agreement with the values deduced from other techniques. Also, this value of band gap is close to that of the insulating high-T_c compounds (1.6-2.0 eV). This indicates that the on-site energy difference between the Cu 3d and O 2p states for both compounds is quite similar.

Figure 3.5 Shows the plot of thermoelectric voltage (ΔV) versus the temperature difference (ΔT) across the sample. The linearity of the plot shows that the thermoelectric power ($S = \Delta V/\Delta T$) can be measured by varying the ΔT across the sample from 2

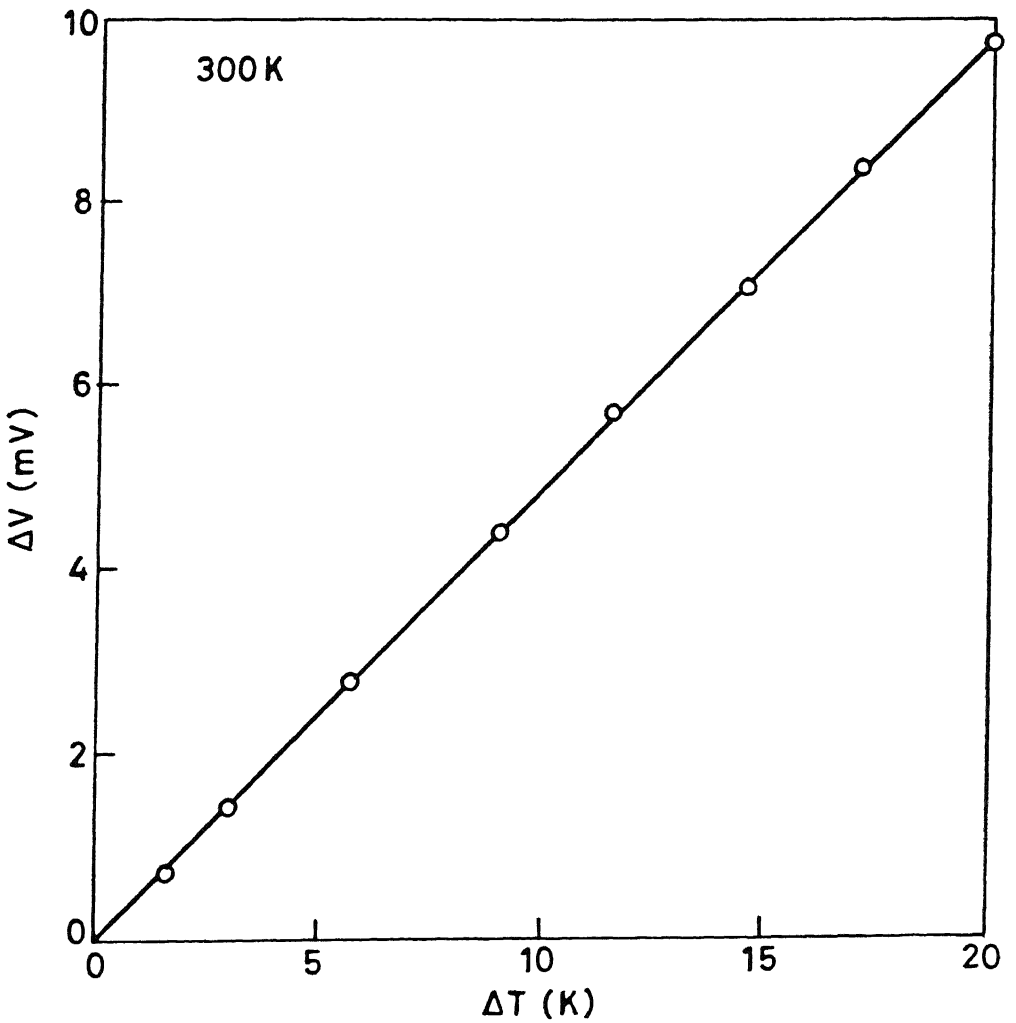

Fig. 3.5. Plot of thermoelectric voltage (ΔV) versus the temperature difference (ΔT) across the sample.

to 20 K without much affecting the accuracy. Figure 3.6 shows the plot of S versus 1000/T for CuO in the temperature range 160-1000 K. The value of S is ~480 μV/K at room temperature. It is to be noted that the S versus 1000/T plot also exhibits a slope change around 230 K. Moreover, here also there are four distinct regions. These results are consistent with the conductivity versus temperature behavior. The positive sign of the TEP suggests that CuO is a p-type (hole type) semiconductor. It may be pointed out that the most HTSC materials also conduct via holes at $T>T_c$. The reported existence of intrinsic hole states at the top of the valence band (VB) is consistent with the observed p-type conductivity. Figure 3.7 shows the behavior of the resistivity and the thermopower versus 1000/T for CuO in the intrinsic region. The negative temperature coefficient and the range of the resistivity, the behavior and magnitude of thermoelectric power, and the value of activation energy in the intrinsic region (0.71 eV) all provide testimony to the semiconducting behavior of CuO.

The observed nature of the optical absorption on thin layers of powdered CuO (Fig. 3.8) suggests that it is an indirect band gap (1.4 eV) semiconductor. This value of 1.4 eV is close to that of the insulating high-T_c compounds (1.6-2.0 eV). This indicates that the on-site energy difference between Cu 3d and O 2p states for both the compounds is quite similar.

Figure 3.9 shows the real part of the dielectric constant (ε_r) versus temperature plot for CuO at various frequencies in the temperature range 100-250 K. The dielectric constant varies from 10 to 700 depending upon the frequency and temperature.

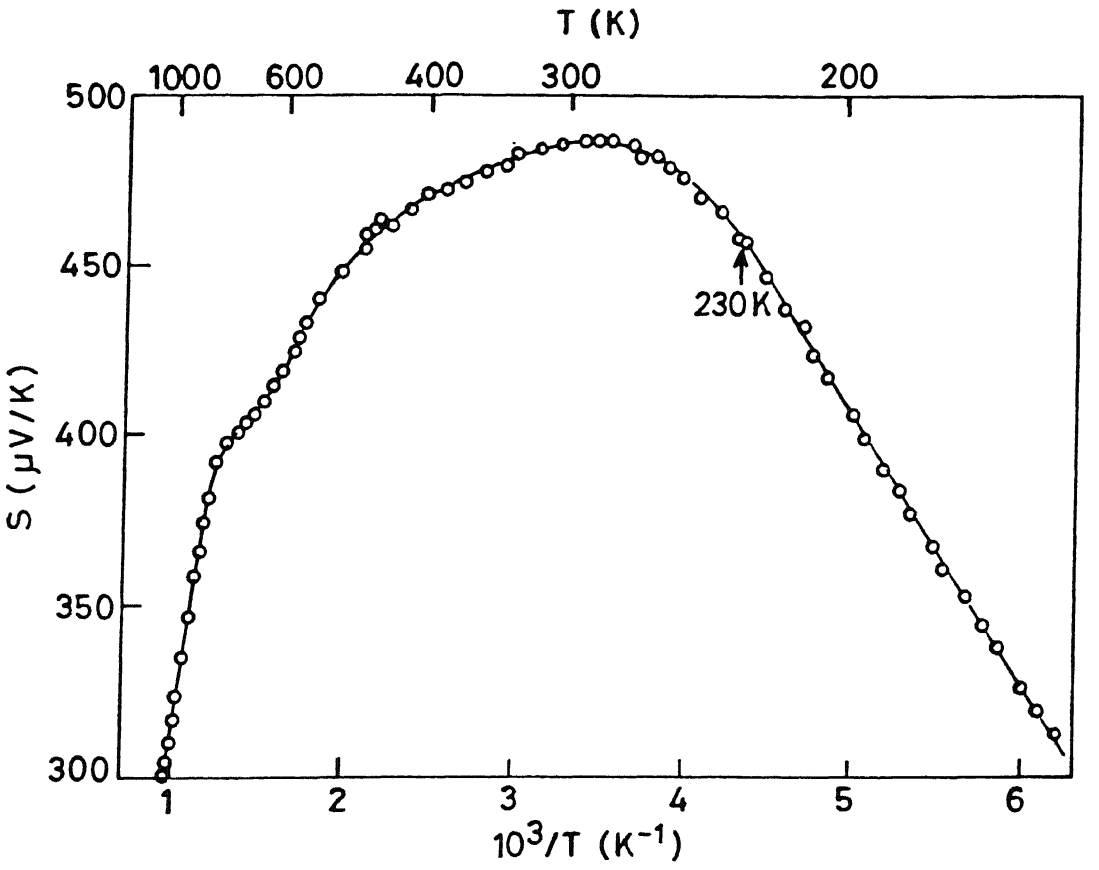

Fig. 3.6. Plot of S versus 1000/T for CuO.

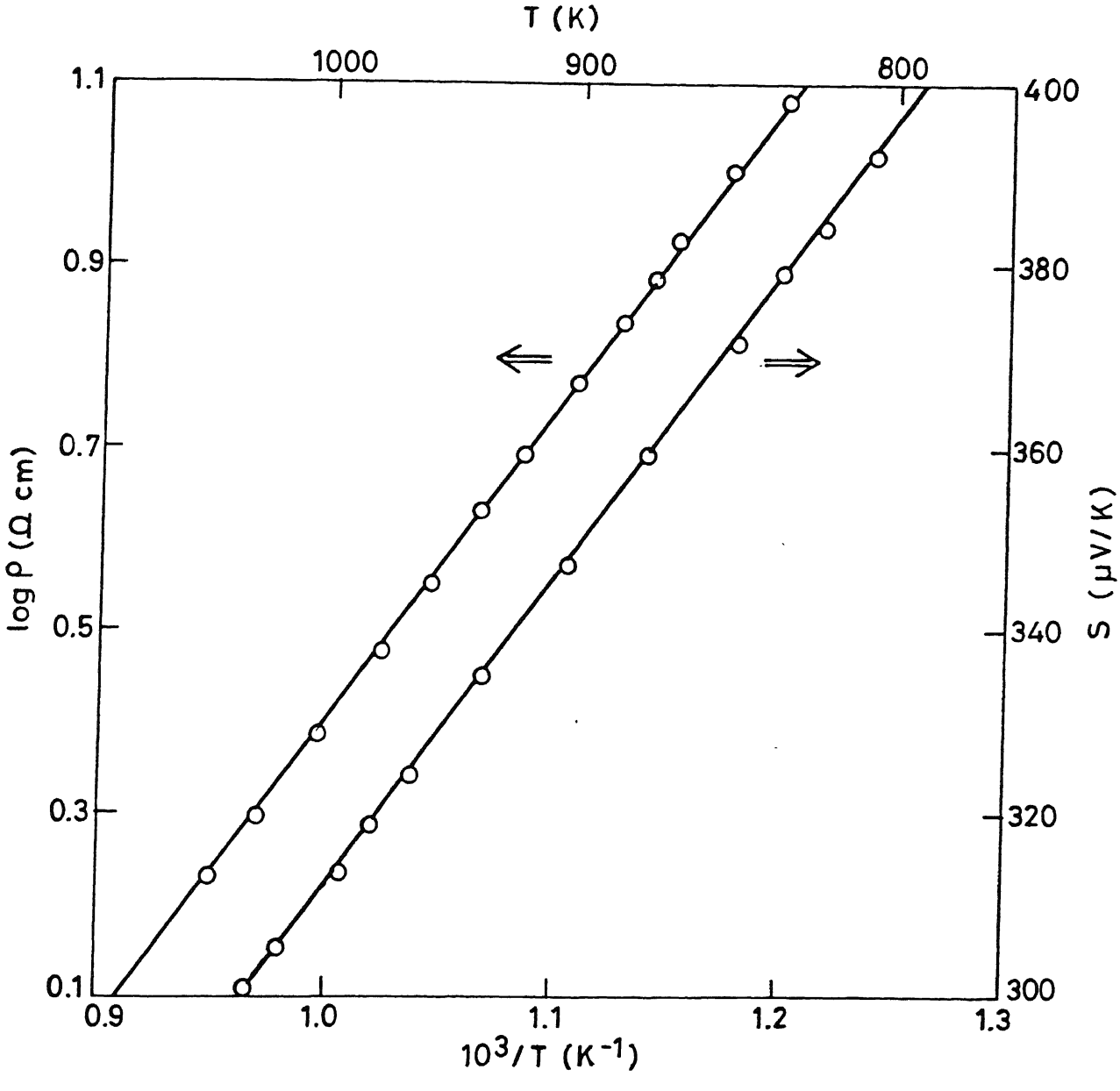

Fig. 3.7. Resistivity and thermopower versus 1000/T for CuO in the intrinsic region.

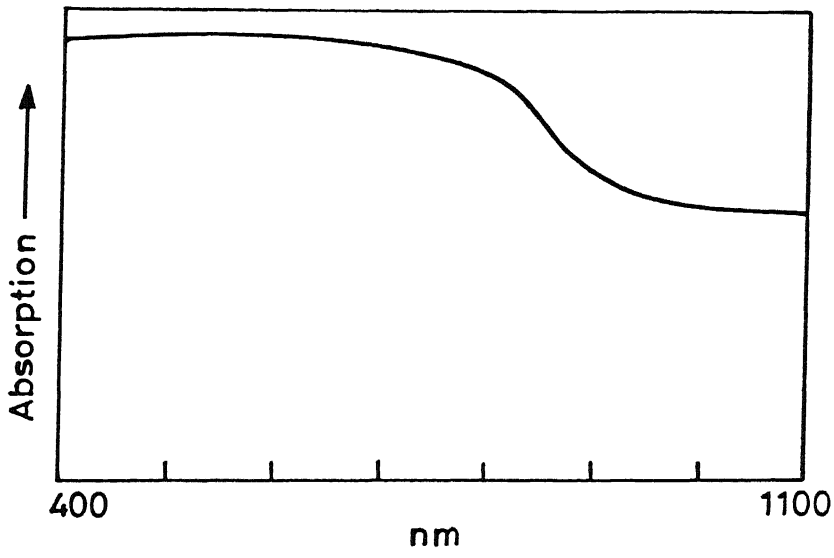

Fig. 3.8. Plot of the absorption spectrum of CuO.

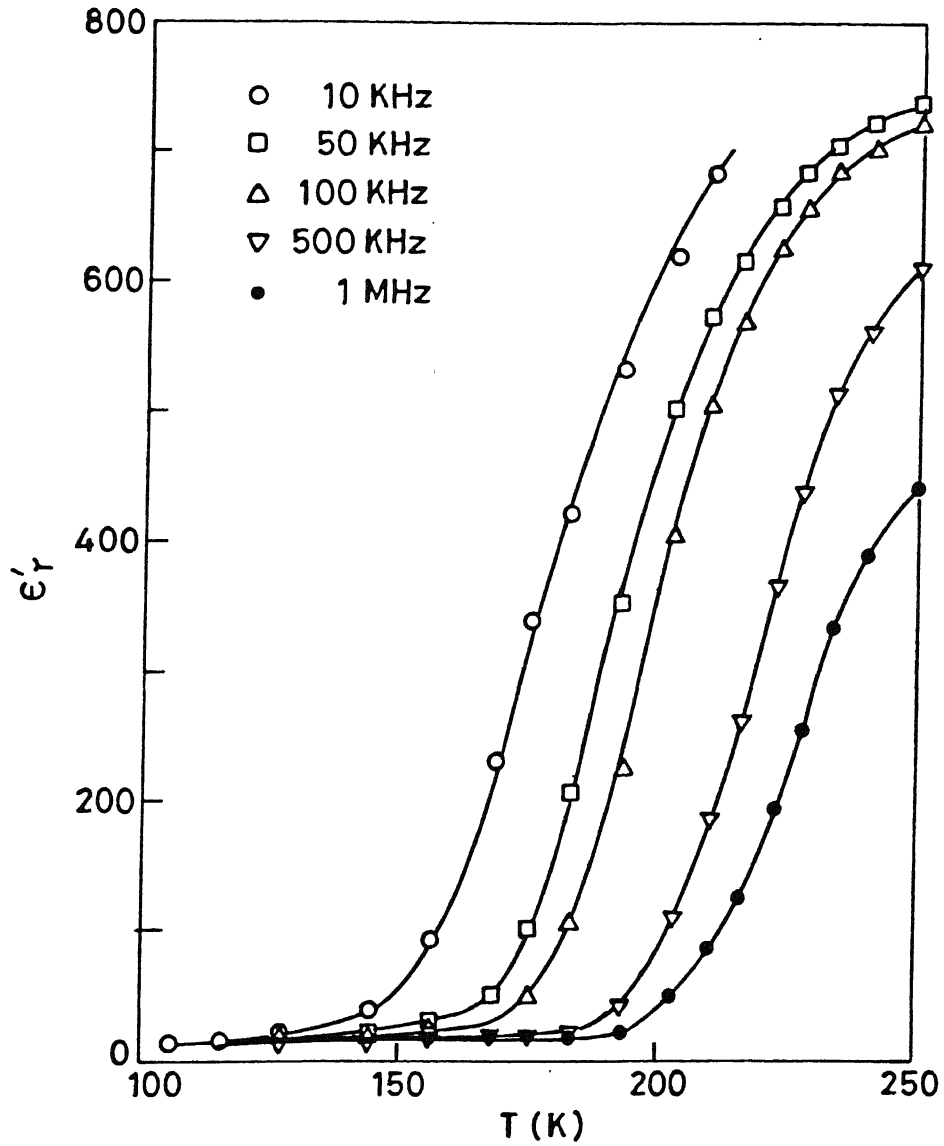

Fig. 3.9. Plot of the real part of the dielectric constant (ε'_r) versus temperature of CuO.

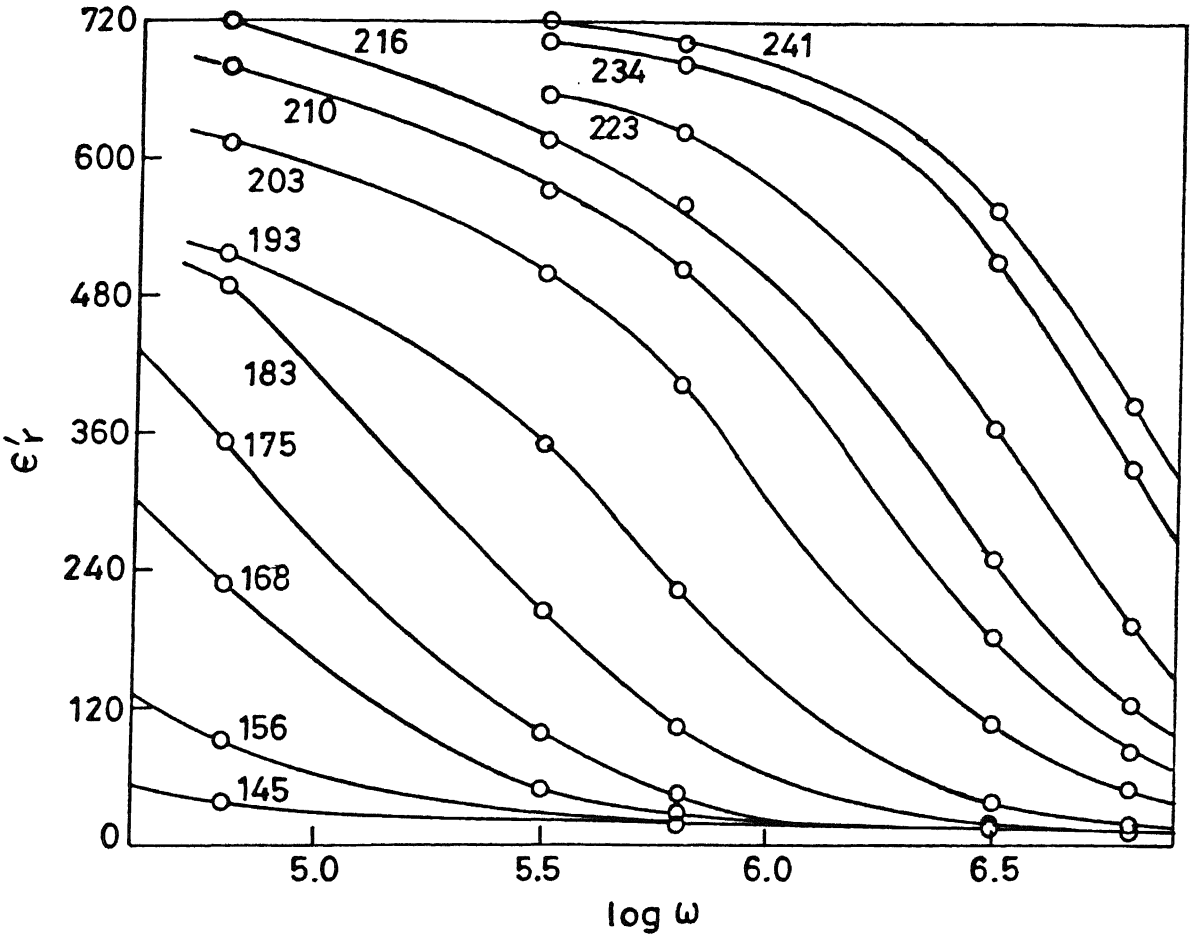

Fig. 3.10. Plot of the real part of the dielectric constant (ε'_r) as a function of frequency.

Figure 3.10 shows the plot of dielectric constant as a function of frequency.

The static dielectric constant (ε_o) of CuO at low temperatures is ~ 10 which is comparable to those of semiconductors such as Si and GaAs (ε_o = 11.5 and 16 respectively). However, the large value of ε_r' at high temperatures and low frequencies is consistent with the anomalous behavior of the resistivity and the thermopower of CuO. The value of dielectric constant is unusually large for a nonferroelectric material. Of course, there is no evidence for a ferroelectric transition in CuO. Since the electronic and ionic polarizabilities cannot account for the observed large values of ε_r', it must be assumed that CuO is a polar semiconductor and that its molecules have a net dipole moment. Figure 3.11 shows the plot of tan δ (loss) versus temperature for CuO. It is noticed that the dielectric loss increases initially as temperature increases (as expected) and then goes through a peak before it starts increasing very rapidly. The observed high value of the dielectric loss is consistent with the high value of conductivity of CuO. Fig. 3.12 shows the behavior of relaxation time τ for dipole relaxation in CuO as a function of reciprocal temperature of CuO. This log τ versus 1000/T shows a linear behavior, as expected.

3.4 Conclusions

In summary, CuO is a p-type semiconductor with an indirect band gap of 1.42 eV. There is evidence for an antiferromagnetic ordering near 230 K. Also there is a large dispersion in the

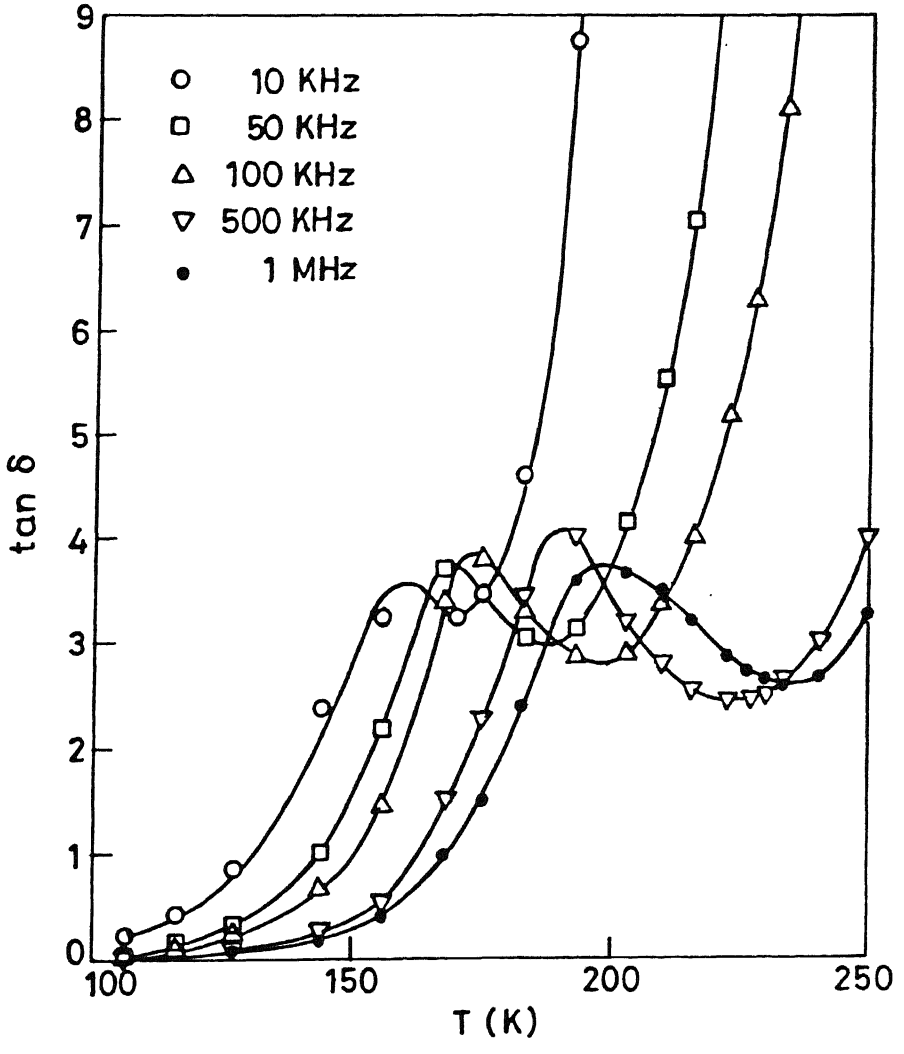

Fig. 3.11. Plot of tan δ (loss) versus temperature for CuO.

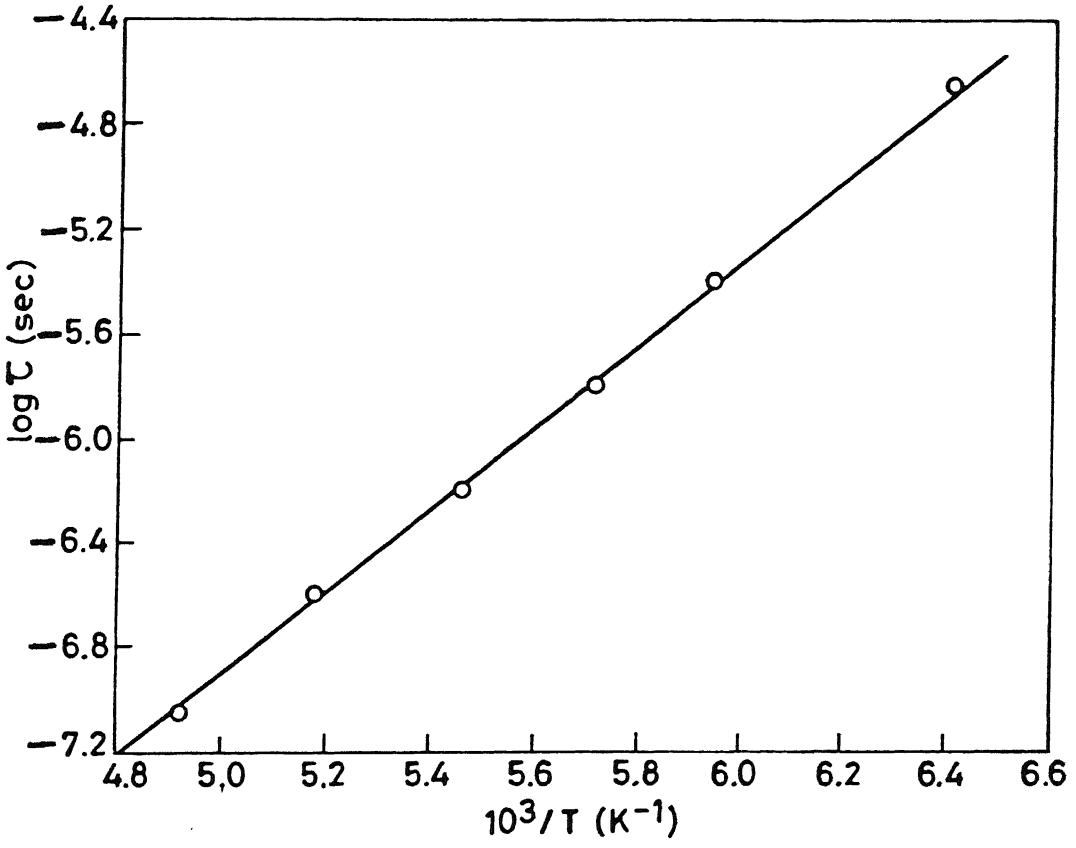

Fig. 3.12. Relaxation time τ for dipole relaxation in CuO as a function of reciprocal temperature.

dielectric constant around this temperature. Anomalies in this temperature region are also reported in χ versus T, neutron diffraction, and specific heat versus T studies. There are reasons to believe that CuO plays an important role in HTSC materials unless the former is present in the latter as a second phase which is ruled out in view of extensive experimental evidence against it. Some of the feature of CuO, for example, the 230 K anomaly in ρ-T, S-T, ε-T curves, the p-type conduction behavior, the large value of ε_r', the EPR silence, and the reported antiferromagnetism at low temperatures, etc., may lead to possible clues to the high temperature superconductivity. Interestingly, some of the anomalies observed in CuO are evidently also present in the CuO based HTSCs, which supports the view that CuO plays a key role in stabilizing the high T_c superconductors.

The band structure calculations show the presence of Fermi surface in CuO, thus resulting in the existence of exactly four intrinsic holes at the top of the valence band (VB). It is interesting to note that the $YBa_2Cu_3O_{7-\delta}$ also has four intrinsic holes at the top of the VB. The existence of intrinsic hole states at the top of the VB is consistent with the reported p-type conductivity in CuO. Although CuO has a Fermi surface and therefore will normally be regarded as a metal, its (static) dielectric constant, ε_0~10 as obtained from the interband optical conductivity data and measured in the present work (Figs. 3.9 and 3.10), is comparable to those of semiconductors such as Si and GaAs (ε_0 = 11.5 and 16, respectively). Thus based on the

magnitude of ε_0 and the behavior of $\rho(T)$ and S (T) curves, CuO should be regarded a semiconductor-like material rather than a metal.

An interesting experimental measurement of resistance in CuO as a function of pressure showed a discontinuous drop of four orders of magnitude at ~390 K at a pressure of 187 kbar, which was not observed in other transition metal oxides. This was explained as being indicative of the occurrence of some type of pressure-induced phase transition in CuO. It is conceivable that at such a high pressure the semiconductor-like gap may collapse, transforming CuO into a normal-metal.

Thus, the interesting anomalous physical and the structural properties (Jahn-Teller effect) of CuO and other insulating phase materials of the high-T_c cuprates such as $YBa_2Cu_3O_6$, La_2CuO_4, etc., suggest that it is difficult to exactly classify them as Mott or Heisenberg insulators (two classes of AFM insulators). However, it does seem that there is some connection between AFM and the superconductivity. Based on the above facts, undoped $YBa_2Cu_3O_{7-\delta}$, Ti, V, and Ni-doped Y-Ba-Cu-O, and (Bi, Pb, Sb)-Sr-Ca-Cu-O systems have been studied and the results are presented in the following Chapters.

CHAPTER 4

STUDIES ON $YBa_2Cu_3O_{7-\delta}$

4.1 INTRODUCTION

Following the discovery of high-T_c superconductivity in the multiphasic Y-Ba-Cu-O system [53] and the subsequent identification of structure and composition of the single-phase responsible for it [54-61], numerous investigations have been carried out to raise the T_c and to improve the superconducting properties. Besides, serious attempts have been made to understand (1) the dimensionality of the system, (2) the electronic structure, and (3) the mechanism of high-T_c superconductivity. Many of the physical properties of the high-T_c oxides have not been well explained. For example, these oxides exhibit some of the following anomalous transport properties in their normal state:

(a) linear temperature dependence of the resistivity (the absence of saturation in the linear $\rho(T)$ behavior).

(b) anomalous temperature dependence of the Seebeck coefficient,

(c) strong temperature dependence of the Hall coefficient, etc.

Some of these anomalous properties, viz, the absence of saturation in $\rho(T)$ plots, the low dimensionality, the anomalous behavior of thermoelectric power (TEP), etc., have of course been to helpful in elucidating the possible mechanisms of HTSC.

Several groups have investigated the resistivity and thermopower both at low- and high-temperatures, and the paraconductivty ($\Delta\sigma$). It is evident from these reports that there

exists a large discrepancy among the results from different laboratories which may be partly attributed to differing qualities of the samples used in their investigations. It is, thus, highly desirable to perform the above measurements at low- as well as at high-temperatures on the same well-processed samples for consistent results. The high-temperature (HT) measurements are expected to yield useful information on the transport mechanisms, and the nature of the ordering transition and its dependence on the oxygen concentration in the materials.

This Chapter reports the results of XRD, SEM, EDXA, DTA, EPR, iodometry, low- and high-temperature resistivity, paraconductivity, and low- and high-temperature TEP measurements in order to elucidate (1) the nearly linear temperature dependence of the resistivity in the normal-state, (2) the nature of the high-temperature orthorhombic-to-tetragonal transition, (3) the other normal-state anomalies, (4) the dimensionality of the system, and (5) the possible mechanisms which give rise to these behavior and the implications of the phenomena to superconductivity.

4.2 RESULTS AND DISCUSSION

4.2.1 XRD, SEM, EDXA, and DTA

The experimental details regarding (1) the sample preparation and (2) the various materials and physical characterization techniques are given in Chapter 2.

The $YBa_2Cu_3O_{7-\delta}$ samples were prepared by the solid-state reaction method as reported in Section 2.2. According to the XRD

analysis, the $YBa_2Cu_3O_{7-\delta}$ samples are single-phase with orthorhombic structure. All the observed peaks were indexed according to Cava et al. [57]. The calculated cell parameters, viz., a=3.820 A°, b=3.885 A°, c=11.670 A°, and V=173.19 $A^{\circ 3}$ are found to be in good agreement with the reported literature values.

The SEM and EDXA analyses also suggest the single-phasic nature of the samples with an average grain size of ~5 μm. The temperature at the endothermal peak in the DTA curve is taken as the decomposition temperature (T_d) of the sample. In this study, the single endothermal peak observed at ~1020°C (in air) suggests that the single-phase nature of the samples.

4.2.2 EPR and Iodometry

The near zero-field strong non-resonant microwave absorption at 77 K signals the superconducting state of the sample. There is no Cu^{2+} resonant absorption signal near g≃2 in the temperature range 77-300 K, suggesting that the Y-Ba-Cu-O samples are of monophase and of reasonably good quality. This EPR-silence also indicates the absence of localized moment on Cu, and also the absence of a highly oxygen-deficient composition as an impurity phase. Indeed, in properly annealed single crystals of Y-Ba-Cu-O, no Cu^{2+} EPR signal is observed, although in unannealed single-phase samples with the optimal oxygen composition it has been suggested that the observed Cu^{2+} EPR signal originates from an impurity phase. The absence of EPR for HTSC cuprates in which the Neel temperature is less than, or comparable to, the

observation temperature also reflects the strong 2D antiferromagnetic coupling within the CuO_2 planes [233].

The oxygen contents of the samples were determined by iodometry [214,215]. The details of the measurements are given in Section 2.8. The value of the oxygen content of Sample 1 is 6.85±0.02 and that of Sample 2 is 6.94±0.02.

4.2.3 Low-Temperature Resistivity

The experimental details of the electrical resistivity measurements are given in Section 2.11. Figure 4.1 shows the variation of the resistivity with temperature for the two varieties of the $YBa_2Cu_3O_{7-\delta}$ samples. Thè ac four-probe ρ-data (not shown in Fig.4.1) measured in the frequency range 1-100 KHz were, within the experimental error, in good agreement with the dc values. All the samples are characterized by a linear temperature dependence of resistivity from at least $2T_c$ to room temperature, and by a smooth rounding off above T_c which is a characteristic of superconducting thermodynamic fluctuations. Here T_c is defined as the temperature at which $d\rho/dT$ versus T plot shows a maximum, or ρ versus T plot has its inflexion point. This $T_c=T_{cI}$ will be used in the paraconductivity analyses (see Section 4.2.4) as the mean-field critical temperature (T_{co}), as justified by Veira et al. [234].

While the samples marked 1 have considerable extrapolated residual resistivities $\rho(0)$, the samples 2A and 2B have extrapolated intercept that approaches the origin (ρ~0) at T=0. The small values of $\rho(o)$ indicate that the samples 2A and 2B are of high-quality and contain very few defects, i.e., δ in

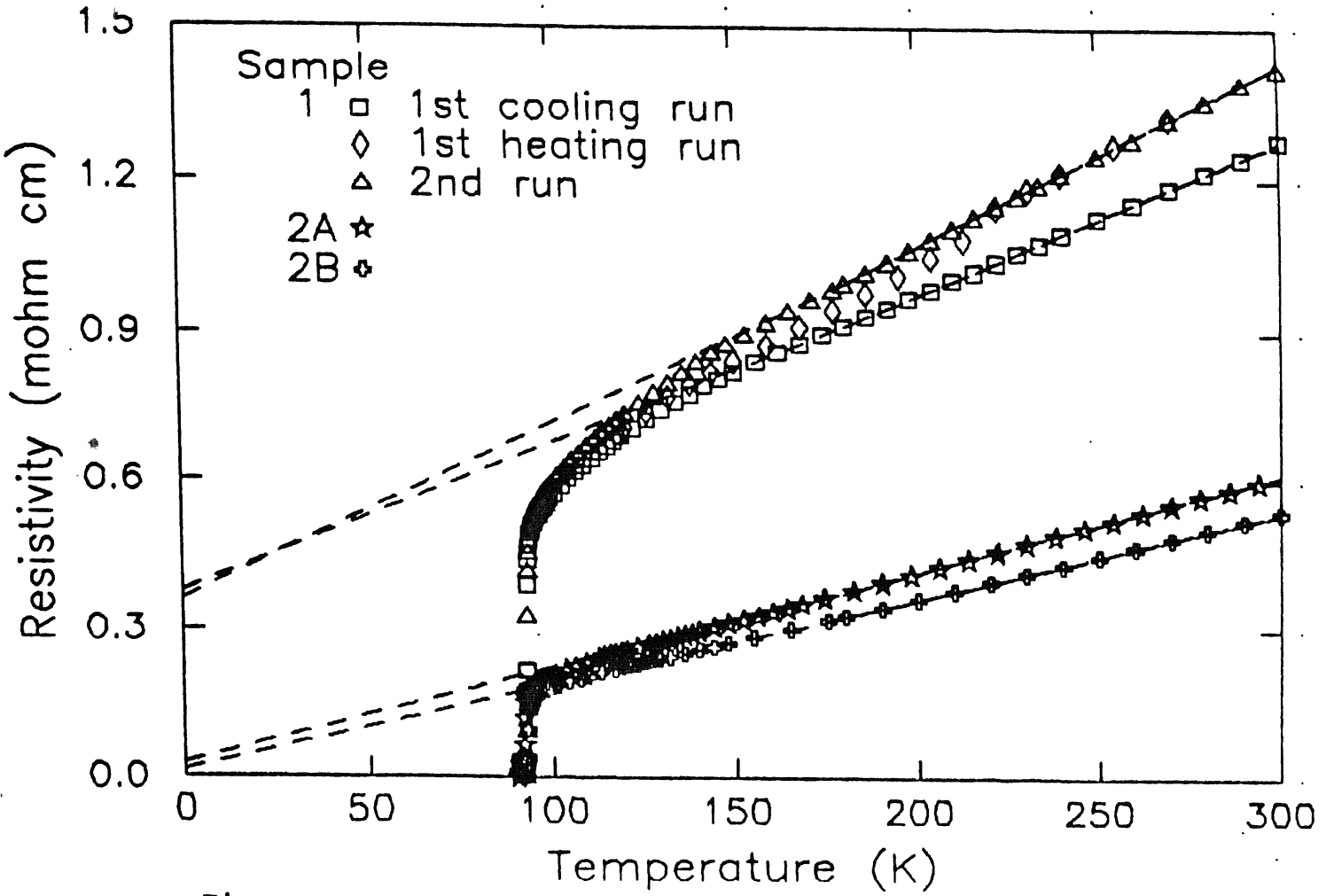

Fig. 4.1. Temperature dependence of the resistivity of three samples of $YBa_2Cu_3O_{7-\delta}$ with different room temperature resistivities. An anomaly is seen at around 220 K in sample 1. The dashed lines are the noncritical normal resistivity fitted to the form a+bT.

$YBa_2Cu_3O_{7-\delta}$ approaches zero [140,141]. When the linear part of the $\rho(T)$ is extrapolated to zero temperature (T=0), typical high-T_c samples show a positive residual resistivity, $\rho(0)>0$. This is usually attributed to electron-impurity interaction. Experiments also reveal that quite a few high-T_c samples unexpectedly show negative residual resistivity. Furthermore, it has been reported that for high-quality samples of Y-Ba-Cu-O, the linear ρ versus T plots have an extrapolated intercept that approaches the origin (ρ = 0 at T = 0). The origin of the difference in signs and magnitudes of the extrapolated resistivity at 0 K in the high-T_c samples is not yet well understood. It is expected that the normal-state resistivity of these oxides is essentially caused by both phonon and impurity scattering. The impurities may be regarded as charged-oxygen vacancies (or defects) in the oxide compounds. The charge carriers will be considered as fermions (electrons or holes) or bosons, respectively, corresponding to a different mechanisms for the high-T_c superconductivity.

The samples marked 1 not only have higher resistivity at all temperatures and higher values of temperature coefficient of resistivity (see Fig. 4.1), but also the ρ-data are not very reproducible; the ρ-data in the first cooling run differs from that in the first heating run leading to an apparent anomaly at ~220 K. The ρ measurements in subsequent cooling and heating cycles are, however, quite reproducible, suggesting perhaps that some kind of phase transition takes place at ~220 K. It should be noted that this is the first report in which an anomaly in the ρ versus T behavior has been observed. Nevertheless, the evidence

for existence of such an anomaly in Y-Ba-Cu-O is also recorded in an ultrasonic study by Toulouse et al. [235]. A detailed study on pure CuO (see Section 3.3) suggests that the 220 K anomaly observed above is, in some way, related to the Cu-O in Y-Ba-Cu-O structure and is probably of magnetic origin [236]. Further it should be pointed out that the resistivity data on samples 2A and 2B are quite reproducible in the heating and cooling cycles. These results, especially on Samples 2B, could be interpreted to mean that it is not just the value of δ, but also the oxygen ordering (occurring at very slow cooling rate at the time of sample preparation) plays an important role in these samples [237,238].

The room temperature resistivities, ρ(300 K), of the Y-Ba-Cu-O samples prepared differently range from 0.5 to 1.5 mΩ cm. The error in the determination of the absolute resistivity values is ±10% and is mainly due to the uncertainty in the correction terms related to sample geometry. The $d\rho/dT$ values in the normal linear region vary from 1.7 to 3.5 $\mu\Omega$ cm K^{-1}. Various transport parameters including ρ(300 K), ρ(100 K), $d\rho/dT$, etc. are listed in Table 4.1. These results are in good agreement with those of Cava et al. [57]. In fact, it would seem that the ceramic samples having densities in excess of 90% of the theoretical value, highest T_c's and sharp transitions, all have similar values of ρ(300 K) and $d\rho/dT$ [137]. All the three types of samples (viz, 1, 2A and 2B) investigated in this work show very sharp transitions (~92.5 K) with a transition width, ΔT_c, provided by the width of the peak in the $d\rho/dT$ versus T curve at half height (unambiguous method), ≤ 0.4 K (Fig.4.2.) which is

TABLE 4.1. Some resistivity parameters of $YBa_2Cu_3O_{7-\delta}$ samples.

sample	ρ(300 K) ($\mu\Omega$ cm)	ρ(100 K) ($\mu\Omega$ cm)	ρ(0 K)[a] ($\mu\Omega$ cm)	dρ/dT ($\mu\Omega$ cm/K)	Tc (K)	ΔTc[b] (K)	AZ-fit A (mΩcm K)	AZ-fit B ($\mu\Omega$cm/K)
1	1424	598	363	3.5	92.8	0.3	42.5	4.3
2A	612	206	28	1.9	92.1	0.4	3.1	2.0
2B	537	182	14	1.7	93.0	0.3	1.6	1.8

[a]Extrapolated residual resistivity.

[b]Full Width at Half Maximum (FWHM) of the dρ/dT versus T graph.

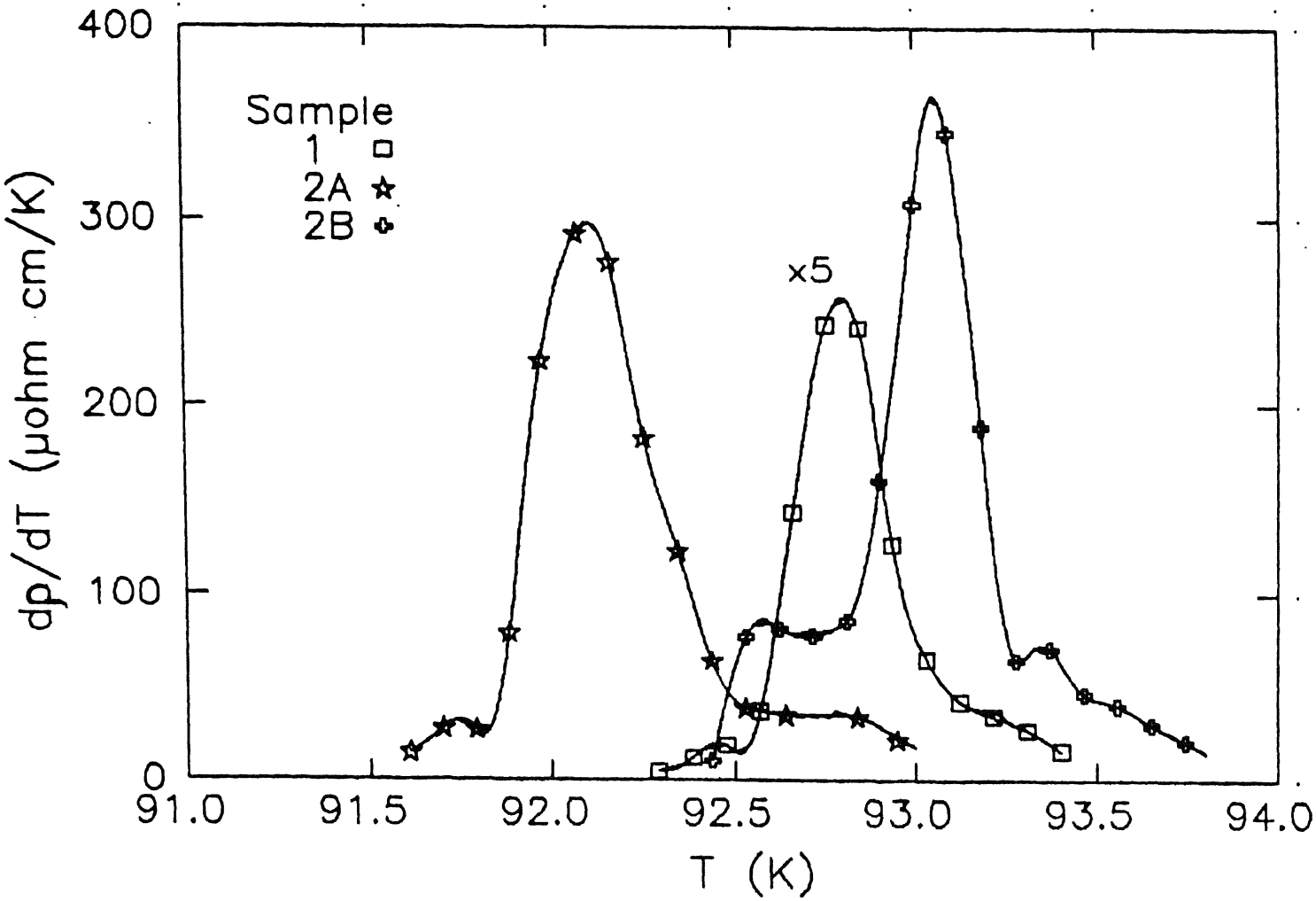

Fig. 4.2. Plot of (dρ/dT) vs. T for samples 1, 2A and 2B. The transition widths (measured at half height) are ≤ 0.4 K.

comparable only to those found in some of the best pc [110] Y-Ba-Cu-O samples. A plausible explanation for the sharp drop in ρ at T_c, i.e., for the narrow transition width (ΔT_c), may appear to be the existence of percolative path which first becomes superconducting, thereby shorting out the current. However, this is ruled out in view of the absence of any non-ohmic behavior and the presence of a single, well-defined peak in $d\rho/dT$ versus T graph.

Although a polycrystalline (pc) sample consists of randomly oriented crystallites, due to anisotropy the low in-plane resistivity will dominate in the equivalent parallel resistor network. Thus in a dense, good-quality polycrystalline sample, the resistivity should essentially have the same behavior, and hence yield the same type of information, as does the ρ_{ab} in a single crystal (sc) study. To test this further, Anderson-Zou (AZ) analysis is applied to our ρ-data in the normal-state. According to these authors the normal-state ρ is given by

$$\rho(T) = A/T + BT \qquad (4.1)$$

where the hyperbolic term is introduced to model the inter-plane hopping of the charge carriers. Figure 4.3. shows a replot of the ρ-data in the form ρT versus T^2 which is linear over most of the investigated temperature range. The values of constants A and B (eq.4.1) determined from these linear plots are also listed in Table 4.1. These values are in good agreement with those found by Anderson and Zou [187] using the single crystal data of Tozer et al. [131], which implies that the resistivity behavior in dense,

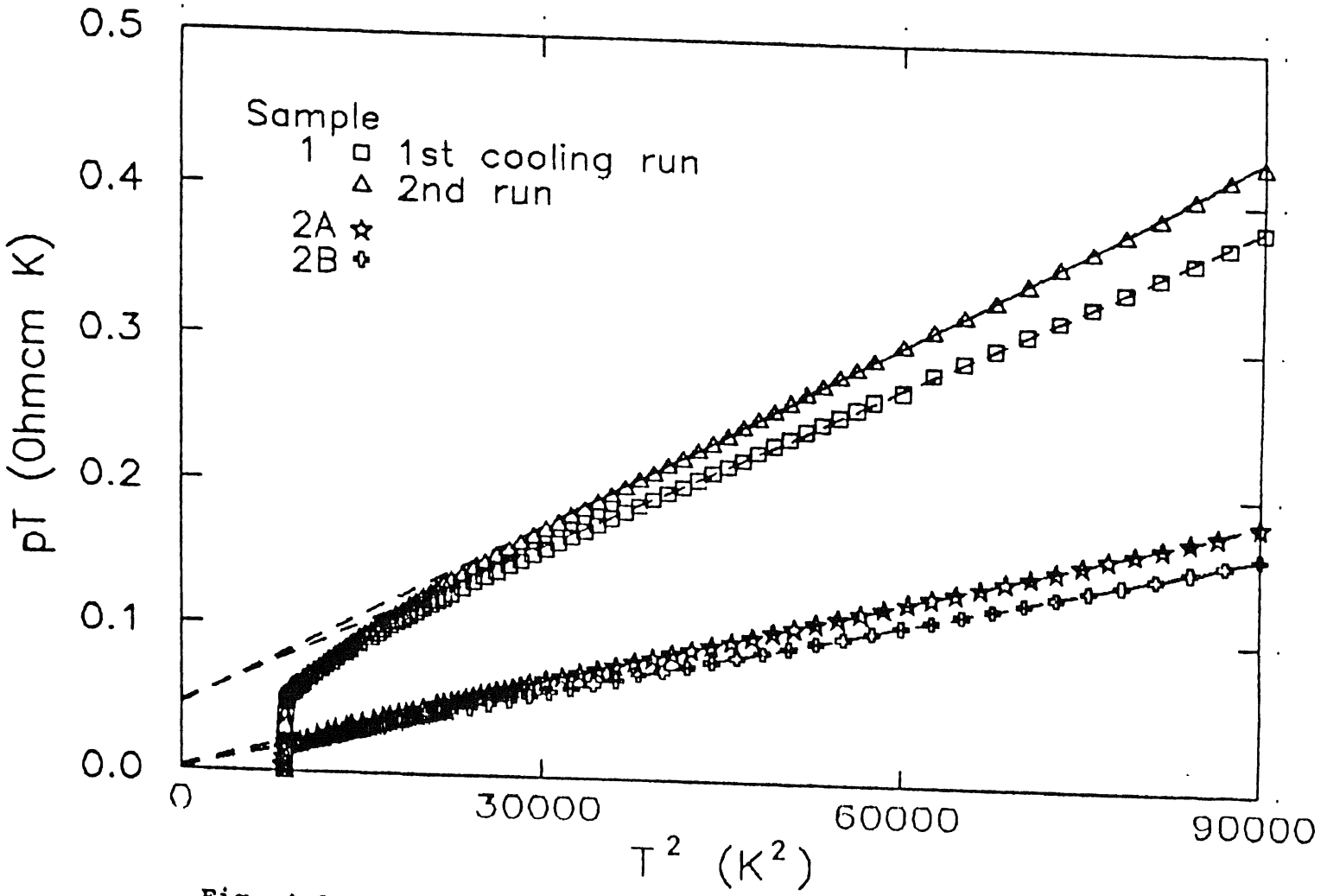

Fig. 4.3. Anderson-Zou plot of the data in Fig.4.1. Fewer data points have been plotted for clarity.

high-quality polycrystalline materials is intrinsic to single grain and thus similar to that of ρ_{ab} in single crystals. Thus, all these qualities make our samples 2A and 2B good candidates for paraconductivity analysis (see Section 4.2.4).

4.2.4 Paraconductivity

An effective attraction between electrons may cause the scattering amplitude between the electrons and the phonons, impurities, or the lattice atoms to vanish and lead to the superconducting behavior, including the absence of any electric resistance at low temperatures. Even in the situation where the superconducting state is destroyed because of the thermal fluctuations particularly in low dimensional systems, the electrical conductivity can be greatly enhanced at LT in various cases, a phenomenon usually called the superconducting fluctuation effect. Thus the fundamental explanation for the observed rounding off of the resistivity-temperature, $\rho(T)$, curve near and above the T_c is that the thermodynamic fluctuations can produce short-lived cooper-pairs, leading to an apparent increase in the conductivity. The excess conductivity ($\Delta\sigma$) in a superconductor in the mean-field approximation in the BCS theory may be written as [239]

$$\Delta\sigma/\sigma_{300} = A\,\epsilon^{x} \qquad (4.2)$$

where σ_{300} is the normal conductivity at room temperature (300 K), A the temperature-independent amplitude, $\epsilon = (T-T_c)/T_c$ the reduced temperature and x the critical exponent. Both A and x

strongly depend on the superconducting dimensionality. For two (2D) and three (3D) dimensions, these are given by

$$A(2D) = e^2 \rho_{300} / 16 \hbar d \quad ; \quad x = -1.0 , \qquad (4.3)$$

and,

$$A(3D) = e^2 \rho_{300} / 32 \hbar \xi(o) \quad ; \quad x = -0.5 \qquad (4.4)$$

where d is the characteristic length of the 2D system and $\xi(o)$ is the zero-temperature coherence length.

The dimensionality in $YBa_2Cu_3O_{7-\delta}$ (Y-Ba-Cu-O) system has been widely studied, but is still a matter of some debate. Since the first report on the excess conductivity measurement on Y-Ba-Cu-O pellets by Freitas et al. [240], there have been several investigations on single crystals (sc) [135,241-243], on polycrystals (pc) [244-249], on c-axis oriented thin films [250], and on single-crystal film [251] specimen of this material. The results of these studies are reviewed by Srinivasan [252].

Freitas et al. [240], Goldenfield et al. [245], Vidal et al. [246] and Veira et al. [244] have found evidence for a 3D fluctuation induced conductivity in Y-Ba-Cu-O (pc) samples. Fontana et al. [249] have observed an apparent crossover from 2D to 3D behavior in Y-Ba-Cu-O pellets. However, the experimental values of the exponent do not agree very well with the theoretical ones. On the other hand, Ausloos et al. [248] have reported the opposite, i.e., a 3D to 2D (from high temperature to low) crossover behavior in Y-Ba-Cu-O (pc) samples which is highly unusual.

Hagen et al. [241] have fitted their conductivity data on single crystals to the following equation

$$\sigma T = T/(aT+b) + CTT_o/(T-T_o) \qquad (4.5)$$

and used a,b,c, and T_o as adjustable parameters to get the best fit. This equation presupposes that the $\Delta\sigma$ is 2D in character. The values of T_o determined from the best-fits were about three-degrees below the temperature of zero-resistance. Their data did not fit with the Lawrence-Doniach (LD) [253] expression for crossover from 2D to 3D. Weigang et al.'s [135] single crystal ρ-data fits well with the LD expression in the temperature range $T_{co} + 1 \leq T \leq T_{co} + 10$ K. However, these authors use $T_c=T_{co}$ where the ρ (in a-b plane) is zero. Also the analysis leads to an ambiguous value of lattice periodicity along c-axis. Friedmann et al. [2420] have fitted their single crystal ρ-data with AL, LD and MT (Maki-Thompson) [254,255] paraconductivity theories. They found that the LD model gives the best fit to the data with physically reasonable parameters. However, the value of $\xi(o) = 0.44$ Å obtained from the best LD fit was surprisingly small. Also their mean-field transition temperature (T_c^{mf}) lies 1 to 3 K below T_c, and the 2D to 3D crossover temperature T_o was around 2 K below $T_c^{R=0}$. Ong et al. [243] by fitting their single crystal ρ-data in the range 120-200 K to the equation

$$\sigma_n(T) = 1 / \{(A/T) + BT\} \qquad (4.6)$$

found 3D fluctuation very close to T_c.

Oh et al. [250] have measured the paraconductivity in epitaxial films of Y-Ba-Cu-O oriented perpendicular to the c-axis and have explained their results in terms of the LD equation of the form

$$\Delta\sigma = e^2 / 16\,\hbar\,\epsilon\,d\,\{1 + [2\xi_c(o) / d]^2\,\epsilon^{-1}\}^{-1/2} \qquad (4.7)$$

This expression predicts a crossover from 2D to 3D behavior as the temperature approaches T_c.

In the theoretical paper Lobb [256] concludes that the Ginzburg-Landau (GL) theory will fail within around 0.1 K of T_c. In the mean field regime the excess conductivity will obey the 3D-AL equation. At lower temperatures their should be a crossover regime in which the exponent of ϵ will be -2/3. On further cooling, the exponent should change to -1/3 in the critical dynamics regime. Veira et al. [257] found that a plot of $\ln(\Delta\sigma/\sigma_{300})$ versus $\ln\,\epsilon$ indeed showed a region in which the exponent was -1/2 followed by a crossover region in which the exponent was -2/3 and finally a third region in which the exponent was -1/3 as the temperature approached T_c from above. However, in this work the value of T_c was determined by adjusting the slope in the crossover regime to -2/3.

It is evident that there exists considerable discrepancy among various investigations mainly because the excess conductivity analyses have to deal with the following questions: (1) How to estimate the background resistivity, in the absence of any quantitative model for the ρ-T dependence in the normal

state, in order to determine $\Delta\sigma$? (2) How to fix the value of T_c? and (3) How to choose, in the absence of any specific theory, the functional dependence of $\Delta\sigma$ on ϵ ?. Moreover, the requirement of high-quality single-phase specimen often imposes additional problem. For example, the reported measurements on most pc samples generally have (1) higher room temperature resistivities (probably due to lower density or the presence of impurities), (2) considerable positive magnitude of the extrapolated residual resistivity, $\rho(o)$ at T=0, (signifying the presence of impurities such as charged-oxygen vacancies or defects) and (3) large transition width of the order of 1 K or higher. These affect the paraconductivity analyses leading to considerable inconsistencies in the reported results.

This section deals with the measurements on high-quality and high-density (≥90%) Y-Ba-Cu-O pellets with very sharp transitions comparable to that of the single crystals. Also two different fitting procedures are used to estimate the background resistivity in order to calculate the $\Delta\sigma$ and the related parameters.

The excess conductivity $\Delta\sigma$ above T_c is defined by

$$\Delta\sigma(T) = \sigma_m(T) - \sigma_n(T) = 1/\rho_m(T) - 1/\rho_n(T) \qquad (4.8)$$

where $\rho_m(T)$ is the measured resistivity and $\rho_n(T)$ is the normal state resistivity, i.e., the resistivity the sample would have had in the absence of superconducting transition. The resistivity data in the linear region ($2T_c \leq T \leq RT$) were fitted in each case to the formulae (i) $\rho(T)=a+bT$ (N) and (ii) $\rho(T)=A/T+BT$ (AZ) and

these equations were used to calculate the normal resistivity in the fluctuation region. The dashed lines in Figs. 4.1 and 4.3 represent these fittings. From the actual measured resistivity and the extrapolated normal resistivity, the excess conductivity ($\Delta\sigma$) was calculated.

In order to test the theoretical expressions for 2D and 3D fluctuations and afford a comparison with the previous results on Y-Ba-Cu-O, the normalized excess conductivity, $(\Delta\sigma/\sigma_{300})$, is plotted against the reduced temperature ϵ. The results shown in Fig.4.4 correspond to the second (cooling/heating) run on sample 1. The reduced temperature range and the exponent of AL equation for this sample are listed in Table 4.2. The ln $(\Delta\sigma/\sigma_{300})$ versus ln ϵ plot is reasonably linear in the reduced temperature range -2.7 to -5.1 with an exponent X=-0.4 in the normal metal (N) case. As the temperature increases further, there is an apparent rise in the slope which indicates that the system perhaps enters the crossover region as the temperature approaches T_c.

Figure 4.5 shows the excess conductivity versus reduced temperature behavior of the sample 2A. In this case three distinct linear regions are identified. There is a high-temperature region in which the exponent (X) is -1.0, followed by a mean-field region in which the exponent is -0.42, and a third region where the exponent (X) is -0.56. The results on sample 2B are presented in Fig.4.6. In this case four linear regions are identified: the high-temperature region in which the exponent is -1.0, followed by a mean-field region with an exponent of -0.43, then a crossover region where the exponent is -2/3 and a fourth region with an exponent of -0.43. This behavior

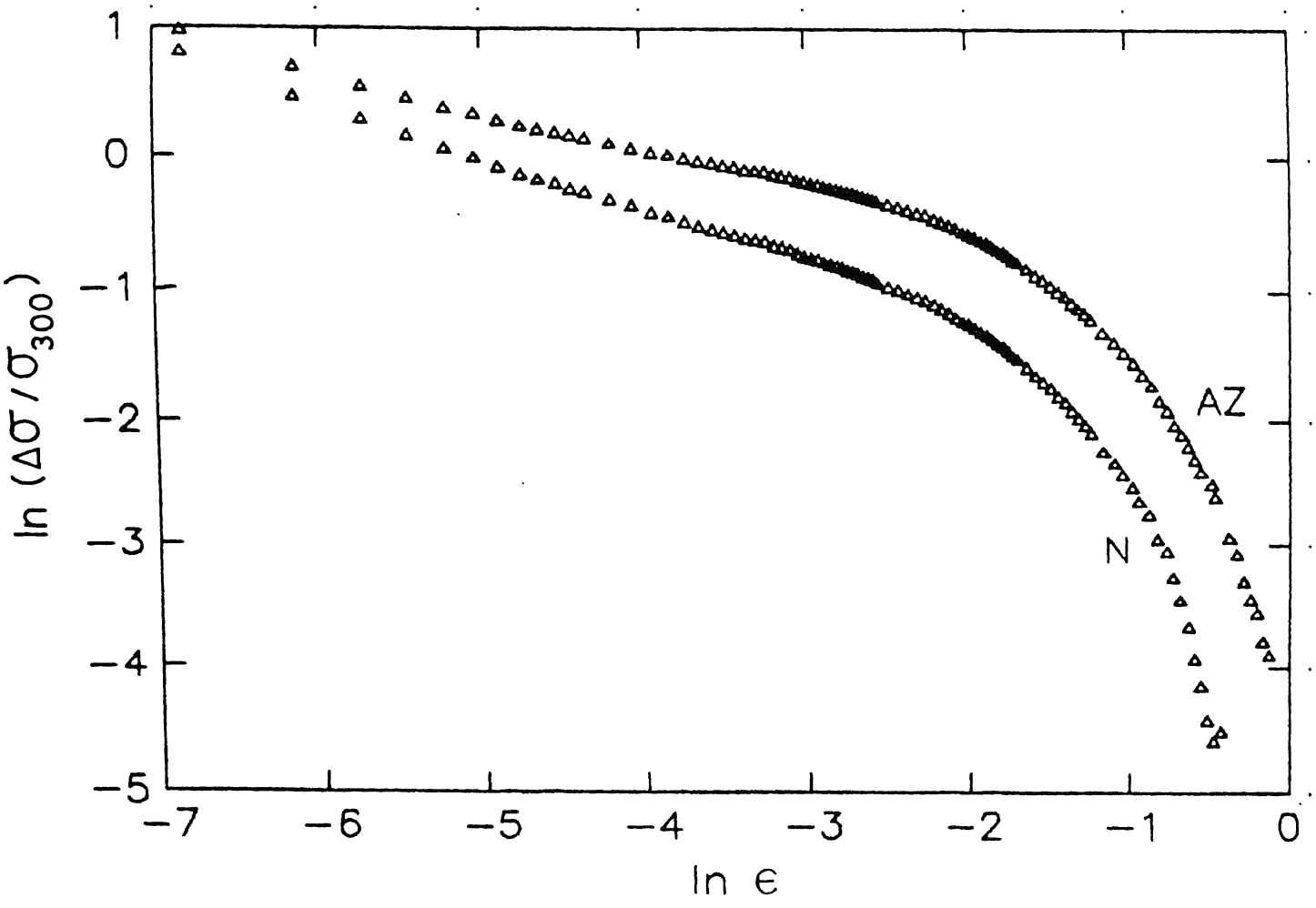

Fig. 4.4. Log-log plot of the normalized excess conductivity ($\Delta\sigma/\sigma_{300}$) versus reduced temperature (ϵ) for sample 1 (2nd run); (N): $\Delta\sigma$ obtained by normal metal extrapolation ; (AZ): $\Delta\sigma$ obtained from the Anderson-Zou fit to the data.

TABLE 4.2. The reduced-temperature range and exponent of AL equation, $\Delta\sigma = A\ \epsilon^{x}$, for three differently processed YBCO polycrystalline samples.

Sample	T_c (K)	ln ϵ - range	T - range (K)	Exponent (x) (N-fit)	(AZ-fit)
1	92.8	-2.7 to -5.1	T_c+6.2 to T_c+0.6	-0.40	-0.30
		< -5.1	< T_c+0.6	upward slope	
2A	92.1	-1.8 to -2.8	T_c+15.2 to T_c+5.6	-1.00	-0.80
		-2.8 to -4.5	T_c+5.6 to T_c+1.0	-0.42	-0.35
		-4.5 to -6.9	T_c+1.0 to T_c+0.1	-0.56	-0.50
2B	93.0	-1.9 to -3.4	T_c+13.9 to T_c+3.1	-1.00	-0.83
		-3.4 to -4.4	T_c+3.1 to T_c+1.1	-0.43	-0.41
		-4.4 to -6.0	T_c+1.1 to T_c+0.2	-0.67	-0.58
		< -6.0	< T_c+0.2	-0.43	-0.41

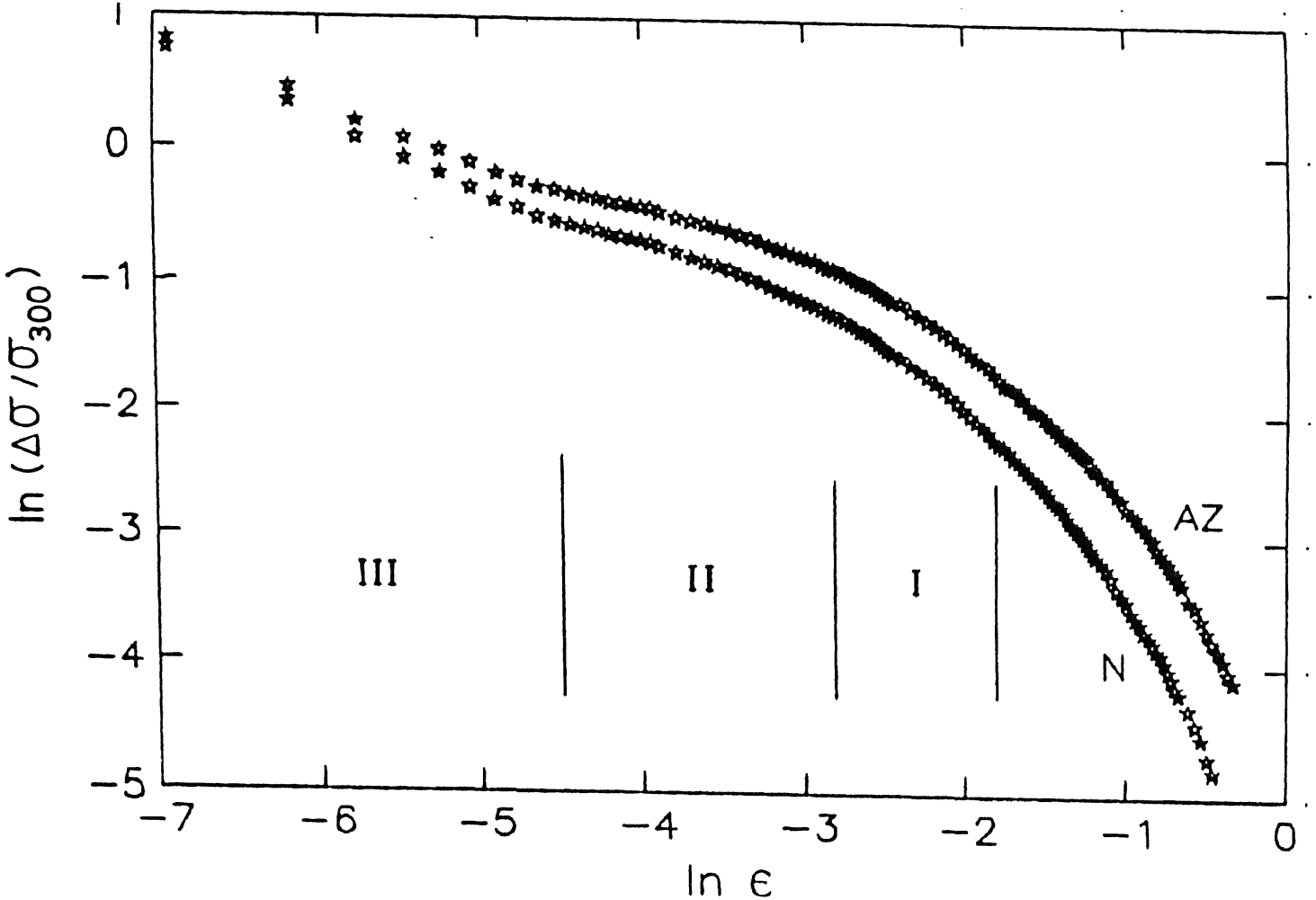

Fig. 4.5. Log-log plot of the normalized excess conductivity ($\Delta\sigma/\sigma_{300}$) vs. reduced temperature (ϵ) for sample 2A ; (N): $\Delta\sigma$ obtained by normal metal extrapolation ; (AZ): $\Delta\sigma$ obtained from the Anderson-Zou fit to the data.

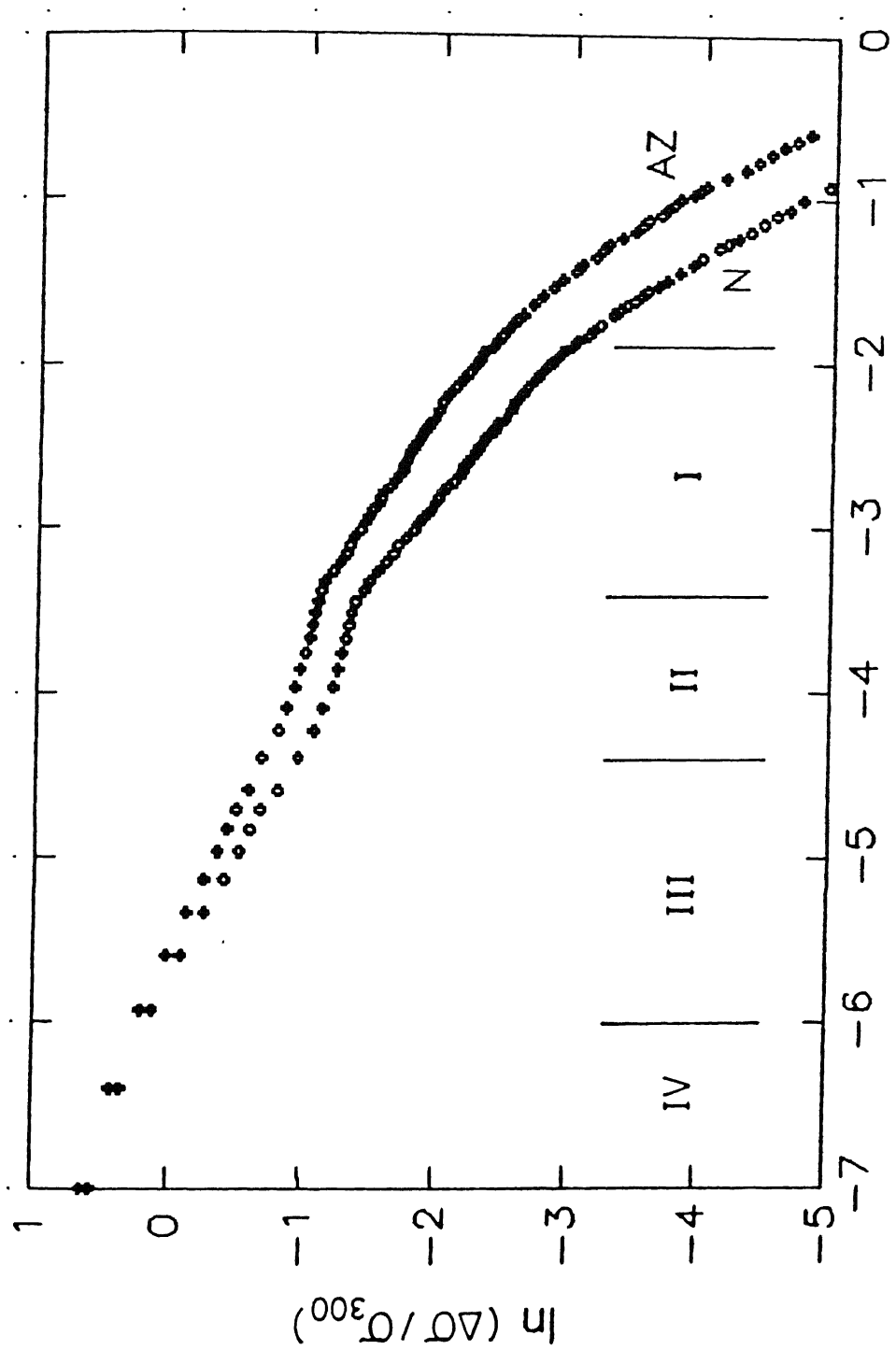

Fig. 4.6. Log-log plot of the normalized excess conductivity ($\Delta\sigma/\sigma_{300}$) vs. reduced temperature (ϵ) for sample 2B ; (N): $\Delta\sigma$ obtained by normal metal extrapolation ; (AZ): $\Delta\sigma$ obtained from the Anderson-Zou fit to the data.

is in close agreement with that predicted by Lobb [256]. The reduced temperature range and the exponent of AL equation for samples 2A and 2B are also listed in Table 4.2. It may be emphasized here that it is for the first time that a 2D to 3D fluctuation followed by a crossover and critical dynamics region has been observed in high-quality pc samples. Although a similar behavior was reported by Veira et al. [257] but their samples apparently had large room temperature resistivity (ρ), and large ΔT_c, etc. Moreover, in their analysis they have used T_c as an adjustable parameter to obtain the required value of the exponent in the crossover region. In our samples marked 1, the absence of various different regions and the lower value of the critical exponent in the mean-field region is probably due to its anomalous behavior in the cooling and heating cycle, which might have caused error in $\rho_n(T)$ and $\rho(T_c)$. In all the samples for ϵ exceeding 0.1 the paraconductivity falls steeply, much faster than any of the power laws [245-249] can predict. The critical exponent in region II is affected by the precise choice of T_c and it is, in all cases studied here, close to -1/2 as predicted by the AL theory for 3D fluctuations in the mean-field region.

The constant A given by eq. (4.4) {with $\xi(o)$=20 Å} has a value of 0.054 for sample 1, 0.023 for sample 2A and 0.020 for sample 2B whose room temperature conductivities are respectively, 7.02×10^2 $(\Omega\ cm)^{-1}$, $1.63 \times 10^3 (\Omega\ cm)^{-1}$, and 1.86×10^3 $(\Omega\ cm)^{-1}$. This observed normal conductivity dependence of the excess conductivity amplitude (A) follows the general trend predicted by the 3D-AL theory, though its magnitudes for different samples are are not in very good agreement, in contrast to other reports

[246,257]. However, the reduced temperature limits of region II are generally in agreement with the earlier reports [240-246,135, 250,257].

In the Anderson-Zou (AZ) case, the behavior of $\ln(\Delta\sigma/\sigma_{300})$ versus $\ln \epsilon$ for all the three samples is identical with the normal metal case but with different values of the exponent. This clearly demonstrates how extrapolation dependent is the observed critical behavior in the absence of any quantitative model of the normal-state resistivity.

4.2.5 Low Temperature Thermoelectric Power

The measurement of thermoelectric power (TEP) is advantageous vis-a-vis resistivity on granular and sometimes multiphasic materials. The electrical resistance between the grains will have less effect on TEP (S) than on the electrical resistivity, because the temperature drop between the grains will usually be much less significant than the voltage drop. Several groups have reported the TEP on single crystal [258-274] and polycrystal [275-300] samples of undoped and doped $YBa_2Cu_3O_{7-\delta}$. However, there are conflicting reports in the literature concerning the value of S and especially its sign. Positive as well as negative values of TEP are reported for both undoped or doped Y-Ba-Cu-O systems. Such wide variations in the measured transport coefficients have been attributed to different methods of sample processing, oxygen deficiency, and the granular structure of the pc samples. Surprisingly, there seems to be relatively more disagreement among the sc results than the pc results with respect to both the magnitude and the nature of

temperature dependence of TEP. Contrary to the behavior of most metallic-diffusion thermopowers, the measured TEP (above T_c) of many HTSCs decreases in magnitude as temperature increases, even near room temperature where phonon drag is usually less important. Thus the measurement of TEP would not merely reveal the sign of the majority charge carriers but can also lead to a better understanding of the nature of the superconducting mechanisms in these materials.

Figure 4.7 shows the thermopower of $YBa_2Cu_3O_{7-\delta}$ as a function of temperature. The absolute thermopower of the various samples were obtained by subtracting the TEP of Cu metal (used as leads) from the observed values. The TEP is quite sensitive to the oxygen content. While the sample with $(7-\delta)=6.85$ shows a positive TEP (holes as majority carriers), the sample with $(7-\delta)=6.93$ shows a negative TEP (electrons as majority carriers). The former has a positive slope and the latter has a negative slope at higher temperatures. That is, there is a linear section where TEP is proportional to T. This result together with the fact that the magnitude of TEP is very small, demonstrate the metallic nature of the Y-Ba-Cu-O superconductors. The deviation from the linearity takes place at successively higher temperatures as the concentration of oxygen vacancies increases. These thermopower results are surprisingly in good agreement with those of Ouseph and O'Bryan [294] even though they have used samples which have unreasonably large $\Delta T_c \leq 3^\circ$ K.

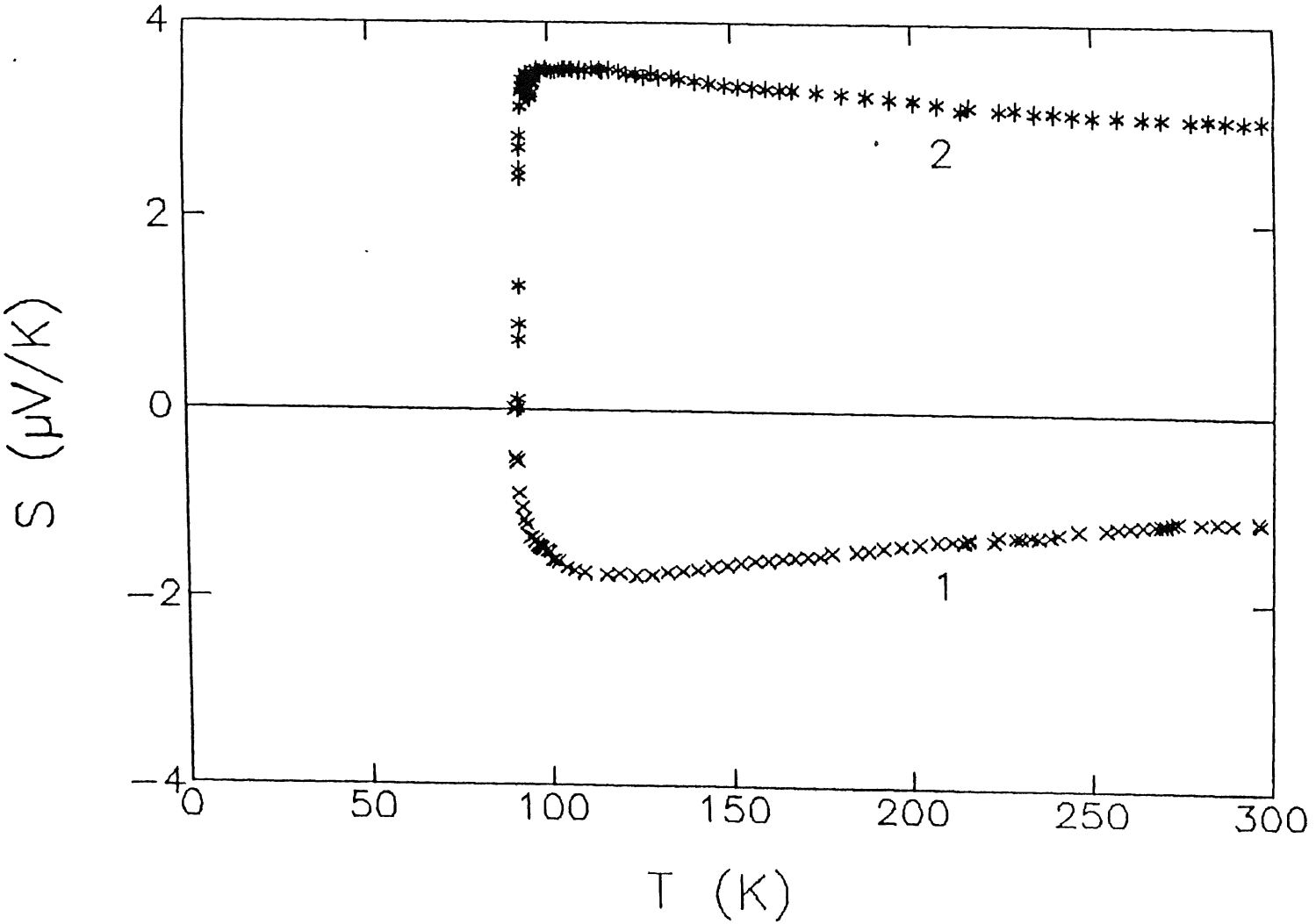

Fig. 4.7. Thermopower as a function of temperature for $YBa_2Cu_3O_{7-\delta}$ compounds with different oxygen content (7-δ). 7-δ for curve 1 is 6.94 ± 0.02; for curve 2 is 6.85 ± 0.02.

In the conventional metallic picture, the contributions to S are due to carrier diffusion and phonon drag. The phonon drag thermopower (S_g) for a single band of carriers with isotropic scattering rate may be written as [272]

$$S_g \propto 1/T \ . \tag{4.9}$$

The diffusion thermopower S_d for a gas of free electrons can be described by the expression

$$S_d = - (\pi^2/3|e|) \ (k_B^2 \ T/\mu) \text{ or } \quad S_d \propto T \ . \tag{4.10}$$

Combining Eqs. (4.9) and (4.10) leads to the following simple expression for the high-temperature metallic TEP:

$$S = S_g + S_d \ = (A/T) + BT \ . \tag{4.11}$$

Thus, it follows that a plot of ST versus T^2 should be a straight line. Figure 4.8 shows this plot for undoped Y-Ba-Cu-O samples in the range 160 K $\leq$ T $\leq$ 300 K. The observed changes in the intercept and the slope of the Y-Ba-Cu-O samples show that the phonon drag and the band-filling effects are responsible for the changes in S.

The Mott formula for the TEP of a normal metal shows that the sign of TEP depends not just on the energy derivative of the Fermi surface area, but also on that of the scattering rate. Crabtree et al. [301] argue that since Y-Ba-Cu-O consists of a

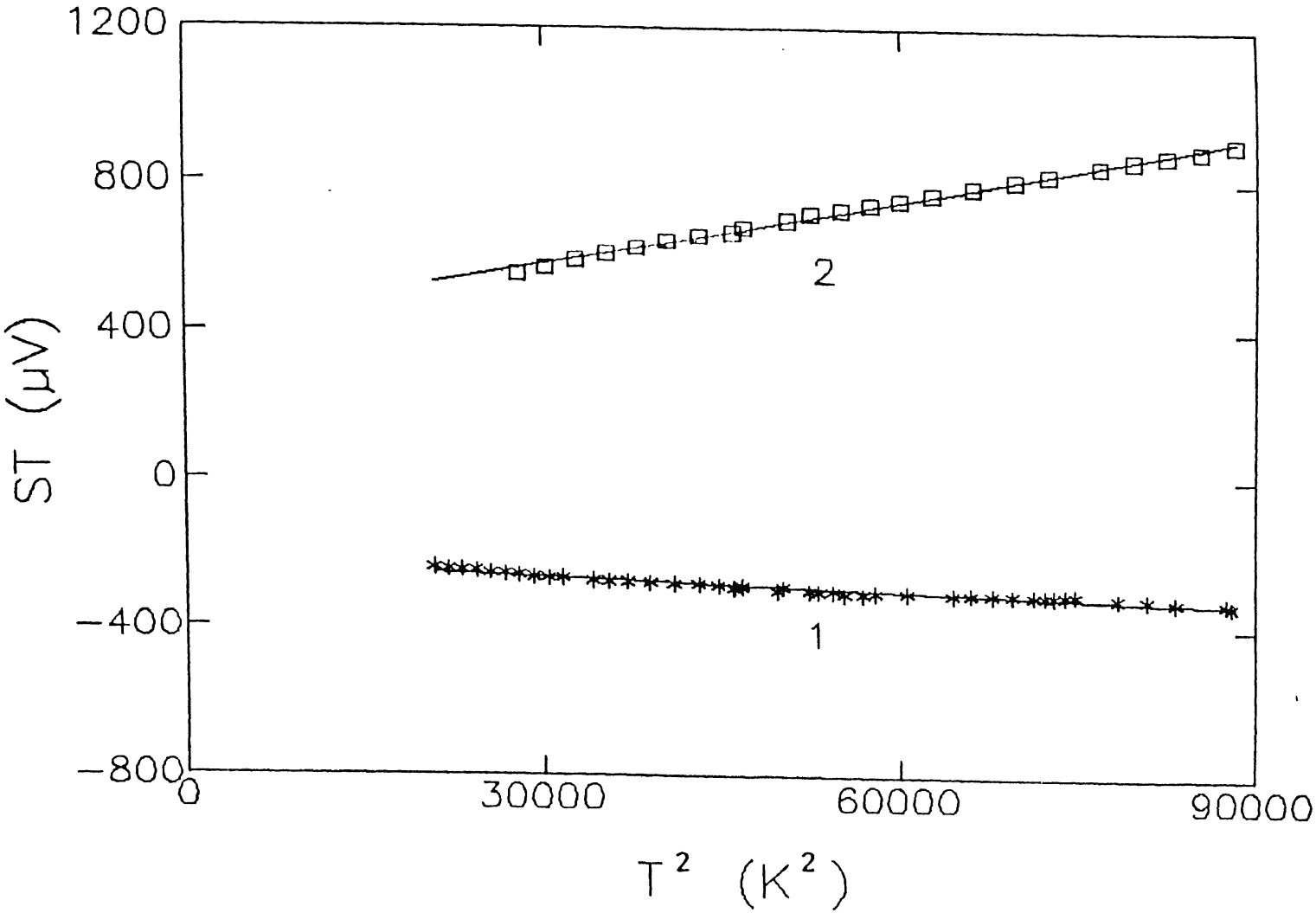

Fig. 4.8. ST vs. T^2 plots for $YBa_2Cu_3O_{7-\delta}$ samples with different oxygen content (7-δ). 7-δ for curve 1 is 6.94 ± 0.02; for curve 2 is 6.85 ± 0.02.

square lattice of CuO_2 units, the Fermi surface is basically cylindrical and essentially hole-like. The observed temperature dependence is rather unusual and more complicated than can be explained under the assumption of a single conduction-band model. In a two-conduction band, electron and hole, the total Seebeck coefficient S is described as [279]

$$S = (\sigma_e S_e + \sigma_h S_h) / (\sigma_e + \sigma_h) , \qquad (4.12)$$

where S_e and S_h are the Seebeck coefficients and σ_e and σ_h are the conductivities due to electrons and holes, respectively. Since S_e and S_h have opposite signs, S, according to Eq. (4.12), may be positive, negative or zero depending on whether $|\sigma_e S_e|$ is less or greater than, or equal to $|\sigma_h S_h|$. A somewhat complicated variation of S with impurity substitution in the present systems may originate in this scheme. Typically, one expects electron-like behavior for an almost empty band, and hole-like behavior for an almost filled band, based on the energy dispersion in these cases. In case of near half-filling, the sign of the charge carriers is difficult to predict.

Thus the observations of positive and negative TEP seem to indicate that the Y-Ba-Cu-O HTSCs involve a multiband conduction picture with a partially filled electron band and a hole band, as proposed by Lee and Ihm [302]. With a slight shift in the Fermi energy, possibly caused by internal strain from the excessive oxygen deficiency, structural deformation, or ionic site difference, the sign of the TEP could have changed due to the

change in occupation of the electron band and the hole band. S_g is overwhelmed by the band-filling effects when the carrier concentration is significantly reduced, e.g., by depleting the oxygen content or by this substitution. The large enhancement in S due to doping in both cases suggests that the chemical potential is close to the midlevel of a band in undoped Y-Ba-Cu-O. The approximate electron-hole symmetry which occurs near midbands causes cancellations from different parts of the band, leading to a small diffusion part of S, as has been emphasized by Anderson [207]. Therefore, raising the chemical potential away from the half-filling level by doping increases the diffusion TEP to large positive values. So, in general, the sign and the temperature dependence of the thermopower may be accounted for by conventional metallic theory, which incorporates diffusion and phonon drag contributions with the involvement of two carrier species.

4.2.6 High Temperature Resistivity

All the high temperature (HT) experiments for reasons of convenience, are carried out at constant oxygen partial pressure, $p(O_2)$ and thus, at sufficiently high-temperatures, are accompanied by changes of the oxygen content of the material. In equilibrium, each temperature and oxygen partial pressure corresponds to a definite oxygen content $(7-\delta)$. The required time to achieve equilibrium depends on the temperature, temperature jump, change in the oxygen pressure, dimensions of the sample, and its grain size, porosity, etc. Thus the composition and hence

the transport properties of these ceramic samples might well depend on their previous history. Also, the changes as a function of the (degree of) oxygen nonstoichiometry, δ, provide important insight into the dependence of the transport parameters on the oxygen doping, which was previously studied by quenching [303-305], getter annealing [306], *in-situ* resistivity at elevated temperatures [303-336], and *in situ* TEP at high-temperature [330,334,337-339]. The δ is also a function of temperature and oxygen partial pressure [340,341]. In thermally quenched samples, where a partial loss of oxygen is frozen in, both the σ and the Hall number density $n_H = 1/eR_H$ decrease systematically with increasing δ, together with a depression of the T_c [303-305]. Another important issue is the atomic scale ordering of the oxygen vacancies [340, 342-344] which may be related to the normal-state electronic properties and the superconducting mechanisms.

Some structural studies (for example, see ref. 340) treated the orthorhombic-tetragonal phase transformation as a discrete process which occurred near δ~0.5 where the occupancies of the O(4) and O(5) sites are equal and the material becomes tetragonal. However, observations of intermediate oxygen-ordering states between the ideal orthorhombic (δ=0) and tetragonal (δ=1) structures [345,346], and theoretical models of oxygen ordering [342,347,348], suggest that the orthorhombic-tetragonal phase transformation is more of an evolutionary process controlled by the oxygen diffusion kinetics [333,349,350]. Thus, in addition to the temperature and oxygen partial pressure, one should also

consider other parameters such as heating/cooling rates and the grain size as the driving forces for the orthorhombic-tetragonal transformation.

Anomalies in the temperature dependence of the resistivities have been reported for the bulk ceramics [307-316] at the orthorhombic-tetragonal transformation temperature, though some investigators have noticed no anomaly whatsoever [317-325]. From simple valence considerations, a semiconducting behavior should be expected at δ~6.5, assuming all the O and Cu ions are in O^{2-} and Cu^{2+} states [330]. However, at and above RT there is no discontinuity in the transport properties as the oxygen content is varied through $(7-\delta)$~6.5. It is suggested that the transport properties are due to the presence of a narrow conduction band with two electrons per formula unit. For δ=0, the band is half-filled, and as δ increases by the removal of oxygen, the population of the electrons in the conduction band increases (the conduction is p-type, by holes) up to about δ=1, where the conduction band is completely filled and the number of effective charge carriers tends to zero.

Anomalies are also reported by LaGraff et al. [333] near the orthorhombic-tetragonal transformation in sc $YBa_2Cu_3O_{7-\delta}$, which were detected by a sensitive bridge electrode configuration. The resistance anomaly manifests itself not as a change in the slope as has been reported [307-316], but as fine structure (or noise) near the transition temperature. No anomalous resistance behavior is observed in the sc study of LaGraff et al. [335] near the orthorhombic-tetragonal transformation temperature which suggests

that the anomalies reported in the literature may not be intrinsic to $YBa_2Cu_3O_{7-\delta}$, but may be due to impurities or additional phases at the grain boundaries or to residual stresses at the grain boundaries resulting from transformational strain.

Figures 4.9 and 4.10 show the $\rho(T)$ behavior at high temperatures for the $YBa_2Cu_3O_{7-\delta}$ samples. The resistivity data on two samples of different batches [$7-\delta = 6.85\pm0.02$ and 6.94 ± 0.02] are found to have almost identical trend but different magnitudes of resistivity in the heating and the cooling cycles, due to their different oxygen content. In the heating cycle the resistivity increases linearly up to ~670 K, except for a small hump, peak at ~570 K, and faster than linearly at T >700 K. The $\rho(T)$ curve changes its slope at ~975 K, and shows an anomaly at ~1080 K. In the cooling cycle, there is a slope change at ~975 K, and beyond that the curve is identical with that in heating cycle except that there is a shift in the absolute values of resistivity. Also, the minor hump observed at ~570 K during the heating cycle is absent. As long as the temperature remains less than ~500 K, the heating and cooling curves are almost identical. However, when the sample is cycled above ~525 K, the $\rho(T)$ curves become hysteretic, and the initial resistivity at RT can no longer be recovered at the end of the cycle; the final resistivity at the end of the cycle being less than the initial value. As a matter of fact the final ρ might be higher or lower than the initial value depending on the prior history of heat treatment and O_2 content.

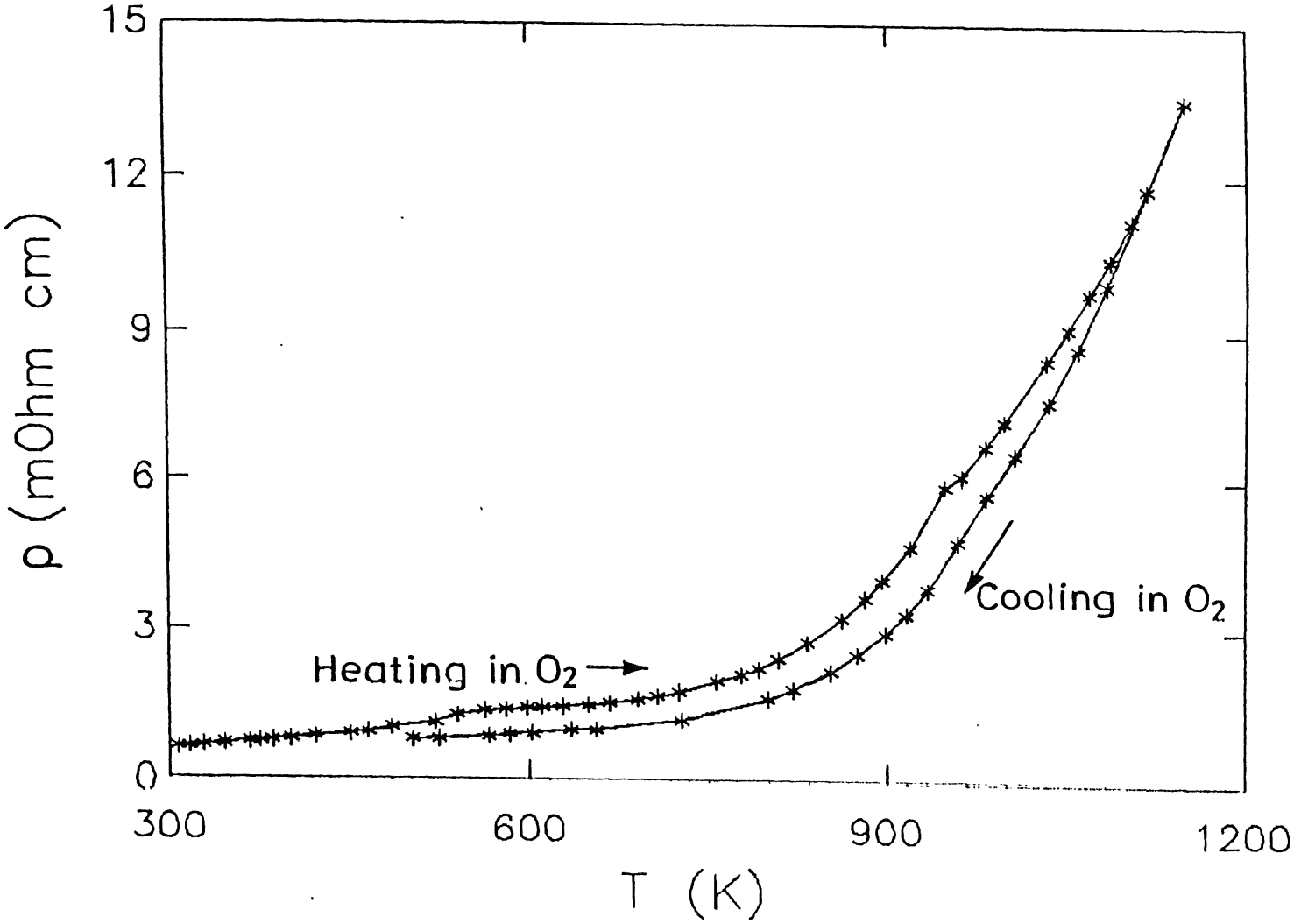

Fig. 4.9. *In situ* resistivity vs. temperature curves for $YBa_2Cu_3O_{7-\delta}$ in oxygen ambient of sample 1 of Fig. 4.1.

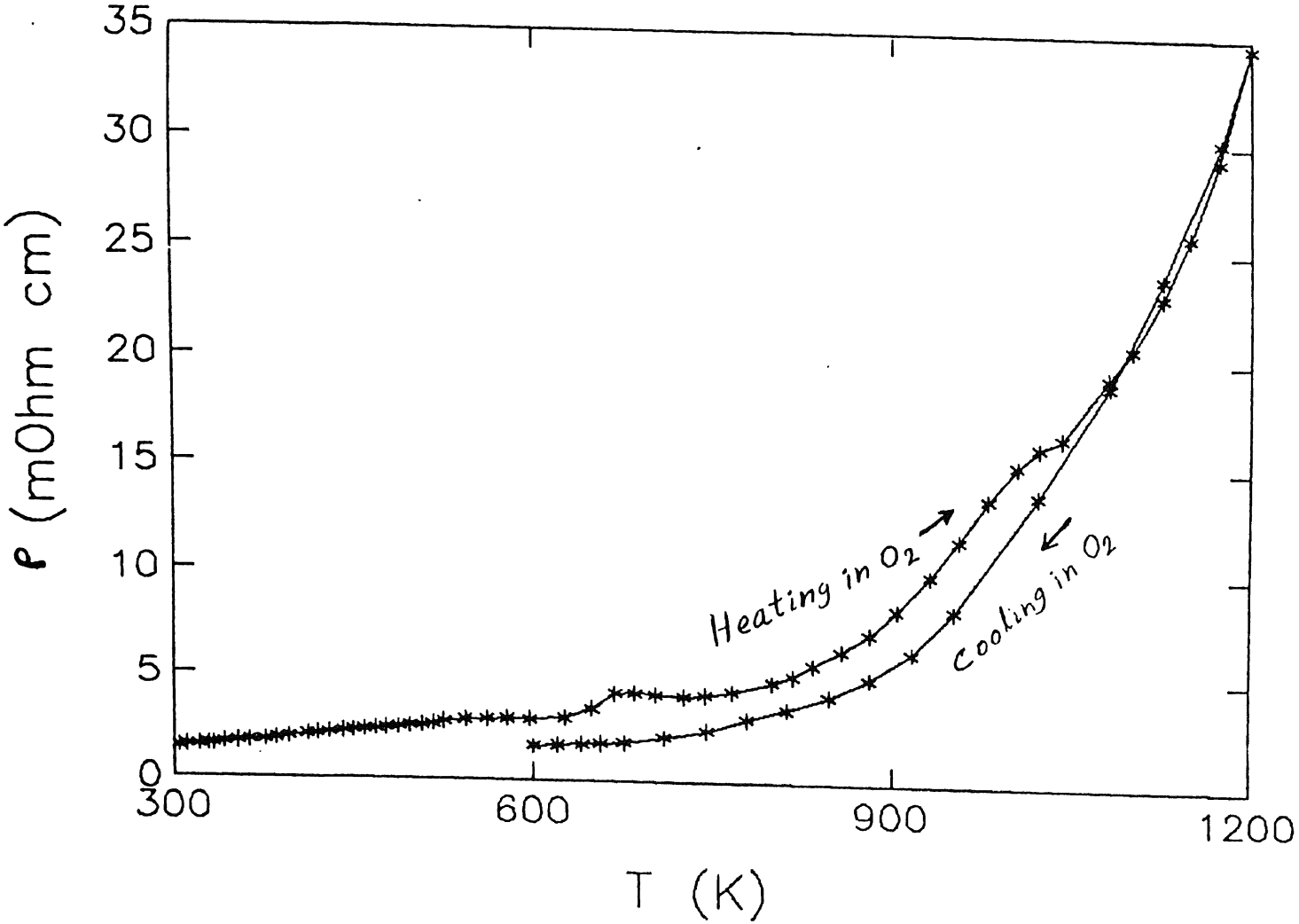

Fig. 4.10. *In situ* resistivity vs. temperature curves for $YBa_2Cu_3O_{7-\delta}$ in oxygen ambient of sample 2 of Fig. 4.1.

The observation that ρ(T) is linear with $d\rho/dT$ = 2.0 $\mu\Omega$cm/K, up to ~670 K is in broad agreement with the previous studies which have reported that ρ(T) is linear in general up to 575-675 K in bulk ceramics [315] and up to ~775 K in single crystal [329,333]. This difference between the sc and pc behavior is attributed to the lower surface-area to volume ratios in the single-crystals [333].

The observed linear ρ(T) characteristic up to relatively high-temperatures (absence of saturation) implies weak electron-phonon coupling [312]. If ρ(T) were to have a non-phonon origin, then the phonon coupling would be weaker yet. This also reveals that the mean free paths '*l*' are much longer than the interatomic spacings '*a*' at temperatures below ~700 K [312,351]. In contrast, ρ(T) curves for metals with *l*=*a* always display strong deviations from linearity at high-temperatures, known as resistivity saturation (e.g. V_3Si). Also, at low-temperatures the mean free path should be much longer than the extremely short coherence lengths which have been deduced [352] for these materials, which should accordingly be treated as clean superconductors. In addition to this the linear temperature behavior of ρ is to be expected at temperatures larger than θ_D, the Debye temperature of the solid (if it is due to electron-phonon interaction). What is deemed unusual is that in these materials the linear region in the ρ(T) curve can start at temperatures markedly lower than θ_D. Thus the increase in ρ upon heating may not only be due to a change in carrier concentration

as oxygen leaves the material, but may also be due to either a temperature or oxygen concentration dependence of the mobility of the charge carriers.

Oxygen is quite mobile in many oxide systems and apparently $YBa_2Cu_3O_{7-\delta}$ system is no exception. In and out diffusion studies from normal-state ρ measurements [310, 315, 318-320, 323, 324] have shown that it can be transported at temperatures as low as 570 K. This seems to be consistent with the observed hump in the $\rho(T)$ curve during the heating cycle. The out-diffusion of oxygen in Y-Ba-Cu-O is independent of δ and is surface-reaction limited by a 1.7 eV activation energy barrier, which is larger than that for the diffusion-controlled oxygen in-diffusion (~1.3 eV for δ~0 sample) [315, 318]. Consequently, the final δ distributions in the slow furnace-cooled and He-annealed samples should be uniform because of the fast oxygen diffusion in the CuO planes with $\delta>0$. In slow oxygen annealing process, the outer shell of a grain can reach its oxygen solubility very rapidly, thereby slowing down the subsequent oxygen in-diffusion process and resulting in an inhomogeneous sample. This finding is extremely important from the processing view point. Thus under those conditions it require much longer annealing time to homogenize the sample. Also, in the orthorhombic phase the oxygen atoms and vacancies are ordered so that there are linear Cu-O chains parallel to the b-axis and Cu-V chains parallel to the a-axis. As a result, the physical and the structural properties of the material are affected by the oxygen content, the ordering, the density, the heat treatment, and the ambient [340]. In the present work this is reflected in the low- and high-temperature ρ and S data.

The sharp upturn of $\rho(T)$ above ~700 K can be ascribed to the temperature dependence of the oxygen deficiency which plays the dual role of reducing the number of carriers and increasing the number of scattering centers. This sharp upturn behavior in $\rho(T)$ of Y-Ba-Cu-O at ~675 K has been accounted for by a model of homogeneous oxygen desorption, characterized by a value of oxygen deficiency δ [309]. In this model, as δ increases with temperature, the density of electronic states decreases and the elastic scattering rate caused by the oxygen-vacancy disorder increases. Both factors contribute to the increase in $\rho(T)$. The contribution due to phonon scattering appears to be independent of δ in this regime; it is assumed to be determined by the electron-phonon coupling constant and the temperature, as usual.

In principle the resistivity can be expressed in terms of two scattering rates; the elastic scattering by quasistatic oxygen-vacancy disorder, and the inelastic scattering by lattice vibrations-phonons and possibly tunneling states. The resistivity, ρ, is given by

$$\rho = m^*/ne^2\tau \ , \qquad (4.13)$$

where m^* is the effective mass. Thus the large enhancement in ρ as δ increases may be attributed to the increased defect-scattering rate $(1/\tau)$, in addition to the decrease in the carrier concentration n [317].

The change in the slope of the $\rho(T)$ curve at ~975 K is due to the orthorhombic-tetragonal structural transition. This change in slope also appears in the cooling cycle more or less at the

same temperature. Jorgenson [340] observed a change in the slope in the c-axis lattice-parameter and the cell volume versus temperature at the transition temperature, ~975 K, which is consistent with a second order transition. That is, there is no hysteresis associated with the transition temperature when the temperature is swept slowly enough to allow for the temperature and oxygen equilibration. This is characteristic of a second order phase transition, and is also consistent with the scanning calorimetric measurements which failed to detect any latent heat at the transition temperature confirming the lack of first-order character. Also the general shape of the $d\rho/dT$ curve is characteristic of a second order phase transition showing a specific heat like anomaly at the orthorhombic-tetragonal(T_{ot}) transition temperature [309]. The observed hysteresis in the present work (Figs. 4.9 and 4.10)is possibly because of the lack of equilibration with respect to temperature and oxygen. Besides the sudden gain or loss of oxygen near the orthorhombic-tetragonal transformation temperature may also be responsible for the anomaly [353].

The observed hysteresis could also be related to the formation of twin boundaries occurring after the onset of the orthorhombic ordered phase, as twinning is observed in TEM studies in [307,333]. Since long-range order is necessary before twin boundaries can be formed, a sharp second-order transition will occur on cooling. However, on heating disorder occurs within each domain at a well-defined temperature, but twin boundaries

still persist as scattering centers at higher temperatures due to pinning forces. This will limit the divergence of the coherence length at T_{ot} leading to a broader transition upon heating.

The observed behavior is in good agreement with the reported TGA results [308]. That is, the O_2 content does not change until ~500 K, and the oxygen uptake during the warming curve increases at ~600 K. The cooling curve shows that the O_2 content of Y-Ba-Cu-O increases monotonically with decreasing temperature from ~1173 K (where δ ~0.94) to RT (where δ ~0.18). The order disorder transition occurs at 1000 K in flowing O_2. The hysteresis observed at higher temperature in both TGA and ρ measurements is most probably a kinetic effect which can be minimized by sweeping the temperature at a much slower rate.

To control the oxygen deficiency δ in $YBa_2Cu_3O_{7-\delta}$, the oxides with $\delta \simeq 0$ have been annealed in air up to a chosen temperature, and then furnace-cooled in high-purity He (99.999+%) ambient back to RT. By selecting the final temperature and the ambient, the oxygen deficiency δ can be controlled. Figure 4.11 shows the $\rho(T)$ behavior at high temperatures for the sample 2B as a function of temperature. While the heating cycle measurement were performed in air the cooling cycle was performed in He. The $\rho(T)$ behavior in air (with a T_{ot} ~950 K) in the heating cycle is more or less similar to that of $\rho(T)$ in O_2 . On the other hand a semiconductor like behavior is observed in the atmosphere in the cooling cycle which is in good agreement with the literature [320]. According to Molenda et al. [334] at δ~0.7

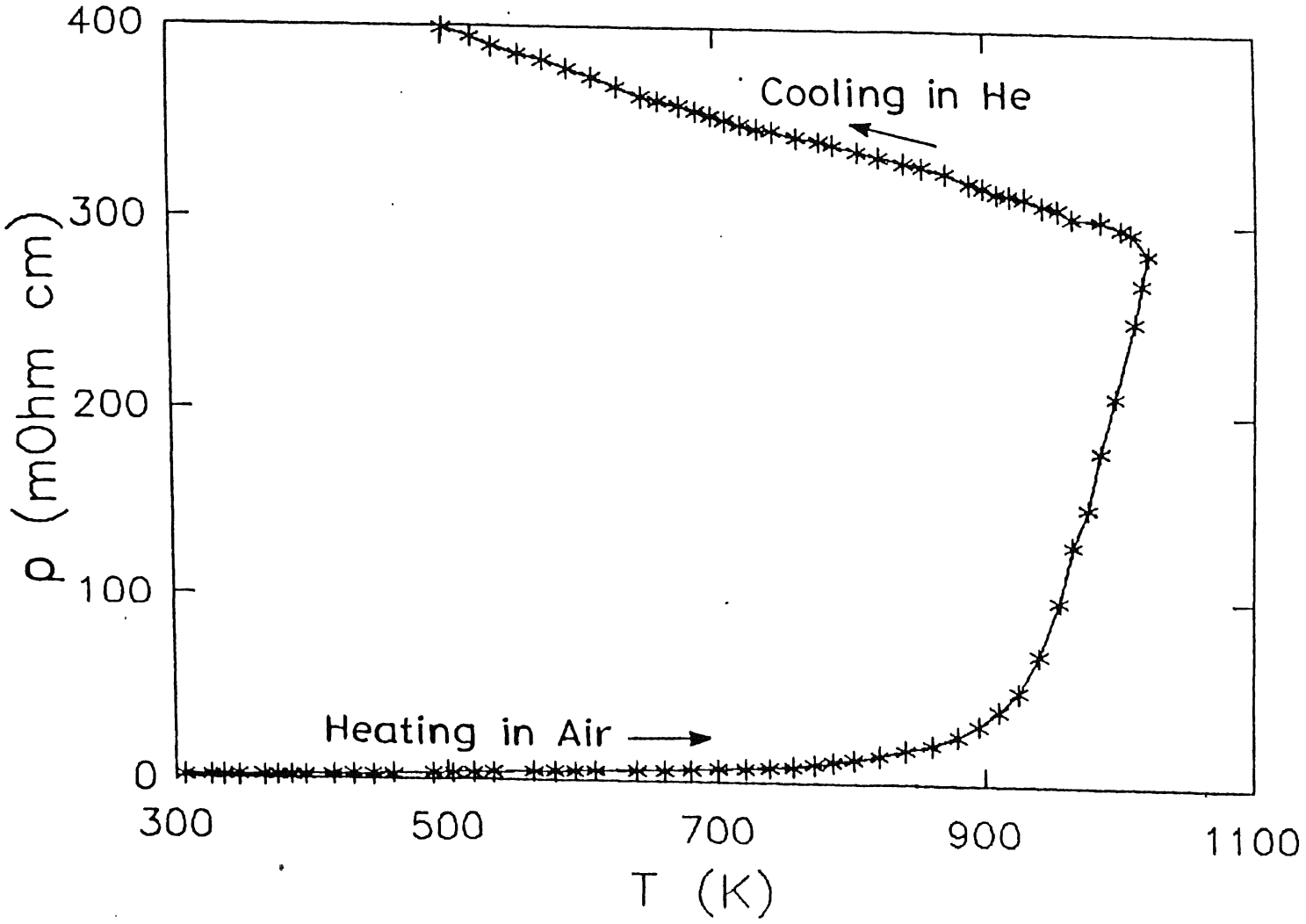

Fig. 4.11. *In situ* resistivity vs. temperature curves for $YBa_2Cu_3O_{7-\delta}$ in Air (heating) and in helium (cooling) ambient.

the splitting of the effective energy band and the appearance of an energy gap of the order of 1 eV (metal-insulator transition) take place. In fact, within the tetragonal phase Grader et al. [311], as well as others [327,354] have established the existence of a metal-semiconductor phase transition , and within the semiconductor phase a transition from the dominant p-type to n-type conduction [316, 330, 354]. For δ >0.7 the transport takes place in more than one band and typical semiconductive properties can be observed. These findings suggest that monitoring the resistivity of a sample can serve as an *in situ* quality control parameter in the manufacturing of the superconducting material.

4.2.7 High Temperature Thermoelectric Power

Figures 4.12 and 4.13 show the variation of thermopower (S) as a function of temperature for the Y-Ba-Cu-O samples in the O_2 atmosphere. The thermopower in the heating cycle is negative at all temperatures below 840 K, changes its sign there (at 840 K) and remains positive over the investigated temperature range (up to ~1100 K). During the cooling cycle the TEP follows more or less the same behavior observed in the heating cycle down to about 550 K. However below this temperature, the thermopower increases more rapidly as the sample is cooled, and crosses the S=0 line once again (~400 K) and becomes positive near the room temperature. This suggests that the oxygen content of the sample has increased after the slow cooling during the thermopower measurement. The fact that S versus T curve (cooling cycle)

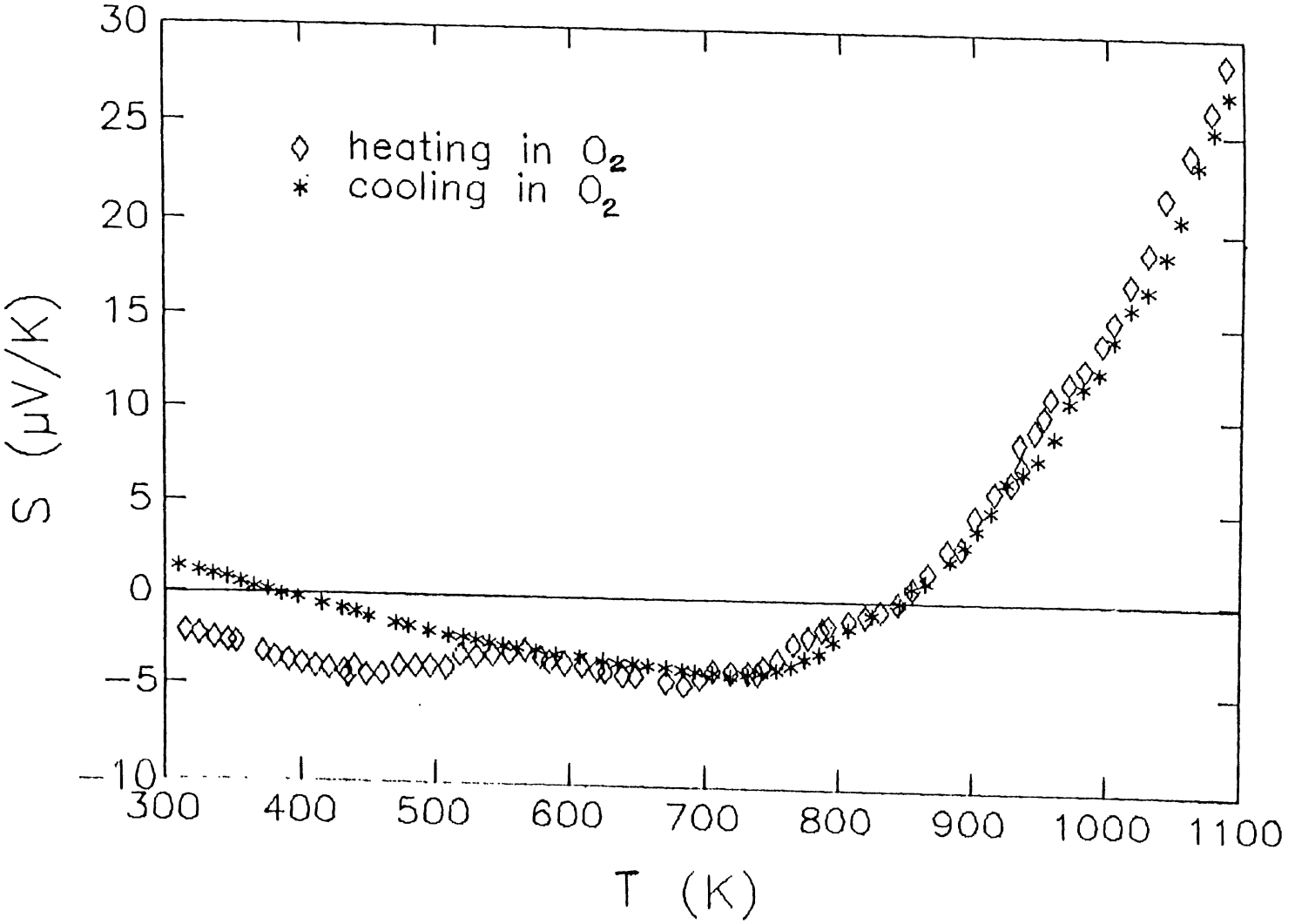

Fig. 4.12. *In situ* thermopower vs. temperature curves for $YBa_2Cu_3O_{7-\delta}$ in oxygen ambient of sample 1 of Fig. 4.1.

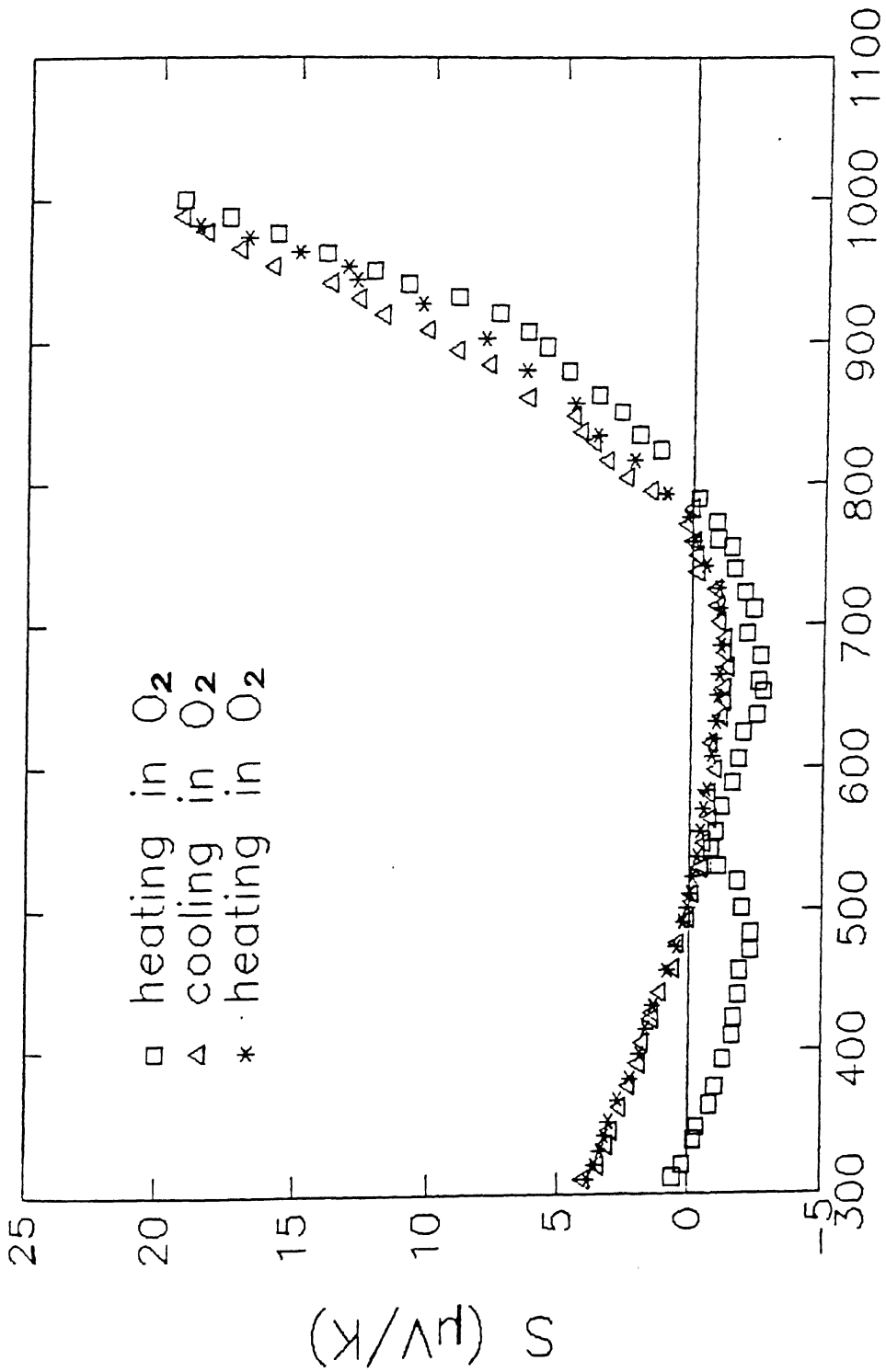

Fig. 4.13. *In situ* thermopower vs. temperature curves for $YBa_2Cu_3O_{7-\delta}$ in oxygen ambient of sample 2 of Fig. 4.1.

intersects the S=0 line at ~400 K, is inconsistent with the conventional theory of thermopower for simple metals which predicts that curve intersects at the origin [338].

The S versus T curve exhibits a negative minimum at ~725 K and crosses the S=0 line at ~840 K. Deviation in the S value is observed at ~950 K close to the (orthorhombic-tetragonal transition), in the heating cycle, whereas it is observed at ~1000 K and at ~935 K in the cooling cycle. The observed behavior of S is compatible with that of normal metals but contrary to the simple diffusion theory of thermopower that predicts a linear temperature dependence. This would suggests the presence of a complex scattering mechanism in these oxides.

Figure 4.14 shows the TEP versus T behavior for $YBa_2Cu_3O_{7-\delta}$ in air (heating cycle) and He (cooling cycle) atmospheres. The S values measured in air are negative up to ~800 K, having a minimum at ~700 K. This is in good agreement with the previous reports [337, 338]. With increasing temperature S changes the sign from minus to plus at ~800 K followed by a sharp increase up to 1000 K. A slight change in the slope of the S(T) curve is noticeable at ~935 K which is close to the (orthorhombic-tetragonal transition) temperature. In the cooling cycle, the magnitude of S remains constant until ~700 K and then it increases.

The upturn behavior of S(T) curve at ~725 K corresponds to the beginning point of oxygen release in the $YBa_2Cu_3O_{7-\delta}$. Simply considering that the sign of S corresponds to that of majority carriers, the negative S below ~800 K implies that the conduction is dominantly due to electrons. The conclusions drawn from the

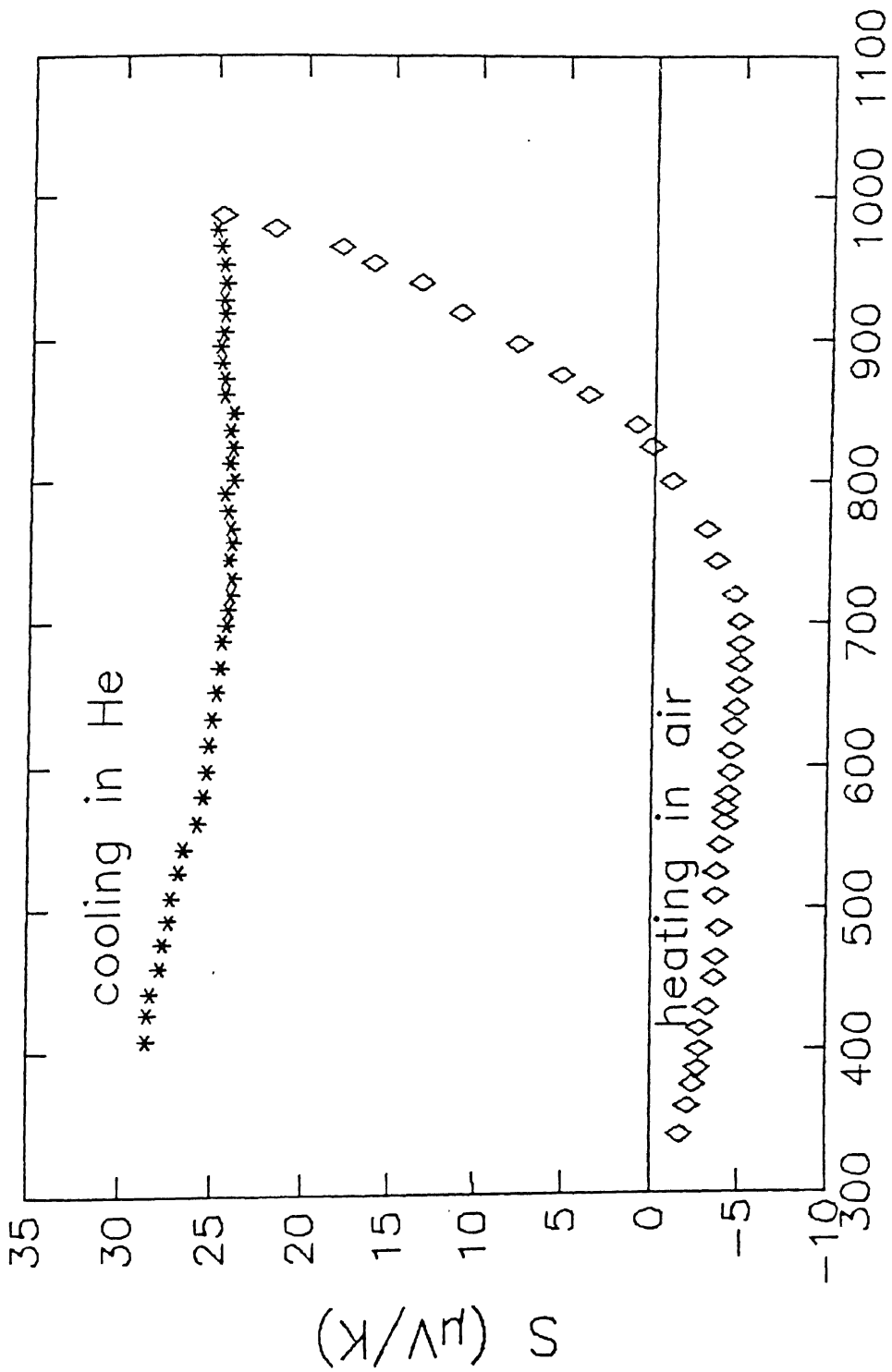

Fig. 4.14. *In situ* thermopower vs. temperature curves for $YBa_2Cu_3O_{7-\delta}$ in air (heating) and in helium (cooling) ambient.

S(T) behavior are generally consistent with these from ρ(T) behavior. The above facts also suggest the conduction mechanism in the $YBa_2Cu_3O_{7-\delta}$ system is of mixed types rather than one-carrier type. Also, the complicated behavior of S(T) suggests that the simple narrow conduction band model is not sufficient to explain all the observations.

4.3 Conclusions

High-quality $YBa_2Cu_3O_{7-\delta}$ samples are prepared by the solid-state reaction method. It is concluded that the major source of the existing discrepancies in the experimental values of transport parameters is the differing processing conditions used by various investigators. The Anderson-Zou fit to the data is found to work as well in polycrystals as in single crystals. Paraconductivity studies show a 2D to 3D crossover when it passes from high-temperature to mean-field region. The TEP data are found to follow a relation of the type S=A/T + BT. The present results and discussion suggest the midband-filling and the phonon drag with the involvement of two carrier species (multiband conduction) mechanisms to be operative in these systems. The high temperature measurements suggest that monitoring the resistivity and TEP of a sample can serve as an *in situ* quality control parameter in the manufacturing of the superconducting material.

CHAPTER 5

STUDIES ON $YBa_2(Cu_{1-X}M_X)_3O_{7-\delta}$ (M = Ti, V, AND Ni)

5.1 INTRODUCTION

Attempts to raise the T_c as well as to improve the superconducting properties of $YBa_2Cu_3O_{7-\delta}$ (Y-Ba-Cu-O) have revealed that the superconductivity is, (1) unaffected by the substitution of Y by isoelectronic rare-earth elements that have a large localized magnetic moment [54], (2) partially affected by the substitution of Ba by an alkali metal [62], and (3) severely suppressed by the substitution of Cu by a number of elements such as Al, Ga, Ag, Sn, Ti, V, Cr, Mn, Fe, Co, Ni, and Zn [355-360]. These studies suggest that the Cu-O assembly is primarily responsible for the superconductivity, and the main contribution to the density of states at the Fermi level, $DOS(E_F)$, comes from the Cu 3d and the O 2p hybridization states. The expected local DOS (E_F) should be small around the Y^{3+} and Ba^{2+} sites because of the stable Kr and Xe core electron structure respectively. The role of Y and Ba is supportive in nature, helping to stabilize the structure and to the charge transfer mechanism between the chain Cu(1) and plane Cu(2) sites. Thus, the substitution of Cu by other metallic elements, particularly the 3d transition-metals, should produce substantial changes in the superconducting properties which in turn will elucidate the electronic structure, the mechanism, and the possible technological applications. Also, a good understanding of such defects can guide our search for new superconducting compounds.

Several groups [361-370] have studied the effect of Ti-doping on the superconductivity of Y-Ba-Cu-O. Xiao et al. [361] and Dou et al. [362] observed a decrease in the zero-resistance transition temperature (T_{CRO}). Okura et al. [363] and Nishi et al. [364] reported an increase in the onset temperature (T_{CO}), but a decrease in the T_{CRO}. An enhancement in the (T_{CRO}) up to ~100 K is reported by Talik et al. [365]. Kammlott et al. [366] observed a decrease in T_c for the sintered samples and almost no change of T_c for partially melt-processed samples. Vasilchenko et al. [367] reported the occupation of Ti at Cu sites and the distortion in orthorhombicity. Mehta et al. [368,369] reported the occupation of Ti at Cu sites and the systematic decrease in T_c with negligible change in orthorhombicity. Muralidharan et al. [370] studied the variation of resistivity and TEP with the density of materials. Similarly, the effect of vanadium doping at the Cu site has been studied by few groups [366,369-371]. The electrical and the magnetic properties of vanadium oxides have been studied [372,373,374]. It is known that the vanadium oxides in the reduced form, VO_2 and V_2O_3, become highly conductive. A crystallographic phase transformation at about 160 K causes a resistivity change by a factor of 10^7. In this case, of course, the resistance increases as temperature is lowered. Despite these studies on Ti and V-doping [361-371], a number of issues are yet to be settled. These include (1) the structural distortion, (2) the solubility limit, (3) the T_c, (4) the oxidation state, and (5) the site occupancy, and hence the role of the dopants (Ti,V) in Y-Ba-Cu-O

superconductors. Besides, no critical fluctuation and TEP studies are available on these doped systems.

Ni-doped Y-Ba-Cu-O system has also been studied by several groups [361,375-393]. However, there are discrepancies regarding (1) the lattice constant, (2) the solubility limit, (3) the T_c, (4) the site occupancy, and (5) the oxidation state and hence the role of Ni in Y-Ba-Cu-O. While Clayhold et al. [386] have studied the TEP of Ni-doped Y-Ba-Cu-O, no critical fluctuation study is available on these samples. Ni was chosen as a dopant for Cu because of (a) the high DOS(E_F) expected due to its d electrons, (b) its ionic size and orbital structure which are close to those of Cu, (c) its structure (fcc) which is same as Cu, and (d) its ferromagnetic nature over diamagnetic Cu (to see the interplay between magnetism and superconductivity).

As a part of our systematic investigations on the role of some of the selected 3d-metal dopants in Y-Ba-Cu-O, this Chapter reports the synthesis and the results of XRD, DTA, TGA, SEM, EDXA, iodometry, EPR, electrical resistivity, paraconductivity, and TEP measurements of $YBa_2(Cu_{1-x}M_x)_3O_{7-\delta}$ (M = Ti, V, and Ni). An attempt has also been made to explain the reason(s) behind the existing discrepancies in the literature. While Sections 5.2 and 5.3 deal with the Ti-, V-doped Y-Ba-Cu-O systems, Section 5.4 deals with the Ni-doped system. The method of sample preparation and other experimental details of various techniques used are given in Chapter 2.

5.2 RESULTS ON $YBa_2(Cu_{1-X}M_X)_3O_{7-\delta}$ (M = Ti, V)

5.2.1 XRD, SEM, and EDXA

High-quality polycrystalline Ti- and V-doped samples have been synthesized by the solid-state reaction method as described in Section 2.2. According to XRD analysis, the $YBa_2(Cu_{1-X}M_X)_3O_{7-\delta}$ (M = Ti,V) samples containing as much as 10 at.% (X = 0.1) of Ti or V are single phasic with orthorhombic structure (negligible change in lattice parameters and hence orthorhombicity). In the case of vanadium samples, extra weak Bragg peaks were detected for X = 0.2; for higher additions (X = 0.5 and 1) the superconducting phase does not form. SEM analysis show that the particle size is ~5 μm. Figures 5.1 and 5.2 show the typical EDXA spectra of $YBa_2(Cu_{1-X}M_X)_3O_{7-\delta}$ with X = 0.025, for Ti- and V-doped samples, respectively.

5.2.2 DTA, TGA, and Iodometry

The temperature at the endothermal peak of the DTA curves of the samples is taken as the decomposition temperature (T_d). In this study, T_d decreases as X increases (Tables 5.1 and 5.2). The presence of other minor endothermal peak(s) for samples with X $\geq$ 0.025 suggests that these samples have some additional phase(s), possibly Ti- or V-rich phase(s), which obviously melts at a lower temperature. TGA of mass loss in air for temperatures up to 850°C of Ti- and V-doped samples show that less mass (oxygen) is lost for samples with higher X.

The oxygen contents of the samples were determined by iodometry (see Section 2.8). In Ti-doped samples there is an increase in the oxygen content (6.98 ± 0.02) of the X = 0.025

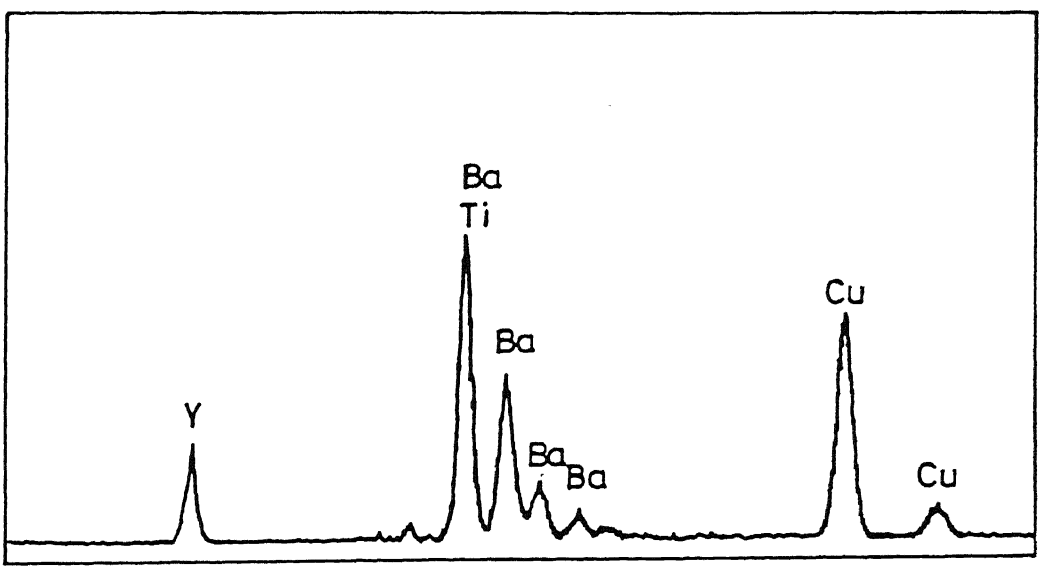

Fig. 5.1. Typical EDXA spectra (at 20 kV) of $YBa_2(Cu_{1-X}Ti_X)_3O_{7-\delta}$ (X = 0.025) sample.

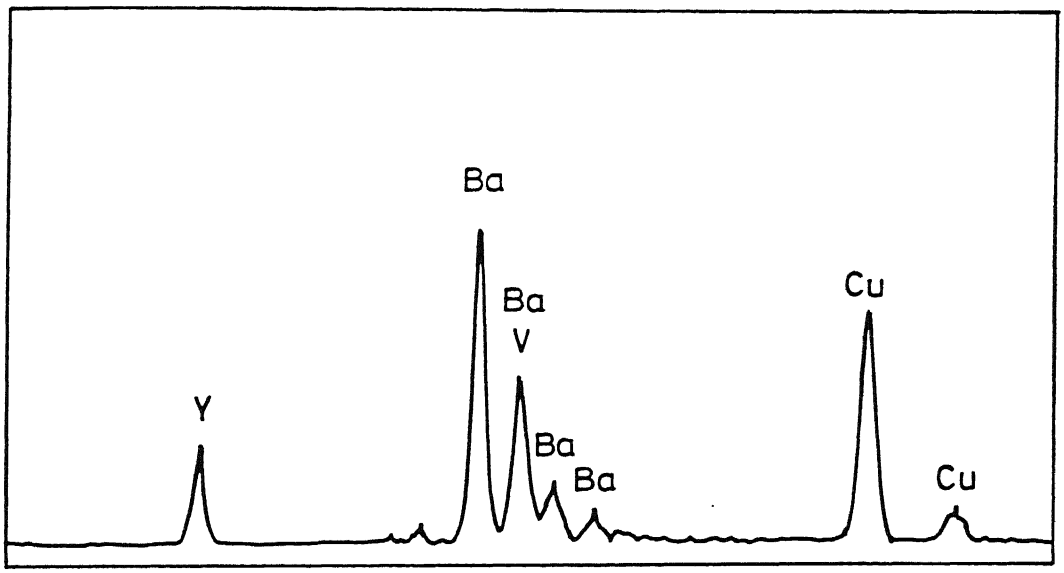

Fig. 5.2. Typical EDXA spectra (at 20 kV) of $YBa_2(Cu_{1-X}V_X)_3O_{7-\delta}$ (X = 0.025) sample.

TABLE 5.1. Some resistivity parameters of $YBa_2(Cu_{1-X}Ti_X)_3O_{7-\delta}$ samples.

X	ρ(300 K) (mΩ cm)	ρ(0 K)[a] (mΩ cm)	$d\rho/dT$[b] ($\mu\Omega$ cm/K)	T_c (K)	ΔT_c[c] (K)	T_d[d] ($^\circ$C)	$(7-\delta)$ ($\pm$ 0.02)
0	0.54	0.014	1.7	93.0	0.3	1020	6.94
0.025	2.30	0.988	4.4	90.8	0.6	1000	6.98
0.05	4.20	2.030	7.3	91.3	0.8	--	
0.075	5.79	2.800	10.1	91.4	0.9	--	
0.1	10.42	4.677	19.0	91.3	0.8	--	

a) Extrapolated residual resistivity.

b) Slope of the normal-state region ($2T \leq_c T \leq RT$) fitted to a+bT.

c) Full width at half maximum (FWHM) of the $d\rho/dT$ versus T graph.

d) Thermal decomposition temperature.

TABLE 5.2. Some resistivity parameters of $YBa_2(Cu_{1-X}V_X)_3O_{7-\delta}$ samples

X	ρ(300 K) (mΩ cm)	ρ(0 K)[a] (mΩ cm)	dρ/dT[b] ($\mu\Omega$ cm/K)	T_c (K)	ΔT_c[c] (K)	T_d[d] ($^\circ$C)	7-δ ($\pm$ 0.02)
0.0	0.54	0.014	1.7	93.0	0.3	1020	6.94
0.025	0.89	0.194	2.2	92.1	0.5	1014	7.07
0.05	0.95	0.310	2.2	92.5	0.6	-	7.14
0.075	1.45	0.306	3.8	92.9	0.6	-	7.16
0.1	1.55	0.390	3.9	92.6	0.5	-	-
0.2	5.16	0.827	14.4	92.3	0.4	-	-

[a] Extrapolated residual resistivity.

[b] Slope of the normal-state region ($2T \leq_c T \leq$ R.T.) fitted to a+bT.

[c] Full width at half maximum (FWHM) of the dρ/dT vs T graph.

[d] Thermal decomposition temperature.

sample with respect to that (6.94 ± 0.02) of the X = 0 sample (Table 5.1). Similarly, an increase in oxygen content as X increases is observed in V-doped samples (Table 5.2).

5.2.3 EPR studies

No evidence of Cu^{2+} EPR signal was observed in the pure Y-Ba-Cu-O sample. This EPR-silence indicates the absence of localized moment on Cu and also the absence of a highly oxygen-deficient composition as an impurity. All the Ti- and V-doped Y-Ba-Cu-O samples show the Cu^{2+} EPR signal.

5.2.4 Electrical resistivity

The experimental details of the resistivity (ρ) measurements have been given in Section 2.11. The temperature dependencies of the resistivity of the Ti- and V-doped Y-Ba-Cu-O samples are shown in Figs.5.3 and 5.4, respectively. All the samples are characterized by a linear temperature dependence of resistivity from at least $2T_c$ to room temperature, and by a smooth rounding off above T_c which is a characteristic of superconducting thermodynamic fluctuations. The room temperature resistivity, the residual resistivity, $\rho(0)$, and the temperature coefficient of the resistivity ($d\rho/dT$), increase systematically as the concentration (X) of Ti or V increases (see Tables 5.1 and 5.2). This can be explained in terms of increased impurity scattering of the charge carriers as X increases. In the case of higher vanadium addition, while the X = 0.5 sample forms a green phase semiconductor, X = 1 forms a white-phase insulator. All the

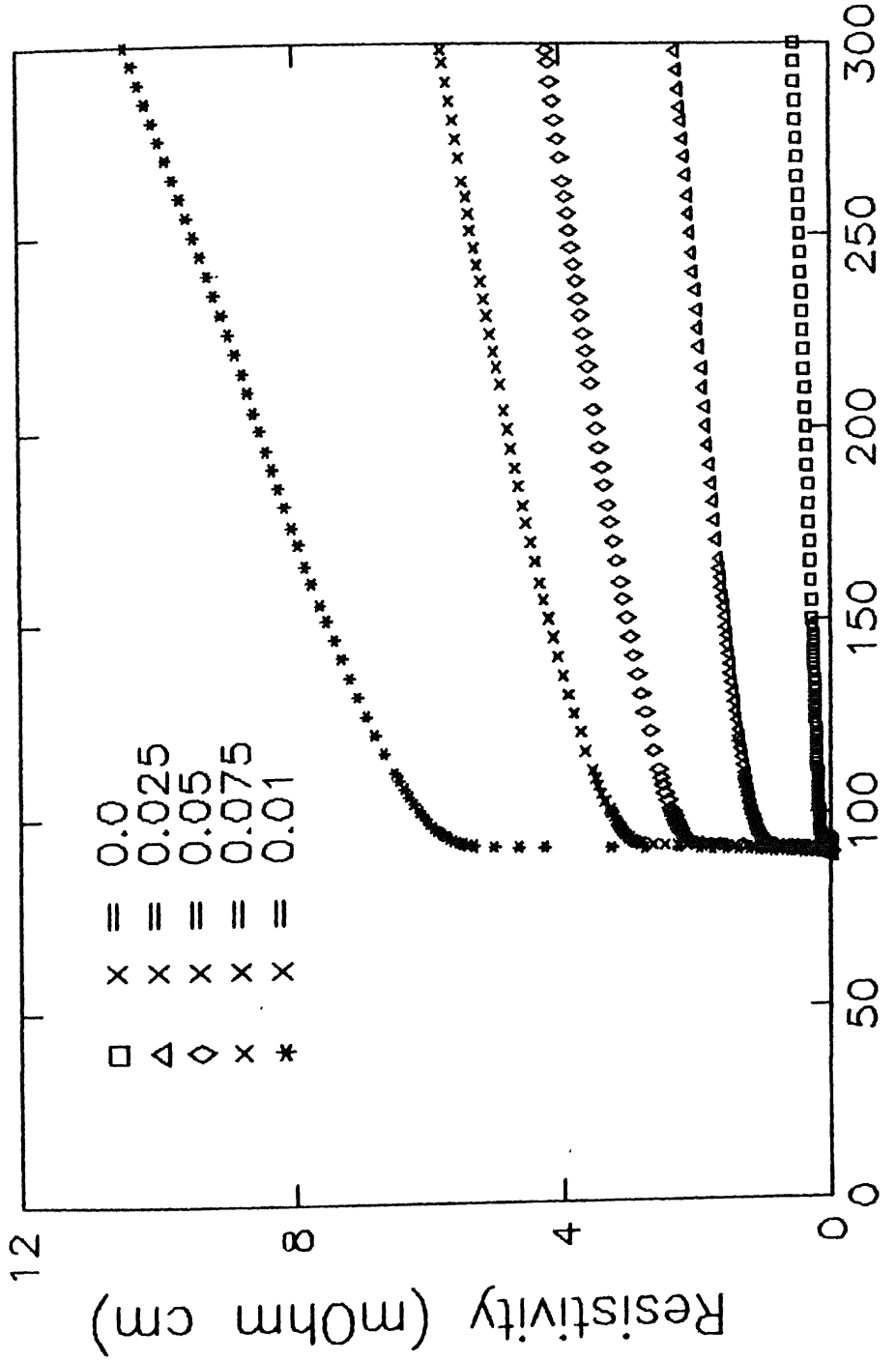

Fig. 5.3. Temperature dependence of the resistivity of $YBa_2(Cu_{1-x}Ti_x)_3O_{7-\delta}$ (X = 0 to 0.1) samples.

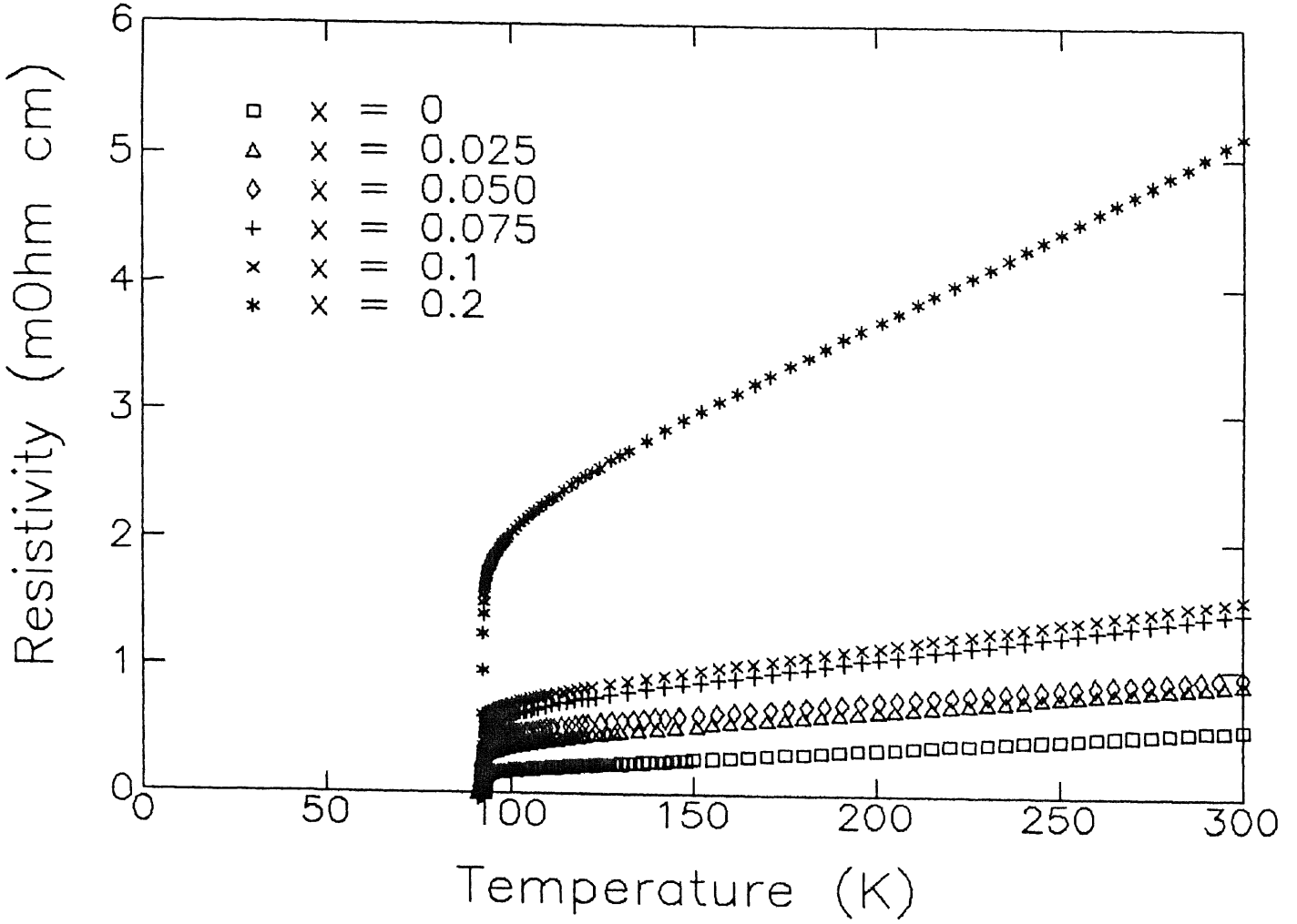

Fig. 5.4. Temperature dependence of the resistivity of $YBa_2(Cu_{1-X}V_X)_3O_{7-\delta}$ (X = 0 to 0.2) samples.

samples of $YBa_2(Cu_{1-X}M_X)_3O_{7-\delta}$ (M = Ti,V) investigated in this work show very sharp transitions around 91 K, with narrow transition widths, $\Delta T_c \leq 0.9$ K, provided by the width of the peak in the $d\rho/dT$ versus T graph at half height (Fig.5.5).

Figures 5.6 and 5.7 show replots of the ρ-data in the form ρT versus T^2 for Ti- and V-doped samples, respectively, to test the Anderson-Zou fit. In order to test the 2D and 3D fluctuations and afford a comparison with the previous results on Y-Ba-Cu-O, the normalized excess conductivity, $(\Delta\sigma/\sigma_{300})$, is plotted against the reduced temperature ε. Figures 5.8 and 5.9 show these results on Ti- and V-doped samples, respectively. In these cases, two distinct linear regions are identified. There is a high-temperature region in which the exponent is nearly -0.8 (region I), followed by a mean-field region in which the exponent is approximately -0.4 (region II).

5.2.5 Thermoelectric Power (TEP)

The thermopower behavior of the undoped $YBa_2Cu_3O_{7-\delta}$ as a function of temperature has been discussed in Chapter 4. The experimental details of TEP measurements are given in Section 2.12. Figures 5.10 and 5.11 show the thermopower of $YBa_2(Cu_{1-X}M_X)_3O_{7-\delta}$, M = Ti and V, respectively, as a function of temperature. All the doped samples show positive values of TEP. The magnitude of TEP at 300 K keeps increasing as X increases.

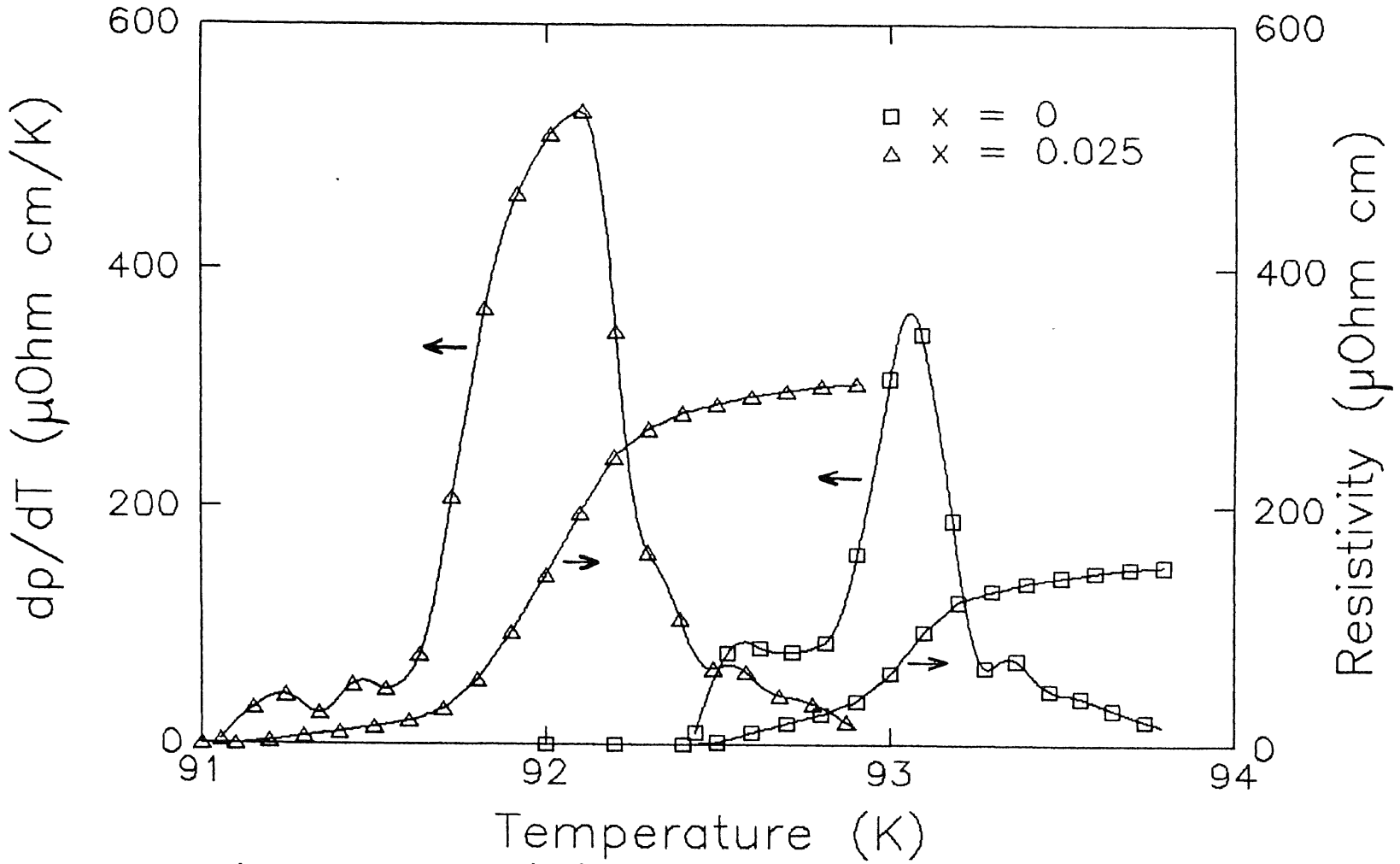

Fig. 5.5. The variation of $(d\rho/dt)$ versus T for $YBa_2(Cu_{1-X}V_X)_3O_{7-\delta}$ (X=0 to 0.025) samples. The temperature dependence of the resistivity in the transition region is also shown.

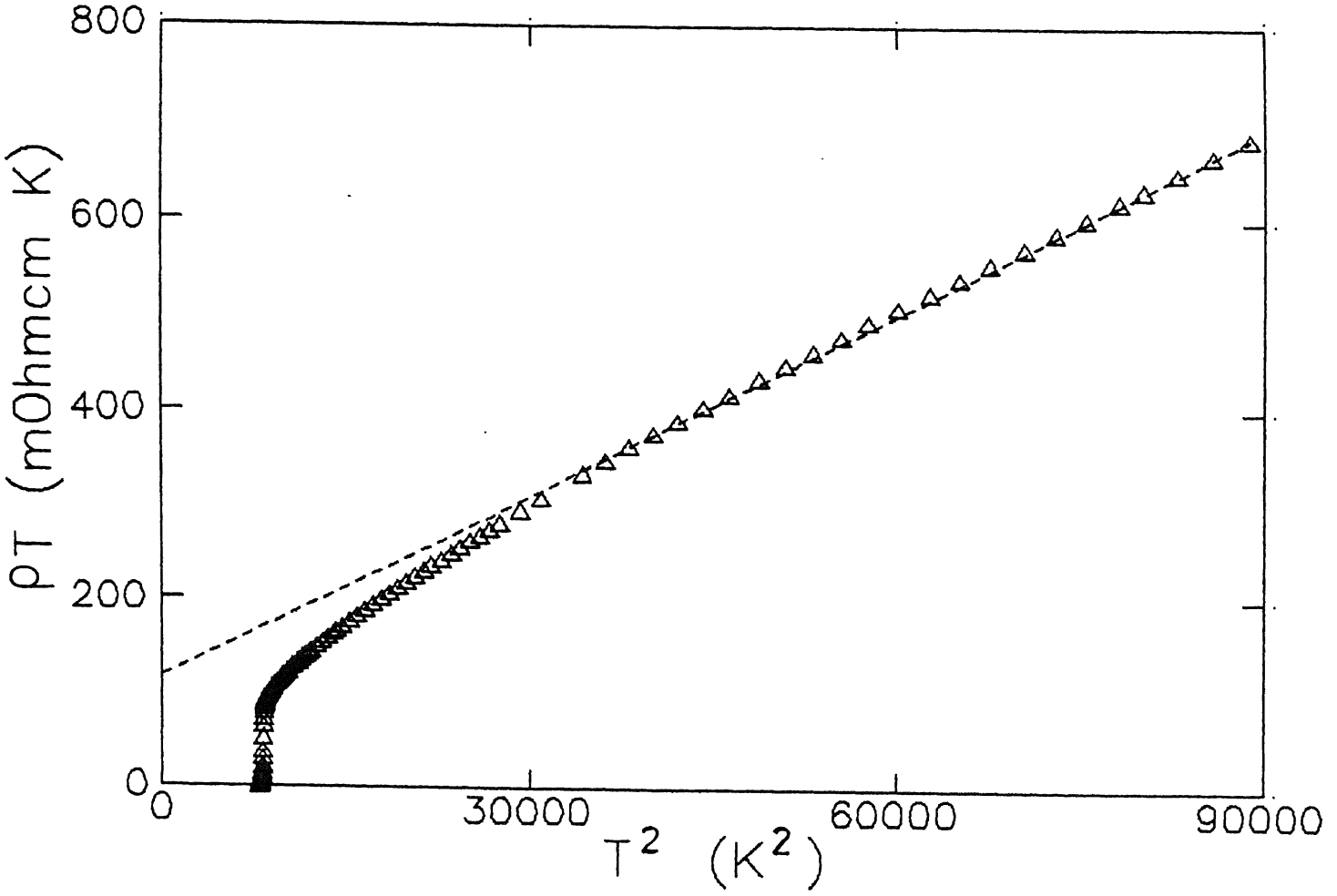

Fig. 5.6. Anderson-Zou plot of the data (with X=0.025) in Fig. 5.3.

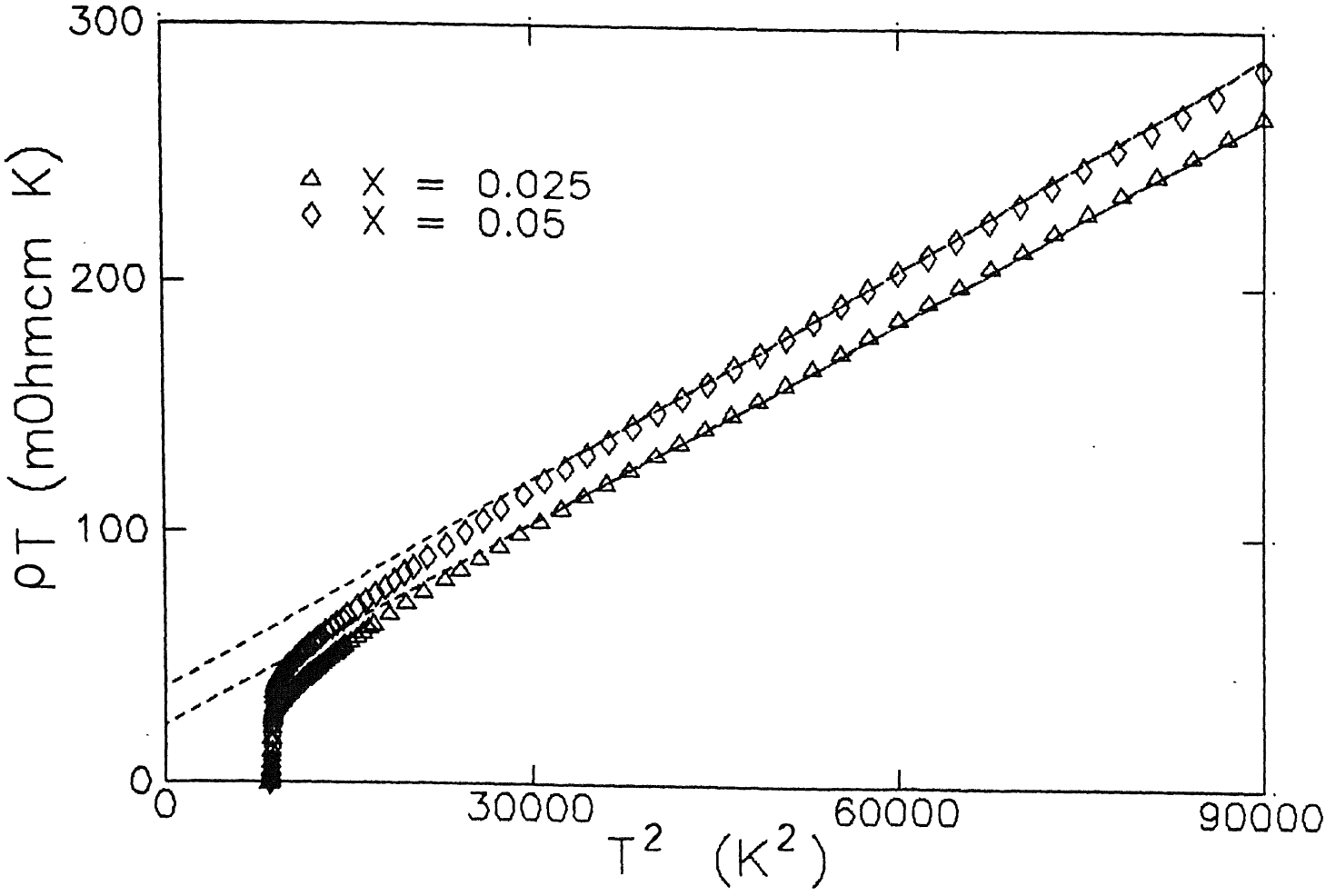

Fig. 5.7. Anderson-Zou plot of the data (with X = 0.025, 0.05) in Fig. 5.4.

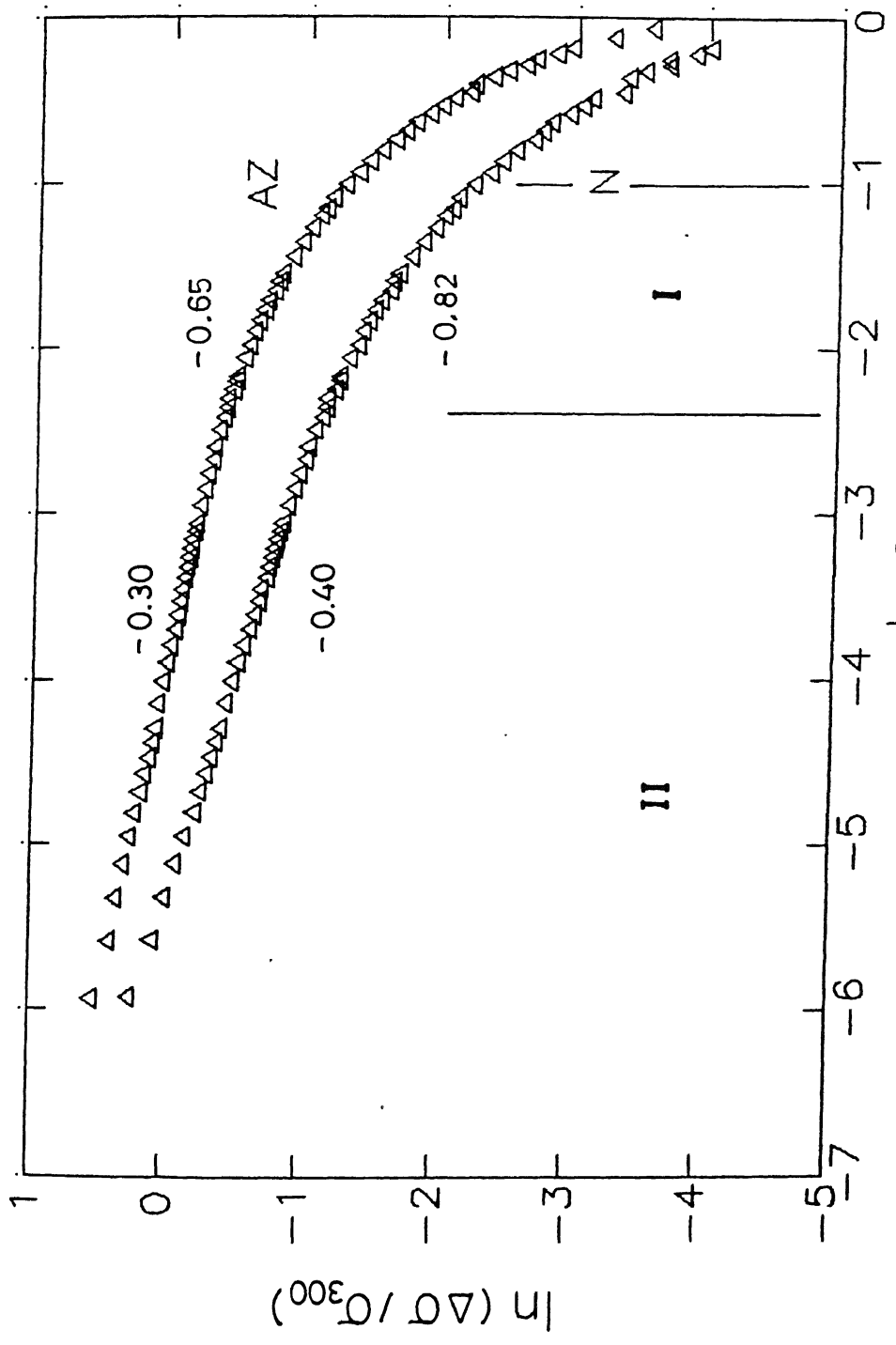

Fig. 5.8. Log-log plot of the normalized excess conductivity ($\Delta\sigma/\sigma_{300}$) vs. reduced temperature (ε) for the Ti-doped sample with X = 0.025; (N): $\Delta\sigma$ obtained by normal metal extrapolation; (AZ): $\Delta\sigma$ obtained from the Anderson-Zou fit to the data.

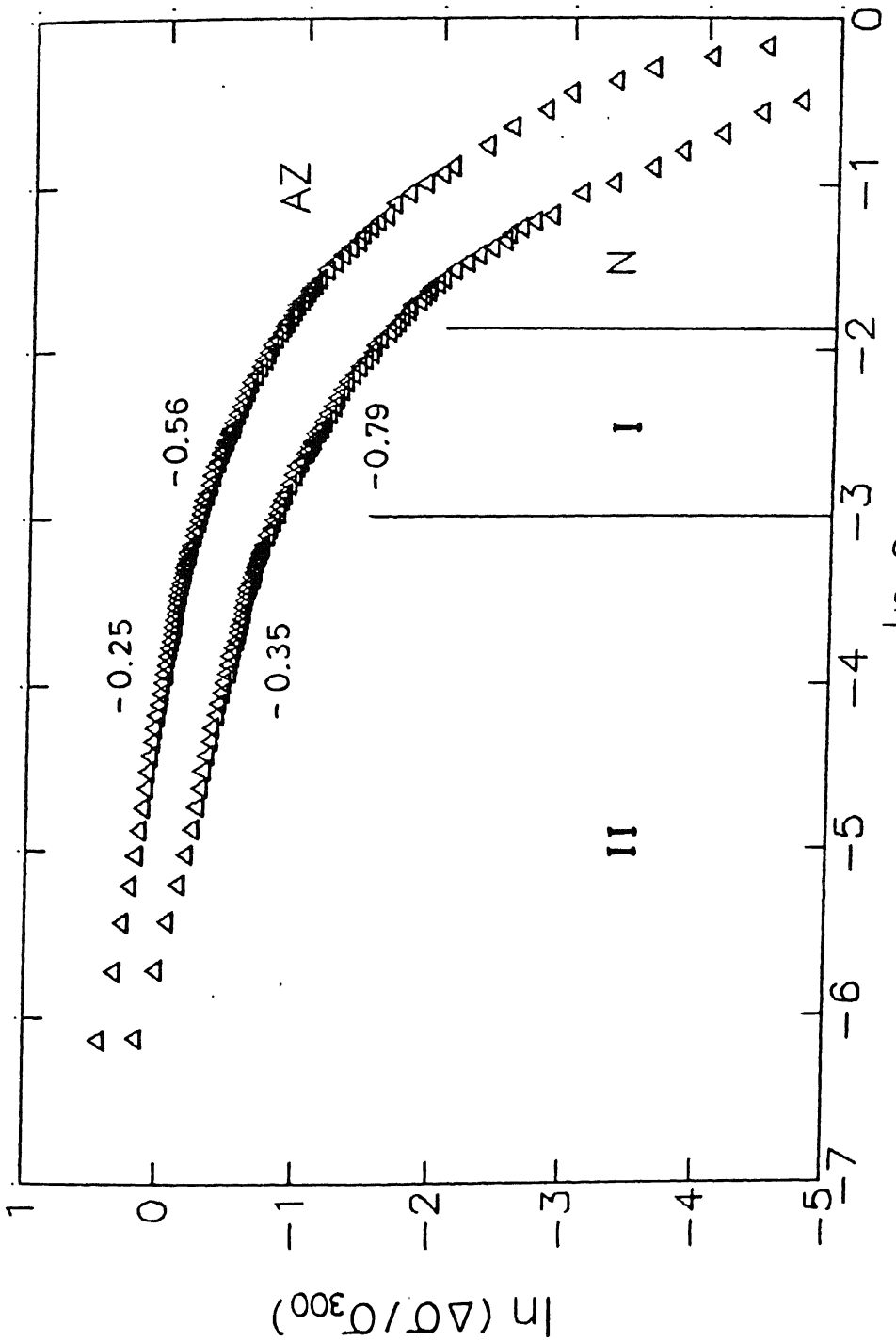

Fig. 5.9. Log-log plot of the normalized excess conductivity ($\Delta\sigma/\sigma_{300}$) vs. reduced temperature (ε) for the V-doped sample with X = 0.025; (N): $\Delta\sigma$ obtained by normal metal extrapolation; (AZ): $\Delta\sigma$ obtained from the Anderson-Zou fit to the data.

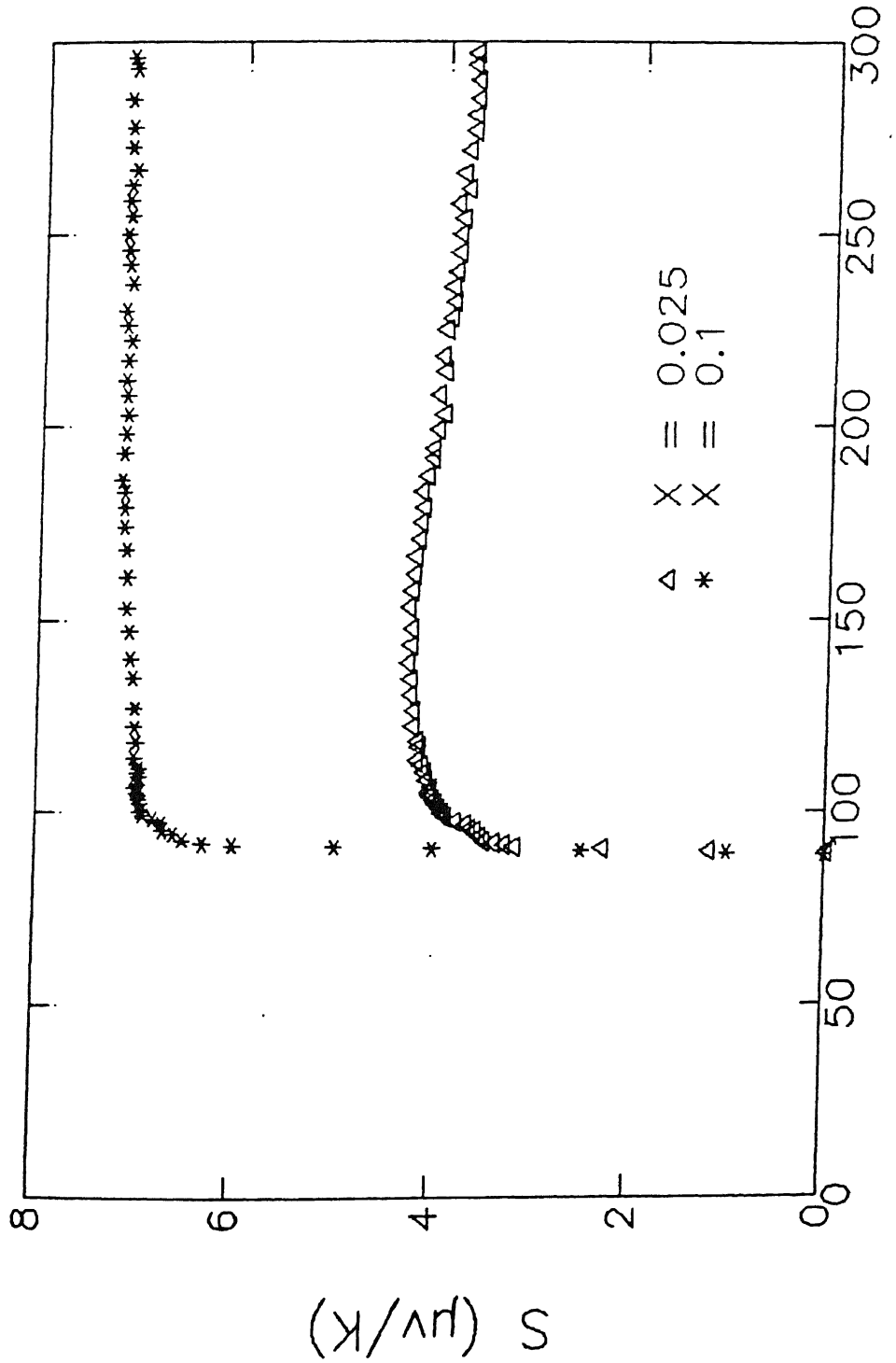

Fig. 5.10. Thermopower as a function of temperature for $YBa_2(Cu_{1-X}Ti_X)_3O_{7-\delta}$ (X = 0.025, 0.1) samples.

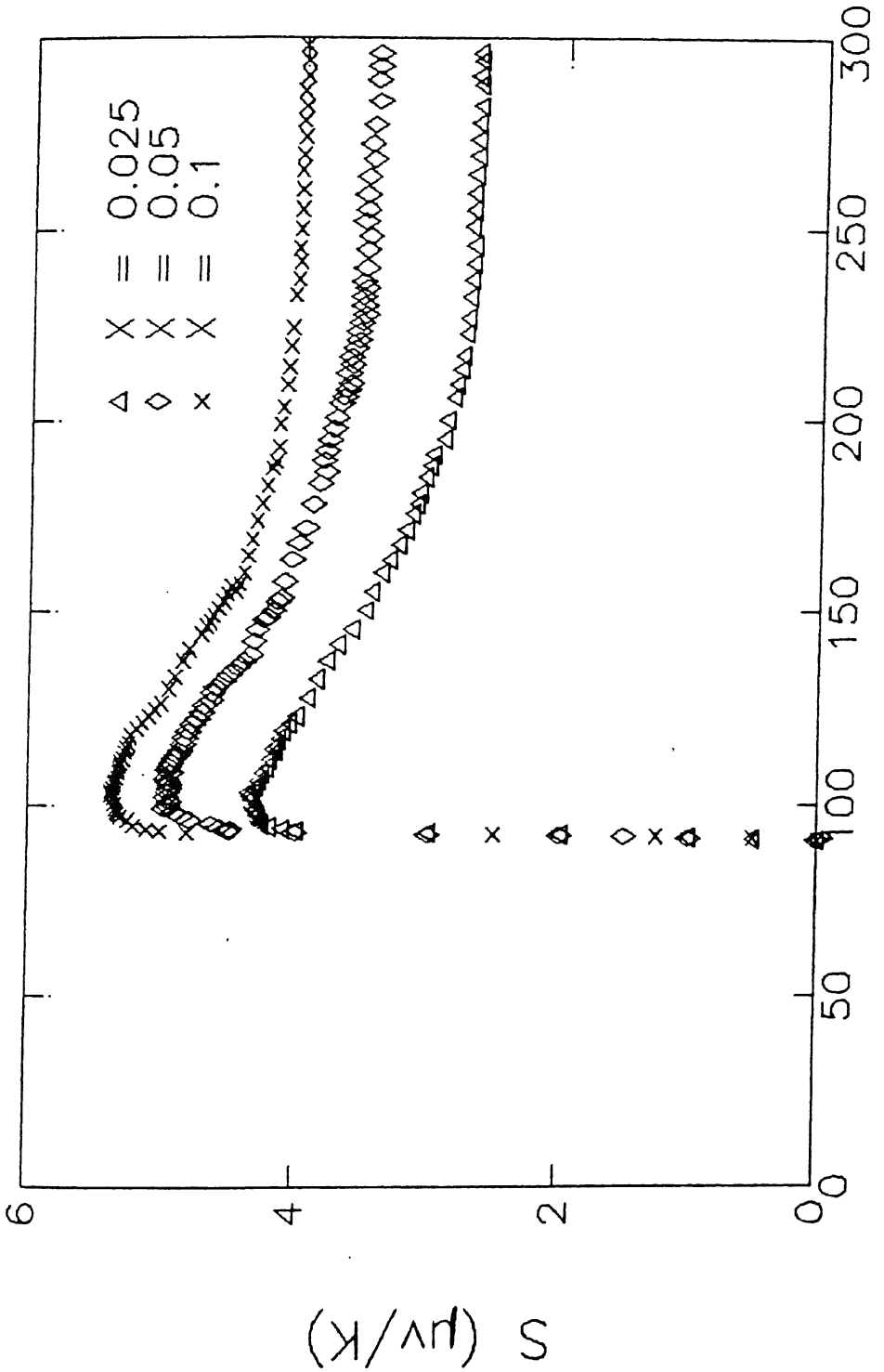

Fig. 5.11. Thermopower as a function of temperature for $YBa_2(Cu_{1-X}V_X)_3O_{7-\delta}$ (X = 0.025, 0.05, 0.1) samples.

5.3 DISCUSSION ON $YBa_2(Cu_{1-X}M_X)_3O_{7-\delta}$ (M = Ti, V)

5.3.1 Solubility

While the oxygen content determined by iodometry (Tables 5.1 and 5.2), and the mass (oxygen) loss obtained from TGA indicate a limited solubilities of Ti and V in Y-Ba-Cu-O, the DTA, SEM, and EDXA suggest (indirectly) that the solubility of Ti or V, in any case, is not more than 2.5 at.% . However, the XRD patterns do not reveal the presence of any second phase even in samples containing dopants up to ~10 at%, probably due to the limited resolution of the XRD technique. Although there are several investigations [361-371] on Ti- and V-doped Y-Ba-Cu-O samples, the solubility limits of these dopants are not clearly established. However, all these studies do indicate that the solubility is very limited. An upper limit of 2.5 at.% solubility inferred in this work is in good agreement with that of Mehta et al. [368,369].

5.3.2 Oxidation state

There is no Cu^{2+} EPR signal near g~2 in undoped Y-Ba-Cu-O samples. This indicates the absence of a localized moment on Cu and suggest that the samples are monophasic, and the volume of Cu is greater than 2+, as reported earlier. The presence of the Cu^{2+} EPR signal near g~2 in all the Ti, V-doped samples indicates that the Ti or V perhaps reduces the valence of copper, to 2+. In this process, the dopants (Ti or V) are likely to assume a higher oxidation state. Possible states of Ti and V are Ti^{3+}/Ti^{4+} and V^{4+}/V^{5+}, respectively. No EPR signal related to Ti^{3+} has been

observed down to 77 K. Similarly, the absence of 8 line series EPR-signal rules out the possibility of V in the V^{4+} valence state. So the possible oxidation state of Ti is Ti^{4+} and that of V is V^{5+}, which are EPR inactive. These results are in agreement with the XPS results of Mehta et al. [368,369].

Although the size of the Ti^{4+} ion (0.68 A°) is comparable to that of the Cu^{2+} ion (0.69 A°), its poor solubility in Y-Ba-Cu-O may be due to its different valence (4+) and structure (hexagonal) from Cu, which is divalent and cubic in structure. The poor solubility of V in Y-Ba-Cu-O may be due to its (1) smaller size (0.59 A°versus 0.72 A° for Cu^{2+}) and (2) different structure. To maintain the charge neutrality, in addition to the reduction of Cu valence, the dopants might have entered the Cu(1) site with higher oxygen coordination, for instance, in an octahedral environment.

5.3.3 Electrical Resistivity

Figures 5.3 and 5.4 show the temperature dependence of the resistivity of the Ti- and V-doped Y-Ba-Cu-O samples. The pure (X=0) sample has a T_c~93 K. The sharp drop in ρ at T_c, leading to narrow transition widths (ΔT_c), might appear to be due to the existence of percolative paths which first become superconducting, thereby shorting out the current. However, this is ruled out in view of the absence of any non-ohmic behavior and the presence of a single, well-defined peak in $d\rho/dT$ versus T plots (Fig. 5.5). While the samples other than X=0 have considerable extrapolated residual resistivities, the sample with

X=0 has an extrapolated intercept that approaches the origin (ρ=0) at T=0. The small values of ρ(0) indicate that the samples are of reasonably high quality and contain fewer defects.

According to Anderson-Zou (see Section 4.2.3), the normal-state resistivity is given by $\rho(T) = A/T+BT$, where the hyperbolic term is introduced to model the inter-plane hopping of carriers. The AZ plots (see Figs.5.6 and 5.7) are linear over most of the investigated temperature range, which implies that the resistivity behavior in dense, high quality polycrystalline materials is intrinsic to a to a single grain and thus similar to that of ρ_{ab} in single crystals. These results indicate that the samples of Ti and V with x=0.025 respectively, are suitable for paraconductivity analyses (see Section 5.3.4).

All the Ti-doped samples (X=0.025, 0.05, 0.075, and 0.1) have T_cs ~91 K. That is, the T_c and also the ΔT_c are affected only slightly by the initial doping, and remain almost constant on further addition. The possible reason for this behavior is that, when the dopant concentration is large, the excess dopant drains (precipitates) out of the superconducting matrix. This superconducting-impurity phase mixture superconducts by short circuiting the current via the least resistance paths and exhibits a particular T_c which is a characteristic of the superconducting matrix and largely independent of the nature and concentration of the impurity phase. Thus, an almost unchanged T_c is obtained by sintering the pellets at 970-985°C (depending upon the Ti concentration in the sample). These results are in broad agreement with those of Kammlott et al. [366] who have reported

(1) a severe suppression of T_c with a varying degree of broadening of the ΔT_c in the case of pellets sintered at ~950°C , and (2) an unchanged T_c with the formation of pure 1:2:3 phase in the case of partially melt-processed samples.

The reported decrease in T_c by Xiao et al. [361], Dou et al. [362], and Mehta et al. [368,369] is possibly due to the lower sintering temperature employed by them. A higher T_{CO} with lower T_{CRO} and thereby the much varying degree of broadening of the superconducting transition, reported by Okura et al. [363] and Nishi et al. [364] also appears to be mainly due to the sample processing conditions. Talik et al. [365] reported a T_{CRO} ~100 K. However, this result is contradicted by their own XRD results and the AC susceptibility data which show the presence of a second phase with a lower T_{CRO} . The possible reason for their contradictory observations may be (1) the inconsistency in their sample preparation (lower sintering temperature with fast cooling rate) and (2) the lower current values used by them, which might have reduced the resolution of their resistivity measurements and thus led to the higher estimate of T_{CRO} .

The results on V-doped Y-Ba-Cu-O samples are similar to those of Ti-doped samples, viz. the T_c and the ΔT_c are almost unaffected. The solubility of V is also very limited (not more than 2.5 at.%). The observed results (viz. an almost unchanged T_c) in V-doped samples can be explained in a way similar to that of Ti-doped samples. Thus, it is evident that an almost no change of T_c and a narrow ΔT_c is possible in a product that has been sintered at a temperature close to the melting point in case

of Ti or V-doped Y-Ba-Cu-O samples. These results are (1) different from those of Kammlott et al. [366], who have reported severe suppression of T_c associated with a varying degree of broadening of the ΔT_c in both the sintered and the partially melt-processed samples, and (2) in broad agreement with those of Brnicevic et al. [371], who have reported no change in the orthorhombic phase and in the T_c up to 6 at.% .

It is concluded that the small fraction of dissolved Ti or V ions possibly occupy Cu(1) sites with an oxidation state of Ti^{4+}/ V^{5+}, and thus do not much affect the density of states at the plane sites and hence the T_c. Thus, it is argued that the existing discrepancies in the literature are mainly due to the different processing conditions used by various investigators, leading to variations in the solubility limits of the dopants and the oxygen content which affects the defect concentration, and possibly also due to the lower resolution in the resistivity measurements of some investigators.

5.3.4 Paraconductivity

The details of the paraconductivity analysis have been given in Section 4.2.4. In all the doped samples for ϵ exceeding 0.1, the paraconductivity falls steeply, much faster than any power laws proposed in the literature for the pure 1:2:3 system can predict. The critical exponent in region II is affected by the precise choice of T_c,and it is, in all cases studied here, close to -1/2 as predicted by the AL theory for 3D fluctuations in the mean-field region. Also, the reduced temperature limits of region II are generally in agreement with others for pure Y-Ba-Cu-O.

In the Anderson-Zou (AZ) case, the behavior of ln $(\Delta\sigma/\sigma_{300})$ versus ln ϵ for the samples is identical with the normal metal case but with different values of the exponent. This clearly demonstrates how extrapolation-dependent is the observed critical behavior in the absence of any quantitative model of the normal-state resistivity.

5.3.5 Thermoelectric Power (S)

While pure Y-Ba-Cu-O samples with different oxygen contents show positive and negative TEP (see Section 4.2.5), all the Ti- and V-doped samples show positive TEP. The systematic increase in the magnitude of the TEP with the increase in the values of dopant concentration(X) shows that the impurity or defect scattering keeps increasing as the doping concentration increases, a result consistent with the resistivity behavior. Also, the estimated T_c (with $\Delta T_c \sim 0.5$ K) is quite consistent with that estimated from resistivity studies.

It follows from the eq. (4.11), that a plot of ST versus T^2 should be a straight line. Figures 5.12 and 5.13 show these plots for Ti and V-doped Y-Ba-Cu-O samples, respectively, in the range 160 K $\leq$ T $\leq$ 300 K. It is evident that the TEP data for both undoped (see Section 4.2.5) and doped samples fit Eq. (4.11) quite well. Thus, the observed changes in the intercept and the slope of the undoped and doped samples of Y-Ba-Cu-O show that the phonon drag and the band-filling effects are responsible for the changes in S.

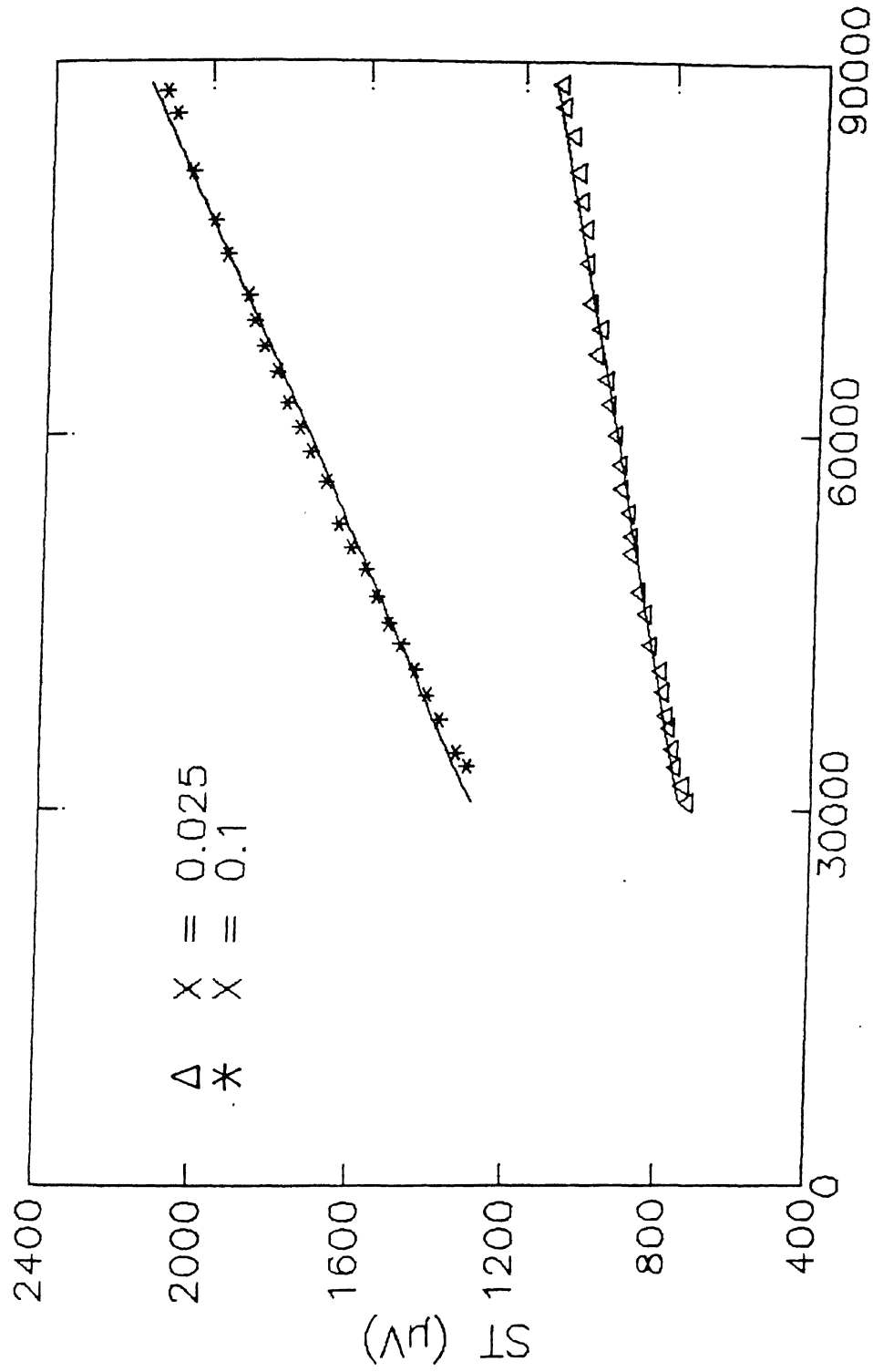

Fig. 5.12. ST vs. T^2 plots for $YBa_2(Cu_{1-x}Ti_x)_3O_{7-\delta}$ (X = 0.025, 0.1) samples.

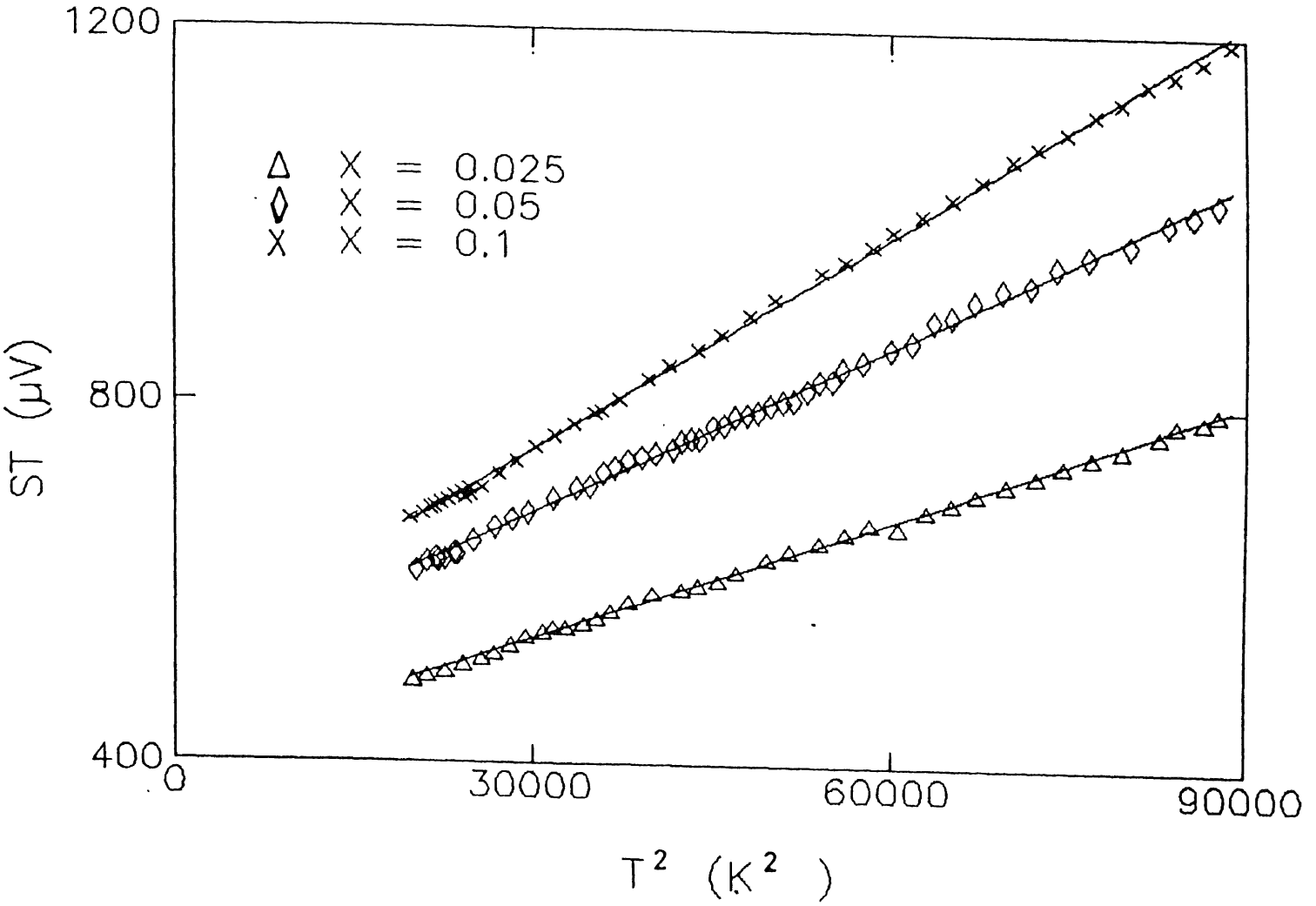

Fig. 5.13. ST vs. T^2 plots for $YBa_2(Cu_{1-X}V_X)_3O_{7-\delta}$ (X = 0.025, 0.05, 0.1) samples.

There is no convincing explanation for the surprising enhancement of the TEP just above the T_c. It is argued that the TEP enhancement is a precursor feature related to the existence of superconducting fluctuations. The reduced electron-phonon scattering leads to an enhanced phonon flux in the normal regions of the mixed state near a superconducting boundary, which in turn enhances the phonon drag. The diffusion TEP is, of course, not enhanced. The net TEP as T_c is approached from higher temperatures is then a weighted average of the normal and the superconducting TEP. Since the superconducting regions contribute no TEP, the mixed state will simply show a reduced normal-state TEP, but the enhancement described above causes the drag TEP to fall significantly more slowly than the diffusion TEP. Within this picture, the precursor peak can be interpreted as no more than a falling negative diffusion TEP lying under a broad positive phonon drag feature. The phonon drag TEP at low temperatures is simply given by

$$S_g = C_g / 3ne , \qquad (5.1)$$

where C_g is the lattice specific heat per unit volume and e is the carrier charge. Also, the small carrier density favors a large drag TEP, as of course does a strong carrier-phonon interaction. A decrease in the carrier density n and in increase in the phonon current due to superconducting fluctuations above T_c would tend to enhance the phonon drag thermopower. However, that is difficult to understand as a mechanism contributing to

the sharpness of the peak near 100 K , since superconducting pairs will tend to short out the thermoelectric voltage arising from phonon drag as well as that from diffusion.

5.4 RESULTS AND DISCUSSION ON $YBa_2(Cu_{1-X}Ni_X)_3O_{7-\delta}$

5.4.1 Solubility

The Ni-doped Y-Ba-Cu-O samples were prepared by solid-state reaction method as discussed in Section 2.2. According to XRD analysis, the $YBa_2(Cu_{1-X}Ni_X)_3O_{7-\delta}$ samples with X = 0.1 are single-phase with orthorhombic structure. The presence of minor impurity peaks was detected in samples with X = 0.2. The cell parameters are reported in Table 5.3. The cell volume increases slightly initially and then decreases as X increases. This change is due to the ionic size variation (which depends upon the oxidation state) of Ni in comparison to Cu ion. This variation of lattice parameters is in broad agreement with the literature.

Both the SEM and EDXA analyses suggest that the solubility limit of Ni in Y-Ba-Cu-O is ~10 at.%. The endothermal peaks in the DTA curves are taken as the decomposition temperature (T_d). The T_d values are also reported in Table 5.3. All but the sample with X = 0.2 show well defined single endothermal peak. The multiple endothermic peaks in the DTA curve of X = 0.2 sample suggest the presence of other phases which obviously melt at different temperatures. Within the experimental error, the TGA of mass loss in air for temperatures up to 850°C of $YBa_2(Cu_{1-X}Ni_X)_3O_{7-\delta}$ ($0 \leq X \leq 0.1$) samples show no significant mass (oxygen) loss. All the samples with $X \leq 0.1$ are EPR silent.

TABLE 5.3 Variation of cell parameters, thermal decomposition temperature, and oxygen content for $YBa_2(Cu_{1-X}Ni_X)_3O_{7-\delta}$ as a function of nominal Ni composition X.

X	a(A°)	b(A°)	c(A°)	V(A^{o3})	T_d(°C)	(7-δ) ±0.02
0	3.820	3.885	11.670	173.19	1020	6.93
0.025	3.825	3.889	11.668	173.56	1013	6.94
0.05	3.826	3.890	11.660	173.53	1008	6.92
0.075	3.821	3.883	11.665	173.07	1004	6.93
0.1	3.824	3.882	11.651	172.96	1000	6.94
0.2	3.822	3.870	11.620	171.87	--	6.85

The Cu^{2+} EPR signal in X = 0.2 sample shows the presence of second impurity phase. The oxygen content (Table 5.3) was determined by iodometry. While there is almost no change in the oxygen content up to X = 0.1, there is some decrease in the value for the X = 0.2 sample.

All the above studies suggest the solubility limit of Ni in Y-Ba-Cu-O to be ~ 10 at.%. This is in good agreement with the results of Maeno et al. [376], Xu et al. [381], Liang et al. [382], and Kammlott et al. [385]. However, the presence of only minor impurity phase(s) in the X = 0.2 sample suggests that the value of ~10 at.% may be an underestimate of the solubility limit of Ni in Y-Ba-Cu-O. It may possibly be some what higher than that (~10 at.%) as reported by Tarascon et al. [375] but very unlikely to be as low as 4 at.% [390] or as high as 20 at.% as reported by Bringley et al. [378]. These discrepancies in the observed solubility limits of Ni in Y-Ba-Cu-O may probably be attributed to varying sample processing procedures and the resolution of the characterization techniques.

5.4.2 Oxidation state

The Cu^{2+} EPR silence in the undoped Y-Ba-Cu-O samples indicates the absence of a localized moment on Cu; it also shows that the samples are monophasic, as reported earlier [394]. Besides, in samples doped up to 10 at.% Ni are EPR silent. The observed Cu^{2+} EPR signal in the 20 at.% Ni-doped sample shows the presence of a second (impurity) phase. Also there is almost no change in the oxygen content in the samples with X up to 10 at.%

Ni. To preserve the charge neutrality of the system either the Cu might have acquired a higher oxidation state (Cu^{3+}) as suggested by Clayhold et al. [386] or the doped Ni possibly might have entered into higher oxidation state (Ni^{3+}), at least for higher doping concentration (X) of Ni, as suggested by Liang et al. [382].

5.4.3 Electrical Resistivity

The temperature dependence of the resistivity of the Ni-doped Y-Ba-Cu-O samples is shown in Fig.5.14. The samples with $X \leq 0.075$ are characterized by a linear temperature dependence of resistivity from at least $2T_c$ to room temperature, and by a smooth rounding off above T_c which is a characteristic of the superconducting thermodynamic fluctuations. The samples with $X \geq 0.1$ show metallic behavior at higher temperatures and semiconductor behavior at lower temperatures before entering into the superconducting state. This suggests that the electrons are getting weakly localized before the superconductivity sets-in. As in case of Ti- and V- doped samples, the room temperature resistivity, the temperature coefficient of the resistivity ($d\rho/dT$), and the residual resistivity [$\rho(0)$] increase systematically as the concentration of Ni (X) increases (see Table 5.4). This may be explained in terms of increased impurity scattering as X increases.

The $YBa_2(Cu_{1-X}Ni_X)_3O_{7-\delta}$ samples of compositions X = 0.0, 0.025, and 0.05, investigated in this work show very narrow transition width, $\Delta T_c \leq 0.5$ K, provided by the width of the peak

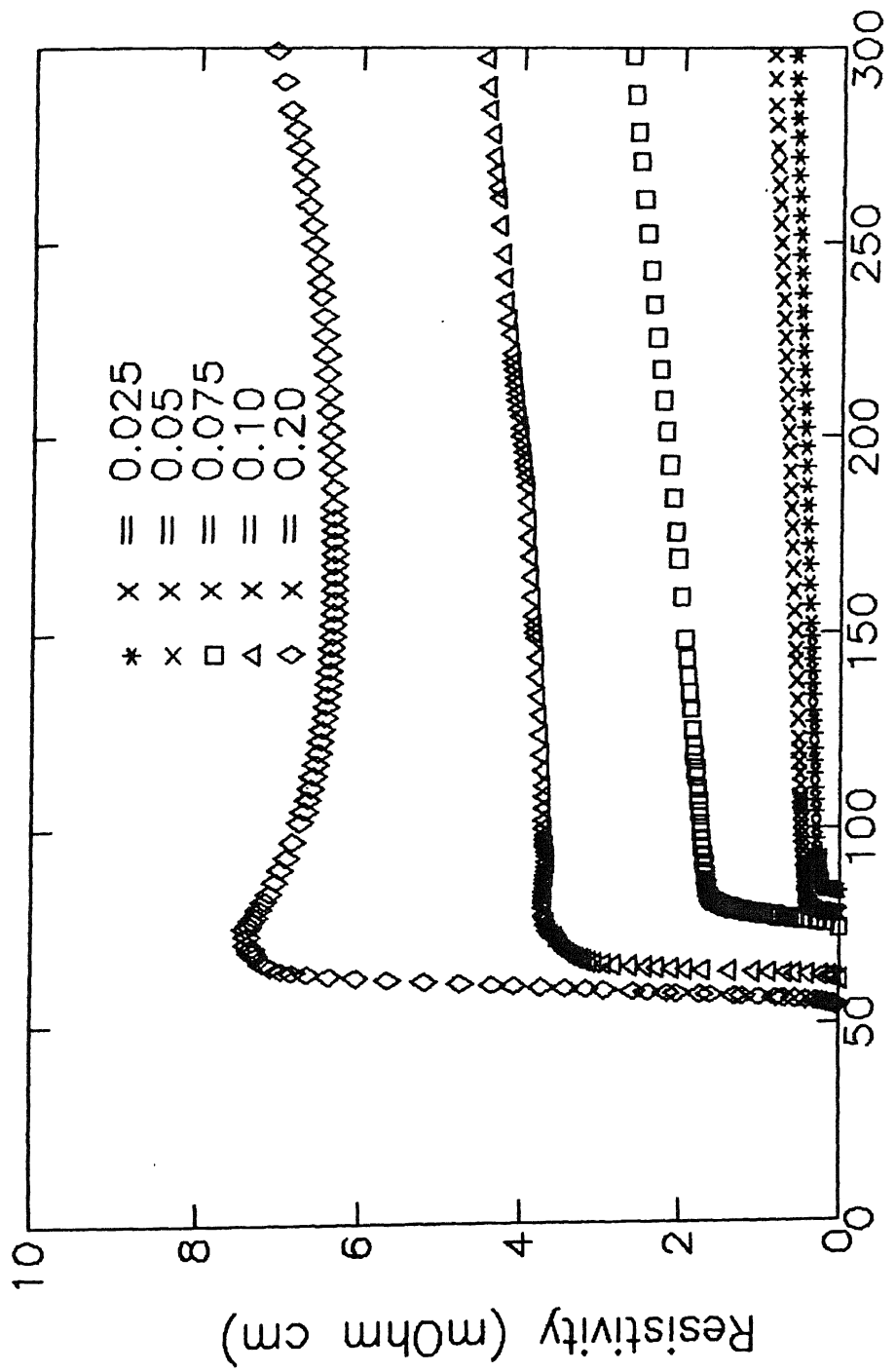

Fig. 5.14. Temperature dependence of the resistivity of $YBa_2(Cu_{1-x}Ni_x)_3O_{7-\delta}$ (X = 0.025 to 0.2) samples.

TABLE 5.4 Some resistivity parameters of $YBa_2(Cu_{1-X}Ni_X)_3O_{7-\delta}$.

X	ρ(300 K) ($\mu\Omega$ cm)	ρ(0 K)[a] ($\mu\Omega$ cm)	$d\rho/dT$[b] ($\mu\Omega$ cm/K)	T_c (K)	ΔT_c[c] (K)
0	537	14	1.7	93.0	0.32
0.025	613	135	1.7	84.0	0.56
0.05	888	242	2.2	78.4	1.00
0.075	2643	1250	4.5	77.3	1.72
0.1	4503	3170	4.7	63.1	2.10
0.2	7072	--	--	58.5	3.02

a) Extrapolated residual resistivity.

b) Slope of the normal-state linear region ($2T_c \leq T \leq RT$) fitted to a+bT.

c) Full Width at Half Maximum (FWHM) of the $d\rho/dT$ versus T graph.

in the $d\rho/dT$ versus T graph at half height. A typical $d\rho/dT$ versus T graph for X = 0.025 sample is shown in Fig.5.15. This is comparable to those found in single crystals (sc) [241,242] and some of the best polycrystalline (pc) Y-Ba-Cu-O samples [110]. The sharp drop in ρ at T_c, leading to narrow transition widths (ΔT_c), may seem to be due to the existence of percolative paths which first become superconducting, thereby shorting out the current. However, this is ruled out in view of the absence of any non-ohmic behavior and the presence of a single, well-defined peak in $d\rho/dT$ versus T plots. While the samples other than X = 0 have considerable extrapolated residual resistivities, the sample with X = 0 has an extrapolated intercept that approaches the origin at T = 0. The small positive value of $\rho(0)$ indicates that the samples are of reasonably high-quality and contain fever defects [140,141]. The pure (X = 0) sample has a T_c ~ 93 K. In Ni-doped samples the T_c gets suppressed from 93 K (X = 0) to 59 K (X = 0.2). Figure 5.16 shows the variation of T_c versus concentration (X). The singlet state, which is formed from the hybridization of $3d_{x^2-y^2}$ - $2p\sigma$ orbitals and thought to be crucial to superconductivity [395], cannot occur at the Ni site. Thus, one possibility for the observed suppression of superconductivity is due to the substitution of Ni and the effective removal of Cu-O sites, rather than from a decrease in available itinerant holes as suggested by Clayhold et al. [386]. However, Xiao et al. [361] have attributed the decrease in the T_c to magnetic effects, while Tarascon et al. [375] have ascribed this to disorder effects. The observed decrease in T_c versus X in this work is in good agreement with that of Bringley et al. [378], Xu et al.

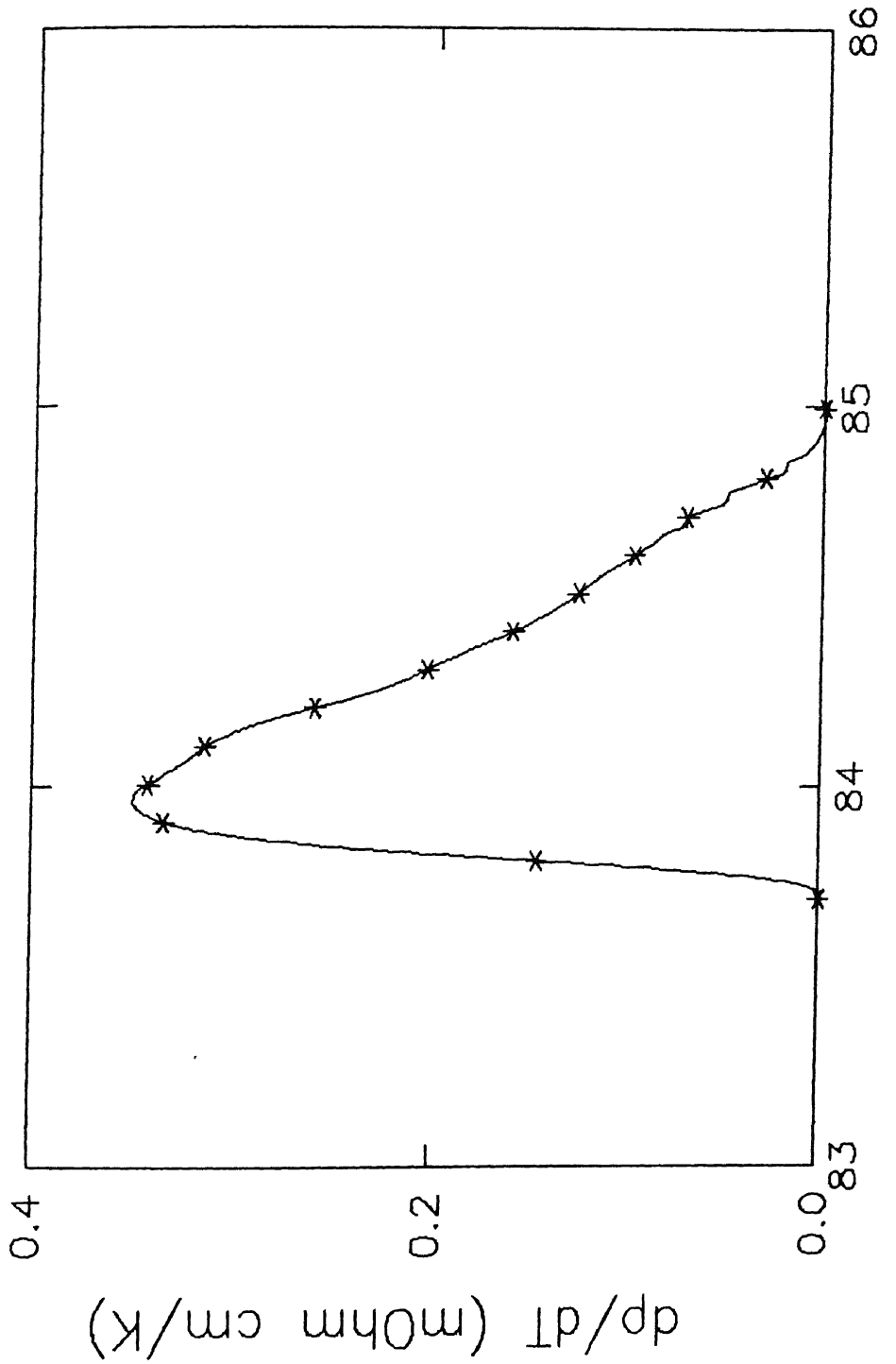

Fig. 5.15. The variation of ($d\rho/dt$) versus T for $YBa_2(Cu_{1-X}Ni_X)_3O_{7-\delta}$ (X=0.025) sample.

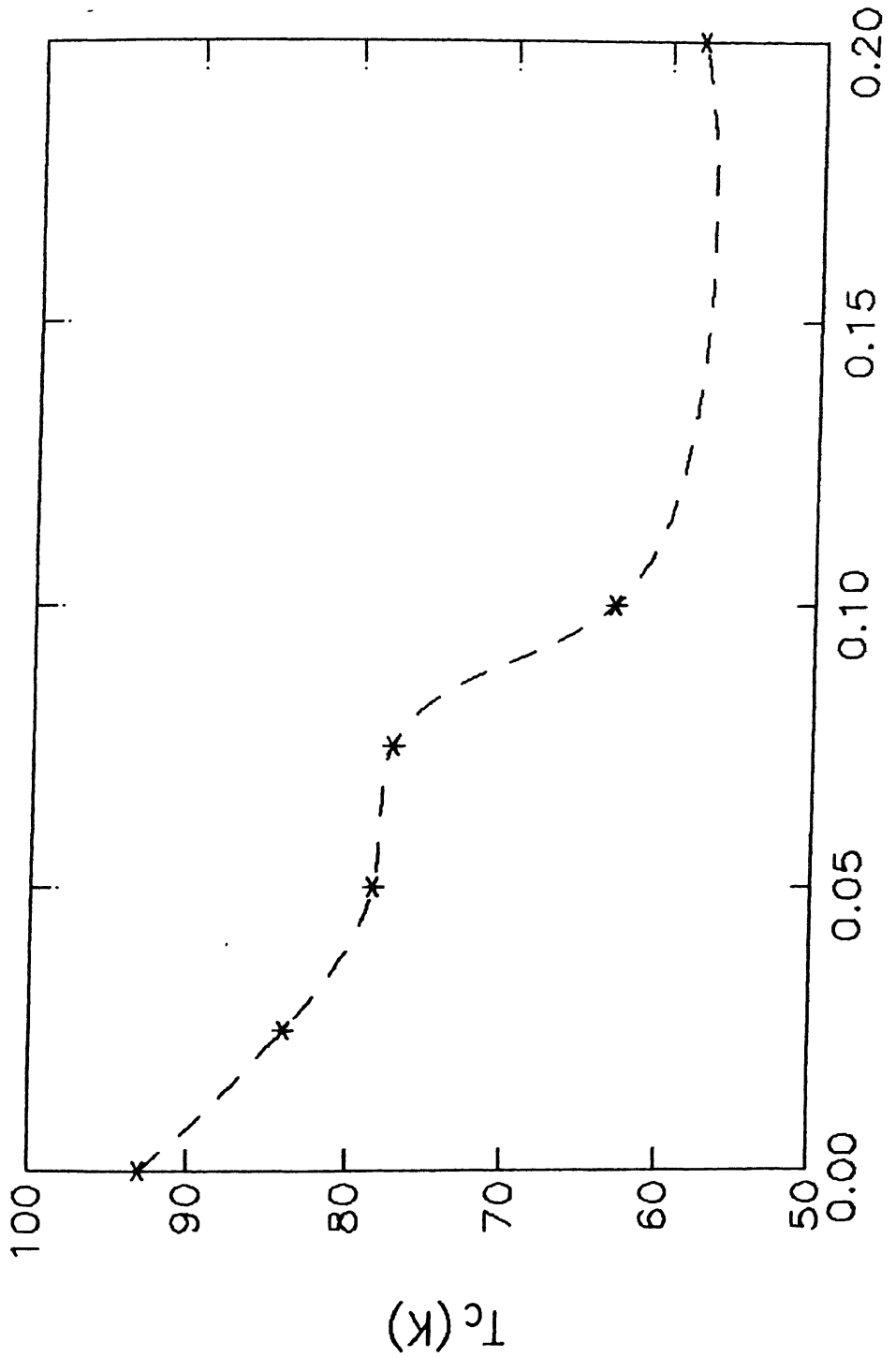

Fig. 5.16. The variation of transition temperature of $YBa_2(Cu_{1-X}Ni_X)_3O_{7-\delta}$ with concentration X. The dashed curve is a guide to the eyes.

[381], Liang et al. [382], Zhang et al. [384], and Clayhold et al. [386], but differs with Bridges et al. [391]. These differences in the T_c versus X behavior may also be due to different processing conditions adopted by various investigators. Strictly speaking, a comparison of our T_c versus X behavior with these reported in literature is not possible because of the lack of oxygen content data in several cases. Also, the presence of small amount of impurity phases may affect the intake of oxygen and consequently the value of T_c.

Although a pc sample consists of randomly oriented crystallites, due to anisotropy the low in-plane resistivity will dominate in the equivalent parallel resistor network. Thus, in a dense, good quality pellet, the resistivity should essentially have the same behavior, and hence yield the same type of information, as does the ρ_{ab} in a single crystal study. To test this further, the Anderson-Zou (AZ) analysis is applied to the ρ-data in the normal state. According to these authors, the normal-state resistivity is given by $\rho(T) = A/T + BT$, where the hyperbolic term, as mentioned earlier, is introduced to model the inter-plane hopping of carriers. Figure 5.17 shows the replots of the ρ-data on the basis of Anderson-Zou analysis (see Section 4.2.3) in the form ρT versus T^2 for Ni-doped samples. The plots are linear over most of the investigated temperature range, which implies that the resistivity behavior in dense, high quality pc materials is intrinsic to a single grain and thus similar to that of ρ_{ab} in single crystals. In view of these qualities, the resistivity data may be utilized for the paraconductivity studies, as discussed below.

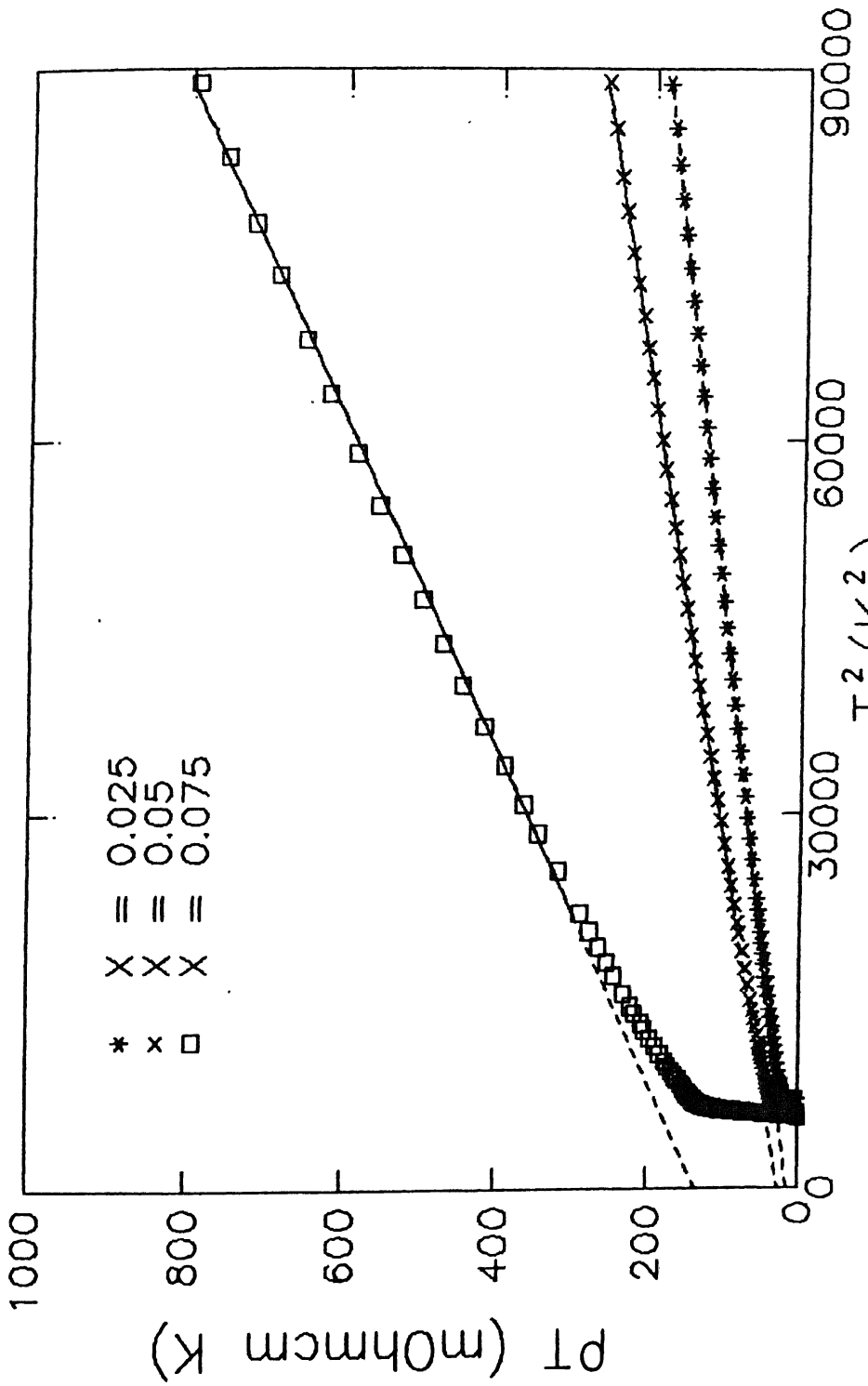

Fig. 5.17. Anderson-Zou plot of the resistivity data reported in Fig. 5.14. for $YBa_2(Cu_{1-X}Ni_X)_3O_{7-\delta}$ samples (X = 0.025, 0.05, 0.075).

5.4.4 Paraconductivity

In order to test the 2D and 3D fluctuations and afford a comparison with the previous results on undoped Y-Ba-Cu-O samples, the normalized excess conductivity, $(\Delta\sigma/\sigma_{300})$, is plotted against the reduced temperature ε and the results are shown in Fig. 5.18 for $YBa_2(Cu_{1-X}Ni_X)_3O_{7-\delta}$ samples with X = 0.025. It suggests a 2D behavior in the normal metal (N) fit and a 3D behavior in the AZ fit in the mean-field like regime.

5.4.5 Thermoelectric Power

Figure 5.19 shows the TEP of $YBa_2(Cu_{1-X}Ni_X)_3O_{7-\delta}$ ($0.025 \leq X \leq 0.2$) samples as a function of temperature. The estimated T_c (with $\Delta T_c \sim 1$ K) is quite consistent with that estimated from the resistivity studies. It is observed that the thermopower is driven to negative values even for small doping concentrations of Ni. When the doping concentration is further increased the TEP systematically changes from negative to positive values. This suggests that the undoped Y-Ba-Cu-O sample should have a value of TEP around zero as observed. It is evident that the TEP is very sensitive to the type of defects. These results are in broad agreement with those of Clayhold et al. [386].

Equation (4.11) suggest that a plot of ST versus T^2 should be a straight line. Figure 5.20 show this plot for Ni-doped Y-Ba-Cu-O samples. It is evident that the TEP data for both undoped (see Section 4.2.5), Ti-, and V-doped (Section 5.3.5) and Ni-doped samples fit Eq. (4.11) quite well. Thus, the observed changes in the intercept and the slope of the undoped and doped samples of Y-Ba-Cu-O show that the phonon drag and the

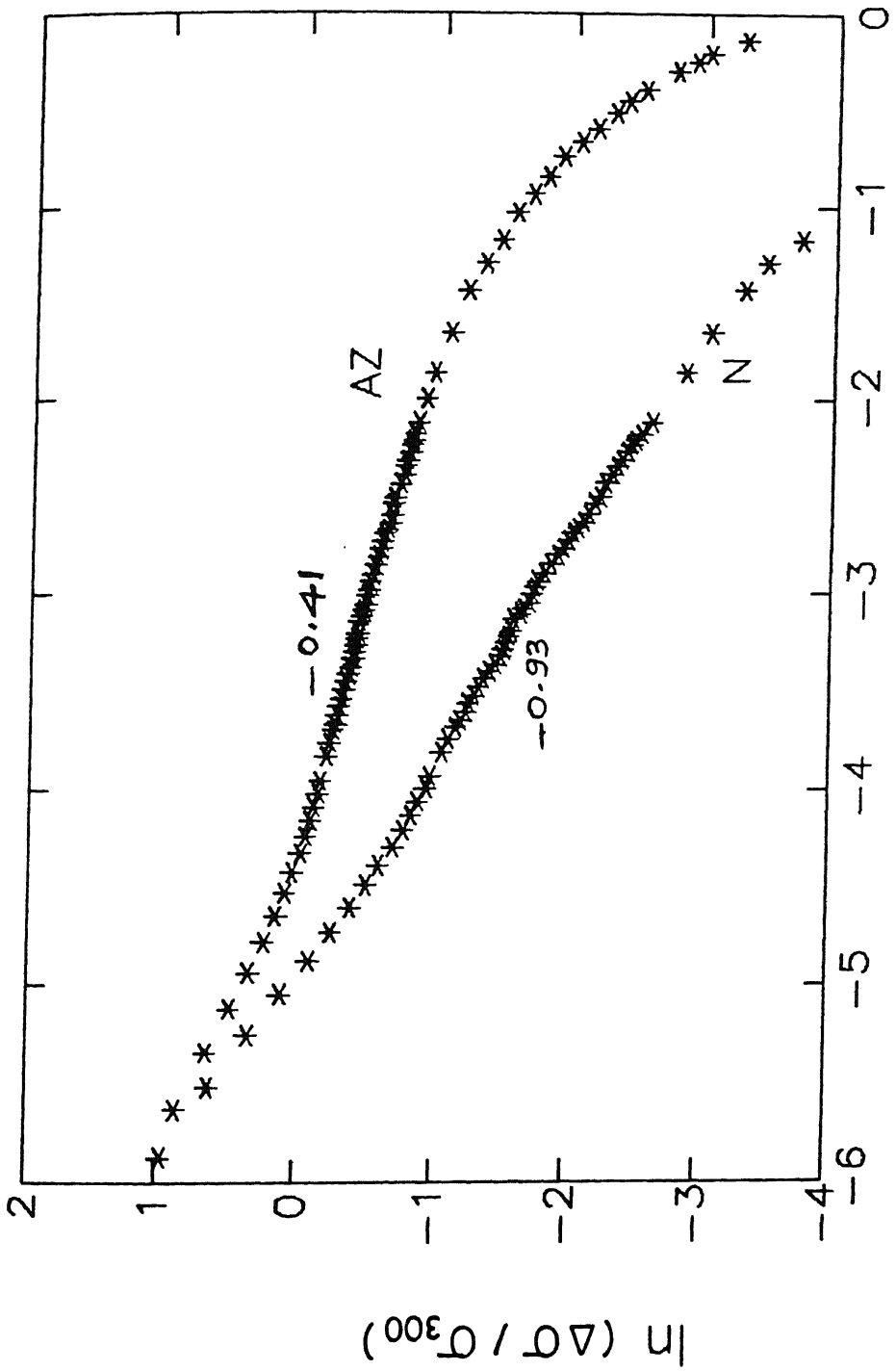

Fig. 5.18. Log-log plot of the normalized excess conductivity ($\Delta\sigma/\sigma_{300}$) versus reduced temperature (ϵ) for the Ni-doped sample with X = 0.025; (N): $\Delta\sigma$ obtained by normal metal extrapolation; (AZ): $\Delta\sigma$ obtained from the Anderson-Zou fit to the data.

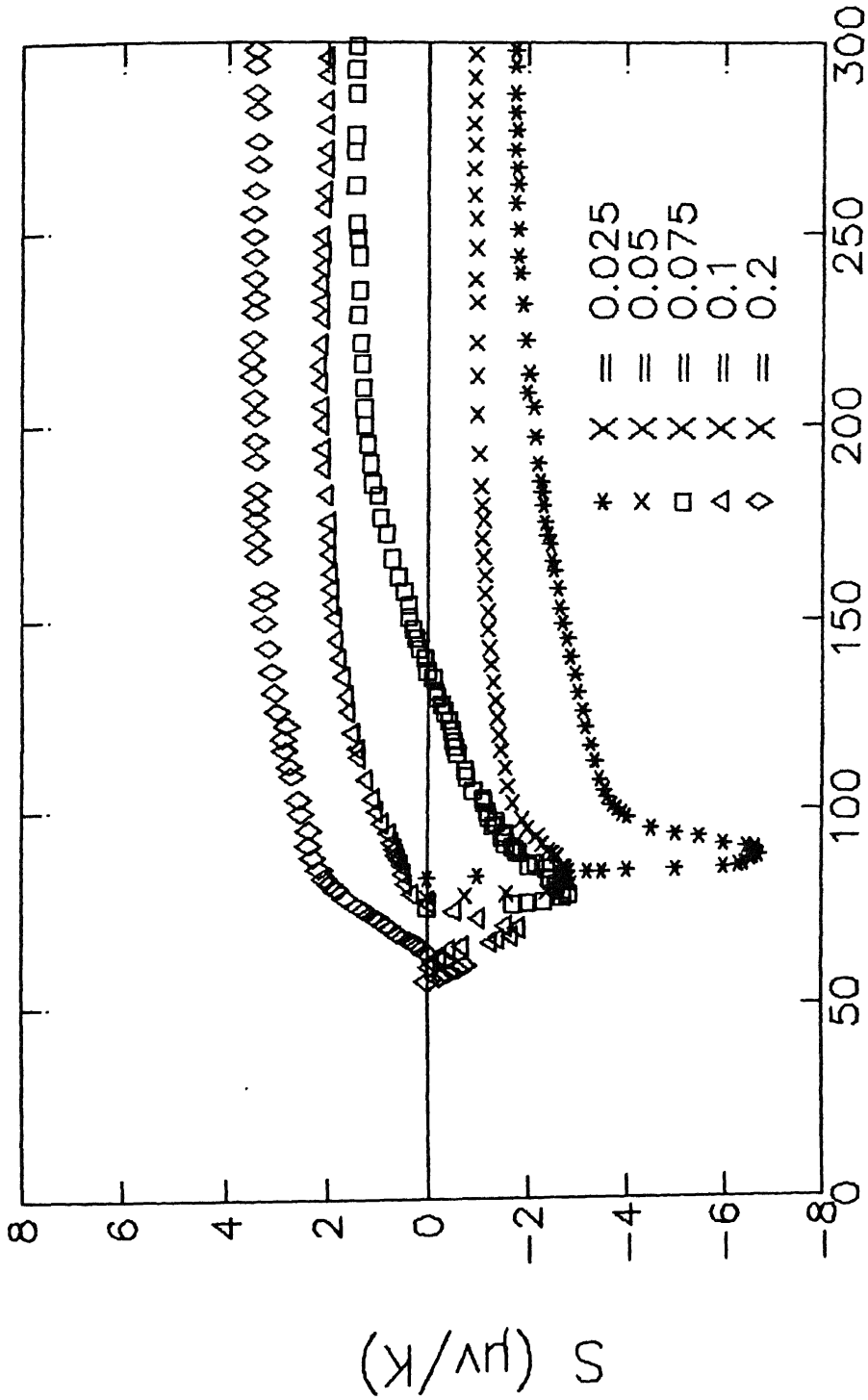

Fig. 5.19. Thermopower as a function of temperature for $YBa_2(Cu_{1-x}Ni_x)_3O_{7-\delta}$ ($0.025 \leq X \leq 0.2$) samples.

band-filling effects are responsible for the changes in S. Here it is appreciated that the phonon drag becomes significant in the clean limit ($\ell > \xi$), i.e., in sc or sinters with minimal lattice defects, generally observed in the temperature range $\Theta_D/10$ to $\Theta_D/5$, where Θ_D is the Debye temperature. Besides, the very small TEP measured in good ceramics and the sharp increase to large positive values when Y-Ba-Cu-O is doped with Pr [287] or oxygen is removed [294] have been suggested by Anderson [207] as evidence for midband filling. The fact that thermopower can be driven to negative values with systematic doping of Ni is also consistent with the midband filling. The large S is suppressed as one approaches the pure system because of the cancellations, arising from electron-hole symmetry in the midband situation.

5.5 Conclusions

The solubility of the Ti- or V-dopants in Y-Ba-Cu-O is very limited and, in any case, not more than 2.5 at.% . Higher concentrations of the dopants (X) result in Ti- or V-rich second phase formation. However, up to X = 0.1, the structure, the T_c, and the ΔT_c remain almost the same as in the case of pure 1:2:3 phase. For all the $YBa_2(Cu_{1-X}Ni_X)_3O_{7-\delta}$ ($0 \leq X \leq 0.2$) samples the structure remains orthorhombic. However, minor impurity peaks were detected in the XRD pattern of X = 0.2 sample. The solubility of the Ni in Y-Ba-Cu-O is found to be ~ 10 at.% .

It is concluded that a major source of the existing discrepancies in the experimental values of transport parameters is the differing processing conditions used by various investigators. The sintering of the samples at temperatures very

close to the melting point seems to have certain advantages. The fact that the T_c of the Ti- and V-doped Y-Ba-Cu-O compounds remains almost unaffected is of technological interest in view of the need for non-poisonous and high melting point materials that could be used as a substrates in high-temperature processing of Y-Ba-Cu-O.

Both room temperature resistivity and TEP increase systematically as the dopant (Ti, V and Ni) concentration increases, as expected in view of impurity scattering. The Anderson-Zou fit to the ρ-data is found to work as well in polycrystals as in single crystals. Paraconductivity studies on Ti and V doped samples show a 2D to 3D crossover when it passes from high-temperature to mean-field region. However in case of Ni doped YBCO samples the paraconductivity studies show a 2D behavior in normal-metal fit and 3D behavior in AZ fit, in the mean field like regime (MFR). The TEP data on all the three doped systems are found to follow a relation of the type $S = A/T + BT$. The present results and discussion suggest the midband-filling and the phonon drag with the involvement of two carrier species (multiband conduction) mechanisms operative in these systems.

CHAPTER 6

STUDIES ON (Bi, Pb, Sb)-Sr-Ca-Cu-O

6.1 INTRODUCTION

Following the initial work of Michel et al. [396] and Maeda et al. [65] a number of studies have reported HTSC in Bi-Sr-Ca-Cu oxide system. It has been found that there exists a series of compounds with general formula $Bi_2Sr_2Ca_{n-1}Cu_nO_{2n+4}$ with n=1,2,3, etc. The transition temperature with zero-resistance (T_{CRO}) is obtained at 10, 85, and 110 K for n=1,2, and 3, respectively. Although single phase materials could be prepared corresponding to n=1 and 2, the material corresponding to n=3 occurs in mixed phase only. Several attempts have been made to obtain the pure 110 K-phase, $Bi_2Sr_2Ca_2Cu_3O_y$ (2223), without the presence of 85 K-phase $Bi_2Sr_2Ca_1Cu_2O_8$ (2212) in this system. However, the amount of high-T_c 2223 phase is very sensitive to the preparational procedure. As a result, under normal conditions, it is difficult to obtain a superconductor with a T_{CRO} higher than 85 K.

Sunshine et al. [66] discovered that Pb substitution for Bi stabilizes the 2223 phase and raises the T_{CRO} above 100K. Hongbao et al. [397] reported that the substitution of Sb for Bi in the Pb-doped compounds gives a T_c~132 K. Chandrachood et al. [398] reported that the substitution of Sb for Bi in the Pb-free compound leads to superconductivity at 132 K. It is generally agreed upon that the preparation of 2223 monophase is quite difficult [68,71] and to obtain a nearly single phase 2223, it requires long-term sintering [71] except in case of reduced

oxygen partial pressure [67]. A three step reaction process with a short sintering time for the preparation of nearly 110 K-phase in the Pb-doped system has been reported by Zhengping et al. [399]. Recently, Huang et al. [400] reported that Ca and Cu rich liquid-phase-aided process in Pb-doped system gives nearly monophasic 110 K-phase. However, the overall mechanism of the formation of 2223 phase is still not very clear. In view of this, a systematic study of the above systems was undertaken.

The samples corresponding to n=2 and 3 with or without Pb and/or Sb substitutions have been prepared under different ambient conditions. Melt quenching method has been used for the preparation of glassy systems. Further experimental details have been given in Chapter 2. The characterization of (Bi, Pb, Sb)-Sr-Ca-Cu-O superconductors by XRD, DTA, resistivity, dielectric, and thermoelectric power (TEP) measurements is discussed below.

6.2 RESULTS AND DISCUSSION

6.2.1 $Bi_2Sr_2CaCu_2O_Y$

Figures 6.1 and 6.2 shows the resistivity as a function of temperature for several samples of $Bi_2Sr_2CaCu_2O_Y$ (2212) system. The T_c's of the samples A, B, C, D, and E are 65, 60, 68, 70, and 93 K, respectively. These Figs. 1 and 2 demonstrate that the room temperature resistivity (ρ_{RT}), the slope ($d\rho/dT$), the onset temperature, the T_c, etc., are all very sensitive to the preparational conditions. The sample E is characterized by a linear temperature dependence of resistivity from at least $2T_c$ to room temperature, and by a smooth rounding off above T_c which is

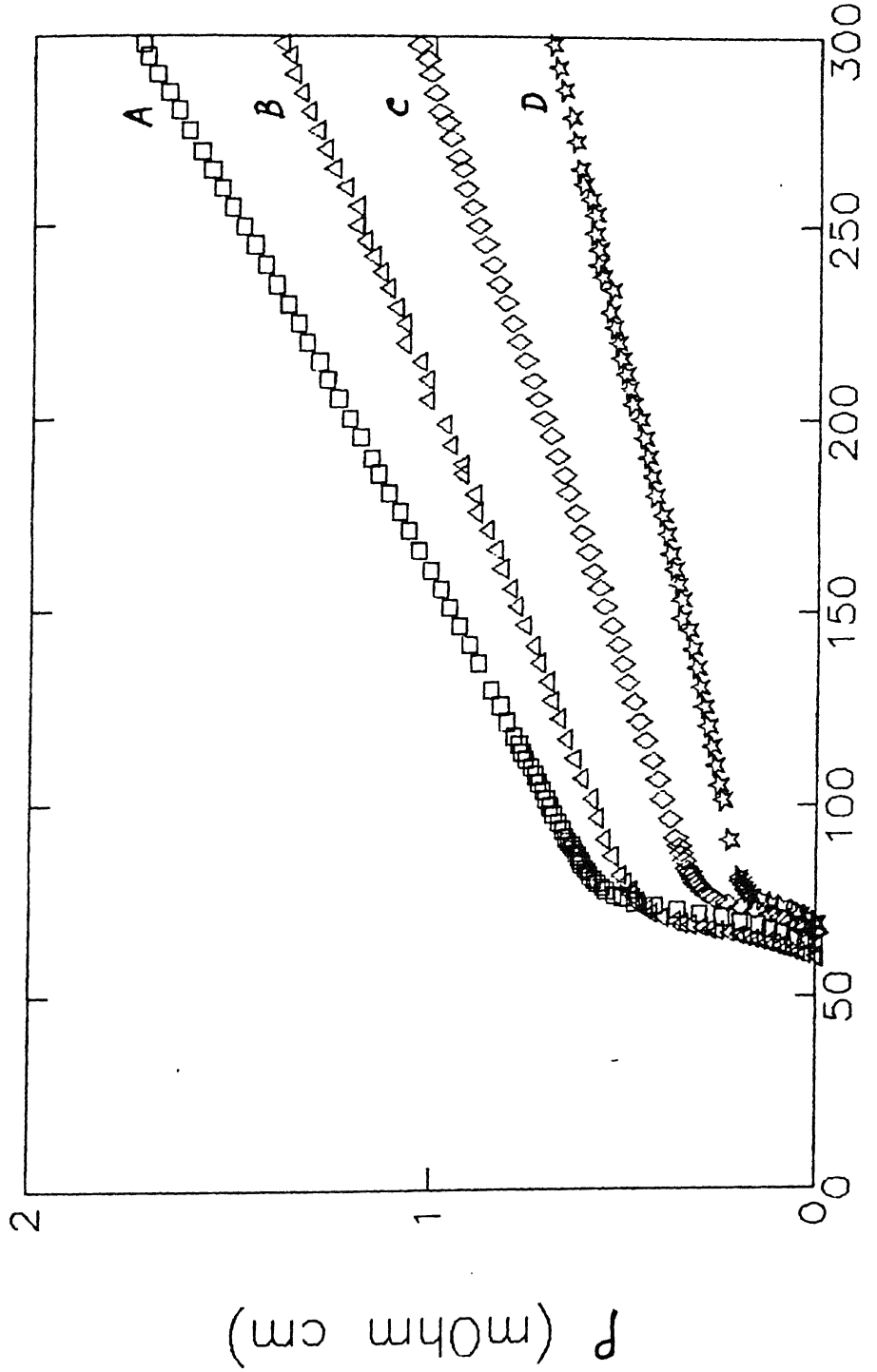

Fig. 6.1. Ressistivity as a function of temperature for several samples of $Bi_2Sr_2CaCu_2O_y$ (2212) system.

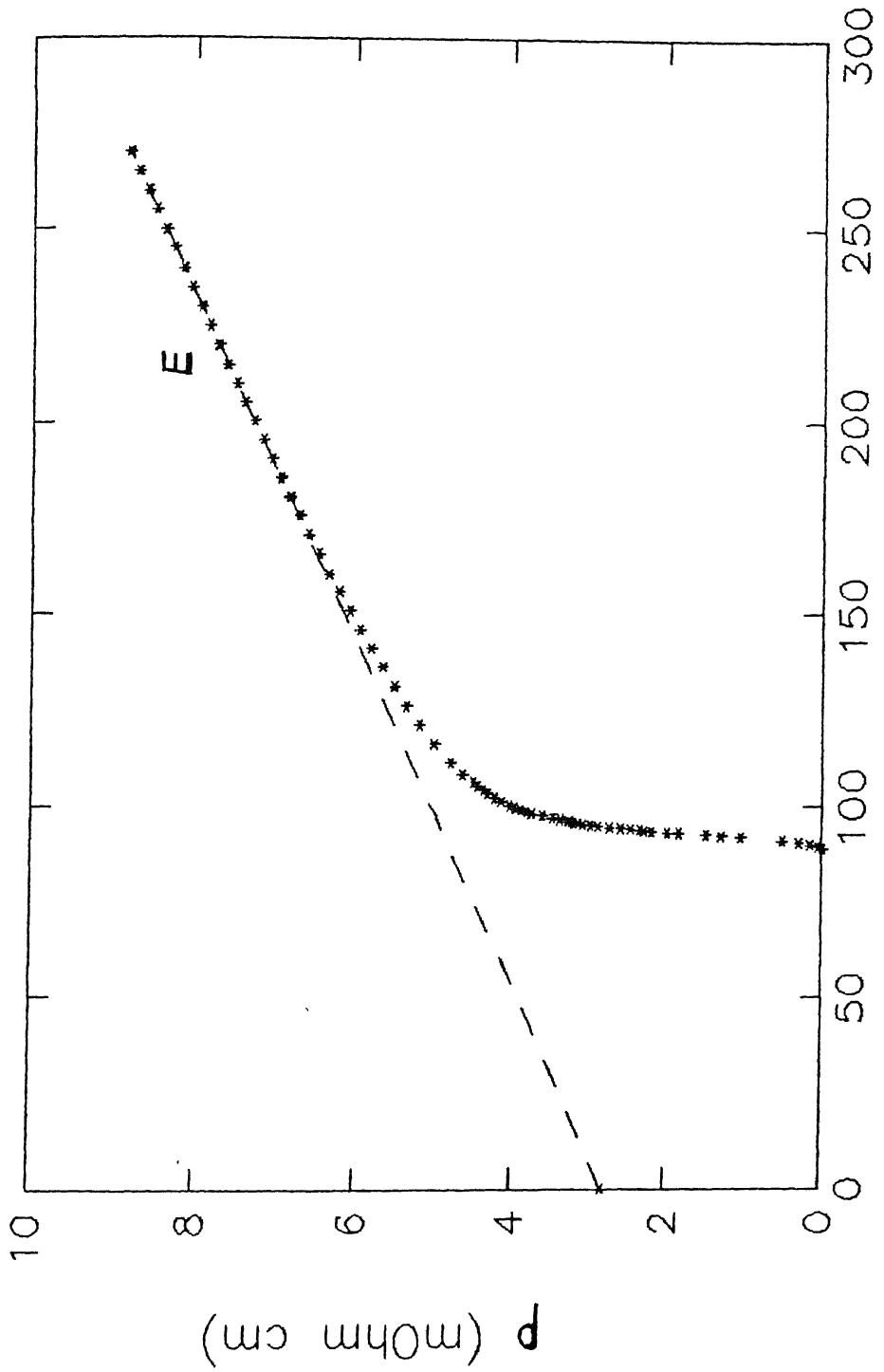

Fig. 6.2. Resistivity as a function of temperature of sample E of $Bi_2Sr_2CaCu_2O_y$ (2212) system.

characteristic of superconducting thermodynamic fluctuations. Here T_c (93.2 K) is defined as the temperature at which $d\rho/dT$ versus T shows a maximum or ρ versus T exhibits a point of inflexion. This $T_c = T_{cI}$ is used in the paraconductivity analysis as the mean-field critical temperature (T_{co}). The value of ρ_{270} is ~ 8.83 mΩ cm. The normal-state resistivity fit to the equation of the form $\rho = a+bT$ yields the temperature coefficient of resistivity $b = (d\rho/dT) \sim 0.02$ mΩ cm/K, and the constant a ~ 2.82 mΩ cm. The transition width, ΔT_c, provided by the width of the peak in the $d\rho/dT$ versus T graph at half height (FWHM) is ~2K.

Although a pc sample consists of randomly oriented crystallites, due to very high anisotrophy the low in-plane resistivity will dominate in the equivalent parallel resister network. Thus in a dense, good quality pellet the resistivity should essentially have the same behavior, and hence yield the same type of information, as does the ρ_{ab} in single-crystal study. To test this, Anderson-Zou (AZ) analysis is applied to our ρ-data in the normal state. According to these authors the normal-state resistivity is given by ρ (T) = A/T + BT where the hyperbolic term is introduced to model the inter-plane hopping of carriers. Figure 6.3 shows a replot of the ρ-data in the form ρT versus T^2 which is linear over most of the investigated temperature range. This implies that the ρ behavior in dense, high quality pc materials is intrinsic to single grain and thus similar to that of ρ_{ab} in single crystals. The values of the constants, A and B are 315 mΩ cmK and 0.028 mΩ cm/K, respectively.

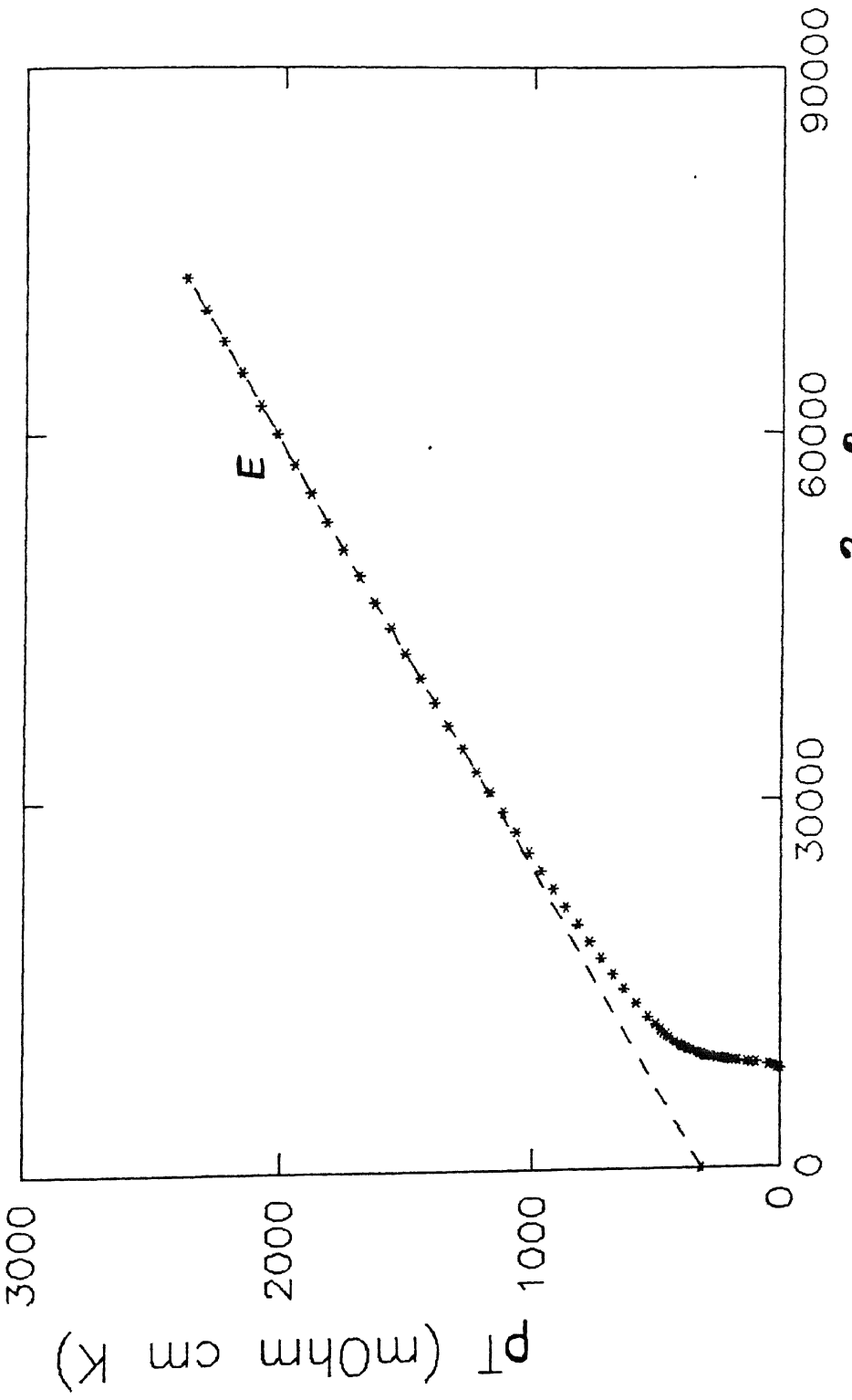

Fig. 6.3. ρT versus T^2 plots for $Bi_2Sr_2CaCu_2O_y$ (2212) system.

Figure 6.4 shows the typical log-log plot of the normalized excess conductivity, $(\Delta\sigma/\sigma_{270})$, versus reduced temperature, $\varepsilon = (T-T_c)/T_c$, with the normal-metal background fitting. Two distinct linear regions are identified. There is a high-temperature region in which the exponent is -0.9, followed by a mean-field region in which the exponent is -0.5. This is in very good agreement with the results on single-crystal studies on $Bi_2Sr_2CaCu_2O_y$ by Mandal et al. [401], although they did not observe similar behavior in pc samples of the same system. To the best of our knowledge, this is the first time that a crossover from 2D to 3D is observed in Bi-2212 polycystal. Similar 2D to 3D crossover behavior is observed in $YBa_2Cu_3O_{7-\delta}$ samples (see Chapter 4).

Figure 6.5 shows the log-log plot of the normalized excess conductivity, $(\Delta\sigma/\sigma_{270})$, versus reduced temperature, $\varepsilon = (T-T_c)/T_c$, with the Anderson-Zou background fitting. Here also two distinct linear regions are identified. There is a high-temperature region in which the exponent is -0.66, followed by a mean-field region in which the exponent is -0.44. This demonstrates how extrapolation dependent is the observed critical behavior in the absence of any quantitative model for the normal-state resistivity. Figure 6.6 shows the thermoelectric power (S) versus temperature behavior for the Sample E of Fig. 6.2. The TEP increases with decreasing temperature, and starts decreasing at ~110 K and becomes zero at ~92 K. The drop in S near 110 K corresponds to the onset of superconductivity and the zero value of S corresponds to the superconducting state. The positive sign of S indicates that the conduction is via holes. The changes in S near 110 K and the zero value of S at ~92 K are

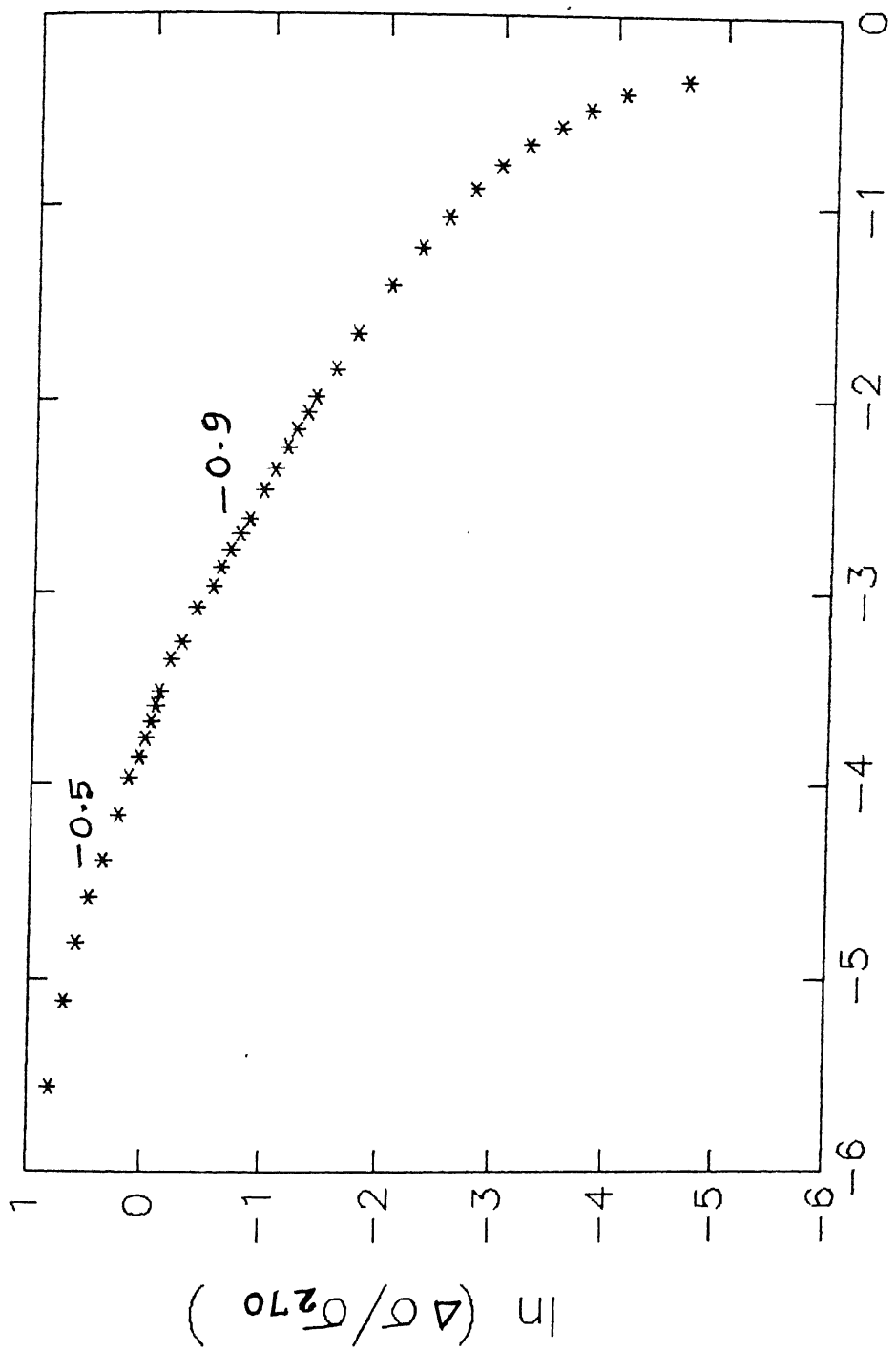

Fig. 6.4. Log-log plot of the normalized excess conductivity ($\Delta\sigma/\sigma_{300}$) versus reduced temperature (ε) for the Bi-2212 sample, with normal-metal background fitting.

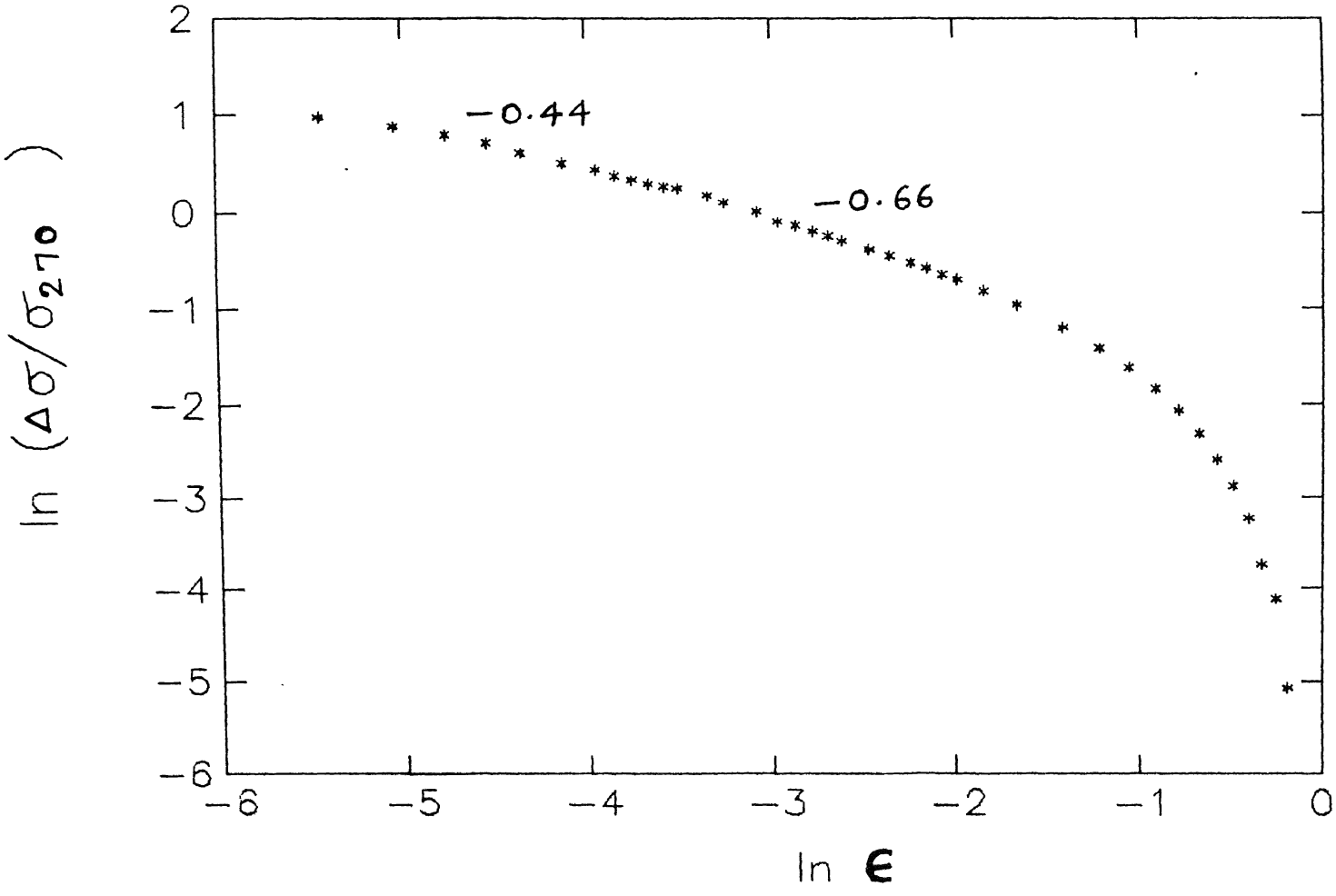

Fig. 6.5. Log-log plot of the normalized excess conductivity ($\Delta\sigma/\sigma_{300}$) versus reduced temperature (ε) for the Bi-2212 sample, with Anderson-Zou background fitting.

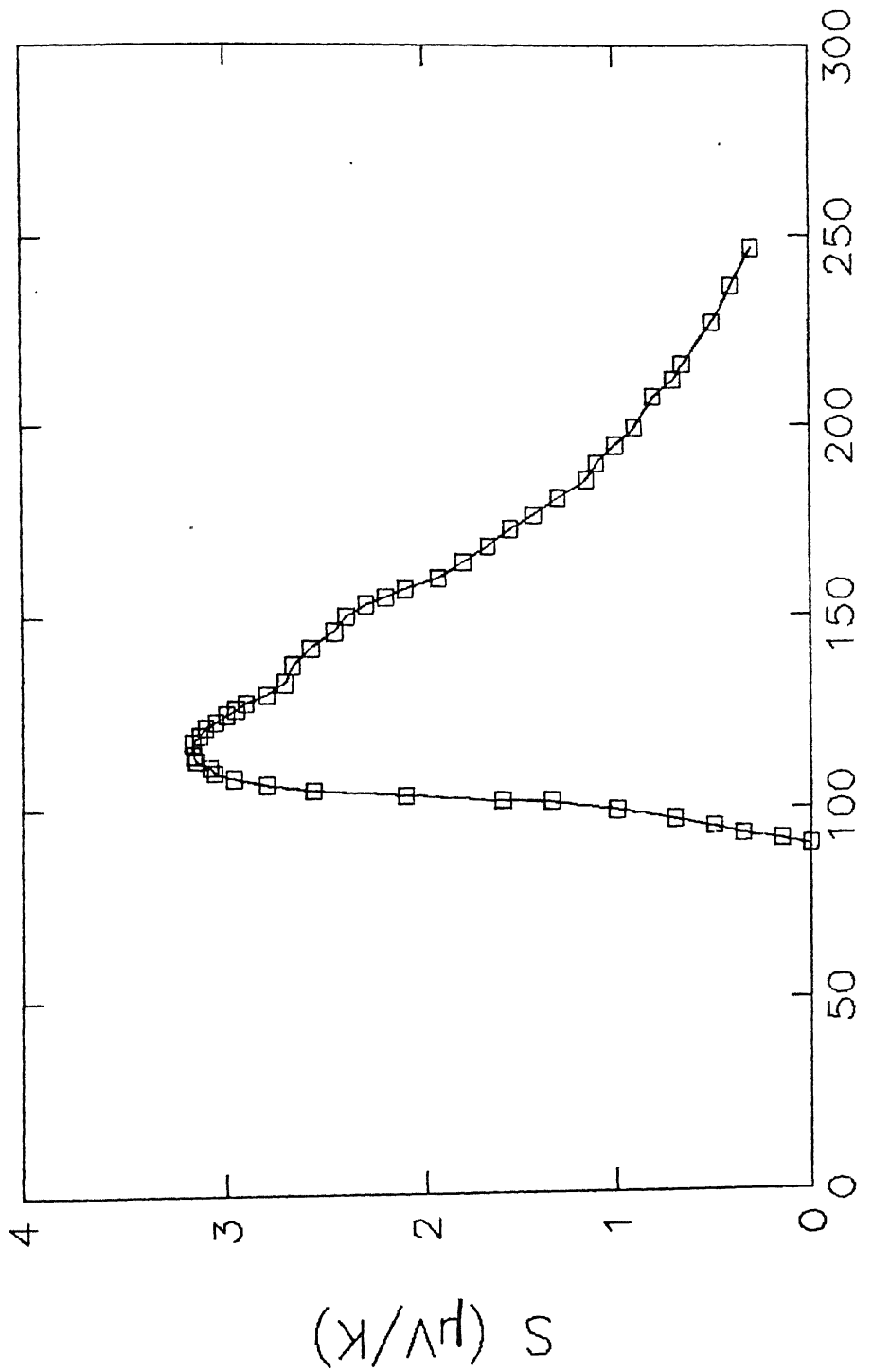

Fig. 6.6. Thermopower (S) versus temperature behavior for the sample E of Fig. 6.2.

consistent with those in the resistivity versus temperature behavior (Fig. 6.2.).

It was relatively difficult to prepare pure 110 K $Bi_2Sr_2Ca_2Cu_3O_Y$ (2223) phase (n=3), as it required precise temperature control over long reaction time (more than a week), otherwise n=2 phase (2212) as well as the binary Ca_2CuO_3 (in form of gold colored needles) get stabilized. Hence, the following composition of the above 2223 system involvong Pb and/or Sb have been tried.

6.2.2 $Bi_{1.7}Pb_{0.3}Sr_{1.6}Ca_2Cu_{3.4}O_X$ and $Bi_{1.9}Sb_{0.1}Sr_2Ca_2Cu_3O_Y$

The experimental details regarding the sample preparation are described in section 2.2. First Pb has been substituted for Bi with the nominal composition $Bi_{1.7}Pb_{0.3}Sr_{1.6}Ca_2Cu_{3.4}O_X$ (samples 1, 1a, 2, 2a,2b). This composition was chosen to see the effect of Ca and Cu-rich sample. Then Sb was substituted for Bi with the nominal composition $Bi_{1.9}Sb_{0.1}Sr_2Ca_2Cu_3O_Y$ (samples 3, 4, 4a) to study the effect of Sb^{+3} on the large ion sites (Bi, Sr, Ca). The polycrystalline material obtained by glass crystallization has the following advantages over the ceramic counterpart: (1) the glass-derived material has a much dense matrix; (2) it is much more homogeneous and could be a candidate for a high-current carrier; and (3) since the starting material is a very uniform glass, the microstructure and the high-T_c phase is much easier to control. Also, it could solve some of the technological problems faced by the ceramic counterpart.

Figure 6.7 shows the XRD pattern of sample 1 which contains both 85 and 110 K phases. The non-resonant microwave absorption

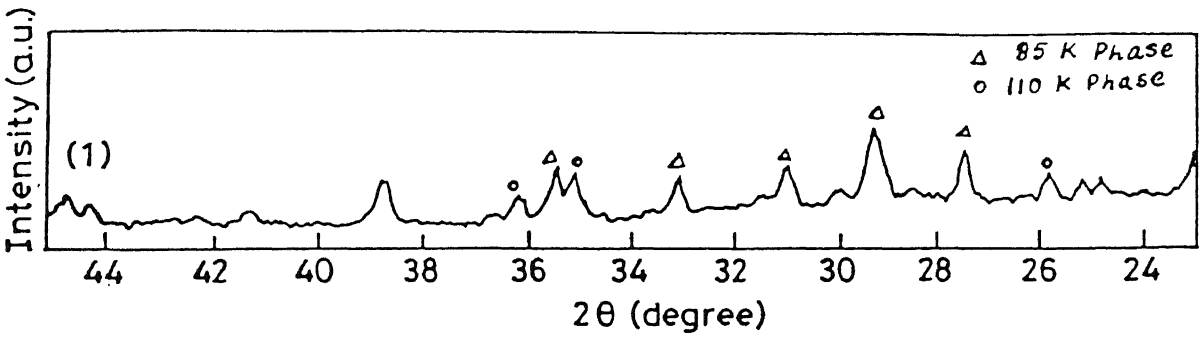

Fig. 6.7. XRD pattern for the sintered (840°C, 72h) $Bi_{1.7}Pb_{0.3}Sr_{1.6}Ca_2Cu_{3.4}O_X$ sample.

spectrum is shown in Fig.6.8 at 77 K, while Fig.6.9 shows the electrical resistivity versus temperature behavior. This sample initially behaved semiconductor-like up to 74 K and then showed a metallic behavior with a T_{CRO} = 40K. When Sample 1 was further annealed at 400°C for 24 h, followed by air quenching (henceforth reffered to as sample 1a), there was no detectable change in the XRD pattern. However, the ρ-T behavior of this sample 1a changed dramatically and became metal-like with a deviation from the linear behavior which starts at 127 K, followed by a T_c onset (T_{CO}) at about 92 K with a T_{CRO}= 74 K. Figure 6.10 shows the DTA curve of the melt-quenched sample of $Bi_{1.7}Pb_{0.3}Sr_{1.6}Ca_2Cu_{3.4}O_X$ (sample 2). The kink toward the endothermic direction at 382°C is the glass transition temperature (T_g), the sharp exothermic peak at 443°C is the crystallization temperature (T_X). From T_g and the XRD pattern (Figure 6.11) it is concluded that the rapidly quenched sample is almost a "glass".

Sample 2 was heat-treated for crystallization in air at 840°C for 15 h, followed by furnace-cooling (sample 2a). The temperature dependence of the resistance of this as-grown sample is shown in Fig.6.12. Its ρ(T) behavior is semiconductor-like at higher temperatures which becomes metal-like at and below 110 K with a T_{Co} of 85 K followed by a T_{CRO} = 70.5 K. The room temperature resistance of the Sample 2a with a few layers removed (sample 2b) was higher than that of as-grown sample 2a. The difference between these two samples, viz, 2a and 2b, is also clearly evident in their XRD patterns (Fig.6.13). This indicates that the annealing time was very short and calls for much longer annealing time for the possible growth of 110 K high-T_c phase.

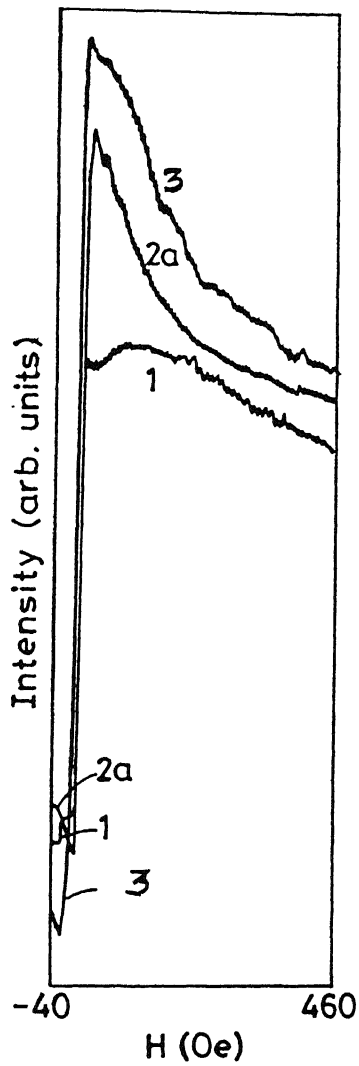

Fig. 6.8. Non-resonant microwave absorption signals of samples with the nominal compositions : ceramic $Bi_{1.7}Pb_{0.3}Sr_{1.6}Ca_2Cu_{3.4}O_X$ (1), crystallized glass $Bi_{1.7}Pb_{0.3}Sr_{1.6}Ca_2Cu_{3.4}O_X$ (2a) and ceramic $Bi_{1.9}Sb_{0.1}Sr_2Ca_2Cu_3O_Y$ (3) at 77K as a function of magnetic field H.

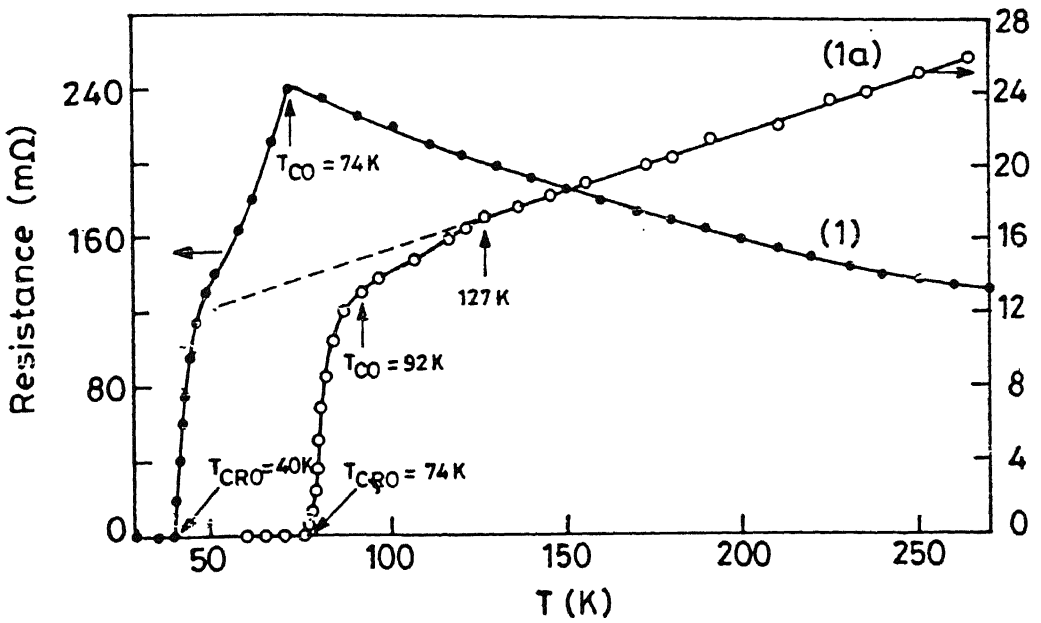

Fig. 6.9. Temperature dependence of the electrical resistance of sintered (840°C, 72h) $Bi_{1.7}Pb_{0.3}Sr_{1.6}Ca_2Cu_{3.4}O_X$ (1) and further annealed (400°C, 24h) and air quenched (1a) samples.

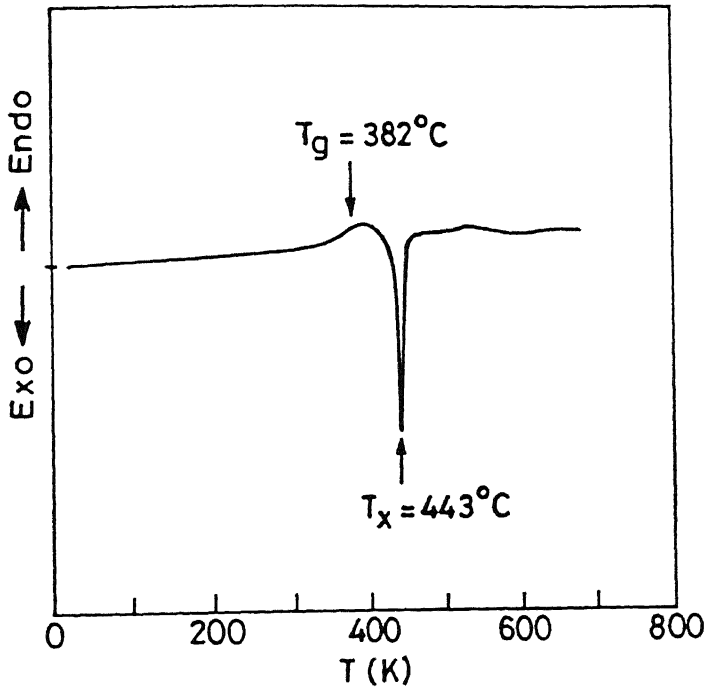

Fig. 6.10. DTA curve of melt-quenched sample of $Bi_{1.7}Pb_{0.3}Sr_{1.6}Ca_2Cu_{3.4}O_x$ (2).

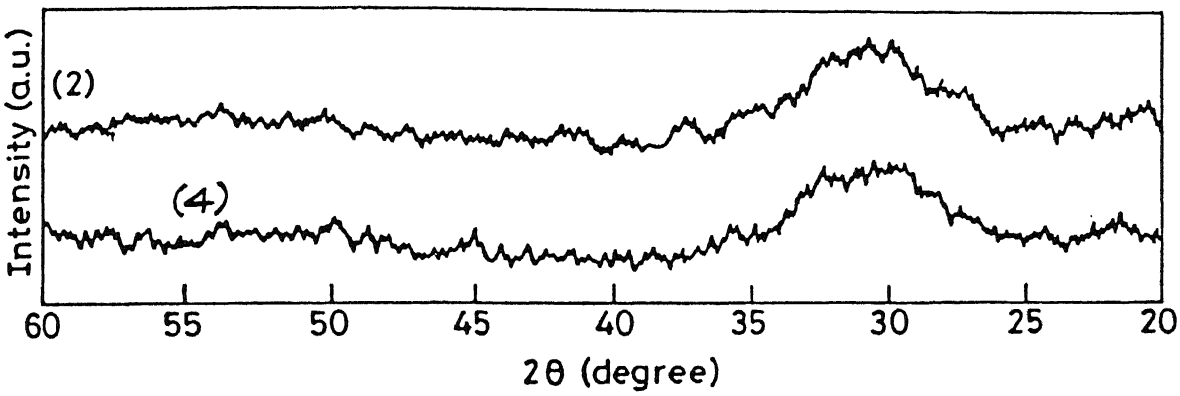

Fig. 6.11. XRD patterns for the melt-quenched samples with the nominal compositions :

$Bi_{1.7}Pb_{0.3}Sr_{1.6}Ca_2Cu_{3.4}O_X$ (2)

$Bi_{1.9}Sb_{0.1}Sr_2Ca_2Cu_3O_Y$ (4).

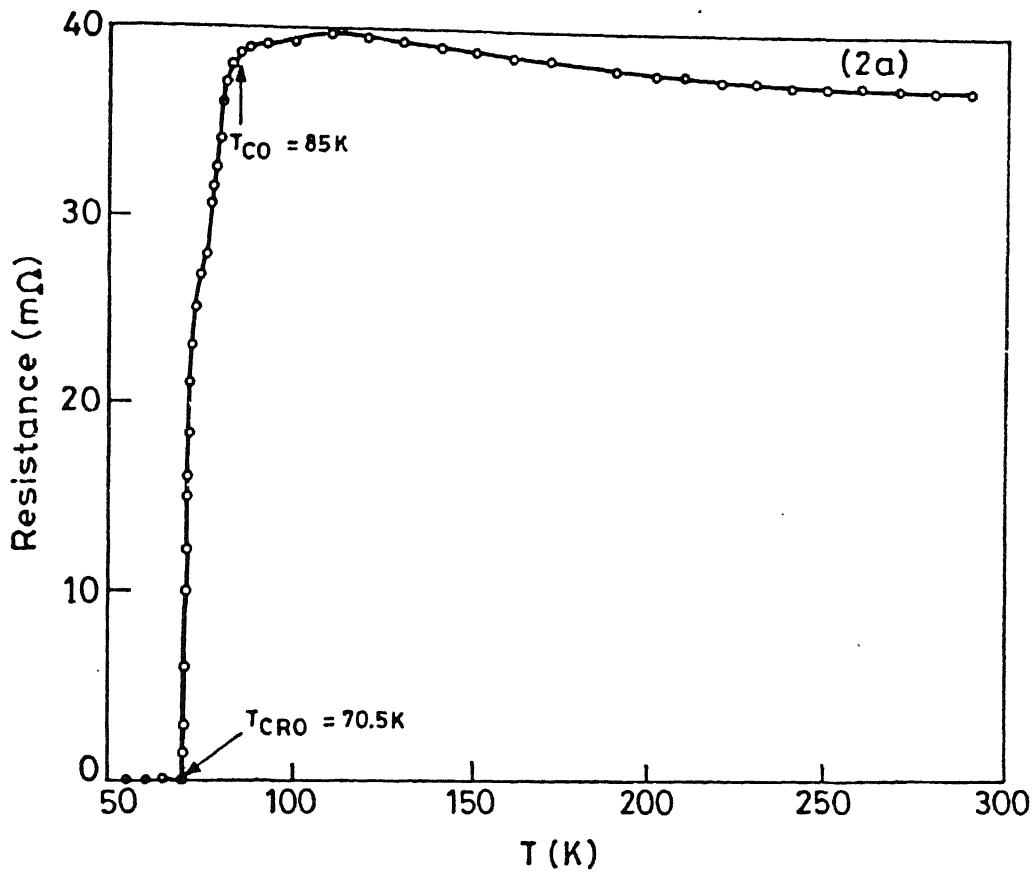

Fig. 6.12. Temperature dependence of the electrical resistance of crystallized $Bi_{1.7}Pb_{0.3}Sr_{1.6}Ca_2Cu_{3.4}O_X$ glass.

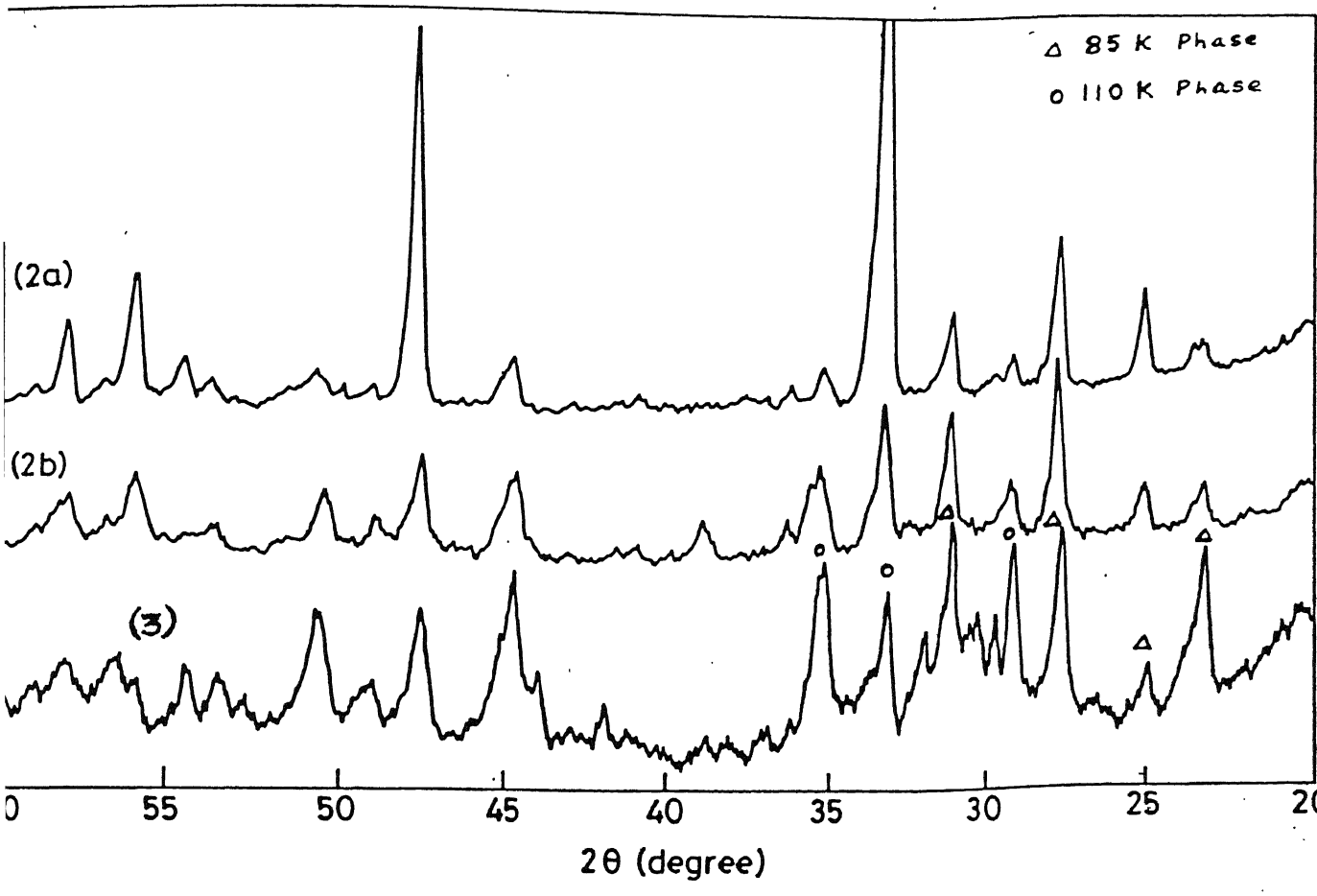

Fig. 6.13. XRD patterns of samples with the nominal compositions : annealed (840°C, 15h) $Bi_{1.7}Pb_{0.3}Sr_{1.6}Ca_2Cu_{3.4}O_X$ [as grown few layers removed (2b)] and sintered (890°C, 15h) $Bi_{1.9}Sb_{0.1}Sr_2Ca_2Cu_3O_Y$ (3).

Superconductivity in sample 3 was ensured by the non-resonant microwave absorption at 77 K. X-ray measurements reveal that this sample contains both 2212 and 2223 phases (Fig.6.9). Figure 6.14 shows the resistance as a function of temperature for Sample 3. Deviation from the linear metallic behavior indeed starts at 130 K with a sharp drop in resistance at ~115 K. This sample exhibits a T_{CO} of 85 K and a T_{CRO} = 70 K. These results are in contrast to those reported earlier [398,402].

Figure 6.11 also shows the XRD pattern of the crystallized glass of nominal composition $Bi_{1.9}Sb_{0.1}Sr_2Ca_2Cu_3O_y$ (Sample 4). Preliminary studies on these samples did not show any sign of superconductivity. It is believed that the sintering temperature (890°C) employed in this case is too high and needs to be reduced to 860-880°C to induce possible superconductivity.

For the dielectric constant measurements, silver paste was used as electrode. The real part (ε'_r) of the complex dielectric constant was calculated from $\varepsilon'_r = (\Delta C_p)t/A_s\varepsilon_o + 1$ where ΔC_p is the difference between the capacitances of the cell with and without the sample, t and A_s the thickness and the area of the sample respectively, and ε_o the permittivity of free space. It was found that for the glass samples 2 and 4 of the above systems ε'_r varies from 40 at 1 KHz to 20 at 10 MHz. This dispersion in dielectric constant with frequency, at room temperature, dies out at low temperatures and approaches a common value of ~10 at 77 K. Also, no non-resonant microwave absorption was found at 77 K in these samples 2 and 4. The resistivities of the quenched glass samples were about 5×10^6 Ohm-cm at room temperature.

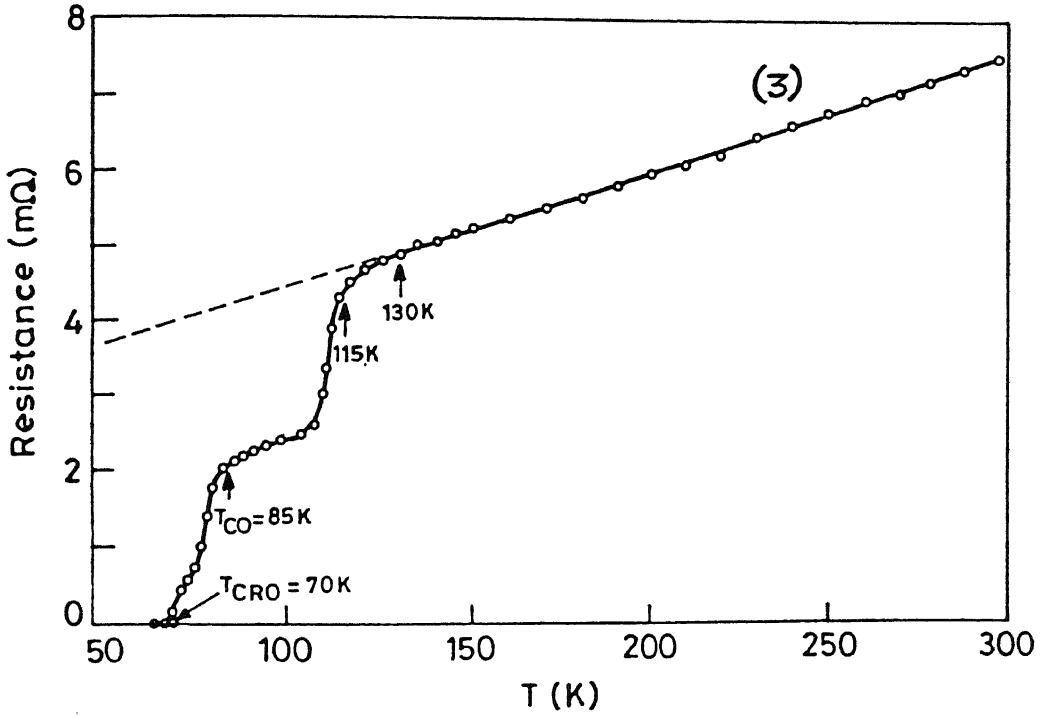

Fig. 6.14. Temperature dependence of the electrical resistance of sintered $Bi_{1.9}Sb_{0.1}Sr_2Ca_2Cu_3O_Y$ sample (3).

6.2.3 $Bi_{1.9}Pb_{0.3}Sr_2Ca_2Cu_3O_y$ and $Bi_{1.6}Pb_{0.3}Sb_{0.1}Sr_2Ca_2Cu_3O_y$

The experimental details regarding the preparation of samples have been given in section 2.2. Figure 6.15 shows the resistivity behavior as a function of temperature for $Bi_{1.9}Pb_{0.3}Sr_2Ca_2Cu_3O_y$ samples. Sample A shows a zero-resistance state (T_{CRO}) at ~91 K, whereas in sample B this state is achieved at ~105 K. However, the onset temperature (T_{CO}) for both the samples is nearly the same (116 K). While samples A clearly show two superconducting transitions, one at ~110 K and the other at ~90 K, samples B show only one at ~110 K. This improved behavior of sample B over sample A is due to the sintering of the former at a higher temperature, i.e. very close to the decomposition temperature. According to DTA analysis, the above compound decomposes at ~862°C (evidenced by an endothermic peak). The sintering temperature and time, and the superconducting transport parameters are displayed in Table 6.1. Sample B has lower values of ρ(300 K) and extrapolated residual resistivity [ρ(o)] than sample A. This suggests that the impurity scattering is higher in sample A than that in B. Figures 6.16 and 6.17 shows the TEP (S) versus temperature plots for both sample A and sample B of Fig. 6.15. In both cases the TEP increases with decreasing temperature. The positive sign of S indicates that the conduction is primarily via holes. The TEP shows a drop at ~122 K and becomes zero at ~95 K in case of sample A and at ~112 K in case of sample B. This is consistent with the observed drop in resistance and is the manifestations of the superconducting transition of the samples around these temperatures.

TABLE 6.1 Some parameters of (Bi,Pb,Sb)-Sr-Ca-Cu-O superconductors.

Sample	sintering temperature (°C)	sintering time (h)	ρ(300K) (mΩ cm)	$\rho(0)$[a] (mΩ cm)	T_{CO}[b] (K)	T_{CRO}[c] (K)
			$Bi_{1.9}Pb_{0.3}Sr_2Ca_2Cu_3O_y$			
A	852	20	4.10	1.05	116	91
B	860	16	3.15	0.56	116	105
			$Bi_{1.6}Pb_{0.3}Sb_{0.1}Sr_2Ca_2Cu_3O_y$			
C	860	12	6.42	3.25	114	72
D	850	12	4.31	2.00	114	101

a) Extrapolated residual resistivity.

b) Onset temperature.

c) Zero-resistance temperature.

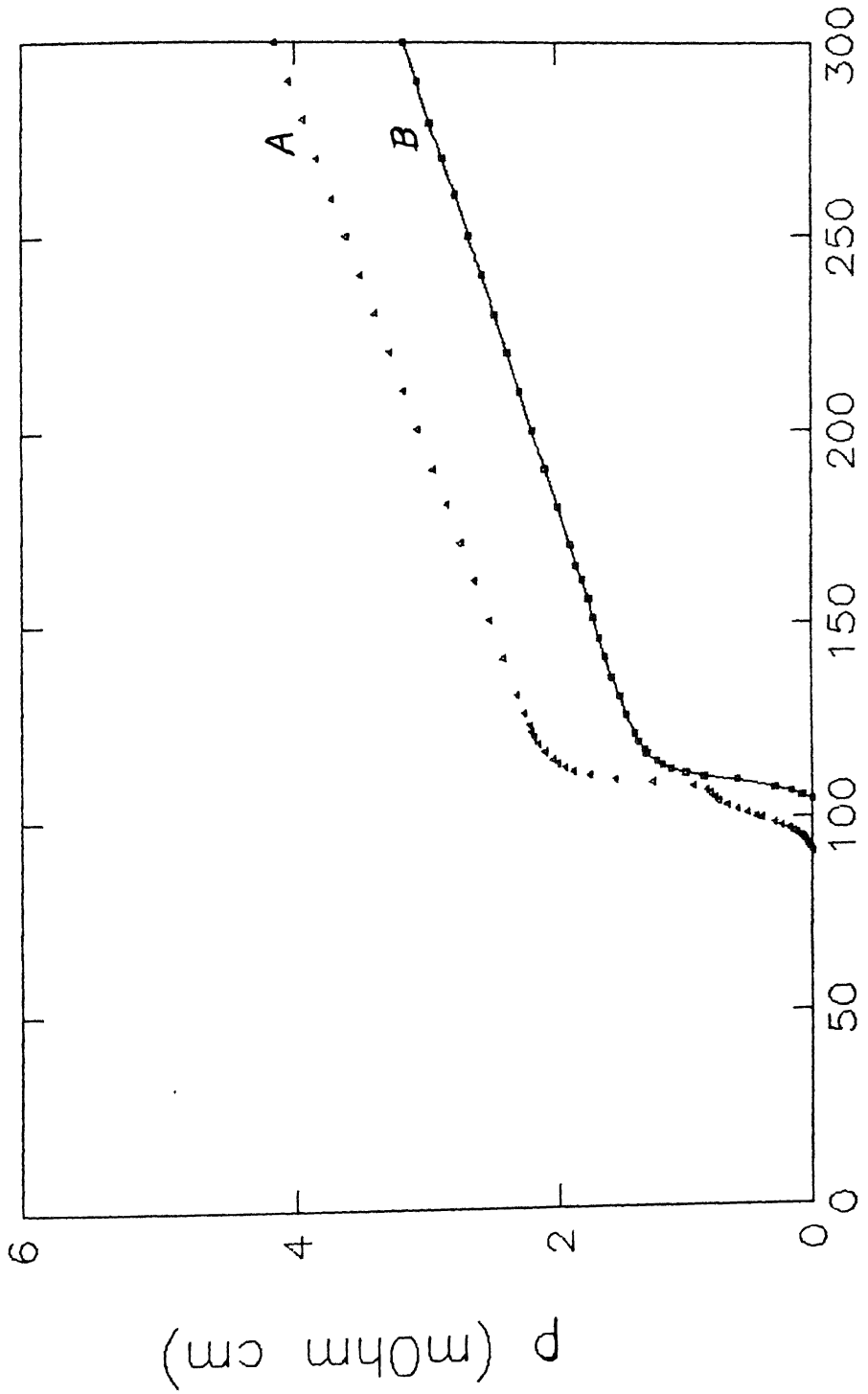

Fig. 6.15. Temperature dependence of the resistivity plots of $Bi_{1.9}Pb_{0.3}Sr_2Ca_2Cu_3O_y$ samples.

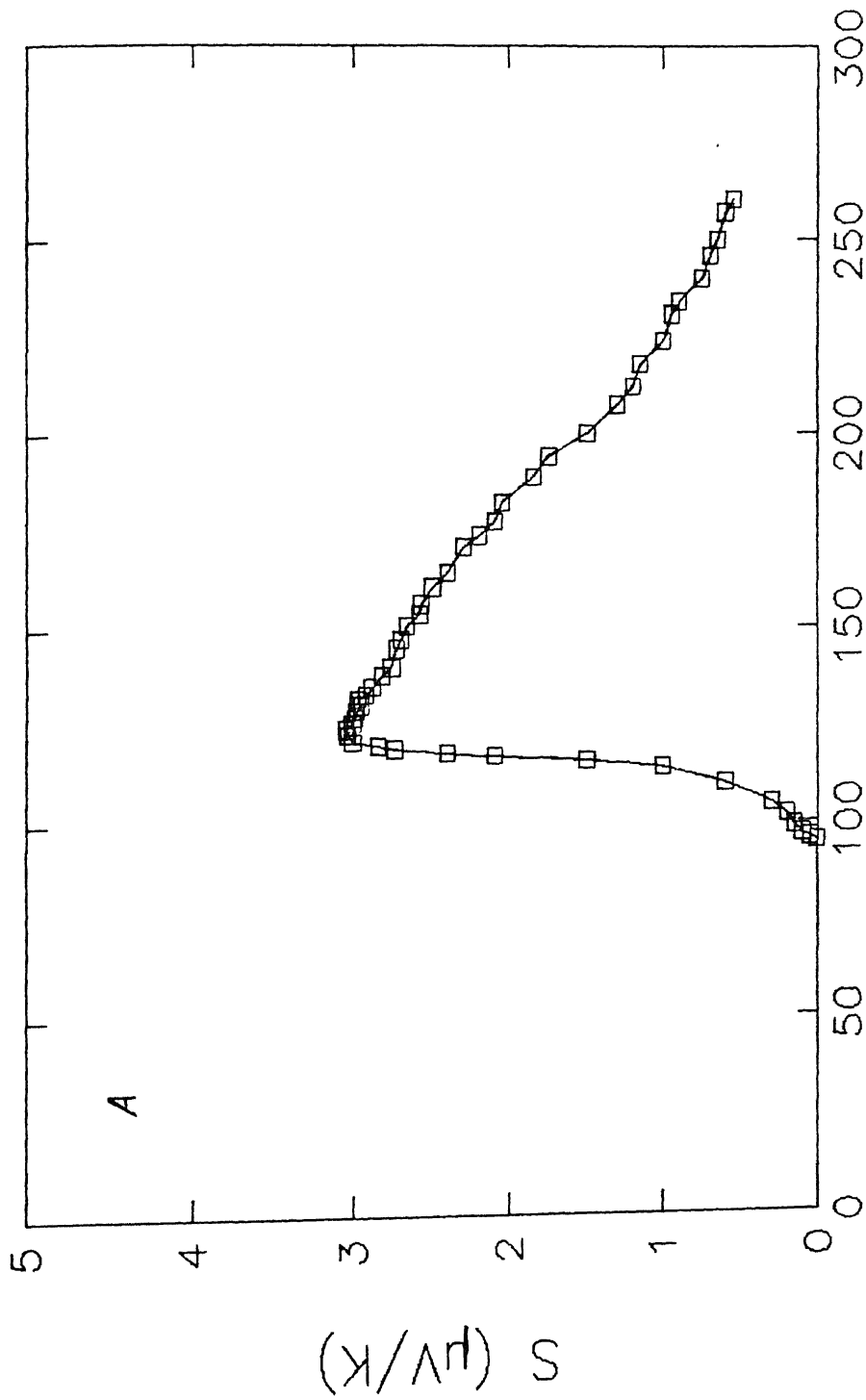

Fig. 6.16. S versus T plot of Sample A of Fig. 6.15.

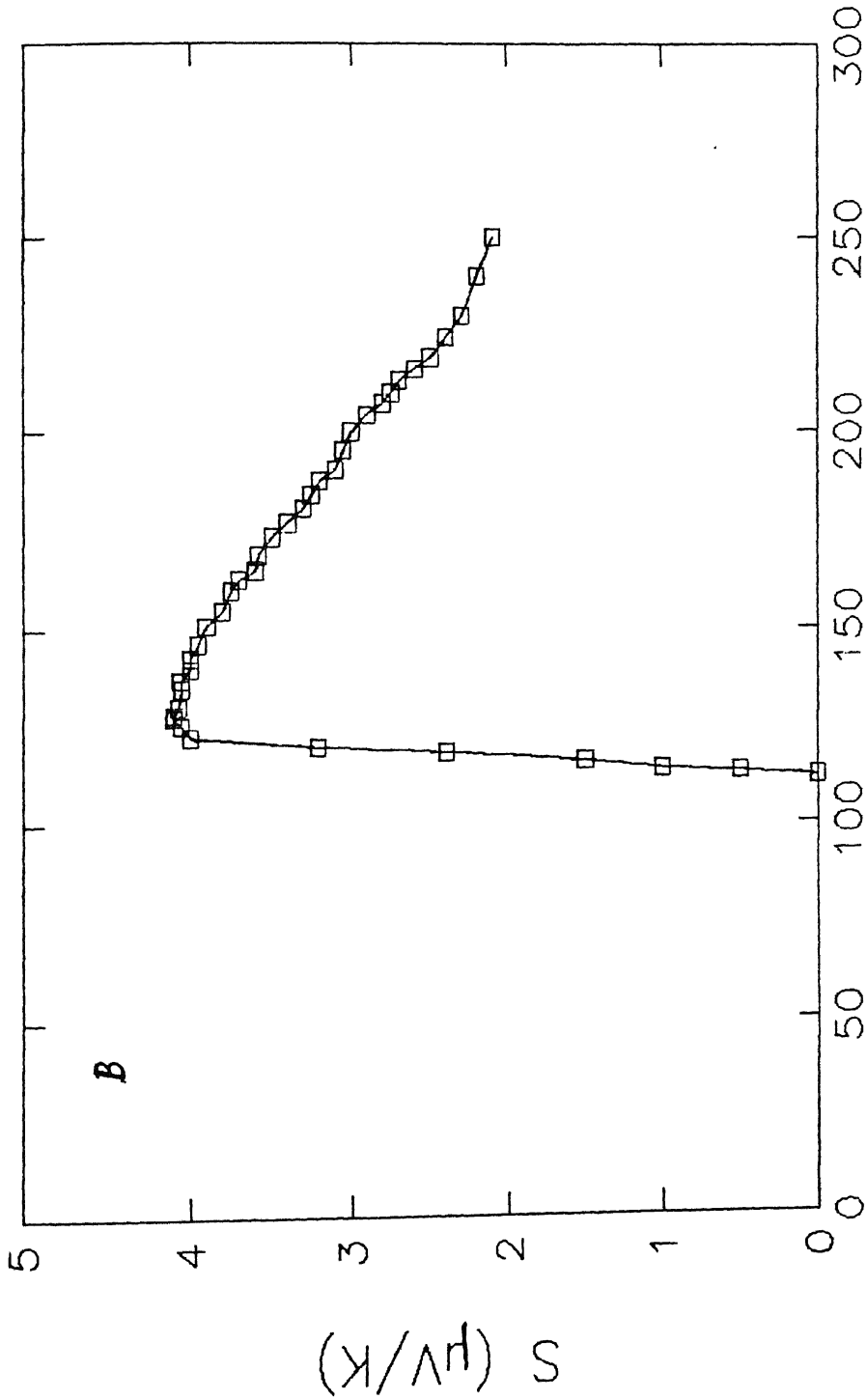

Fig. 6.17. S versus T plot of sample B of Fig.6.15.

Proper sample preparation conditions possibly reduce this impurity or defect scattering and help in stabilization of the three Cu-O layer structure over much longer region along the c-axis. It is important to note that the short-time heat treatment at 900°C as a second step in the synthesis process possibly helps achieve T_C above 100 K as suggested by Zhengping et al [399]. In absence of such short-time high-temperature heat treatment, the samples showed T_C much lower than 100 K, unless these are prepared via the long-term sintering procedure. From the XRD patterns of these samples (Fig.6.18), it is observed that while the sample A is dominated by 85 K-phase, sample B largely consists of 110 K-phase. Since 2223 phase is developed from 2212 phase and both are preferentially oriented along the c-axis in bulk samples, it is proper to examine the formation of 2223 by monitoring the XRD peak intensities of (0010) in 2223 (2θ = 23.9) and the neighboring peak (008) in 2212 (2θ = 23.1). It is interesting to note that although sample B contains the 2212 phase, it still shows a T_{CRO} = 105 K. It is believed that the precursor-matrix reaction technique coupled with a short-time high temperature heat treatment (forming a liquid-phase which enhances the diffusion rate) facilitates the formation of 2223 phase within 20 h of the sintering process.

Figure 6.19 shows the resistivity behavior as a function of temperature for $Bi_{1.6}Pb_{0.3}Sb_{o.1}Sr_2Ca_2Cu_3O_y$ samples . Some of the superconducting properties are listed in Table 6.1. While sample C shows a zero-resistance state (T_{CRO}) at 72 K, the sample D shows T_{CRO} ~101 K. The T_{CO} in both cases is ~114 K. Though the reaction process is same as followed in the preparation of

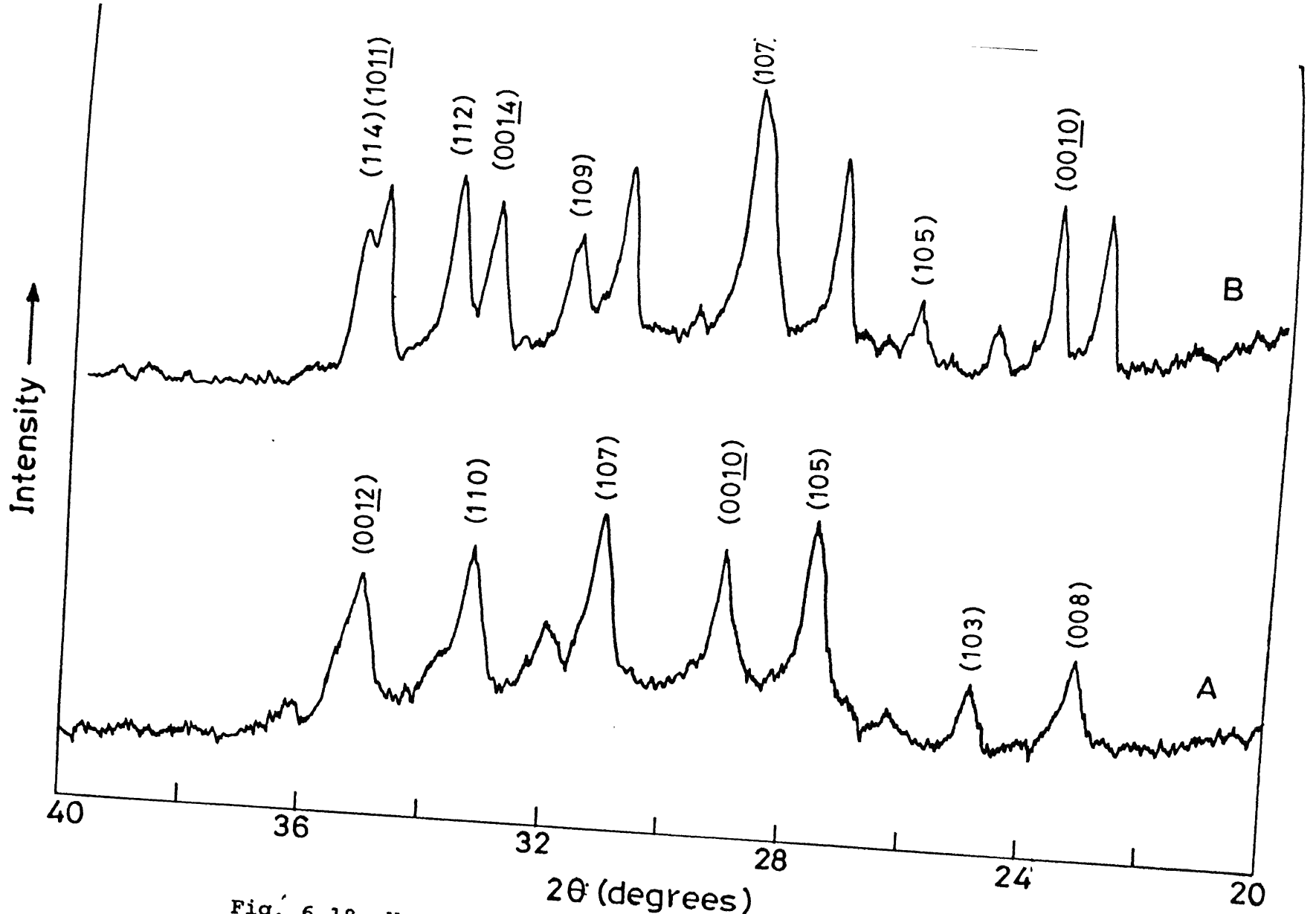

Fig. 6.18. X-ray diffraction patterns for samples A and B of nominal composition $Bi_{1.9}Pb_{0.3}Sr_2Ca_2Cu_3O_y$. The Miller indices are noted above each peak.

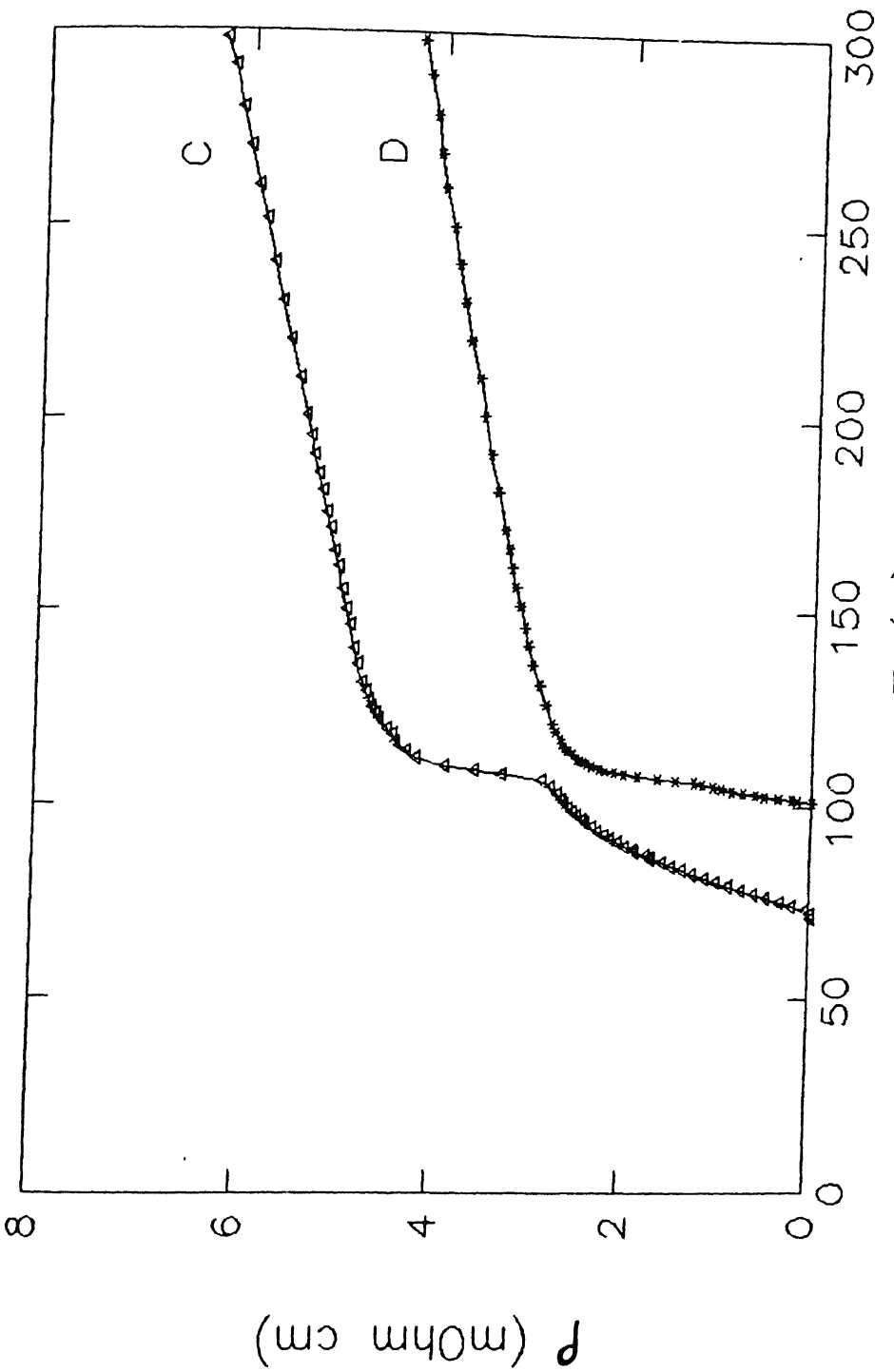

Fig. 6.19. Temperature dependence of the resistivity plots of $Bi_{1.6}Pb_{0.3}Sb_{0.1}Sr_2Ca_2Cu_3O_y$ samples.

samples A and B, the sample C shows a much less T_{CRO} , i.e. 72 K , because in this case the final sintering was carried out at 860°C, a temperature somewhat higher than the decomposition temperature (855°C) found from the DTA analysis. This sample C was also found to be in a slightly molten state and somewhat deformed. This possibly induced the growth of the 2212 and other phases. XRD patterns of the samples C and D (Fig.6.20) show the reflections attributable to 2223 and 2212 phases. However, the XRD pattern of the sample D is mainly dominated by 2223 phase. Figure 6.21 shows the TEP versus temperature of sample D of Fig. 6.19. At RT the value of S is ~4 μV/K and increases with decreasing temperature, showing a broad peak around 200 K. The positive sign of S indicates that the conduction is by holes. The TEP shows sharp drop around 125 K and becomes zero at ~112 K. Abrupt changes in S near 125 K is consistent with the resistance drops of the sample (Fig.6.19, sample D) and is the manifestations of the superconducting transitions of the sample around these temperatures.

In both the series of samples the transition to the superconducting state stretches over few Kelvin. It seems, this transition width can be reduced further and the pure 110 K-phase is possible to achieve by controlling the sintering temperature and duration . Though the samples B and D show XRD reflections from 2223 and 2212 phases they have the T_{CRO} at 105 and 101 K respectively, possibly due to the formation of the current conduction path via 110 K-phase, which is generally shown by resistivity measurements. It is often observed that a sample showing clear diffraction peaks due to the 2223 phase in the XRD

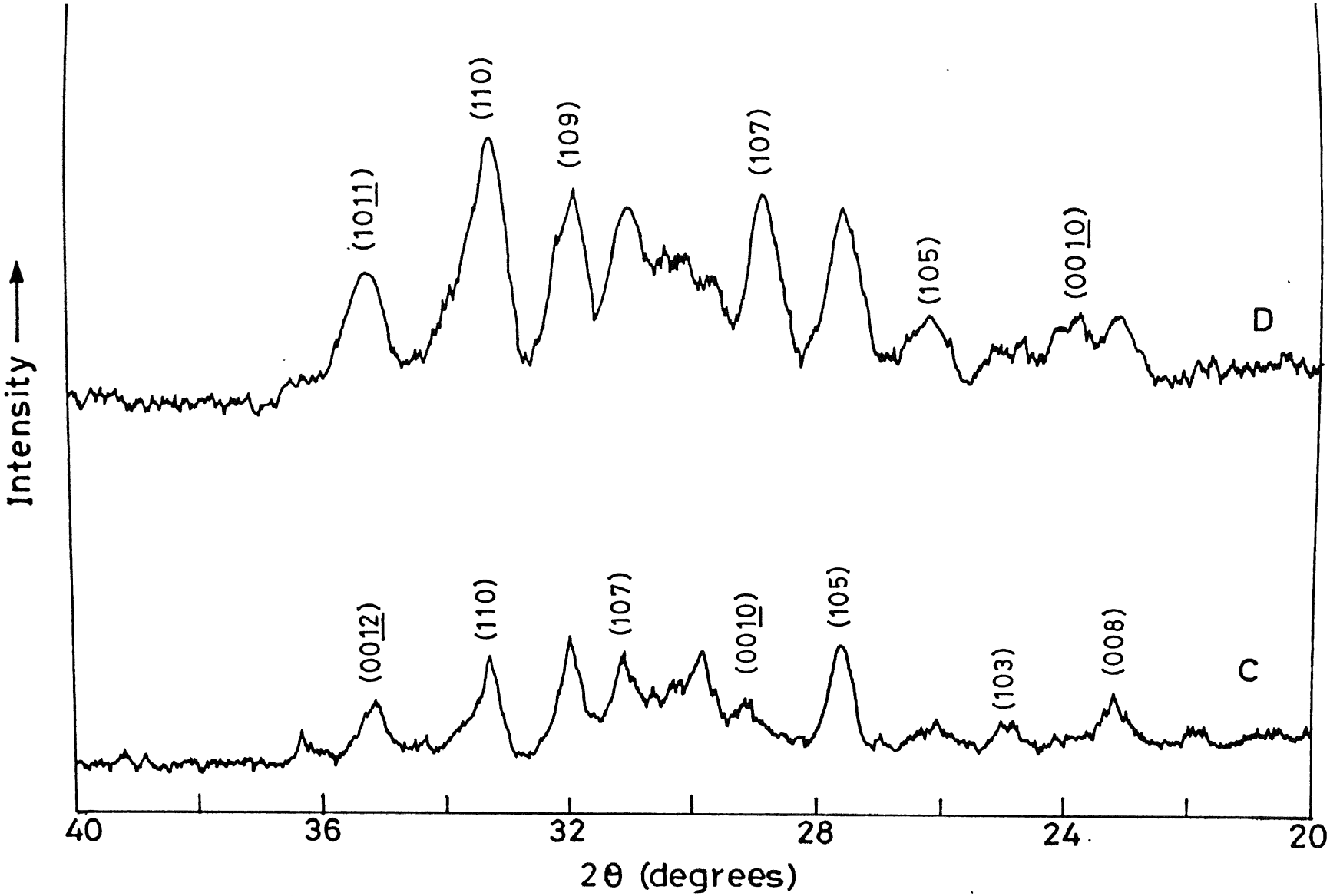

Fig. 6.20. X-ray diffraction patterns for samples C and D of nominal composition $Bi_{1.6}Pb_{0.3}Sb_{0.1}Sr_2Ca_2Cu_3O_y$. The Miller indices are noted above each peak.

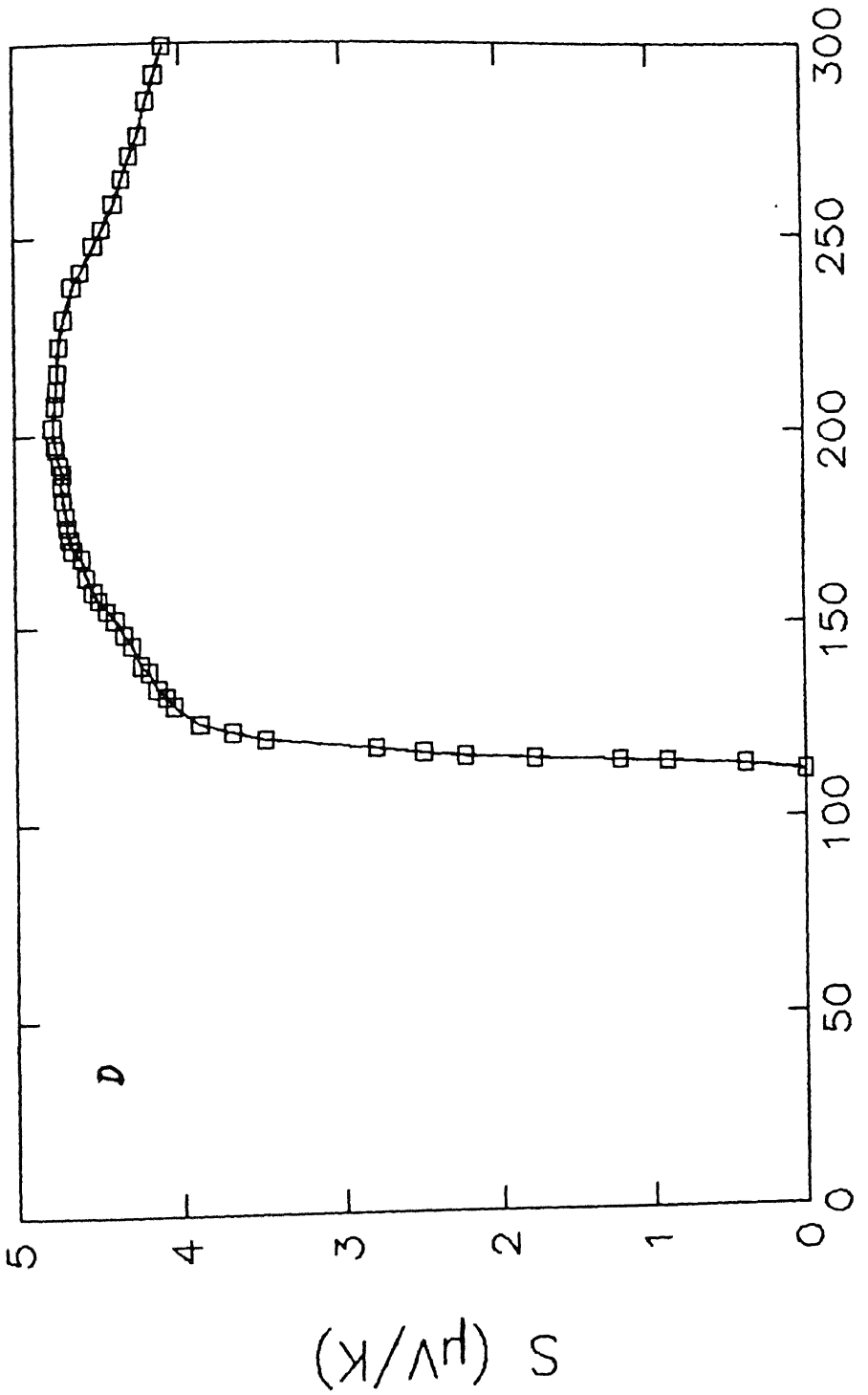

Fig. 6.21. S versus T plot of sample D of Fig. 6.19.

pattern and/or a large diamagnetic signal due to superconductivity caused by the 2223 phase does not exhibit zero resisitivity above 100 K. It is also not unusual that superconductivity observed in an electrical resisitivity measurement does not correspond to the phase of the largest amount present, but rather depends on the degree of linkage of the superconducting current paths; both the starting composition and the sintering conditions have great influence on the formation of such paths. All the four samples, viz., A,B,C, and D, invariably show the metallic behavior throughout the temperature region. It is also evident from Table 6.1 that the extrapolated residual resistivity can be reduced by controlling the sintering temperature. That is, the impurity or defect scattering due to the formation of different phases can be controlled by proper sample processing conditions.

The improvement in T_{CRO} in the Bi compound when Pb alone or Pb and Sb are added appears related to some changes in the kinetics of the solid-state reaction, which is obviously speeded up by the dopants. This is evident as attempts to prepare 110 K-phase samples without Pb or Sb for the same period of sintering time failed. Pb atoms are easily incorporated into the structure due to their similar electronic configuration of $6s^2$ $6p^0$ when in the +2 state as Bi in a +3 oxidation state. The role of Sb doping is to bring down the sintering temperature as well as duration. That is, it makes the kinetics of the reaction faster as suggested earlier [403-406]. The TEP data suggest that these are hole type superconductors.

6.3 CONCLUSIONS

Single-phase samples of $Bi_2Sr_2CaCu_2O_y$ system (n=2 phase) with T_c~85 K have been prepared. This required careful control of the composition, temperature, annealing time, etc. ; otherwise phases with T_c varying from 60 to 95 K gets stabilized. It was relatively difficult to prepare pure 110 K $Bi_2Sr_2Ca_2Cu_3O_y$ phase (n=3) under normal conditions. Further studies on $Bi_{1.7}Pb_{0.3}Sr_{1.6}Ca_2Cu_{3.4}O_X$ and $Bi_{1.9}Sb_{0.1}Sr_2Ca_2Cu_3O_Y$ systems suggested that the exact composition responsible for the 110 K or a still higher temperature phase is not clear but it exists in a narrow composition with a particular preparation process, sintering temperature, time, etc.

Nearly 110 K-phase samples of nominal compositions $Bi_{1.9}Pb_{0.3}Sr_2Ca_2Cu_3O_y$ and $Bi_{1.6}Pb_{0.3}Sb_{o.1}Sr_2Ca_2Cu_3O_y$ have been synthesized by a three-step reaction process involving a matrix method. The 110 K-phase formation mechanism is believed to be the liquid-phase-aided reaction at a higher temperature which enhances diffusion rate and promotes the 2223 phase formation. It is further believed that by keeping this method of preparation as a basis and by carefully controlling the short-time high-temperature heating, sintering temperature and duration, it is possible to prepare a pure 110 K monophasic compounds. Partial Pb and Sb combined doping in place of Bi has an obvious advantage over the simple Pb-doping in that it brings down the sintering temperature and duration. That is, addition of Sb with Pb makes the kinetics of the reaction faster. Paraconductivity analysis show the 2D to 3D crossover behavior in Bi-2212 polycrystals.

CHAPTER 7

SUMMARY AND CONCLUSIONS

1. Cupric Oxide (CuO) System

The critical point concerned with the high-T_c cuprates is that, for transition-metal compounds (mainly oxides), the parent compounds are antiferromagnetic (AFM) insulators (CuO, La_2CuO_4, Nd_2CuO_4, $YBa_2Cu_3O_6$, etc.). CuO is considered to be a key material in synthesis of most of the Cu-O based HTSCs. Besides, the Cu-O assembly is seemingly responsible for the superconductivity, and the main contribution to $DOS(E_F)$, comes from the Cu 3d and the O 2p hybridization states. The role of Y and Ba is probably supportive in nature; they help to stabilize the structure and the charge transfer mechanism between the Cu sites.

High-quality polycrystalline samples of CuO, $YBa_2Cu_3O_{7-\delta}$, $YBa_2(Cu_{1-x}M_x)_3O_{7-\delta}$ (M = Ti, V, and Ni), and (Bi, Pb, Sb)-Sr-Ca-Cu-O systems have been synthesized by solid-state reaction, glass, and matrix routes. Preliminary studies on the samples have been carried out by XRD, SEM, EDXA, DTA, TGA, EPR, density, optical absorption, and iodometry measurements. Further detailed studies on the samples have been carried out by low-and high-temperature resistivity, low- and high-temperature thermoelectric power, paraconductivity, and dielectric constant measurements.

In CuO, the antiferromagnetic (AFM) ordering temperature (Neel transition temperature, T_N) is found to occur around 230 K, in electric, thermoelectric, and dielectric measurements. This anomaly at ~230 K is also observed in some of the

non-superconducting and high-temperature superconducting cuprates. For such compounds the prevailing consensus appears to be that the one-electron band theory is inadequate to describe the ground-state electronic structure.

CuO is a p-type semiconductor, a fact also observed in most of the high-T_c cuprates. The reported existence of intrinsic hole states at the top of the valence band (VB) is consistent with the observation of p-type conductivity in CuO. The indirect band gap (E_g ~1.4 eV) of CuO is close to that of the insulating high-T_c compounds (1.6-2.0 eV). This indicates that the on-site energy difference between the Cu 3d and O 2p states for both the compounds is quite similar.

It is interesting to note that the as-received high-purity CuO has no Cu^{2+} EPR signal near g=2 from 77-400 K, although the impure CuO displayed Cu^{2+} signal at RT with varying intensity depending on the impurity concentration. Similarly, single-phase $YBa_2Cu_3O_{7-\delta}$ with optimal oxygen composition, has no Cu^{2+} EPR signal near g~2, because it has no curie moment, although multiphase Y-Ba-Cu-O gives Cu^{2+} EPR signal of varying intensity depending on the concentration of the impurity phase(s). It seems that the effective density of states of the VB is probably influenced by the magnetic transition at Neel temperature (T_N).

Thus, based on the value of ε_o at T<200 K and from the resistivity behavior, CuO should be regarded as a semiconductor-like material rather than a metal. However, the reported Fermi surface of CuO (many of the high-T_c cuprates show similar characteristics in their band structure, namely the existence of a semiconductor-like or semimetal-like gap, and a

Fermi surface) and the observations of (1) a high values of static dielectric constant (100-700) at T>230 K (a fact also observed in the insulating phase(s) of the high-T_c cuprates) and the anomalous behavior of TEP suggest some kind of metallike character in this system. In essence, the absence of Cu^{2+} EPR signal around g=2 in the so called paramagnetic temperature (T>230 K) regime, the anomalous behavior of resistivity, TEP, and dielectric constant, and the reported anomalous behavior in neutron diffraction, magnetic susceptibility, and specific heat around this temperature T=230 K suggest that some kind of complex electric, thermoelectric, dielectric, magnetic, and spin transitions occur in CuO around this temperature regime.

In pure CuO, there is intense competition for the lone electron between copper and oxygen ions. It would appear that the oxygen "wins" because a filled oxygen orbital is a slightly more stable configuration than a filled outer copper orbital. Thus, bonding between nominal Cu^{2+} and O^{2-} has both ionic and covalent character and involves the Cu 3d and O 2p orbitals. If copper and oxygen are mixed with other elements in a crystal lattice, the delicate energy balance can be shifted, so that Cu and O can share electrons to complete their outer shells. This sharing of electrons forms a "covalent" bond between copper and oxygen. Because the electrons are now free to move between the Cu and O atoms, materials containing copper, oxygen, and other elements can be good conductors. Hence, the properties of CuO may be varied from insulator to semiconductor to semimetal to metal and to superconductor. Copper can donate 1,2, or 3 electrons in a chemical bond with oxygen. The most stable of the three valence

states is 2+. Hence, the 1+ state (found for example, in Cu_2O) is called "reduced" Cu and the 3+ state (found, for instance in $NaCuO_2$) is known as "oxidized" copper.

Thus, the interesting physical and the reported structural properties (Jahn-Teller effect) of CuO and other insulating phase materials of the high-T_c cuprates such as $YBa_2Cu_3O_6$, La_2CuO_4, etc., suggest that it is difficult to exactly classify them as whether they are Mott or Heisenberg insulators (two classes of AFM insulators). There seems a likely close connection between AFM and superconductivity. Inspired by these findings, undoped and Ti, V, and Ni-doped $YBa_2Cu_3O_{7-\delta}$, and (Bi, Pb, Sb)-Sr-Ca-Cu-O systems have been studied.

2. $YBa_2Cu_3O_{7-\delta}$ System

The following are the some of the parameters observed for the single-phase $YBa_2Cu_3O_{7-\delta}$ (123) samples:
The calculated cell parameters : a=3.820 A° ; b=3.885 A° ; and c=11.670 Å; grain size ~5 μm; oxygen content(7-δ): 6.94±0.02 and 6.85±0.02; calculated density : 90-95 % ; The RT resistivity ~600 μΩ cm ; $\Delta T_c \leq$ 0.5 K; T_c ~92 K; $\rho(o)$ = 15 μΩ cm ; and the slope $d\rho/dT$ = 1.5-2.0 μΩ cm/K.

For all the undoped and doped Y-Ba-Cu-O systems, and for most of the (Bi, Pb, Sb)-Sr-Ca-Cu-O systems studied, the normal-state (linear region) resistivity is fitted to the following equations:

$\rho = A + BT$ (Normal-metal) and $\rho = A/T + BT$ (Anderson-Zou).

The fact that the ac (1-100 kHz) resistivity values agree reasonably well with the ρ_{dc} values demonstrates that the grain boundary effects on dc resistivity are negligible. Also, the Anderson-Zou fit to the ρ-data is found to work as well in polycrystals as in single crystals.

The *In situ*, high-temperature resistivity measurements in the controlled atmosphere up to ~ 1200 K have furnished information regarding the exact annealing temperature required for the preparation of high oxygen content $YBa_2Cu_3O_{7-\delta}$ samples, the oxygen out diffusion temperature, and the type and temperature of the occurrence of the structural (orthorhombic to tetragonal) phase transition. Besides, the observed linear $\rho(T)$ curves to high temperatures (absence of saturation) implies weak electron-phonon coupling. This also reveals that the mean free paths 'l' are much longer than the interatomic spacings 'a' at temperatures below ~700 K. Also, at low-temperatures the mean free path should be much longer than the extremely short coherence lengths for these materials, which should accordingly be treated as clean superconductors. Even if electronic contribution to ρ is dominant, a crossover from T^5 to T behavior arising from a phonon background contribution should be evident somewhere below 50 K. That there is no deviation from the linearity and thus no clear evidence for any additional (i.e., non-electronic) component of ρ is surprising. In general, the linear $\rho(T)$ behavior is to be expected at temperatures higher than Θ_D, the Debye temperature of the solid (if it is due to electron-phonon interaction). What is unusual is that in these materials it can start at temperatures markedly lower than Θ_D.

3. $YBa_2(Cu_{1-x}M_x)_3O_{7-\delta}$ (M = Ti, V, and Ni)

The solubility of the Ti- or V-dopants in Y-Ba-Cu-O is ~2.5 at.% . Higher dopant concentration (x) results in Ti- or V-rich second phase formation. However, up to x = 0.1, the structure, the T_c, and the ΔT_c remain almost the same as in the case of pure 1:2:3 phase. For all the $YBa_2(Cu_{1-x}Ni_x)_3O_{7-d}$ ($0<x<0.2$) samples the structure remains orthorhombic. The solubility of the Ni in Y-Ba-Cu-O is determined to be ~10 at.% . The T_c of the Ti- and V-doped Y-Ba-Cu-O compounds remains almost unaffected is of technological interest in view of the need for non-poisonous and high melting point materials that could be used as a substrate in high-temperature processing of Y-Ba-Cu-O.

EPR studies show the possible oxidation state of Ti is Ti^{4+} and that of V is V^{5+}. The dopants might have entered the Cu(1) site with higher oxygen coordination, for instance, in an octahedral environment.

Both room temperature resistivity and TEP increase systematically as the dopant concentration (x) increases, as expected in view of the impurity scattering. The high value of the slope ($d\rho/dT$) and the very small value of the $\rho(T=0)$ rules out the electron-phonon scattering mechanism as a dominant source of resistivity.

4. Paraconductivity or Excess Conductivity

The paraconductivity analyses, for the first time, for almost all the Y and Bi systems studied, showed the 2D to 3D crossover when the system enters, from high-temperature to the mean-field regime. In the case of $YBa_2Cu_3O_{7-\delta}$ a further cross

over regime followed by a critical dynamics regime have been observed as T approaches T_c. This behavior is in close agreement with that predicted by Lobb. In general, the excess conductivity plot is sensitive to the fitting procedure used in the normal-state to determine the background resistivity and the quality of the specimen used for such studies. The observed value of the exponent in different regimes is generally affected by the precise choice of T_c and it is, in all cases studied here, close to -0.5 as predicted by the Aslamazov and Larkin theory for 3D fluctuations in the mean-field region. Besides, the observed 2D to 3D crossover is quite consistent with the expected behavior for systems with large anisotrophy and smaller GL coherence length than any separation between Cu-O planes.

5. Thermoelectric Power (S)

The TEP (S) data are found to follow a conventional simple metallic relation of the type $S = S_g + S_d = (A/T) + BT$, where the contribution to S are due to carrier diffusion and phonon drag. The midband-filling and the phonon drag with the involvement of two carrier species (multiband conduction) mechanisms seem operative in these systems. There is no convincing explanation for the surprising enhancement of the TEP observed just above the T_c in some of the samples. Some authors have suggested that this TEP enhancement is a precursor feature related to the existence of superconducting fluctuations. The reduced electron-phonon scattering leads to an enhanced phonon flux in the normal regions of the mixed state near a superconducting boundary, which in turn enhances the phonon drag.

6. (Bi, Pb, Sb)-Sr-Ca-Cu-O System

Bi-series superconductors with n=2 and 3 (2212 and 2223) phase samples have been prepared with or without Pb and/or Sb doping. It was relatively difficult to synthesize pure phase corresponding to n=3. Single phase Bi 2212 and Pb- and/or Sb-doped 2223 phase samples have been prepared by a relatively short-time sintering via matrix method. The dielectric constant of Bi-based glasses at room temperature is around 30.

In conclusion, CuO seems to be the key material in most of the high-T_c cuprates. These HTSCs exhibit low-dimensional behavior in the normal-state. All the systems studied, showed the 2D to 3D crossover when they enter from high-temperature to mean-field regime. In the case of $YBa_2Cu_3O_{7-\delta}$ a further cross over regime followed by a critical dynamics regime have been observed as T approaches T_c. Many of the normal-state properties of these HTSCs are anomalous and are unlike those observed in any other metal or expected for a Fermi-liquid. There seems to be a likely close connection between AFM and superconductivity. The observed linear $\rho(T)$ curves to high-temperatures (absence of saturation) implies weak electron-phonon coupling. This also reveals that the mean free paths 'l' are much longer than the interatomic spacings 'a' at temperatures below ~700 K. Also, at low-temperatures the mean free path should be much longer than the extremely short coherence lengths for these materials, which should accordingly be treated as *clean* superconductors. The midband-filling and the phonon drag with the involvement of two carrier species (multiband conduction) mechanisms seem operative in these systems.

REFERENCES

[1] H.K. Onnes, Leiden Comm. **119b, 120b,** and **122b** (1911).

[2] H.K. Onnes, Leiden Comm. **133a** (1913).

[3] D.J. Quinn and W.B. Ittner, J. Appl. Phys. **33**, 748 (1962).

[4] H.K. Onnes, Leiden Comm. **139f** (1914).

[5] H.K. Onnes, Leiden Comm. **133d** (1913).

[6] F.B. Silsbee, J. Wash. Acad. Sci. **6**, 597 (1916).

[7] W. Meissner and R. Ochsenfeld, Naturwiss **21**, 787 (1933).

[8] E. Maxwell, Phys. Rev. **78**, 477 (1950).

[9] C.A. Reynolds, B. Serin, W.H. Wright, and L.B.Nesbitt, Phys. Rev. **78**, 487 (1950).

[10] H. London, Proc. Roy. Soc. A **176**, 522 (1940).

[11] A.B. Pippard, Proc. Roy. Soc. A **191**, 385 and 399 (1947).

[12] I. Giaever, Phys. Rev. Lett. **5**, 147 and 464 (1960).

[13] I. Giaever and K. Megerle, Phys. Rev. **122**, 1101 (1961).

[14] J. Bardeen, Phys. Rev. Lett. **6**, 57 (1961).

[15] B.D. Josephson, Phys. Lett. **1**, 251 (1962).

[16] B.B. Goodman, Proc. Roy. Soc. Lond. A **66**, 217 (1953).

[17] A. Brown, M.W. Zemansky, and H.A. Boorse, Phys. Rev. **92**, 52 (1953).

[18] H.E. Bömmel, Phys. Rev. **96**, 220 (1954).

[19] L.C. Hebel and C.P. Slichter, Phys. Rev. **113**, 1504 (1959).

[20] P.L. Richards and M. Tinkham, Phys. Rev. **119**, 575 (1960).

[21] C.J. Gorter and H.B.G. Casimir, Phys. Z. **35**, 963 (1934).

[22] H. London and F. London, Physica **2**, 341 (1935).

[23] L.D. Landau, J. Phys. USSR **5**, 71 (1941).

[24] V.L. Ginzburg, Sov. Phys. JETP, **14**, 177 (1944).

[25] V.L. Ginzburg and L.D. Landau, Zh. Eksp. Teor. Fiz. 20, 1064 (1950).

[26] A.A. Abrikosov, Zh. Eksp. Teor. Fiz. 32, 1442 (1957).

[27] F. London, Proc. Roy. Soc. A 152, 24 (1935).

[28] H. Fröhlich, phys. Rev. 79, 845 (1950); H. Fröhlich, Proc. Roy. Soc. A 215, 291 (1952).

[29] M.R. Schafroth, Helv. Phys. Acta 24, 655 (1951).

[30] M.R. Schafroth, Phys. Rev. 96, 1442 (1954).

[31] M.R. Schafroth, S.T. Butler, and J.M. Blatt, Helv. Phys. Acta, 30, 93 (1957).

[32] L.N. Cooper, Phys. Rev. 104, 1189 (1956).

[33] J. Bardeen, L.N. Cooper, and J.R. Schrieffer, Phys. Rev. 108, 1175 (1957).

[34] J.R. Schrieffer, Phys. Rev. 106, 162 (1957).

[35] N.N. Bogoliubov, Zh. Eksp. Teor. Phys. 34, 58 (1958); N.N. Bogoliubov, Nuovo Cimento 7, 794 (1958).

[36] J.G. Valatin, Nuovo Cimento 7, 843 (1958).

[37] G.M. Eliashberg, Zh. Eksp. Teor. Phys. 38, 966 (1960).

[38] Y. Nambu, Phys. Rev. 117, 648 (1960).

[39] P. Morel and P.W. Anderson, Phys. Rev. 125, 1263 (1962).

[40] M.L. McMillan, Phys. Rev. 167, 331 (1968).

[41] A.W. Sleight, J.L. Gillson, and P.E. Bierstedt, Solid State Comm. 17, 27 (1975).

[42] R. Chevrel, M. Sergent, and J. Prigent, J. Solid State Chem. 3, 515 (1971).

[43] B.T. Matthias, M. Marezio, E. Corenzwit, A.S. Cooper, and H.E. Barz, Science 175, 1465 (1972).

[44] J.R. Gavaler, Appl. Phys. Lett. 23, 480 (1973).

[45] J.G. Bednorz and K.A. Müller, Z. Phys. B 64, 189 (1986).

[46] J.G. Bednorz, K.A. Müller, and M. Takashige, Europhys. Lett. 3, 379 (1987).

[47] S. Uchida, H. Takagi, K. Kitazawa, and S.Tanaka, Jpn. J. Appl.Phys. 26, L1 (1987).

[48] C.W. Chu, P.H. Hor, R.L. Meng, L. Gao, and Z.J. Huang, Phys. Rev. Lett. 58, 405 (1987).

[49] J.D. Jorgensen, H.B. Schuttler, D.G. Hinks, D.W. Capone II, K. Zhang, M.B. Brodskym, and D.J. Scalapino, Phys. Rev. Lett. 58, 1024 (1987).

[50] H. Takagi, S. Uchida, K. Kitazawa, and S. Tanaka, Jpn. J. Appl. Phys. 26, L123 (1987).

[51] R.J. Cava, R.B.Van Dover, B.Batlogg, and E.A.Rietmann, Phys. Rev. Lett. 58, 408 (1987).

[52] K. Kishio, K. Kitazawa, S. Kanbe, I. Yasuda, N. Sugii, H. Takagi, S. Uchida, K. Fueki, and S. Tanaka, Chem. Lett. 2, 429 (1987).

[53] M. K. Wu, J. R. Ashburn, C. J. Torng, P. H. Hor, R.L. Meng, L. Gao, Z.J. Huang, Y.Q. Wang, and C.W.Chu, Phys. Rev. Lett. 58, 908 (1987).

[54] P. H. Hor, L. Gao, R. L. Meng, Z. J. Huang, Y. Q. Wang, K. Forster J. Vassilious, C.W. Chu, M.K. Wu, A.R. Ashburn, and C.J. Torng, Phys. Rev. Lett. 58, 911 (1987);
P.H. Hor, R.L. Meng, Y.Q. Wang, L. Gao, Z.J. Huang, J. Bechtold, K. Forster, and C.W.Chu, Phys. Rev. Lett. 58, 1891 (1987).

[55] D.G. Hinks, L. Soderholm, D.W. Capone II, J.D. Jorgensen, I.K. Schuller, C.U. Serge, K. Zhang, and J.D. Grace, Appl. Phys. Lett. 50, 1688 (1987).

[56] R.M. Hazen, L.W. Finger, R.J. Angel, C.T. Prewitt, H.K.Mao, C.G. Hadidiacos, P.H.Hor, R.L. Meng, and C.W.Chu, Phys. Rev. B 35, 7238 (1987);

P.M. Grant, R.B. Beyers, E.M. Engler, G. Lim, S.S.P. Parkin, M.L. Ramirez, V.Y. Lee, A. Nazzal, J.E. Vasquez, and R.J. Savoy, Phys. Rev. B 35, 7242 (1987).

[57] R.J. Cava, B. Batlogg, R. B. Van Dover, D. W. Murphy, S. Sunshine, T. Siegrist, J. P. Remeika, E.A. Rietmann, S.M. Zahurak, and G. Espinosa, Phys. Rev. Lett. 58, 1676 (1987).

[58] C.N.R. Rao, P. Ganguly, A.K. Rayachaudhuri, R.A.Mohanram, and K. Sreedhar, Nature, 326, 856 (1987).

[59] D. W. Murphy, S. Sunshine, R. B. Van Dover, R. J. Cava, B. Batlogg, S.M. Zahurak, and L.F. Schneemeyer, Phys. Rev. Lett. 58, 1888 (1987).

[60] A.R.Moodenbaugh, M. Suenaga, T.Assano, R.N. Shelton, H.C.Ku, R. W. Mc Mallum, and P. Klavine, Phys. Rev. Lett. 58, 1885 (1987);

[61] S. Hosoya, S. Shamoto, M. Onoda, and M. Sato, Jpn. J. Appl. Phys. 26, L325 (1987);

K. Kitazawa, K. Kishio, H. Takagi, T. Hasegawa, S. Kanbe, S. Uchida, S. Tanaka, and K. Fueki, Jpn. J. Appl. Phys. 26, L339 (1987).

[62] M. Oda, T. Murakami, Y. Enomoto, and M.Suzuki, Jpn. J. Appl. Phys. 26, L804 (1987).

[63] J. Karpinski, E. Kaldis, E. Jilek, and B. Bucher, Nature, 336, 660 (1988);

D.E. Morris, J.H. Nickel, J.Y.T. Wei, N.G. Asmar, J.S.Scott, U.M.Scheven, C.T.Hultgren, A.G.Markelz, J.E.Post, P.J.Heaney, D.R. Veblen, and R.M. Hazen, Phys. Rev. B 39, 7347 (1989).

[64] C.N.R. Rao, G.N. Subbanna, R. Nagarajan, A.K. Ganguli, L. Ganapathi, R. Vijayaraghavan, and S.V. Bhat, J. Solid State Chem. 88, 163 (1990).

[65] H. Maeda, Y. Tanaka, M. Fukutomi, and J.Asano, Jpn. J. Appl. Phys. 27, L209 (1988).

[66] S.A. Sunshine, T. Siegrist, L.F. Schneemeyer, D.W. Murphy, R.J. Cava, B. Batlogg, R.B. Van Dover, R.M. Fleming, S.H. Glarum, S.Nakahara, R. Farrow, J.J. Krajewski, S.M. Zahurak, J.V.Waszczak, J.H.Marshall, P. Marsh, L.W.Rupp Jr., and W.F. Peck, Phys. Rev. B 38, 893 (1988).

[67] U. Endo, S. Koyama, and T. Kawai, Jpn. J. Appl. Phys. 27, L1467 (1988).

[68] C.N.R. Rao, L. Ganapathi, R. Vijayaraghavan, G.Ranga Rao, K. Murthy, and R.A. Mohan Ram, Physica C 156, 827 (1988), and references therein.

[69] U. Balachandran, D. Shi, D.I. Dos Santos, S.W. Graham, M.A. Patel, B. Tani, K. Vandervoort, H. Claus, and R.B. Poeppel, Physica C 156, 649 (1988).

[70] H. Sasakura, S. Minamigawa, K. Nakahigachi, M. Kogachi, S. Nakanishi, N. Fukuoka, M. Yoshikawa, S.Noguchi, K.Okuda, and A. Yanase, Jpn. J. Appl. Phys. 28, L1163 (1989).

[71] D. Shi, M. Blank, M. Patel, D.G. Hinks, A.W. Mitchell, K. Vandervoort, and H. Claus, Physica C 156, 822 (1988); S.X. Dou, H.K. Liu, A.J. Bourdillon, M. Kviz, N.X. Tan, and C.C. Sorrell, Phys. Rev. B 40, 5266 (1989).

[72] P.V.P.S.S. Sastry, I.K. Gopalakrishnan, J.V. Yakhmi and R.M. Iyer, Physica C 157, 491 (1989).

[73] Z.Z. Sheng and A.M. Hermann, Nature 332,138 (1988).

[74] R.M. Hazen, D.W. Finger, R.J. Angel, C.T. Prewitt, N.L.Ross, C.G. Adidiacos, P.J.Heaney, D.R.Veblen, Z.Z.Sheng, A.El Ali, and A.M. Hermann, Phys. Rev. Lett. 60, 1657 (1988).

[75] S.S.P. Parkin, V.Y. Lee, E.M. Engler, A.I.Nazzal, T.C.Huang, G. Gorman, R. Savoy, and R.Beyers, Phys. Rev. Lett. 60, 1539 (1988).

[76] C. Politis and H. Luo, Mod. Phys. Lett. B 2, 793 (1988).

[77] C.C. Torardi, M.A. Subramanian, J.C. Calabrese, J. Gopalakrishnan, T.R. Askew, K.J. Morrissey, R.B. Flippen, U. Chowdhry, and A.W. Sleight, Science 240, 631 (1988).

[78] Y. Tokura, H. Takagi, and S. Uchida, Nature 337, 345 (1989).

[79] R.J. Cava, B.Batlogg, J.J. Krajewski, R. Farrow, L.W. Rupp, A.E. White, Jr., K. Short, W.F. Peck, and T.Kometani, Nature 332, 814 (1988).

[80] D.G. Hinks, B. Dabrowski, J.D. Jorgensen, A.W. Mitchell, D.R. Richards, S. Pei, and D. Shi, Nature 333, 836 (1988).

[81] A.F. Hebard, M.J. Rosseinsky, R.C. Haddon, D.W. Murphy, S.H. Glarum, T.T.M. Palstra, A.P. Ramirez, and A.R. Kortan, Nature 350, 600 (1991).

[82] M.J. Rosseinsky, A.P. Ramirez, S.H. Glarum, D.W. Murphy, R.C. Haddon, A.F. Hebard, T.T.M. Palstra, A.R. Kortan, S.M. Zahurak, and A.V.Makhija, Phys. Rev. Lett. 66, 2830 (1991).

[83] P.W. Stephens, L. Mihaly, P.L. Lee, R.L. Whetten, S.M. Huang, R. Kaner, F. Deiderich, and K. Holczer, Nature 351, 632 (1991).

[84] P.A. Heiney, J.E. Fischer, A.R. McGhie, W.J. Romanow, A.M. Denenstein, J.P.McCauley, Jr., A.B.Smith, III, and D.E. Cox, Phys. Rev. Lett. 66, 2911 (1991), and references therein.

[85] T.T.M. Palstra, R.C. Haddon, A.F. Hebard, and J.Z. Zaanen, Phys. Rev. Lett. 68, 1054 (1992).

[86] R.S. Liu, S.F. Hu, D.A. Jefferson, P.P. Edwards, P.D. Hunneyball, Physica C 205, 206 (1993).

[87] S.N. Putilin, E.V. Antipov, O. Chmaissem, and M. Marezio, Nature 362, 226 (1993).

[88] A. Schilling, M. Cantoni, J.D.Guo, and H.R.Ott, Nature, 363, 56 (1993).

[89] M. Lagues, X.M. Xie, H. Tebbji, X.Z. Xu, V. Mairet, C. Hatterer, C.F.Beuran, C.D.Cavellin, Science, 262,1850 (1993).

[90] J.T. Chen, L.E. Wenger, C.J. McEwan, and E.M. Logothetis, Phys. Rev. Lett. 58, 1972 (1987).

[91] R.N. Bhargava, S.P. Herko, and W.N.Osborne, Phys. Rev. Lett. 59, 1468 (1987).

[92] C.Y. Huang, L.J. Dries, P.H. Hor, R.L. Meng, C.W. Chu, and R.B. Frankel, Nature 328, 403 (1987);
H. Ihara, N. Terada, M. Jo, M. Hirabayashi, M. Tokumoto, Y. Kimura, T. Matsubara, and R. Sugise, Jpn. J. Appl. Phys. 26, L1413 (1987).

[93] J. Narayan, V.N. Shukla, S.J. Lukasiewicz, N. Biunno, R. Singh, A.F. Schreiner, and S.J. Pennycook, Appl. Phys. Lett. 51, 940 (1987).

[94] A.V. Narlikar, Nature 327, 357 (1987);
R. Schönberger, H.H. Otto, B. Brunner, and K.F. Renk, Physica C 173, 159 (1991).

[95] A.W. Sleight, Physics Today, June (1991), p.24.

[96] J.B. Goodenough and A. Manthiram, J. Solid State Chem. 88, 115 (1990).

[97] J.D. Jorgensen, H.B. Schuttler, D.G. Hinks, D.W. Capone, K. Zhang, M.B. Brodsky, and D.J.Scalapino, Phys. Rev. Lett. 58, 1024 (1987).

[98] S.W. Cheong, J.D. Thompson, and Z. Fisk, Physica C 158, 109 (1989).

[99] J. Beille, B. Chevalier, G. Demazeau, F. Deslandes, J. Etourneau, O. Laborde, C. Michel, P. Lejay, J. Provost, B. Raveau, A. Sulpice, J.L. Tholence, and R.Tournier, Physica B 146, 307 (1987).

[100] P.M. Grant, S.S.P. Parkin, V.Y. Lee, E.M. Engler, M.L. Ramirez, J.E. Vazquez, G. Lim, and R.D. Jacowitz, Phys. Rev. Lett. 58, 2482 (1987).

[101] S.A. Shaheen, N. Jisrawi, Y.H. Lee, Y.Z. Zhang, M. Groft, W.L. MacLean, H. Zhen, L.Rebelsky, and S.Horn, Phys. Rev. B 36, 7214 (1987).

[102] S.M. Fine, M. Greenblatt, S. Simizu, and S.A.Friedberg, Phys. Rev. B 36, 5716 (1987).

[103] M. Tokumoto, Y. Nishihara, K.Oka, and H.Unoki, Nature, 330, 48 (1987).

[104] J.E. Schirber, B. Morosin, R.M. Merrill, P.F. Hlava, E.L. Venturini, J.F. Kwak, P.J. Nigrey, R.J. Baughman, and D.S. Ginley, Physica C 152, 121 (1988).

[105] R. Yoshizaki, H. Sawada, T. Iwazumi, and H. Ikeda, Solid State Comm. 65, 1539 (1988).

[106] H. Kurahashi, Y. Saito, Y. Abe, and H.Ikeda, Physica C 156, 297 (1988);
J. Beille, G. Demazeau, H.Dupendant, J. Etourneau, P.Lejay, A. Sulpice, and R. Tournier, Physica C 157, 446 (1989).

[107] S. Tanaka, G. Takagi, S. Uchida, and K. Kitazawa, Jpn. J. Appl. Phys. 26, L231 (1987).

[108] W. Wang, G. Collin, M. Ribault, J. Friedel, D. Jerome, J.M. Bassat, J.P.Coutures, and Ph.Odier, J.Phys. 48,1181 (1987).

[109] A.V. Narlikar, in *International Conference on Superconductivity,* Edited by S.K. Joshi, C.N.R. Rao, and S.V.Subramanyam (World Scientific, Singapore, 1990), p.103, and references therein.

[110] R.J. Cava, A.W. Hewat, E.A. Hewat, B. Batlogg, M. Marezio, K.M. Rabe, J.J. Krajewski, W.F.Peck Jr., and L.W.Rupp Jr., Physica C 165, 419 (1990).

[111] R.J. Cava , B. Batlogg, S.A. Sunshine, T. Siegrist, R.M. Fleming, K. Rabe, L.F. Schneemeyer, D.W. Murphy, R.B.van Dover, P.K. Gallagher, S.H. Glarum, S.Nakahara, R.C.Farrow, J.J. Krajewski, S.M. Zahurak, J.V. Waszczak, J.H.Marshall, P. Marsh, L.W. Rupp, Jr., W.F. Peck, and E.A.Rietman, Physica C 153-155, 560 (1988).

[112] R.J. Cava, B. Batlogg, K.M. Rabe, E.A. Rietman, P.K. Gallagher, and L.W. Rupp Jr., Physica C 156, 523 (1988).

[113] B. Raveau, C. Michel, and M. Hervieu, J. Solid State Chem. 88, 140 (1990).

[114] S.S.P. Parkin, V.Y. Lee, A.I. Savoy, R. Beyers, and S.J. La Placa, Phys. Rev. Lett. 61, 750 (1988).

[115] M.A. Subramanian, J.C. Calabrese, C.C. Torardi, J. Gopalakrishnan, T.R. Askew, R.B. Flippen, K.J.Morrissey, U. Chowdhry, and A.W. Sleight, Nature 332, 420 (1988).

[116] C.C. Torardi, M.A. Subramanian, J.C. Calabrese, J. Gopalakrishnan, E.M. Mc Carron, K.J. Morrissey, T.R.Askew, R.B.Flippen, U.Chowdhry, and A.W. Sleight, Phys. Rev. B 38, 225 (1988).

[117] H. Ihava, R. Sugise, K. Hirabayashi, N. Terada, M. Jo, K. Hayashi, A. Negishi, M. Tokumoto, Y. Kimura, and T. Shimomura, Nature 334, 510 (1988).

[118] P. Haldar, K.Chen, B.Maheswaran, A.Roig-Janicki, N.K.Jaggi, R.S. markiewicz, and B.C.Giessen, Science 241, 1198 (1988).

[119] M. KiKuchi, S. Nakajima, y. Syono, K. Hiraga, T. Oku, D. Shindo, N.Kobayashi, H. Iwasaki, and Y.Muto, Physica C 158, 79 (1989).

[120] R.M. Hazen, C.T. Prewitt, R.J. Angel, N.L.Ross, L.W.Finger, C.G. Hadidiacos, D.R. Veblen, P.J. Heaney, P.H. Hor, R.L. Meng, Y.Y. Sun, Y.Q. Wang, Y.Y. Sue, Z.J. Huang, L. Gao, J. Bechtold, and C.W. Chu, Phys. Rev. Lett. 60, 1174 (1988).

[121] M. Hervieu, C. Michel, B. Domenges, Y. Laligant, A. Lebail, G. Ferey, and B. Raveau, Mod. Phys. Lett. 2, 491 (1988).

[122] J.M. Tarascon, Y. Le page, P. Barboux, B.G. Bagley, L.H. Greene, W.R. Mc Kinnon, G.W. Hull, M.Giroud, and D.M.Hwang, Phys. Rev. B 37, 9382 (1988).

[123] J.M. Tarascon, W.R. Mc Kinnon, P. Barboux, D.M. Hwang, B.G. Bagley, L.H. Greene, G.W. Hull, Y. Le Page, N. Stoffel, and M. Giroud, Phys. Rev. B 38, 8885 (1988).

[124] T. Rouillon, R. Retoux, D. Groult, C. Michel, M.Hervieu, J. Provost, and B.Raveau, J. Solid State Chem. 78, 322 (1989).

[125] R.J. Cava, B. Batlogg, J.J. Krajewsky, L.W.Rupp, L.F. Scheemeyer, T. Siegrist, R.B. Van Dover, P.Marsh, W.F.Peck, P.K. Gallagher, S.H. Glarum, J.H.Marshall, R.C.Farrow, J.V. Waszczak, R. Hull, and P. Trevor, Nature 336, 211 (1988).

[126] T. Rouillon, J. Provost, M. Hervieu, D. Groult, C. Michel, and B. Raveau, Physica C 159, 201 (1989).

[127] S. Pei, J.D. Jorgensen, B. Dabrowski, D.G. Hinks, D.R. Richards, A.W. Mitchell, J.M. Newsam, S.K. Sinha, D.Vaknin, and A.J. Jacobson, Phys. Rev. B 41, 4126 (1990).

[128] S. Kondoh, M. Sera, Y. Ando, and M.Sato, Physica C 157, 469 (1989).

[129] B. Batlogg, Physics Today, June (1991), p.44.

[130] S. Martin, A.T. Fiory, R.M. Fleming, L.F.Schneemeyer, and J.V. Waszczak, Phys. Rev. Lett. 60, 2194 (1988);
Q.S. Yang and Z.X. Zhao, in *International Conference on Superconductivity,* Edited by S.K. Joshi, C.N.R.Rao, and S.V. Subramanyam (World Scientific, Singapore, 1990), p.25.

[131] S.W. Tozer, A.W. Klemsasser, T. Penney, D. Kaiser, and F. Holtzberg, Phys. Rev. Lett. 59, 1768 (1987).

[132] S.J. Hagen, T.W. Jing, Z.Z. Wang, J. Hovath, and N.P. Ong, Phys. Rev. B 37, 7928 (1988).

[133] Y. Iye, T. Tamegai, H. Takeya, and H. Takei, Jpn. J. Appl. Phys. 26, L1057 (1987).

[134] Y. Iye, T. Tamegai, T. Sakakibara, T. Goto, N. Miura, H. Takeya, and H. Takei, Pysica C 153-155, 26 (1988).

[135] G. Weigang and K. Winzer, Z. Phys. B, 77, 11 (1989).

[136] M. Charalambous, J.Chaussy, and P.Lejay, Physica B 169, 637 (1991).

[137] A. Esparza, C.A. D'ovidio, J. Guimpel, E. Osquiguil, L. Civale, and F. de la cruz, Solid State Commun. 63, 137 (1987);
R. Micnas, J. Ranninger, and S. Robaszkiewicz, Phys. Rev. B 36, 4051 (1987).

[138] S. Martin, A.T. Fiory, R.M. Fleming, L.F. Schneemeyer, J.V. Waszczak, Phys. Rev. Lett. 60, 2194 (1988).

[139] A.T. Fiory, S. Martin, R.M. Fleming, L.F. Schneemeyer, J.V. Waszak, A.F. Hebard, and S.A. Sunshine, Physica C 162-164, 1195 (1989).

[140] H.L. Stormer, A.F.J. Levi, K.W. Baldwin, M. Anzlowar, and G.S. Boebinger, Phys. Rev. B 38, 2472 (1988).

[141] J.Z. Wu, C.S. Ting, and D.Y. Xing, Phys. Rev. B 40, 9296 (1989).

[142] M.R. Dietrich, W.H. Fietz, J. Ecke, and C. Politis, Jpn. J. Appl. Phys. 26, Suppl. 26-3 (1987).

[143] J. Orenstein, G.A. Thomas, A.J. Millis, S.L. Cooper, D.H. Rapkine, T. Timusk, L.F. Schneemeyer, and J.V. Waszczak, Phys. Rev. B 42, 6342 (1990);
Z. Schlesinger, R.T. Collins, F. Holtzberg, C. Field, S.H. Blaton, U. Welp, G.W. Crabtree, Y. Fang and J.Z. Liu, Phys. Rev. Lett. 65, 801 (1990).

[144] D.W. Reagor, A. Migliori, Z. Fisk, R.D. Taylor, K.A.Martin, and R.R. Ryan, Phys. Rev. B 38, 5106 (1988).

[145] L.R. Testardi, W.G. Moulton, H. Mathias, H.K. Ng, and C.M. Rey, Phys. Rev. B **37**, 2324 (1988).

[146] A. Behrooz and A. Zettl, Solid State Comm. **70**, 1059 (1989).

[147] G.A. Samara, W.F. Hammetter, and E.L. Venturini, Phys. Rev. B **41**, 8974 (1990).

[148] K. Kamaras, S.L. Herr, C.D. Porter, N. Tache, D.B.Tanner, S. Etemad, T. Venkatesan, E. Chase, A. Juan, X.D. Wu, M.S. Hedge, and B. Dutta, Phys. Rev. Lett. **64**, 84 (1990).

[149] J.R. Cooper, B. Alavi, L. -W. Zhou, W.P. Beyermann, and G. Gruner, Phys. Rev. B **35**, 8794 (1987).

[150] M.F. Hundley, A. Zettl, A. Stacy, and M.L. Cohen, Phys. Rev. B **35**, 8800 (1987).

[151] N. Mitra, J. Trefny, B. Yarar, G. Pine, Z.Z.Sheng, and A.M. Hermann, Phys. Rev. B **38**, 7064 (1988).

[152] T. Penney, S. von Molnar, D. Kaiser, F. Holtzberg, and A.M. Kleinasser, Phys. Rev. B **38**, 2918 (1988);
T.R.Chien, D.A.Brawner, Z.Z.Wang, and N.P.Ong, Phys. Rev. B **43**, 6242 (1991).

[153] C.N.R. Rao, J. Gopalakrishnan, A.K. Santra, and V. Manivannan, Physica C **174**, 11 (1991);
H. Zhang and H. Sato, **70**, 1697 (1993).

[154] D. Vaknin, S.K. Sinha, D.E. Moncton, D.C. Johnston, J.M. Newsam, C.R.Safinya, and H.E.King Jr., Phys. Rev. Lett. **58**, 2802 (1987).

[155] J.B. Torrance, A. Bezinge, A.I. Nazzal, T.C. Huang, S.S.P. Parkin, D.P. Keane, S.J. LaPlaca, P.M. Horn, and G.A. Held, Phys. Rev. B **40**, 8872 (1989).

[156] M. Takigawa, P.C. Hammel, R.H. Heffner, Z. Fisk, J.L. Smith, and R.B. Schwartz, Phys. Rev. B 39, 300 (1989); M. Takigawa, A.P. Reyes, P.C. Hammel, J.D. Thompson, R.H. Heffner, Z.Fisk, and K.C. Ott, Phys. Rev. B 43, 247 (1991).

[157] C.H. Pennington, D.J. Durand, C.P. Slichter, J.P.Rice, E.D. Bukowski, and D.M. Ginsberg, Phys. Rev. B 39, 2902 (1989); R.E. Waldstedt, W.W. Warren Jr., R.F. Bell, G.F. Brennert, G.P. Espinosa, R.J. Cava, L.F. Schneemeyer, and J.V. Waszczak, Phys. Rev. B 38, 9299 (1988).

[158] N. Bulut and D.J. Scalapino, Phys. Rev. Lett. 68, 706 (1992), and references therein.

[159] W.W. Warren, R.E. Walstedt, G.F. Brennert, G.P. Espinosa, and J.P. Remeika, Phys. Rev. Lett. 59, 1860 (1987); P.C. Hammel, M. Takigawa, R.H. Heffner, and Z. Fisk, Phys. Rev. B 38, 2832 (1988).

[160] R. Vijayaraghavan, L.C. Gupta, A.K. Rajarajan, P.P. Singh, and A.T. Rane, in *International Conference on Superconductivity,* Edited by S.K. Joshi, C.N.R. Rao, and S.V.Subramanyam (World Scientific, Singapore, 1990), p.284.

[161] M. Cardona, in *International Conference on Superconductivity,* Edited by S.K. Joshi, C.N.R. Rao, and S.V.Subramanyam (World Scientific, Singapore, 1990), p.208, and references therein.

[162] F. Slakey, M.V. Klein, J.P. Rice, and D.M.Ginsberg, Phys. Rev. B 43, 3764 (1991).

[163] C.M. Varma, P.B. Littlewood, S. Schmitt-Rink, E.Abrahams, and A.E. Ruckenstein, Phys. Rev. Lett. 63, 1996 (1989).

[164] L.F. Mattheiss, Phys. Rev. Lett. 58, 1028 (1987); L.F. Mattheiss and D.R. Hamman, Solid State Comm. 63, 395 (1987).

[165] A. Bansil, R. Pankaluoto, R.S. Rao, P.E. Minjarends, W. Dlugosz, R.Prasad, and L.C.Smedskjoer, Phys. Rev. Lett. 61, 2480 (1988).

[166] C.M. Fowler, B.L. Freeman, W.L. Hults, J.C. King, F.M. Mueller, and J.L. Smith, Phys. Rev. Lett. 68, 534 (1992), and references therein.

[167] F.M. Mueller, C.M. Fowler, B.L. Freeman, W.L. Hutts, J.C. King, and J.L. Smith, Physica B 172, 253 (1991).

[168] L.P.Gor'kov and N.B.Kopnin, Usp. Fiz.Nauk. 156, 118 (1988).

[169] L.C. Bourne, M.F. Crommie, A. Zettl, H.C. Loye, S.W.Keller, K.L. Leary, A.M. Stacy, K.J. Chang, M.L. Cohen, and D.E. Morris, Phys. Rev. Lett. 58, 2337 (1987);
B. Batlogg, R.J. Cava, A. Jayaraman, R.B. van Dover, G.A. Kourouklis, S. Sunshine, D.W. Murphy, L.W. Rupp, H.S. Chen, A. White, K.T. Short, A.M. Mujsce, and E.A. Rietman, Phys. Rev. Lett. 58, 2333 (1987);
E.L. Benitez, J.J. Lin, S.J. Poon, W.E. Farneth, M.K. Crawford, and E.M. McCarron, Phys. Rev. B 38, 5025 (1988);
M. Cardona, R. Liu, C. Thomsen, W. Kress, E. Schönherr, M. Bauer, L. Genzel, and W. König, Solid State Commun. 67, 789 (1988).

[170] J.P. Franck, J. Jung, M.A. Mohamed, S. Gygax, and G.I. Sproule, Phys. Rev. B 44, 5318 (1991).

[171] H.J.Bornemann and D.E.Morris, Phys. Rev. B 44, 5322 (1991).

[172] R. Combescot, Phys. Rev. Lett. 68, 1089 (1992).

[173] A.W. Sleight, Science 242, 1519 (1988).

[174] R.J. Cava, Science 247, 656 (1990).

[175] J.H. Nickel, D.E. Morris, and J.W. Ager, III, Phys. Rev. Lett. 70, 81 (1993).

[176] J.-M. Imer, F. Patthey, B. Dardel, W.-D. Schneider, Y. Bayer, Y. Petroff, and A. Zettl, Phys. Rev. Lett. 62, 336 (1989);

C.G. Olson, R. Liu, A.B. Yang, D.W. Lynch, A.J.Arko, R.S. List, B.W. Veal, Y.C. Chang, P.Z. Jiang, and A.P. Paulikas, Science 245, 731 (1989);

C.G. Olson, R. Liu, D.W. Lynch, R.S. List, A.J. Arko, B.W. Veal, Y.C. Change, P.Z. Jiang, and A.P.Paulikas, Phys. Rev. B 42, 381 (1990);

[177] S. Vieira, M.A. Ramos, M. Vallet-Regi, and J.M. Gonzalez-Calbet, Phys. Rev. B 38, 9295 (1988).

[178] Z. Schlesinger, R.T. Collins, D.L. Kaiser, and F.Holtzberg, Phys. Rev. Lett. 59, 1958 (1987);

W. Ose, P.E. Obermayer, H.H. Otto, T. Zetterer, H. Langfellner, J. Keller, and K.F. Renk, Z. Phys. B 70, 307 (1988);

G.A. Thomas, J. Orenstein, D.H. Rapkine, M. Capizzi, A.J. Mills, R.N. Bhatt, L.F. Schneemeyer, and J.V. Waszczak, Phys. Rev. Lett. 61, 1313 (1988).

[179] A.J. Arko, R.S. List, R.J. Bartlett, S.W. Cheong, Z. Fisk, J.D. Thompson, C.G. Olson, A.B. Young, R. Liu, C. Gu, B.W. Veal, J.Z. Liu, A.P. Paulikas, K. Vandervoort, H. Claus, J.C. Campuzano, J.E. Schirber, and N.D. Shinn, Phys. Rev. B 40, 2268 (1989).

[180] P.W. Anderson and J.R. Schrieffer, Physics Today, June (1991), p. 54.

[181] A. Manthiram and J.B.Goodenough, Physica C 159, 760 (1989).

[182] J.B. Torrance, Y. Tokura, A.I. Nazzal, A. Bezinge, T.C. Huang, and S.S.P. Parkin, Phys. Rev. Lett. 61, 1127 (1988).

[183] C.M. Varma, S. Schmitt-Rink, and E. Abrahams, Solid State Comm. 62, 681 (1987).

[184] P.W. Anderson, Science 235, 1196 (1987).

[185] P.W. Anderson, G. Baskaran, Z. Zou, and T. Hsu, Phys. Rev. Lett. 58, 2790 (1987).

[186] P.W. Anderson, Phys. Rev. Lett. 64, 1839 (1990).

[187] P.W. Anderson and Z. Zou, Phys. Rev. Lett. 60, 132 (1988); P.W. Anderson, Phys. Rev. B 42, 2624 (1990).

[188] N. Nagaosa and P.A. Lee, Phys. Rev. Lett. 64, 2450 (1990).

[189] L.B. Ioffe and G.Kotliar, Phys. Rev. B 42, 10348 (1990); L.B.Ioffe and P.B.Wiegmann, Phys. Rev. Lett. 65,653 (1990).

[190] J.R. Schrieffer, X.G. Wen, and S.C. Zhang, Phys. Rev. Lett. 60, 944 (1988);
J.R. Schrieffer, X.G. Wen, and S.C. Zhang, Phys. Rev. B 39, 11663 (1989).

[191] A. Kampf and J.R.Schrieffer, Phys. Rev. B 41, 6399 (1990); 42, 7967 (1990);
D.M. Frenkel, W. Hanke, Phys. Rev. B 42, 6711 (1990).

[192] J.H. Kim, K. Levin, and A. Auerbach, Phys. Rev. B 39, 11633 (1989).

[193] G. Kotliar, P.A. Lee, and N. Read, Physica C 153-155, 538 (1988).

[194] D.M. Newns, P. Pattnaik, M. Rasolt, and D.A. Papaconstantopoulos, Phys. Rev. B 38, 7033 (1988).

[195] N. Bulut, D. Hone, D.J. Scalapino, and N.E. Bickers, Phys. Rev. Lett. 64, 2723 (1990); Phys. Rev. B 41, 1797 (1990).

[196] A.J. Millis, H. Monien, and D. Pines, Phys. Rev. B 42, 167 (1990).

[197] C.M. Varma, Phys. Rev. Lett. 61, 2713 (1988).

[198] C.M. Varma, P.B. Littlewood, S. Schmitt-Rink, E. Abrahams, and A.E. Ruckenstein, Phys. Rev. Lett. 63, 1996 (1989).

[199] Yu.B. Gaididei and V.M. Loktev, Phys. Status Solidi b 147, 307 (1988).

[200] V.L. Ginzburg, Int. J. Mod. Phys. B 1, 651 (1987), and references therein.

[201] A. Virosztek and J. Ruvalds, Phys. Rev. B 42, 4064 (1990).

[202] Y. Guo, J.M. Langlois, and W.A. Goddard, Science 239, 896 (1988);
E.Y. Loh, T. Martin, and P.Prelovsek, Phys. Rev. B 38, 2494 (1988).

[203] E.A. Pashitski and B.L. Vinetskii, Pis'ma Zh. Exp. Teor. Fiz. Suppl., 46, 124 (1987).

[204] A.S. Davydov, Phys. Rep. 190, 191 (1990), and references therein.

[205] S.S. Jha, in *International Conference on Superconductivity,* Edited by S.K. Joshi, C.N.R. Rao, and S.V.Subramanyam (World Scientific, Singapore, 1990), p. 372.

[206] D.S. Dessau, B.O. Wells, Z.-X. Shen, W.E. Spicer, A.J.Arko, R.S. List, D.B. Mitzi, and A. Kapitulnik, Phys. Rev. Lett. 66, 2160 (1991).

[207] P.W. Anderson, G. Baskaran, Z. Zou, J. Wheatley, T. Hsu, B.S. Shastry, B. Doucot, and S. Liang, Physica C 153-155, 527 (1988).

[208] W.E. Pickett, Rev. Mod. Phys. 61, 433 (1989).

[209] R. Lal and S.K. Joshi, Solid State Commun. 83, 209 (1992).

[210] H.E. Castillo and C.A. Balseiro, Phys. Rev. Lett. 68, 121 (1992), and references threrein.

[211] K. Levin, Ju H. Kim, J.P. Lu, and Q. Si, Physica C 175, 449 (1991).

[212] C.M. Varma, Int. J. Mod. Phys. B 3, 2083 (1989).

[213] C.M. Varma, S. Schmitt-Rink, and E. Abrahams, in *Novel Superconductivity,* Edited by V. Kresin and S. Wolf, Plenum Press, New York (1987).

[214] E.H. Appelman, L.R. Morss, A.M. Kini, U. Geiser, A. Umezawa, G.W. Crabtree, and K. Carlson, Inorg. Chem. 26, 3239 (1987).

[215] D.C. Harris and T.A. Hewston, J. Solid State Chem. 69, 182 (1987).

[216] H.C. Montgomery, J. Appl. Phys. 42, 2971 (1971).

[217] R.B. Roberts, Philos. Mag. 36, 91 (1977).

[218] R.S. Crisp, W.G. Henry, and P.A.Schroeder, Philos. Mag. 10, 553 (1964); the data in this paper must be corrected to the new scale of Roberts (Ref. 217).

[219] S. Minomura and H.G. Drickamer, J. Appl. Phys. 34, 3043 (1963).

[220] B.N. Brockhouse, Phys. Rev. 94, 781 (1954)

[221] M. O'keeffe and F.S. Stone, J. Phys. Chem. Solids 23, 261 (1962).

[222] H. Wieder and A.W.Czanderna, J. Appl. Phys. 37, 184 (1966).

[223] B.Roden, E. Braun, and A. Freimuth, Solid State Commun. 64, 1051 (1987).

[224] G.N. Kryukova, V.I. Zaikovskii, V.A. Sadykov, S.F. Tikhov, V.V. Popovskii, N.N. Bulgakov, J. Solid State Chem. 73, 191 (1988).

[225] L. Degiorgi, E. Kaldis, and P. Wachter, Physica C 153-155, 657 (1988).

[226] J.B. Forsyth, P.J. Brown, and B.M. Wanklyn, J.Phys. C 21, 2917 (1988)

[227] B.X. Yang, T.R. Thurston, J.M. Tranquada, G. Shirane, Phys. Rev. B 39, 4343 (1989).

[228] M.S. Seehra, Z. Feng, and R. Gopalakrishnan, J.Phys. C 21, L1051 (1988).

[229] K. Muraleedharan, C.K. Subramaniam, N. Venkataramani, T.K. Gundu Rao, C.M. Srivastava, V. Sankaranarayanan, and R. Srinivasan, Solid State Commun. 76, 727 (1990).

[230] F. Mehran, S.E. Barnes, T.R. Mc Guire, W.J.Gallagher, R.L. Sandstrom, T.R.Dinger, and D.A.Chance, Phys. Rev. B 36, 740 (1987).

[231] F. Mehran, S.E. Barnes, G.V.Chandrashekhar, T.R. Mc Guire, and M.W. Shafer, Solid State Commun. 67, 1187 (1988).

[232] E.Gmelin, T.P.Chattopadhyay, and W. Brill, *International Conference on superconductivity,* Jan. 10-14,1990, Bangalore.

[233] R. Janes, K.K. Singh, S.D. Burnside, P.P. Edwards, Solid State Commun. 79, 241 (1991).

[234] J.A. Veira and F. Vidal, Physica C 159, 468 (1989).

[235] J. Toulouse, X.M. Wang, and D.J.L. Hong, Phys. Rev. B 38, 7077 (1988).

[236] J.W. Loram, K.A. Mirza, C.P. Joyce, and A.J. Osborne, Europhys. Lett. 8, 263 (1989).

[237] H. You, J.D. Axe, X.B. Kan, S.C. Moss, J.Z. Liu, and D.J. Lam, Phys. Rev. B 37, 2301 (1988).

[238] R.M. Fleming, L.F. Schneemeyer, P.K. Gallagher, B. Batlogg, L.W. Rupp, and J.V. Waszczak, Phys. Rev. B 37, 7920 (1988).

[239] L.G.Aslamazov and A.I.Larkin, Phys. Lett. A 26, 238 (1968).

[240] P.P.Freitas, C.C. Tsuei, and T.S. Plaskett, Phys. Rev. B 36 833 (1987).

[241] S.J. Hagen, Z.Z. Wang, and N.P. Ong, Phys. Rev. B 38, 7137 (1988).

[242] T.A. Friedmann, J.P. Rice, J. Giapintzakis, and D.M. Ginsberg, Phys. Rev. B 39, 4258 (1989).

[243] N.P. Ong, Z.Z. Wang, S.J. Hagen, T.W.Jing, J.Clayhold, and J. Horvath, Physica C 153-155, 1072 (1988).

[244] A. Poddar, P. Mandal, A.N. Das, B. Ghosh, and P.Choudhury, Physica C 159, 231 (1989);
P. Mandal, A. Poddar, A.N. Das, B. Ghosh, and P.Choudhury, Physica C 169, 43 (1990).

[245] N. Goldenfield, P.D. Olmsted, T.A. Friedman, and D.M. Ginsberg, Solid State Commun. 65, 465 (1988).

[246] F. Vidal, J.A. Veira, J. Maza, and F. Miguelez, Solid State Commun. 66, 421 (1988);

[247] F.Vidal, J.A.Veira, J.Maza, J.J.Ponte, J.Amador, C.Cascales, M.T. Casals, and I. Rasines, Physica C 156, 165 (1988).

[248] M. Ausloos and Ch. Laurent, Phys. Rev. B 37, 611 (1988).

[249] M.P. Fontana, C. Paracchini, C. Paris De Renzi, P.Podini, F. Licci, and F.C. Matacotta, Solid State Commun. 69, 621 (1989).

[250] B. Oh, K. Char, A.D. Kent, M. Naito, M.R. Beasley, T.H. Geballe, R.H. Hammond, A. Kapitulnik, and J.M. Graybeal, Phys. Rev. B 37, 7861 (1988).

[251] V.A. Gasparov, Physica C **178**, 449 (1991).

[252] R. Srinivasan, in *International Conference on Superconductivity*, edited by S.K. Joshi, C.N.R. Rao, and S.V.Subramanyam (World Scientific, Singapore, 1990), p.147, and references therein.

[253] W.E. Lawrence and S. Doniach, Proc. XII Int. Conf. Low Temp. Phys. Kyoto (1970), ed. E.Kanda (Keigaku, Tokyo, 1971) P.361.

[254] K.Maki, Prog. Theor. Phys. 39, 897 (1968) ; 40, 193 (1968).

[255] R.S. Thompson, Phys. Rev. B 1, 327 (1970).

[256] C.J. Lobb, Phys. Rev. B 36, 3930 (1987).

[257] J.A. Veira, J. Maza, and F. Vidal, Phys. Lett. A **131**, 310 (1988).

[258] M. Sera, S. Kondoh, and M.Sato, Solid State Commun. 68, 647 (1988).

[259] R.C.Yu, M.J. Naughton, X. Yan, P.M. Chaikin, F. Holtzberg, R.L. Greene, J. Stuart, and P. Davis, Phys. Rev. B 37, 7963 (1988).

[260] M.A. Howson, M.B. Salamon, T.A. Friedmann, S.E. Inderhees, J.P. Rice, D.M.Ginsberg, and K.M. Ghiron, J. Phys. Condens. Matter 1, 465 (1989).

[261] M.A. Howson, M.B. Salamon, T.A. Friedmann, J.P. Rice, and D.M. Ginsberg, Phys. Rev. B 41, 300 (1990).

[262] S.-W. Cheong, S.E. Brown, Z. Fisk, R.S. Kwok, J.D.Thompson, E. Zirngiebl, G. Grüner, D.E. Peterson, G. -L. Wells, R.B. Schwarz, and J.R. Cooper, Phys. Rev. B 36, 3913 (1987).

[263] L. Lu, B.H. Ma, S.-Y. Lin, H. -M. Duan, and D. -L. Zhang, Europhys. Lett. 7, 555 (1988).

[264] M.F. Crommie, A. Zettl, T.W. Barbee III, and M.L. Cohen, Phys. Rev. B 37, 9734 (1988).

[265] M. Sera, S. Shamoto, and M. Sato, Solid state Commun. 68, 649 (1988).

[266] Z.Z. Wang and N.P. Ong, Phys. Rev. B 38, 7160 (1988).

[267] L. Forro, M. Raki, J.Y. Henry, and C. Ayache, Solid State Commun. 69, 1097 (1989).

[268] S.-Y. Lin, L. Lu, H.-M. Duan, B. -H. Ma, and D. -L. Zhang, Int. J. Mod. Phys. B 3, 409 (1989).

[269] T.A. Friedmann, M.W. Rabin, J. Giapintzakis, J.P. Rice, and D.M. Ginsberg, Phys. Rev. B 42, 6217 (1990).

[270] A.J. Lowe, S. Regan, and M.A. Howson, Physica B 165 & 166, 1369 (1990).

[271] A.B. Kaiser and G. Mountjoy, Phys. Rev. B 43, 6266 (1991).

[272] J.L. Cohn, S.A. Wolf, V. Selvamanickam, and K.Salama, Phys. Rev. Lett. 66, 1098 (1991).

[273] A.J. Lowe, S. Regan, and M.A. Howson, Phys. Rev. B 44, 9757 (1991).

[274] J.L.Cohn, E.F.Skelton, S.A.Wolf, and J.Z. Liu, Phys. Rev. B 45, 13140 (1992).

[275] U. Gottwich, R. Held, G. Sparn, F. Steglich, H. Rietschel, D. Ewert, B. Renker, W. Bauhoffer, S. von Molnar, M. Wilhelm, and H.E. Hoenig, Europhys. Lett. 4, 1183 (1987).

[276] J.T. Chen, C.J. McEwan, L.E. Wenger, and E.M. Logothetis, Phys. Rev. B 35, 7124 (1987).

[277] Z.G. Khim, S.C. Lee, J.H. Lee, B.J. Suh, Y.W. Park, C.Park, and I.S. Yu, Phys. Rev. B 36, 2305 (1987).

[278] S.C. Lee, J.H. Lee, B.J. Suh, S.H. Moon, C.J. Lim, and Z.G. Khim, Phys. Rev. B 37, 2285 (1988).

[279] W.N. Kang and M.Y. Choi, Phys. Rev. B 42, 2573 (1990).

[280] O. Cabeza, A. Pomar, A. Diaz, C.Torron, J.A.Veira, J.Maza, and F. Vidal, J. Phys. Condens. Matter, 5, 1365 (1993).

[281] O. Cabeza, A. Pomar, A. Diaz, C. Torron, J.A. Veira, J. Maza, and F. Vidal, Phys. Rev. B 47, 5332 (1993).

[282] N. Mitra, J. Trefny, and M. Young, Phys. Rev. B 36, 5581 (1987).

[283] R. Srinivasan, V. Sankaranarayanan, N.P. Raju, S.Natarajan, U.V. Varadaraju, and G.V. Subba Rao, Pramana J. Phys. 29, L225 (1987).

[284] C. Uher and A.B. Kaiser, Phys. Rev. B 36, 5680 (1987).

[285] H.J. Trodahl and A. Mawdsley, Phys. Rev. B 36, 8881 (1987).

[286] A. Mawdsley, H.J. Trodahl, J. Tallon, J. Sarfati, and A.B. Kaiser, Nature 328, 233 (1987).

[287] A.P. Goncalves, I.C. Santos, E.B. Lopes, R.T. Henriques, M. Almeida,and M.O. Figueiredo, Phys. Rev. B 37, 7476 (1988).

[288] Z. Henkie, P.J. Markowski, R. Horyn, Z. Bukowski, and J. Klamut, Phys. Status Solidi B 146, 131 (1988).

[289] Ch. Laurent, S.K. Patapis, M. Laguesse, H.W.Vanderschueren, A. Rulmont, P. Tarte, and M. Ausloos, Solid State Commun. 66, 445 (1988).

[290] V. Radhakrishnan, C.K. Subramaniam, V. Sankaranarayanan, G.V. Subba Rao, and R. Srinivasan, Phys. Rev. B 40, 6850 (1989).

[291] W.N. Kang, K.C.Cho, Y.M.Kim, and Mu-Yong choi, Phys. Rev. B 39, 2763 (1989).

[292] A.K. Bhatnagar, R. Pan, D.G. Naugle, G.R.Gilbert, and R.K. Pandey, Phys. Rev. B **41**, 4002 (1990).

[293] S. Yan, P.Lu, and Q.Li, Solid State Commun. 65, 355 (1988).

[294] P.J. Ouseph and M. Ray O'Bryan, Phys. Rev. B **41**, 4123 (1990).

[295] E. Borchi, S. de Gennaro, and M. Simoncini, Phys. Lett. A **170**, 102 (1992).

[296] A.B. Kaiser and C. Uher, in *Studies of High Temperature Superconductors,* edited by A.V. Narlikar (Nova Science, New York, 1990), vol. 7.

[297] M. Ausloos, K. Durczewski, S.K. Patapis, Ch. Laurent, and H.W. Vanderschueren, Solid State Commun. 65, 365 (1988).

[298] S.R. Jha, Y.S. Reddy, D.K. Suri, K.D. Kundra, R.G. Sharma, and D. Kumar, Pramana J. Phys. 32, 277 (1989).

[299] T.K. Dey, S.K. Ghatak, S. Srinivasan, D. Bhattacharya, and K.L. Chopra, Solid State Commun. 72, 525 (1989).

[300] F. Devaux, A. Manthiram, and J.B. Goodenough, Phys. Rev. B **41**, 8723 (1990).

[301] C.W. Crabtree, W.K. Kwok, and A. Umezawa, in *Quantum Field Theory as an Interdisciplinary Basis,* Edited by F.C. Khanna, H. Umezawa, G. Kunstatter, and H.C. Lee (World Scientific, Singapore, 1988).

[302] D.H. Lee and J. Ihm, Solid State Commun. 62, 811 (1987).

[303] R.C. Budhani, S.H. Tzeng, and R.F.Bunshah, Phys. Rev. B 36, 8873 (1987).

[304] S. Uchida, S. Tajima, H. Takagi, K. Kishio, T.Hasegawa, K. Kitazawa, K. Fueki, and S. Tanaka, Jpn. J. Appl. Phys. 26, 1105 (1987).

[305] Z.Z. Wang, J. Clayhold, N.P. Ong, J.M. Tarascon, L.H. Greene, W.R. McKinnon, and G.W. Hull, Phys. Rev. B 36, 7222 (1987).

[306] R.J. Cava, B. Batlogg, C.H. Chen, E.A. Rietman, S.M. Zahurak, and D. Werder, Nature 329, 423 (1987).

[307] P.P. Freitas and T.S. Plaskett, Phys. Rev. B 36, 5723 (1987).

[308] T.K. Chaki and M. Rubinstein, Phys. Rev. B 36, 7259 (1987).

[309] A.T. Fiory, M. Gurvitch, R.J. Cava, and G.P.Espinosa, Phys. Rev. B 36, 7262 (1987).

[310] J.Park, P.Kostic, and J.P.Singh, Mater.Lett. 6, 393 (1988).

[311] G. S. Grader, P.K. Gallagher, and E.M. Gyorgy, Appl. Phys. Lett. 51, 1115 (1987).

[312] M.Gurvitch and A.T.Fiory, Phys. Rev. Lett. 59, 1337 (1987).

[313] T. Ohtani, T. Okudo, A. Tamaki, and T. Ueda, Jpn. J. Appl. Phys. 27, L61 (1988).

[314] F. Munakata, K. Shinohara, H. Kanesaka, N. Hirosaki, A. Okada, and M. Yamanaka, Jpn. J. Appl. Phys. 26, L1292 (1987).

[315] K.N. Tu, N.C. Yeh, S.I. Park, and C.C. Tsuei, Phys. Rev. B 39, 304 (1989).

[316] H.I. Yoo, J. Mater. Res. 4, 23 (1989).

[317] S.I. Park, C.C.Tsuei, and K.N.Tu, Phys. Rev. B 37, 2305 (1988).

[318] K.N. Tu, C.C. Tsuei, S.I. Park, and A. Levi, Phys. Rev. B 38, 772 (1988).

[319] K.N. Tu, N.C. Yeh, S.I. Park, and C.C. Tsuei, Phys. Rev. B 38, 5118 (1988).

[320] N.-C. Yeh, K.N. Tu, S.I. Park, and C.C. Tsuei, Phys. Rev. B 38, 7087 (1988).

[321] J. Park and H.G. Kim, Jpn. J. Appl. Phys. 27, L191 (1988).

[322] S. Yamaguchi, K. Terabe, A. Imai, and Y. Iguchi, J. Appl. Phys. 27, L220 (1988).

[323] G. S. Grader, P.K. Gallagher, J. Thomson, and M. Gurvitch, Appl. Phys. A 45, 179 (1988).

[324] G. Ottaviani, C. Nobili, F. Nava, M. Affronte, T. Manfredini, F.C. Matacotta, and E. Galli, Phys. Rev. B 39, 9069 (1989).

[325] J. Nowotny, M. Rekas, and W.Weppner, J. Am. Ceram. Soc. 73, 1040 (1990).

[326] K. Schuller, D.G. Hinks, M.A. Beno, D.W. Capone II, L. Soderholm, J.P. Locquet, Y. Bruynseraede, C.U. Segre, and K. Zhang, Solid State Commun. 63, 385 (1987).

[327] P.P.Freitas and T.S.Plaskett, Phys. Rev. B 37, 3657 (1988).

[328] M. Gurvitch and A.T. Fiory, Appl. Phys. Lett. 51, 1027 (1987).

[329] A.T. Fiory, S. Martin, L.F. Schneemeyer, R.M. Fleming, A.E. White, and J.V. Waszczak, Phys. Rev. B 38, 7129 (1988).

[330] J. Genossar, B. Fisher, I.O. Lelong, Y. Ashkenazi, and L. patlagan, Physica C 157, 320 (1989).

[331] M. Gurvitch, A.T. Fiory, L.F. Schneemeyer, R.J. Cava, G. P. Espinosa, and J.V.Waszczak, Physica C 153-155, 1369 (1988).

[332] Z. Gao, Z. Hou, B. Du, D. Zhang, G. Wang, C. Wang, and C. Zhu, Physica C 167, 49 (1990).

[333] J.R. LaGraff, P.D. Han, and D.A. Payne, Physica C 169, 355 (1990).

[334] J. Molenda, A. Stoklosa, and T. Bak, Physica C 175, 555 (1991).

[335] J.R. LaGraff, P.D. Han, and D.A.Payne, Phys. Rev. B 43, 441 (1991).

[336] C. Picard, P. Gerdanian, and M. Ould-Die, Physica C 165, 44 (1990).

[337] T. Ohtani, Mat. Res. Bull. 24, 343 (1989).

[338] T. Ohtani and K.Ohkuma, Solid State Commun. 72, 767 (1989).

[339] T. Ohtani, K. Kobatake, and T. Takehara, Physica C 179, 376 (1991).

[340] J.D. Jorgensen, M.A. Beno, D.G. Hinks, L. Soderholm, K.J. Volin, R.L.Hitterman, J.D. Grace, I.K. Schuller, C.U.Segre, K. Zhang, and M.S. Kleefisch, Phys. Rev. B 36, 3608 (1987).

[341] J.D. Jorgensen, B.W. Veal, A.P. Paulikas, L.J. Nowicki, G.W. Crabtree, H.Claus, and W.K.Kwok, Phys. Rev. B 41, 1863 (1990).

[342] L.T.Willie and D.de Fontaine, Phys. Rev. B 37, 2227 (1988).

[343] G.V. Tendeloo, H.W. Zandbergen, and S. Amelinckx, Solid State Commun. 63, 603 (1987).

[344] L.T. Wille, A. Berera, and D. de Fontaine, Phys. Rev. Lett. 60, 1065 (1988).

[345] D. Shi and D.W. Capone, Appl. Phys. Lett. 53, 159 (1988).

[346] R. Beyers, B.T. Ahn, G. Gorman, V.Y. Lee, S.S.P. Parkin, M.L. Ramirez, K.P. Roche, J.E. Vazquez, T.M. GÜr, and R.A. Huggins, Nature (London) 340, 619 (1989).

[347] D. de Fontaine, M.E. Mann, and G. Ceder, Phys. Rev. Lett. 63, 1300 (1989).

[348] D. de Fontaine, G. Ceder, and M. Asta, Nature (London) 343, 544 (1990).

[349] D. Shi, Phys. Rev. B 39, 4299 (1989).

[350] N. Hudakova and P. Diko, Physica C 167, 408 (1990).

[351] L. Civale and E.N. Martinez, Phys. Rev. B 38, 928 (1988).

[352] E. Osquiguil, R. Decca, G. Nieva, L. Civale, and F. de la cruz, Solid State Commun. 65, 491 (1987).

[353] C.J. Jou and J. Washburn, J. Mater. Res. 4, 795 (1989).

[354] I.A. Leonodov, Ya.N. Blinovskov, E.E. Flyatau, P.Ya. Novak, and V.L. Kozhevnikov, Physica C 158, 287 (1989).

[355] T. Siegrist, L.F. Schneemeyer, J.V. Waszczak, N.P. Singh, R.L. Opila, B. Batlogg, L.W. Rupp, and D.W. Murphy, Phys. Rev. B 36, 8365 (1987).

[356] M. Hiratani, Y. Ito, K. Miyauchi, and T. Kudo, Jpn. J. Appl. Phys. 26, L1997 (1987).

[357] H. Krishnan, V. Sankaranarayanan, V. Radhakrishnan, C.K. Subramaniam, R.Srinivasan, and G.V. Subba Rao, Phys. Rev. B 40, 2639 (1989).

[358] J.J. Neumeier, T. Bjornholm, M.B. Maple, and I.K. Schuller, Phys. Rev. Lett. 63, 2516 (1989).

[359] W.M. Tiernan, R.B. Hallock, J.C.W. Chien, and B.M. Gong, Phys. Rev. B 44, 4661 (1991).

[360] G. Xiao, M.Z. Cieplak, A. Gavrin, F.H. Streitz, A. Bakhshai, and C.L.Chien, Phys. Rev. Lett. 60, 1446 (1988).

[361] G. Xiao, F.H. Streitz, A. Gavrin, Y.W. Du, and C.L. Chien, Phys. Rev. B 35, 8782 (1987).

[362] S.X. Dou, N. Savvides, X.Y. Sun, A.J. Bourdillon, C.C. Sorrell, J.P.Zhou, and K.E.Easterling, J. Phys. C 20, L1003 (1987).

[363] K. Okura, K. Ohmatsu, H. Takei, H. Hitotsuyanagi, and T. Nakahara, Jpn. J. Appl. Phys. 27, L655 (1988).

[364] Y. Nishi, S. Moriya, S. Tokunaga, J. Mat. Sci. Lett. 7, 359 (1988).

[365] E.Talik, J.Szade, and J.Heimann, Physica C 165, 434 (1990).

[366] G.W. Kammlott, T.H. Tiefel, and S. Jin, Appl. Phys. Lett. 56, 2459 (1990).

[367] S.A. Vasilchenko, A.I. Gordienko, V.I. Dotsenko, A.P. Isakina, I.F. Kislyak, A.I. Prokhvatilov, M.N. Sorin, N.M. Chaikovskaya, Supercond. Phys. Chem. Technol 4, 1093 (1991).

[368] P.K. Mehta, B.D. Padalia, Om Prakash, D.T. Adroja, P.D. Prabhawalkar, N. Venkataramani, S.K. Malik, and A.V. Narlikar, Bull. Mater. Sci. 14, 871 (1991).

[369] P.K. Mehta, Ph.D. thesis, I.I.T. Bombay (1991).

[370] P.U. Muralidharan and A.D. Damodaran, Jpn. J. Appl. Phys. 1 30, 280 (1991), and references therein.

[371] N. Brnicevic, Lj Tusek-Bozic, P. Planinic, A. Turkovic, S. Popovic, B. Santic, Z. Toman, G. Leising, E.Scheweiger, and V. Wippel, in *Euro-ceramics,* vol. 2, Edited by G. de With, R.A. Terpstra, and R. Metselaar (Elsevier, London, 1989), p.2.481.

[372] C.N.R. Rao and G.V. Subba Rao, *Transition Metal Oxides* (U.S. Govt., Washington, 1974), P.30;

M.Yethiraj, J.Solid State Chem. 88, 53 (1990).

[373] H. Kuwamoto, J.M. Honig, and J. Apple, Phys. Rev. B 22, 2626 (1980);

[374] S.A. Carter, J. Yang, T.F. Rosenbaum, J. Spalek, and J.M. Honig, Phys. Rev. B 43, 607 (1991).

[375] J.M. Tarascon, L.H. Greene, P. Barboux, W.R. McKinnon, G.W. Hull, T.P. Orlando, K.A. Delin, S. Foner, and E.J. McNiff,Jr, Phys. Rev. B 36, 8393 (1987).

[376] Y. Maeno, T. Nojima, Y.Aoki, M. Kato, K. Hoshino, A. Mitami, and T. Fujita, Jpn. J. Appl. Phys. 26, L774 (1987).

[377] J.M. Tarascon, P. Barboux, P.F. Miceli, L.H. Greene, G.W. Hull M.Eibschutz, and S.A. Sunshine, Phys. Rev. B 37, 7458 (1988).

[378] J.F. Bringley, T.-M. Chen, B.A. Averill, K.M. Wong, and S.J. Poon, Phys. Rev. B 38, 2432 (1988).

[379] Y. Zhao, H. Zhang, S. Sun, Z. Su, Z. Chen, and Q. Zhang, Solid State Commun. 67, 31 (1988).

[393] R.S. Howland, T.H. Geballe, S.S. Lederman, A. Fischer Colbrie, M.Scott, J.M.Tarascon, and P.Barboux, Phys. Rev. B 39, 9017 (1989).

[394] C.N.R. Rao, in *International Conference on Superconductivity,* edited by S.K. Joshi, C.N.R. Rao, and S.V. Subramanyam (World Scientific, Singapore, 1990), p.72.

[395] F.C. Zhang and T.M. Rice, Phys. Rev. B 37, 3759 (1988).

[396]. C. Michel, H. Hervieu, M.M. Bovel, A.Grandin, F.Deslandes, J. Provost, and B. Raveau, Z. Phys. B 68, 421 (1987).

[397] L. Hongbao, C. Liezhao, Z. Ling, M. Zhiqiang, L. Xiaoxian, Y. Zhidong, X. Bai, M. Xianglei, Z. Guien, R. Yaozhong, C.Zhaojia and Z.Yuheng, Solid State Commun. 69, 867 (1989).

[398] M.R. Chandrachood, I.S.Mulla and A.P.B.Sinha, Appl. Phys. Lett. 55, 1472 (1989).

[399] X. Zhengping, J.Chunlin and Z.Lian, Solid State Commun. 72, 1013 (1989) ; 72, 1015 (1989).

[400] Y.T. Huang, C.Y. Shei, W.N. Wang, C.K. Chiang and W.H.Lee, Physica C 169, 76 (1990).

[401] P. Mandal, A. Poddar, A.N.Das, and B. Ghosh, Physica C 169, 43 (1990).

[402] P.V.P.S.S. Sastry, I.K. Gopalakrishnan, J.V. Yakhmi, and R.M. Iyer, Physica C 157, 491 (1989).

[403] L. Hongbao, Z. Weijie, Z.Ling, M.Zhiqiang, L.Biyou, Y.Ming, C. Liezhao, C. Zhaojia, R. Yaozhong, P. Dingkun and Z. Yuheng, Physica C 159, 665 (1989).

[404] M. Pissas and D. Niarchos, Physica C 159, 643 (1989).

[405] T.Maeda, K.Sakuyama, H.Yamauchi and S.Tanaka, Physica C159, 784 (1989).

[406] Q. Xu, T.Cheng, X-G. Li, L. Yang, C. Fan, H.Wang, Z.Mao, D. Peng, Z. Chen and Y. Zhang, Physica C 168, 489 (1990).

BIBLIOGRAPHY

[1] D. Shoenberg, *Superconductivity* (Cambridge, Great Britain, 1962).

[2] A.C. Rose-Innes and E.H. Rhoderick, *Introduction to Superconductivity* (Pergamon, London, 1969).

[3] G. Rickayzen, *Theory of Superconductivity* (Interscience, New York, 1965).

[4] C. Kittel, *Introduction to Solid State Physics* (Wiley, New York, 1986).

[5] V. Daniel Hunt, *Superconductivity Sourcebook* (John Wiley, New York, 1989).

[6] J.C. Phillips, *Physics of High-T_c Superconductors* (Academic Press, USA, 1989).

[7] T.P. Orlando and K.A. Delin, *Foundations of Applied Superconductivity* (Addition-Wesley, New York, 1991).

[8] N.F. Mott and E.A. Davis, *Electronic Processes in Non-crystalline Materials* (Clarendon, Oxford, 1979).

[9] R.R. Heikes and R.V. Ure, *Thermoelectricity* (Interscience, New York, 1961).

[10] D.K.C. Mac Donald, *Thermoelectricity* (Wiley, New York, 1962).

[11] R.D. Barnard, *Thermoelectricity in metals and alloys* (Taylor and Francis, London, 1972).

[12] F.J. Blatt, P.A. Schröder, C.L. Foiles, and D. Greig, *Thermoelectric Power of Metals* (Plenum, New York, 1976).

[13] N.F. Mott, *Metal-Insulator Transitions* (Taylor and Francis, London, 1974).

List of Publications

A. Refereed journals :

[1] V.P.N. Padmanaban and K.Shahi, Fluctuation induced paraconductivity in $YBa_2Cu_3O_{7-\delta}$, Physica C **172**, 427 (1991) .

[2] V.P.N. Padmanaban and K. Shahi, Preparation and characterization of glassy and superconducting (Bi,Pb,Sb)-Sr-Ca-Cu-O systems, Bull. Mater. Sci. **14**, 351 (1991) .

[3] V.P.N. Padmanaban and K.Shahi, 110 K $Bi_2Sr_2Ca_2Cu_3O_y$ superconductors by Pb and Sb doping, Solid State Commun. **83**, 123 (1992).

[4] V.P.N. Padmanaban and K. Shahi, Superconducting properties of $YBa_2(Cu_{1-X}M_X)_3O_{7-\delta}$ (M = Ti,V), Physica C **208**, 263 (1993).

B. Conference proceedings :

[5] V.P.N. Padmanaban and K. Shahi, Some studies on CuO and their relevance to high-Tc superconductivity (HTSC) ; International symposium on high-Tc superconductivity, Jaipur, July 6-8, 1988. Proceedings published in High Temperature Superconductivity, P. 217, 1988, Oxford and IBH, Ed.: K.B. Garg.

[6] V.P.N. Padmanaban and K. Shahi, Transport properties of high-Tc superconductors and their precursor.Presented at the National workshop on high-Tc superconductors, Oct. 3-5, 1989, Indian Institute of Technology, Kanpur, India .

[7] V.P.N. Padmanaban and K. Shahi, Preparation,Phase Characterization and Transport studies on glassy and superconducting, $(Bi,Pb,Sb)_2Ca_2Sr_2Cu_nO_{2n+4+\delta}$ system. Presented at the International conference on superconductivity, Jan. 10-14, 1990, Bangalore, Abst. No. Pre. 4.4 .

[8] V.P.N. PAdmanaban and K. Shahi, Paraconductivity in $YBa_2Cu_3O_{7-\delta}$, Presented at the symposium on Materials Research, Jan. 18-19, 1991, Indian Institute of Technology, Kanpur, India.

PHY-1994-D-PAD-SOM